Determination of Elastic-Plastic and Visco-Plastic Material Properties from Instrumented Indentation Curves

JiJun Kang

MEng

Thesis submitted to The University of Nottingham

for the degree of Doctor of Philosophy

July 2013

For Dad and Mum

Abstract

Instrumented indentation techniques at micro or nano-scales have become more popular for determining mechanical properties from small samples of material. These techniques can be used not only to obtain and to interpret the hardness of the material but also to provide information about the near surface mechanical properties and deformation behaviour of bulk solids and/or coating films. In particular, various approaches have been proposed to evaluate the elastic-plastic properties of power-law materials from the experimental loading-unloading curves. In order to obtain a unique set of elastic-plastic properties, many researchers have proposed to use more than one set of loading-unloading curves obtained from different indenter geometries.

A combined Finite Element (FE) analysis and optimisation approach has been developed, using three types of indenters (namely, conical, Berkovich and Vickers), for determining the elastic-plastic material properties, using one set of 'simulated' target FE loading-unloading curves and one set of real-life experimental loading-unloading curves. The results obtained have demonstrated that excellent convergence can be achieved with the 'simulated' target FE loading-unloading curve, but less accurate results have been obtained with the real-life experimental loading-unloading curve. This combined technique has been extended to determine the elastic and visco-plastic material properties using only a single indentation 'simulated' loading-unloading curve based on a two-layer viscoplasticity model.

A combined dimensional analysis and optimisation approach has also been developed and used to determine the elastic-plastic material properties from loading-unloading curves with single and dual indenters. The dimensional functions have been established based on a parametric study using FE analyses and the loading and linearised unloading portions of the indentation curves. It has been demonstrated that the elastic-plastic material properties cannot be uniquely determined by the test curves of a single indenter, but the unique or more accurate results can be obtained using the test curves from dual indenters.

Since the characteristic loading-unloading responses of indenters can be approximated by the results of dimensional analysis, a simplified approach has been used to obtain the elastic-plastic mechanical properties from loading-unloading curves, using a similar optimisation

procedure. It is assumed that the loading-unloading portions of the curves are empirically related to some of the material properties, which avoids the need for time consuming FE analysis in evaluating the load-deformation relationship in the optimisation process. This approach shows that issues of uniqueness may arise when using a single indenter and more accurate estimation of material properties with dual indenters can be obtained by reducing the bounds of the mechanical parameters.

This thesis highlights the effects of using various indenter geometries with different face angles and tilted angles, which have not been covered previously. The elastic-plastic material parameters are estimated, for the first time, in a non-linear optimisation approach, fully integrated with FE analysis, using results from a single indentation curve. Furthermore, a linear and a power-law fitting scheme to obtain elastic-plastic material properties from loading-unloading indentation curves have been introduced based on dimensional analysis, since there are no mathematical formulas or functions that fit the unloading curve well. The optimisation techniques have been extended to cover time-dependent material properties based on a two-layer viscoplasticity model, has not been investigated before.

Acknowledgement

This thesis would not have been possible without the support of my supervisors at the University of Nottingham. I am greatly indebted to Professor Adib Becker and Wei Sun for their continuous support, guidance and encouragement during my PhD study.

I would like to thank all my friend and colleagues in the Structural Integrity and Dynamics (SID) group, the Department of Mechanical Engineering, The University of Nottingham for sharing their experience and knowledge. They have also made my time as a student enjoyable and memorable.

Thanks to my brother, JunHyuk Kang, for encouraging, understanding, patience and supporting me during this period of time to finish my Ph.D program.

Finally yet most importantly, I would like to thank my parents, who unconditionally support me financially and mentally, so I could complete this long journey without concern.

Nomenclature

$A_{project}$	Projected area of the hardness impression
A_1	$3\sqrt{3}$
A_1	π
a_r	Radius of the circle of contact
a	Ratio of the contact radius
$a\cot\alpha$	Depth of penetration
C	Independent of initial plastic strain
C_f	Compliance of the loading instrument
C_0	Total compliance
C_s	Compliance of indenter material
D	The diameter of indenter (mm)
d	The diameter of indenter (mm)
dP/dh	The initial slope of the unloading curve
E_r	Reduced modulus
$F(x)$	Objective function
$f_{1,2\ and\ 3}$	Dimensional functions
h	Spherical indenter at any point with radius r from the centre of contact
h_c	Circle of contact $(h_{max} - h_s)$
h_f	Final depth of the contact impression after indenter removed
h_{max}	Maximum displacement of indenter
H_{Meyer}	The hardness of Meyer's law
H'	Power law hardening with work hardening exponent
h_s	Distance between the surface of specimen and the edge of contact at full load or $\frac{P_{max}}{dP_u/dh \text{ at } h_{max}}$
h_p	Contact depth
H	Hardness

i	A specific position
K	$E^n\sigma_y^{1-n}$ (Yield coefficient)
K_p	Elastic modulus of the elastic plastic network
K_v	Elastic modulus of the elastic-viscous network
m	Power law index or $\frac{S(h_{max}-h_f)}{F_{max}}$
N	Total number of points
n	Work-hardening exponent
n_1	Work hardening exponent
n_2	Norton creep parameters
P	Indenter load
$P_{Hertzian}$	Hertzian pressure distribution
P_{mean}	Mean contact pressure
P_{max}	Maximum indenter load
P_u	Unloading Force
$\mathrm{P_i^{exp}}$	The (experimental) force from target data
$\mathrm{P}(x)_\mathrm{i}^{\mathrm{pre}}$	The predicted total force
R	Relative radius of the two contacting bodies' curvature $\frac{1}{R}=\frac{1}{R_1}+\frac{1}{R_2}$
R_i	Radius of a rigid indenter
R^n	A vector in the *n*-dimensional space
S	Initial slope of unloading curve or $\frac{mF_{max}}{(h_{max}-h_f)}$
UTS	Ultimate tensile strength
W_{total}	Total work done
W_U	Work done during unloading
Y	Initial yield stress
α	The angle of indenter

β	Correction factor 1.034 for a Berkovich indenter and 1.024 for a Vickers indenter
ϵ	Geometric constant: 0.727 for conical and 0.75 for Berkovich and Vickers
π_α	$\frac{F}{Eh^2}$
π_1	*Y/E*
π_2	h/h_m
σ_r	A representative flow stress
σ_v	Stress in the elastic-viscous network
σ_y	Initial yield stress
σ_p	Stress in the elastic-plastic network
ε_p^i	Initial plastic strain
ε_r	Representative strain
x	Optimisation variable set
$\varepsilon_{\text{total}}$	Total strain
ε_{el}	Elastic strain
ε_{pl}	Plastic strain
ε_p^{el}	The elastic strain in the elastic-plastic network
ε_v^{el}	Elastic strain in the elastic-viscous network
δ	Distance of mutual approach
ν	Poisson's ratio

Abbreviations

BHN	Brinell hardness number
CAX3	Three-Node Axisymmetric Triangular Continuum Elements
CAX4R	Four-Node Axisymmetric Quadrilateral Continuum Elements
C3D4	Four-Node Linear Tetrahedron Continuum Elements
FEA	Finite element analysis
.EXE	Executable File
.INP	ABAQUS Input File
LSQNONLIN	Non-linear Least Square Function

.M	MATLAB Script File
.OBD	ABAQUS Output Data File
PEEQ	Equivalent Plastic Strain
RF1	Reaction Force in X-direction (in Newton)
RF2	Reaction Force in Y-direction (in Newton)
RF3	Reaction Force in Z-direction (in Newton)
R3D4	Four-Node Bilinear Quadrilateral Continuum Elements
2D	Axisymmetric model
3D	3-Dimensional
UTS	Ultimate tensile strength
U1	Displacement in X-direction (in Millimetre)
U2	Displacement in Y-direction (in Millimetre)
U3	Displacement in Z-direction (in Millimetre)
SNRE	The squared norm of the residual error

List of Contents

1 Introduction

1.1 Background

Over the past two decades, increasing attention has been paid to the determination of material properties using indentation techniques. Instrumented indentation tests are used to measure the variation of the penetrated depth of an indenter into a specimen with the applied load and the area of contact. Indentation tests can be used not only to obtain and interpret the hardness but also to provide information regarding the mechanical properties of a specimen, deformation behaviour of bulk solids and coating films.

Traditional indentation testing (macro-micro scale) is a simple method to measure material properties of an unknown specimen with a sharp indenter. Limitations exist using this technique due to the varied shape of the indenter tips. The impression contact area can be measured after removal of the indenter. Nanoindentation improves the traditional indentation testing by indenting on the nano-scale with very precise tip shapes. The distinguishing feature of nanoindentation tests is the indirect measurement of contact area using very high-resolution type of scanning probe microscopy. Instrumented indentation tests can be also used to measure the work-hardening exponent, yield stress post-yield properties, etc. The measurements of elastic modulus, work-hardening exponent and yield stress are the main focus of this thesis.

1.2 Research Aims and Objectives

This work seeks to establish new reliable and accurate approaches for obtaining unique material properties from instrumented load-unloading indentation curves. The key steps to achieving the research aims are listed below:

- Identifying the knowledge gaps in this field
- Understanding the material response of a specimen under the indenter using finite element (FE) analysis

- Development of new optimisation models that can be combined with various approaches: FE analysis, dimensionless mathematical functions and simplified equations.
- Evaluation of elastic-plastic and visco-plastic material properties from instrumented loading-unloading indentation curves.
- Applying the proposed methods to real experimental indentation loading-unloading curves to evaluate the material properties.

1.3 Thesis Outline

Chapter 1 Introduction

The background, research aims and the objective of this study are illustrated

Chapter 2 Literature Review

A general background of instrumented indentation measurement is introduced. This chapter provides a review of the current state of the art in the field of instrumented indentation measurement techniques. Based on the review of instrumented indentation, the knowledge gaps are identified in this field and the concept of estimation of material properties using optimisation techniques is established.

Chapter 3 Research Methodology

In **Chapter 3**, the research methodology to address the knowledge gaps is introduced. In addition, the development of optimisation methods for the determination of material properties is illustrated. For understanding the material behaviour under the indenter, FE analysis using (the FE commercial software ABAQUS) is used in **Chapter 4** and, then, new approaches for obtaining material properties from indentation tests are presented in **Chapter 5, 6, 7** and **8**. In **Chapter 9**, a comprehensive study is performed based on the real experimental indentation curves.

Chapter 4 Effects of indenter geometries on the prediction of material properties

In **Chapter 4**, the influence of indenter geometries on the estimation of the material properties based on the FE simulation of three different indenters with perfectly sharp tips are investigated. Since loading-unloading curves are obtained, the hardness and elastic modulus are calculated using the widely used Olive-Pharr method for extraction material properties from indentation curves. In addition, the material responses under tilted indenter angles are investigated.

Chapter 5 Determining Elastic-Plastic Properties from Indentation Data obtained from Finite Element Simulations and Experimental Results

Chapter 5 presents a combined FE analysis and optimisation method for extracting four elastic-plastic mechanical properties from a given indentation load-displacement curve using only a single indenter. This approach is extended to examine the effectiveness and accuracy of the optimisation techniques using a real-life experimental indentation curve with random errors.

Chapter 6 A Combined Dimensional Analysis and Optimisation Approach for determining Elastic-Plastic Properties from Indentation Tests

In **Chapter 6**, a parametric study using FE analysis is conducted to construct the appropriate dimensional functions. This dimensionless mathematical function is coupled with a numerical optimisation algorithm to extract three elastic-plastic mechanical properties from the indentation load-displacement curves. Linear and power-law unloading fitting schemes are developed. Different sets of materials properties are used and the accuracy and validity of the predicted mechanical properties using a single indenter or dual indenters are assessed.

Chapter 7 Obtaining material properties from indentation loading-unloading curves using simplified equations

Based on the use of dimensional analysis to analyse the characteristic loading-unloading curves in **Chapter 6**, more simplified equations are devised to obtain the material properties. Various optimisation approaches are introduced to obtain material properties from indentation loading-unloading curves with single or dual indenters.

Chapter 8 Determination of elastic and viscoplastic material properties from indentation tests using a combined finite element analysis and optimisation approach

The optimisation approaches are extended to obtain elastic-visco-plastic material properties from indentation loading-unloading curves using optimisation algorithms and FE analysis based on a spherical indenter for a two-layer viscoplasticity model.

Chapter 9 Implementation of optimisation techniques in determining elastic-plastic properties from 'real' instrumented indentation curves

Three different methods (namely, FE analysis, dimensional analysis and a simplified empirical method) are used to determine the elastic-plastic material properties from 'real' loading-unloading test data from a single indenter.

Chapter 10 Conclusion and Further Work

The main conclusion and contributions of this research are discussed, and areas of further work are suggested.

2 Literature Review

This chapter presents a literature review of the various aspects of the development of indentation methods and the analysis techniques for extraction of mechanical properties from loading-unloading curves.

2.1 Basic theory of Indentation

Generally, an indentation test is the application of a controlled load through an indenter into the surface of a test specimen and recording the indenter displacement and the contact area remaining after the removal of the indenter. A typical indentation loading- unloading curve is shown in **Figure 2.1**.

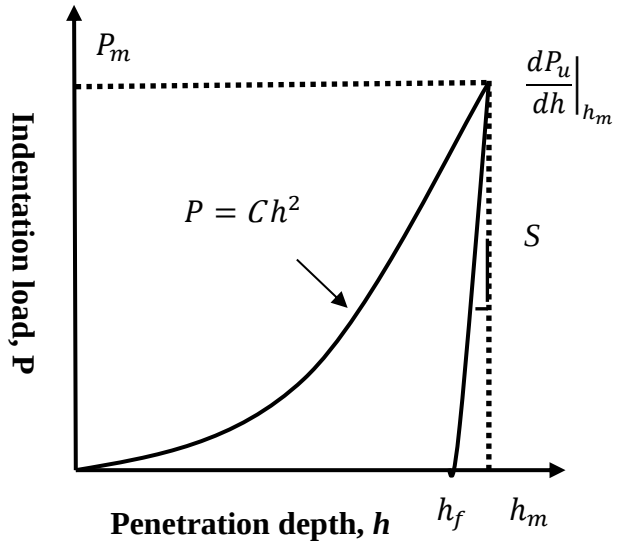

Figure 2.1 Loading and unloading curve from a typical indentation experiment [1].

Figure 2.2 shows the surface profile at the contact region. The relevant quantities are the maximum indenter load P_{max}; the maximum displacement of the indenter h_{max}; the final depth of the contact impression after removing the indenter, h_f; and the initial slope of unloading curve S. Generally, the loading curve, for most materials, contains the transition from elastic contact to plastic behaviour in the specimen beneath the indenter. Unlike the loading curve, the unloading curve near the top of the loading curve consists mostly of elastic recovery.

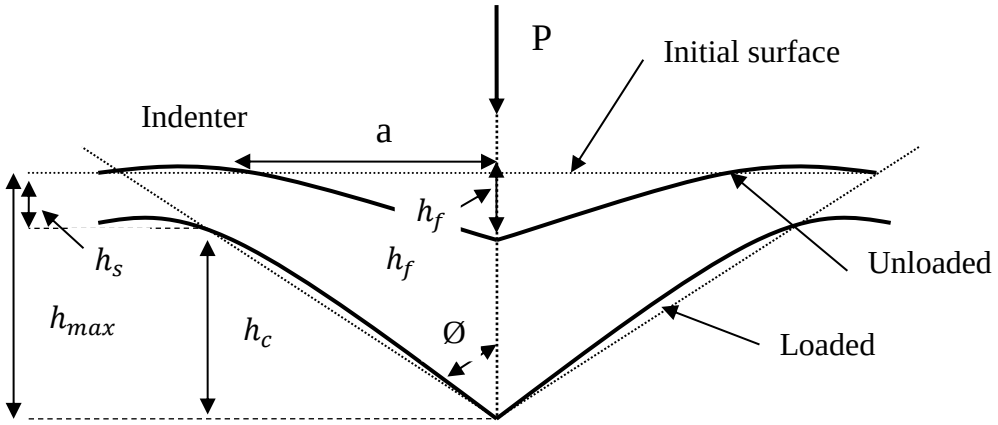

Figure 2.2 Schematic diagram of the surface profile at loading and unloading for indenter [1]

The earliest type of hardness test is the semi-quantitative scale of scratch hardness, which is developed by Moh in 1822. In order to measure the hardness based on Moh's method, the surface of material is scratched by a diamond stylus, and ten minerals are selected as standard material to compare the size of residual scratch imprint on the unknown material surface. Moh's hardness is the fundamental contribution to the development of Brinell, Knoop, Vickers and Rockwell hardness methods. However, it is hard to measure an accurate value of hardness of the material due to the friction between the diamond and the surface of unknown material. [2]

In the Brinell test [3], a very hard ball indenter moves downward to the large part of material specimen by varying the applied load and the size of the ball. The deformation of material specimen can be used to derive the Brinell hardness number as follows:

$$\text{BHN} = \frac{2\text{P}}{\pi\text{D}(\text{D}-\sqrt{\text{D}^2-\text{d}^2})} \qquad (2.1)$$

where P is applied load, D is the diameter of the indenter (mm), and d is the diameter of indentation(mm). The ultimate tensile strength (UTS) can be empirically expressed based on the BHN. In 1908, the empirical concept of the ratio of the load to the projected area of indentation is proposed by Meyer [4] to measure the hardness of material. Meyer hardness can be defined as:

$$\text{Meyer Hardness} = \frac{4P}{\pi d^2} \qquad (2.2)$$

where P is the applied load, and d is chordal diameter of indenter.

This leads to find the Meyer's law using a spherical indenter;

$$P = kd^n \qquad (2.3)$$

The values of k and n are changed by using different sizes of the spherical indenter, D, which gives different chordal diameters, d. The value of k decreased when the ball diameter increases. Therefore, it can be written as:

$$A = k_1 D_1^{n-2} = k_2 D_2^{n-2} = k_3 D_3^{n-2} \qquad (2.4)$$

Combining Eq. (2.2) and Eq. (2.4) gives:

$$H_{Meyer} = \frac{4P}{\pi d^2} = \frac{4P}{\pi}\left(\frac{d}{D}\right)^{n-2} \qquad (2.5)$$

The theoretical indentation test for obtaining elastic modulus was developed by Hertz [5]. The contacts between two elastic solids, a rigid sphere and a flat surface, were analysed and new classical solutions were derived, based on experimental and theoretical work. A spherical indenter can provide the transition of the deformation from elastic to elastic-plastic contact more clearly, compared with a sharp indenter such as conical, Vickers and Berkovich indenters, where the limits of plastic flow are reached immediately and the deformation is inevitably irreversible. The classic Hertzian contact theory [5] can be used to derive a relationship between the indenter load and other parameters, for a flat or curved surface indented by a rigid sphere as follows (see, e.g. Johnson[6]):

$$a^3 = \frac{3}{4}\frac{\mathrm{PR}}{\mathrm{E_r}} \qquad (2.6)$$

where a is the radius of the circle of contact, P is the indenter load, R is given by $\frac{1}{R} = \frac{1}{R_1} + \frac{1}{R_2}$ where R_1 and R_2 refer to the radii of curvature of the two bodies, and E_r is the 'reduced modulus', combining the elastic module of the specimen and the indenter, expressed as $\frac{1}{E_r} = \frac{(1-\nu^2)}{E_i} + \frac{(1-\nu^2)}{E_s}$. A schematic representation of the contact deformations between a rigid spherical indenter and a specimen are shown in **Figure 2.3**, where h_{max} is the maximum indentation depth, h_f is the final depth after the indenter is fully unloaded, h_s is the distance

between the surface of specimen and the edge of contact at full load and h_c is the contact depth at the same position.

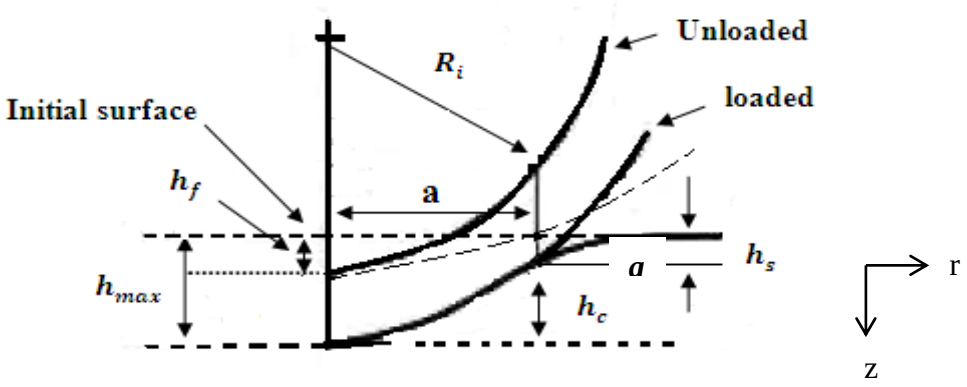

Figure 2.3 Schematic representation of contact between a rigid indenter of radius R_i and a flat specimen [7]

In general, R is the relative radius of the two contacting bodies' curvature, defined as follows:

$$\frac{1}{R} = \frac{1}{R_1} + \frac{1}{R_2} \qquad (2.7)$$

This equation is easily modified if one of the bodies is a flat plane, defined as follows:

$$\frac{1}{R} = \frac{1}{R_1} + 0 = \frac{1}{R_1} \qquad (2.8)$$

The Hertzian contact theory [5] is limited to homogeneous, isotropic materials which satisfy Hook's law, and assumes the contact deformation at contact remains localised. In addition, the contact surfaces are assumed to be continuous, frictionless and non-conforming. The Hertzian pressure distribution proposed by Hertz [5] can be expressed as:

$$P_{Hertzian} = P_{max}(1 - (r/a)^2)^{1/2} \qquad (2.9)$$

The deflection *h* of an elastic half-space under the spherical indenter at any point with radius *r* from the centre of contact can be expressed as follows: [5]

$$h = \frac{1}{E^*}\frac{3}{2}P_{max}\frac{\pi}{4a}(2a^2 - r^2) \quad r \leq a \qquad (2.10)$$

The Hertzian pressures are distributed on both indenter and surface of the specimen, and the deflections of points on the surface in the vicinity of the indenter are given by Eq. (2.10).

From Eq. (2.10), the distance of the edge of the circle contact, which is exactly half that of the total penetrated depth beneath the specimen surface, is given by: h_s=$h_c = h_{max}/2$.

The mutual approach of distant points between the indenter and specimen is obtained from

$$\delta^3 = \left(\frac{3}{4E^*}\right)^2 \frac{P^2}{R} \qquad (2.11)$$

and substituting Eq.(2.9) into Eq. (2.6), the distance of mutual approach can be calculated as:

$$\delta = a^2/R \qquad (2.12)$$

The mean contact pressure P_{mean} can be expressed as:

$$P_{mean} = P/\pi a^2 \qquad (2.13)$$

where the indenter load is divided by the contact area of the spherical indenter. Combining Eq.(2.6) and Eq. (2.13), the mean contact pressure can be obtained as follows:

$$P_{mean} = \left(\frac{4E^*}{3\pi}\right)\frac{a}{R} \qquad (2.14)$$

The indentation stress can be expressed as 'mean contact pressure' and the ratio of the contact radius a over the indenter radius R is called as "indentation strain". The existence of a stress-strain response of the relationship between $P_{mean}$and *a/R* of spherical indenter is similar to that of conventional uniaxial tension and compression tests. However, based on the indentation stress-strain relationship, more valuable information about elastic-plastic properties of the specimen can be obtained owing to the localised nature of the stress field. For a conical indenter, the relationship between the radius of the circle of contact and the indenter, shown in **Figure 2.4** can be expressed by:

$$P = \frac{\pi a}{2} E^* a \, cot\alpha \qquad (2.15)$$

The deformed surface profile within the area of contact is:

$$h = \left(\frac{\pi}{2} - \frac{r}{a}\right) a \cot\boldsymbol{\alpha} \quad r \leq a \qquad (2.16)$$

where α is the face angle of indenter, a cotα is the depth of penetration h_c at the circle of contact. Substituting Eq. (2.15) into Eq. (2.16) with r = 0, gives:

$$P = \frac{2\text{Etan}\alpha}{\pi} {h_t}^2 \qquad (2.17)$$

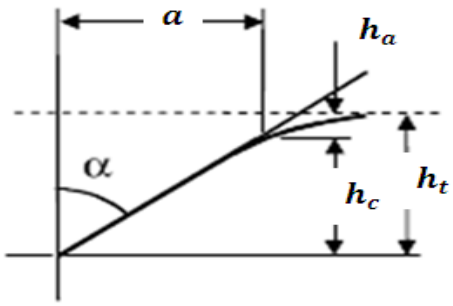

Figure 2.4 The geometry of contact with conical indenter. [7]

In general, a spherical indenter is one of the most common types of indenter, which is covered by the Hertz equation for elastic loading. The three-sided Berkovich indenter and four-sided Vickers are also widely used. The area of contact between specimen and indenter is particularly interesting. For a spherical indenter, the radius of the contact circle is given by:

$$a = \sqrt{2R_i h_c} \qquad (2.18)$$

where R_i is the radius of indenter and h_c is the final depth of the contact impression after unloading. In terms of a conical indenter, the radius of circle contact can be expressed as

$$a = h_c \tan\alpha \qquad (2.19)$$

Based on Hertz's equations, in 1885, Boussinesq [8] introduced an analysis procedure to calculate the stresses and displacements in contacts between two linear elastic solids. Sneddon [9, 10] made major contributions to derive the relationship of load, displacement and contract area for various punch shapes. However, the analysis is much more complex if plasticity is included. Experiments using indentation also have been performed by Tabor et al. [11, 12] to extract the material properties. The major observation from these experiments was that the recovery is truly elastic as the indenter is removed from the material. In addition, elastic contact solutions using spherical and conical indenters can be derived since there are good agreement between the experimental deformation and that obtained from Hertz's equations. Using these results, it was found that the elastic modulus significantly influences the initial portion of the unloading curve.

Research efforts were diversely focused on the indentation test by the mid-20th century. Various aspects of indentation tests such as plasticity [13-16], frictional effects [17-18], viscoelastic and nonlinear elastic solids [19-23] and adhesion [24-30] have been examined. In the early 1970's, depth-sensing indentation tests were developed by many researchers [31-35]. Their research is the foundation for the subsequent development of nanoindentation, especially technological advancements such as reducing the size of indenter tips and improving the accuracy and resolution of the depth measurement using advanced microscopes and load measurements.

Heretofore, instrumented indentation experimental tests have been widely used to estimate the hardness of a material. Ternovskill et al. [35] introduced a stiffness equation from the load and indenter displacement curve to derive the reduced modulus of a specimen material, which includes the elastic modulus and Poisson's ratio. The elastic modulus is extracted from load-displacement data, which is obtained by instrumented micro-hardness testing machines, using the following equation: [35]

$$S=\frac{dP}{dh}=\frac{2}{\sqrt{\pi}}E_r\sqrt{A_{project}} \qquad (2.20)$$

where, S is the contact stiffness, E_r is the reduced modulus of the specimen and $A_{project}$ is the projected area of the hardness impression. For derivation of the elastic modulus, it is assumed that the contact area is equivalent to the projected area of the hardness impression. Pharr et al. [1] have shown that Eq. (2.20) can be applied not only to a conical indenter but also to any indenter geometry that can be described as a body of revolution of a smooth function.

It was recognised in the early 1980's that mechanical properties of very thin films and surface layers can be also extracted using load and depth sensing indentation testing. Since it is difficult to measure the very small contact area of hardness impression, the indenter area function (or shape function) was suggested by Pethica et al [34]. The basic notion of this method is to determine the projected contact area directly from the shape function when the maximum indenter displacement and the residual displacement of the hardness impression after unloading are known. Based on this method, the estimation of contact area using the final depth gives more accurate results than using the displacement at maximum load.

Comprehensive work has been performed by Doerner and Nix [36], who put these ideas together to obtain the elastic modulus and hardness from indentation load-displacement curves. They assumed that the contact area of the indenter does not change during initial unloading. Therefore, the elastic behaviour corresponds to that of a flat-ended cylindrical punch indenter and the initial portion of the unloading curve is also linear. These relationships can be expressed as Eq. (2.21) due to the fact that the slope of the unloading curve is associated with the elastic modulus and contact area.

$$P = S(h - h_c) \qquad (2.21)$$

where, h_c it the true contact indentation depth. For determination of the contact area, they extrapolated the top one-third of the unloading curve and the extrapolated depth with the indenter shape function. After obtaining the contact area, the elastic modulus can be determined by Eq. (2.20). Doerner and Nix's method fits the initial portion of the unloading curve of most metals well.

Many indentation experiments have been performed by Olive and Pharr [37] and they found that the unloading curve is much better to describe as a power law fit rather than a linear fit. They assumed that there is large elastic recovery during the unloading process, which is the major difference compared with Doerner and Nix's method. The Olive-Pharr method is the most popular method for the interpretation of unloading-displacement data from the indentation test, and is used to determine hardness and elastic modulus. The hardness of the material can be determined from the maximum part of the loading curve and the elastic modulus can be determined by the initial part of the unloading curve, which is usually referred to as the contact stiffness. It is assumed that the unloading behaviour of the indenter is fully elastic with no plastic deformation. From the unloading data, the contact area and the plastic depth of penetration can be obtained. Therefore, the unloading stiffness is the most significant part of an indentation load-displacement loop since it is very significantly dependent on the elastic properties of the material. A power law fit is presented as:

$$\mathrm{P} = \mathrm{C}(\mathrm{h} - \mathrm{h_f})^{\mathrm{m}} \qquad (2.22)$$

$$\mathrm{S} = \left(\frac{\mathrm{dP}}{\mathrm{dh}}\right)_{\mathrm{h}=\mathrm{h_{max}}} = \mathrm{Cm}(\mathrm{h_{max}} - \mathrm{h_f})^{\mathrm{m}-1} \qquad (2.23)$$

where *m* is the power law index, and *C* is a constant. The contact stiffness, *S*, see **Figure 2.1**, is then calculated by differentiating Eq. (2.20) at the maximum depth of penetration, $h = h_{max}$. The value of *m* varies between 1.1 to 1.8 for most materials, according to the results of FE modelling studies [37, 38]. The slope of the unloading curve can be found and the depth of contact circle h_c can be determined from the load-displacement data using the following equation:

$$\mathrm{h_c} = \mathrm{h_{max}} - \mathrm{h_s} \qquad (2.24)$$

where $h_s = \epsilon \frac{P_{max}}{S}$, and ϵ is the geometric constant = 0.727 for conical and 0.75 for Berkovich and Vickers indenters [37]. Since the depth of the contact circle is determined, it is possible to obtain the projected area of the indenter. Projected areas for the various types of indenters are given in Ref. [7]. The reduced Young's modulus is given by:

$$\frac{1}{\mathrm{E_r}} = \frac{1-\mathrm{v_s}^2}{\mathrm{E_s}} + \frac{1-\mathrm{v_i}^2}{\mathrm{E_i}} \qquad (2.25)$$

where $\mathrm{E_s}, \mathrm{E_i}$, $\mathrm{v_s}$ and $\mathrm{v_i}$ are the elastic modulus and Poisson's ratio of the specimen and indenter, respectively. For a "rigid" indenter, the second term in Eq. (2.25) is negligible. Therefore; Eq. (2.25) can be rewritten:

$$\frac{1}{\mathrm{E_r}} = \frac{1-\mathrm{v_s}^2}{\mathrm{E_s}} \qquad (2.26)$$

The initial slope of the unloading curve can be used to determine the projected area, $\mathrm{A_{project}}$, shown in Eq.(2.20). It shows the relationship between the initial slope of unloading curve, dP/dh, and the projected area, $\mathrm{A_{project}}$ and the Young's modulus, $\mathrm{E_r}$ for axisymmetric indenters such as conical indenters. Experimental and FE results [37] show that a correction factor, β, corresponding to the axial variation in stress can be introduced for non-axisymmetric, polygonal indenter shapes. β is 1.034 for a Berkovich indenter and 1.024 for a Vickers indenter. The contact stiffness with the correction factor is:

$$\mathrm{S} = \frac{\mathrm{dP}}{\mathrm{dh}} = \frac{1}{\beta}\frac{2}{\sqrt{\pi}}\mathrm{E_r}\sqrt{\mathrm{A_{project}}} \qquad (2.27)$$

Rearranging Eq. (2.27) the elastic modulus can be expressed by

$$\mathrm{E_r} = \left(\frac{\pi}{4\mathrm{A_{project}}}\right)^{1/2}\frac{\mathrm{dP}}{\mathrm{dh}}\,\beta \qquad (2.28)$$

The hardness can be determined by the following:

$$H = P_{max} / A_{project} \quad (2.29)$$

2.2 Type of indenters

In order to determine the hardness and elastic modulus of a specimen, spherical or pyramid-shaped indenters such as Berkovich, Vickers and conical indenters are widely used. The features of Berkovich, Vickers and conical indenters are discussed briefly in this section. For the Berkovich indenter, the half-angle from the centreline is 65.27°. This angle gives the same ratio of projected area to indentation depth as the Vickers indenter and three sided pyramid indenter. It is easier to construct to meet at a sharp point compared with four sided Vickers pyramid indenter. In general, mean contact pressures can be obtained from the projected area of contact, h_c, shown in **Figure 2.2**. Since the geometry of the Berkovich indenter is known, the projected area can be calculated. The details of the geometry of the Berkovich indenter are shown in **Figure 2.5**. The projected area can be calculated as following:

$$\tan 60° = l/0.5a \quad (2.30)$$

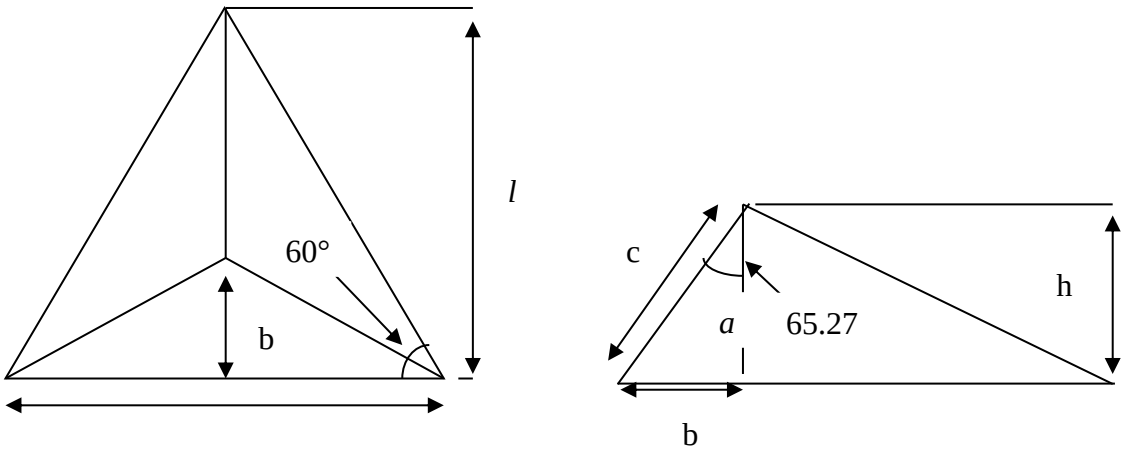

Figure 2.5 Berkovich indenter

This can be rearranged as

$$l = \sqrt{3}a/2 \quad (2.31)$$

The projected area can expressed as

$$A_{projected} = al\ /2 \qquad (2.32)$$

Substituting Eq. (2.31) into Eq. (2.32) gives

$$A_{projected} = \frac{\sqrt{3}}{4}a^2 \qquad (2.33)$$

From Eq. (2.33), the value of *a* is not known yet.

$$cos65.27° = h/c \qquad (2.34)$$

$$h = \frac{a\cos 65.27°}{2\sqrt{3}\sin 65.27°} = \frac{a}{2\sqrt{3}\tan 65.27°} \qquad (2.35)$$

Eq. (2.30) can be rearranging as follows

$$a = 2\sqrt{3}\tan 65.27° \qquad (2.36)$$

Substituting Eq. (2.36) into Eq. (2.33), the projected are of Berkovich indenter is expressed as

$$A_{projected} = 3\sqrt{3}h^2 tan^2 65.27 = 24.49h^2 \qquad (2.37)$$

For the Vickers indenter, the half-angle from the centreline is 68° with a four sided pyramid. **Figure 2.6** shows the geometry of the Vickers indenter.

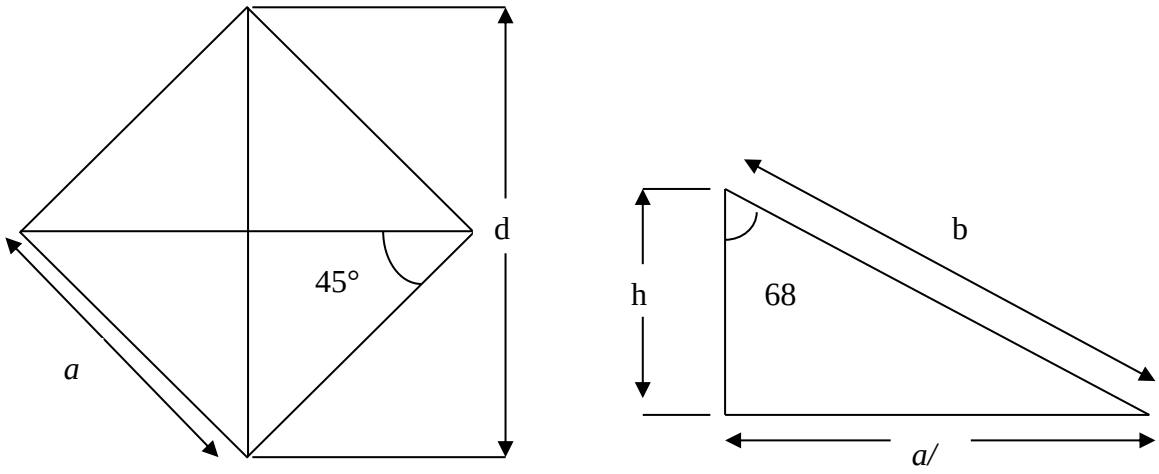

Figure 2.6 Vickers indenter

The projected area can be calculated as following:

$$\sin 45° = d/2a \qquad (2.38)$$

This can be rearranged as follows

$$a = d/\sqrt{2} \quad (2.39)$$

The projected area can expressed as follows

$$A_{projected} = a^2 \quad (2.40)$$

Substituting Eq. (2.39) into Eq. (2.40)

$$A_{projected} = \frac{d^2}{2} \quad (2.41)$$

The value of a can be also expressed as:

$$\tan 68° = a/2h \quad (2.42)$$

$$a = 2h \tan 68° \quad (2.43)$$

Substituting Eq. (2.40) into Eq. (2.43), the projected area of the Vickers indenter is expressed as follows

$$A_{projected} = a^2 = 4h^2 \tan^2 68 = 24.504h^2 \quad (2.44)$$

For the axisymmetric conical indenter, the projected area can be simply expressed as:

$$A_{projected} = \pi h^2 \tan^2 \alpha \quad (2.45)$$

The projected areas of each indenter are summarised in **Table 2.1**.

Table 2.1 Projected area for four different types of indenters and the centreline to face angle of the indenter [3]

Indenter type	Projected Area	Semi-angle θ(deg)	Effective cone Angle, α (deg)
Sphere	$A \approx \pi 2Rh_p$	N/A	N/A
Berkovich	$A = 3\sqrt{3}h^2 tan^2\theta$	65.3°	70.2996°
Vickers	$A = 4h^2 tan^2\theta$	68°	70.32°
Cone	$A = \pi h^2 tan^2\theta$	α	α

As can be seen from **Table 2.1**, the projected area of pyramid-shaped indenters, Berkovich and Vickers indenters, are approximately $A = 24.5h^2$ and the projected area with the angle of 70.3° of the conical indenter is equivalent to that of the pyramid-shaped indenters. Therefore,

for convenience, the axisymmetric conical indenter is widely used as it results in the same projected area of the pyramid indenters. In general, measuring hardness can be used by the concept of geometrical similarity. There are two different types of geometrically similar indentations, as shown in **Figure 2.7**.

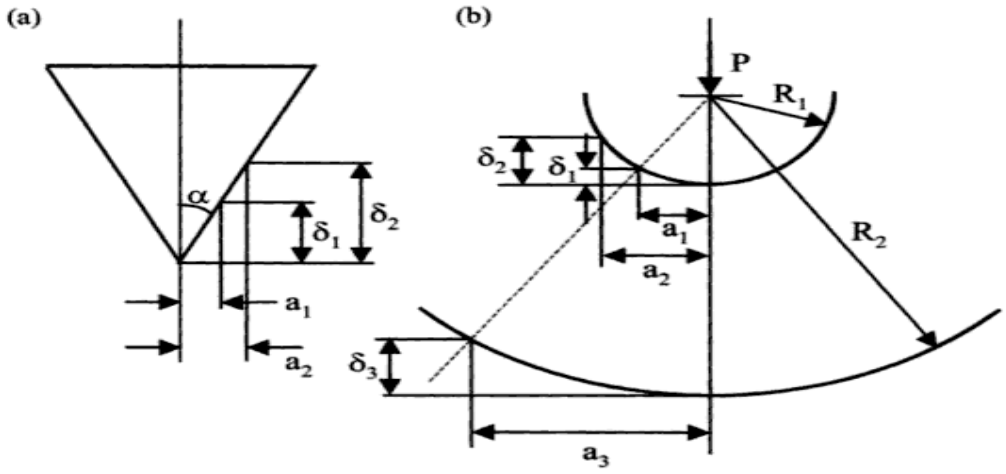

Figure 2.7 Geometrical similarities for a conical or pyramidal indenter [7]

Geometrical similarity for a conical or pyramid indenter is shown in **Figure 2.7**(a). The ratio of the contact circle radius to the depth of the indentation a/δ basically remains constant during load increase. This is important in measuring hardness with a pyramidal or conical indenter due to the fact that the strain within the specimen material remains constant and is independent of the applied load. Unlike the pyramid and conical indenters, a spherical indenter is not a geometrically similar indenter due to the increase in the ratio a/δ as the load increases. However, it can be geometrically similar indentation when the ratio a/R remains constant.

2.3 Review of instrumented indentation measurement

2.3.1 Scaling approach to indentation modelling

A dimensional analysis method for the analysis of load-displacement data is studied by Cheng and Cheng [39-48]. In general, the uniaxial stress-strain ($\sigma - \epsilon$) relationship is assumed to be expressed by

$$\boldsymbol{\sigma} = \begin{Bmatrix} \mathrm{E}\boldsymbol{\varepsilon} \text{ for } \boldsymbol{\varepsilon} \leq \frac{\mathrm{Y}}{\mathrm{E}} \\ \mathrm{K}\boldsymbol{\varepsilon}^{\mathrm{n}} \text{ for } \boldsymbol{\varepsilon} \geq \mathrm{Y}/\mathrm{E} \end{Bmatrix} \qquad (2.46)$$

where E is Young's modulus, Y is initial yield stress, n is the work-hardening exponent, and K is the yield coefficient, where $K=Y(E/Y)^n$. The material is elastic perfectly-plastic if n is zero. The indentation test can be divided into two different parts, loading and unloading. The basic principles for the dimensional analysis method can be introduced as follows. Firstly, the dependent variable should be selected and all independent variables and parameters should then be identified with independent dimensions. Secondly, since dimensionless quantities are formed, relationships among dimensionless quantities can be established. The number of relationships is equivalent to the number of dependent quantities. From the loading curve, the indenter load F and the penetration displacement h are dependent variables. The indenter load is dependent on Young's modulus (E), Poisson's ratio (ν), initial yield stress (Y), work-hardening exponent (n) and the angle of indenter (α). Since the functions of ν, α and n have no dimensions, E or Y can be chosen and E and h are selected as the governing parameters for dimensional analysis. Those can be expressed by the following:

$$\begin{aligned}[\mathrm{Y}] &= [\mathrm{E}] \\ [\mathrm{F}] &= [\mathrm{E}][h]^2\end{aligned} \qquad (2.47)$$

Therefore, the load F for the loading curve can be expressed by

$$\mathrm{F} = \mathrm{f_L}(\mathrm{E}, \boldsymbol{\nu}, \mathrm{Y}, \mathrm{n}, \mathrm{h}, \boldsymbol{\alpha}) \qquad (2.48)$$

By applying the π-theorem in dimensional analysis [45], it becomes:

$\pi_\alpha = \boldsymbol{\pi}_\alpha(\pi_1, \nu, n, \alpha)$, or equivalently $\mathrm{F} = Eh^2\pi_\alpha\left(\frac{Y}{E}, \nu, n, \alpha\right)$ (2.49)

where $\pi_\alpha = \frac{F}{Eh^2}$, $\pi_1 = Y/E$, ν, n, α are all dimensionless.

Also, the contact depth h_p can be expressed as

$$h_p = h\pi_\beta\left(\frac{Y}{E}, \nu, n, \alpha\right) \qquad (2.50)$$

During unloading, a maximum indenter displacement h_m is added. Therefore, the force, F, can be expressed as a function, f_U , of seven independent governing parameters.

$$F = f_U(E, \nu, Y, n, h, h_m, \alpha) \qquad (2.51)$$

Dimensional analysis yields:

$\pi_\alpha = \pi_\alpha(\pi_1, \pi_2, \nu, n, \alpha)$,

or equivalently F = $Eh^2\pi_\alpha\left(\frac{Y}{E}, \frac{h}{h_m}, \nu, n, \alpha\right)$ (2.52)

where $\pi_\alpha = \frac{F}{Eh^2}$, $\pi_1 = Y/E, \pi_2 = h/h_m$ ν, n, α are all dimensionless.

From Eq. (2.52), the load F depends on h^2 and the ratio $\frac{h}{h_m}$.

Now, the initial unloading slope dF/dh can be considered. With regard to the derivative of indenter displacement and estimating it at h=h_m, it can be written as

$$\frac{dF}{dh} = Eh_m\pi_\delta\left(\frac{Y}{E}, \nu, n, \alpha\right) \quad (2.53)$$

where the initial unloading slope is proportional to h_m.

The total work done can be obtained by integrating the load-indenter displacement curves. Total work done by loading is given by

$$W_{total} = \int_0^{h_m} Fdh = \frac{Eh_m{}^3}{3}\pi_\alpha\left(\frac{Y}{E}, \nu, n, \alpha\right) \quad (2.54)$$

The total work is proportional to $h_m{}^3$.

During unloading, the work done on the indenter is written as

$$W_U = \int_{h_f}^{h_m} Fdh = \frac{Eh_m{}^3}{3}\pi_U\left(\frac{Y}{E}, \nu, n, \alpha\right) \quad (2.55)$$

The ratio of irreversible work or energy dissipation for a loading-unloading cycle, $(W_{total} - W_U)/W_{total}$, can be expressed as

$$\frac{W_{total}-W_U}{W_{total}} = 1 - 3\frac{\pi_U(Y/E,\nu,n,\alpha)}{\pi_\alpha(Y/E,\nu,n,\alpha)} \quad (2.56)$$

FE analysis would allow a systematic investigation of the relationship of Eqs (2.49) and (2.52) and also the form of the dimensionless functions. These scaling relationships are important due to the fact that it allows testing the relationship between experimental variables within a theoretical framework, which can lead to better understanding of indentation in elastic-plastic solids.

2.3.2 Numerical approach based on FE Analysis

The technique proposed by Oliver and Pharr [38] is widely used. There are a number of simplifying assumptions for this technique, (i) the specimen is an infinite half-space, (ii) an ideal indenter geometry is used, (iii) the material is linearly elastic and incompressible, and (iv) no adhesive and no frictional forces. FE techniques have been used to compute very complex stress-strain fields of thin film or bulk materials in an indentation process. The first use of FE analysis for the indentation problem has been performed by Hardy [49] and Dumas [50] and their experimental results are in good agreement with the FE analysis. Bhattacharya and Nix [51] in 1988 developed FE models of Ni, Al and Si to compare with experimental results, which showed that the continuum based FE approach, is able to simulate the load-unloading response during a sub-micrometer indenter test.

Laursen and Simo [52] focussed on using the FE analysis to investigate the mechanics of the micro-indentation process of Al and Si. The main observation of their research is that the assumption of a constant projected area during unloading is not supported by FE simulations. In addition, the pile-up and sink-in behaviour could be appreciable. From their work, the estimated contact area is considerably different as compared with the actual contact area. Furthermore, Lichinchi et al [53] found that load-displacement curves from FE simulations using axisymmetric and 3D models with Berkovich indenter and experimental data are generally in good agreement. Bolshakov et al [54] investigated the effect of the indentation process with applied or residual stress on the elastic-plastic material of A1 8009 based on FE analysis. They indicated that the results of nanoindentation measurements are not accurate when pile-up or sink-in is not considered in the contact area determination. They also mentioned that the elastic modulus and hardness are not influenced by the applied stress. FE analysis can be applied to obtain more accurate material properties and to explain the occurrence of pile-up or sink-in.

However, most previous FEA simulations are limited to axisymmetric models rather than 3D models. Few indentation analyses [55-56] have been performed using 3D FE simulation models with Vickers indenters to obtain the material properties. In general, it is assumed that there is no friction between the indenter and the indented material and that the tip of the

indenter is perfectly sharp. Only few researchers [57-58] have compared the behaviour of different indenter geometries. The influence of various indenters such as Berkovich, Vickers, Knoop, and cone indenters on the indentation of elastic-plastic material has been studied by Min et al [57]. They found that the relationship of load-displacement between axisymmetric models of a cone indenter and 3D models of Berkovich and Vickers indenters agree with the rule of the volume equivalence. In addition, three different indenter geometries used on bulk and composite materials have recently been employed by Sakharova et al [58]. They compared load-displacement curves, the values of hardness and the strain distribution using different indenters, such as conical, Berkovich and Vickers indenters and found that the equivalent plastic strain distributions were affected by the geometry of indenters. In recent years, research efforts have been focused on extracting elastic-plastic material properties (E, ν, σ_y, n) using indentation data, in which the power law hardening is generally used to characterise these independent parameters [43-45]. Combinations of dimensional analysis and FE simulations with a single indenter shape have been used to extract the elastic-plastic properties [46, 59]. Based on this method, a unique set of material properties could not be generated [59-62]. Furthermore, many research groups have shown [43, 63] that almost the same indentation load-displacement curves can be generated by different sets of material properties, when a single indenter is used. Therefore, many researchers believed that unique solutions can only be determined by dual (or plural) sharp indenters. [63-67].

2.3.3 The concept of representative strain

The determination of the stress-strain curve of a given material using the elastic-plastic response in indentation tests has been studied in the past. The common method is to construct the dimensionless functions with the concept of representative strain, introduced by Atkins and Tabor [68]. The direct relationships between indentation diameter and average applied strain, average pressure and corresponding stress have been shown by Tabor [2]. He has shown that the constraint factor $C = H/\sigma_y$ is about 3 for most perfectly plastic materials, where H is the Vickers indentation hardness and σ_y is the yield strength. The determination of mechanical properties with micro-spherical indentation has shown by Field and Swain [69]. The use of stepwise indentation with a partial unloading technique can help to divide the

elastic and the plastic components of indentation at each step. Later, the method of determining of the nonlinear part of stress-strain curve with conical indenters with different angles was developed by Jayaraman et al. [70]. Another method for determining the stress-strain curve with spherical indentation was also studied by Taljat et al.[71]. Using their method, relationships between maximum and minimum applied strains and stresses, contact diameter, indenter diameter and hardening exponent were determined, but the hardening exponent was not accurately determined. Methods for determining the stress-strain relationship curve with a neural network and cyclic indentation were developed by Huber and Tsakmakis [72]. In addition, based on FE simulation of successive ball indentations with increasing load, a new procedure has been given by Bouzakis and Vidakis [73]. However, both methods are usually difficult and time consuming due to the fact that cyclic loading is required in Huber's method. Furthermore, FE simulation and the measurement of imprint profile for every stress-strain curve point are required in Bouzakis' method.

Procedures for obtaining the elastic-plastic properties from loading-unloading curves with Vickers indentation are proposed by Giannakopoulos and Suresh [74]. In general, the indentation response of elastic-plastic behaviour can be modelled by the concept of self-similarity. The plastic indentation of a power law plastic material with a spherical indentation, based on a self-similar solution, was developed by Hill et al. [75]. Subsequently, the elastic-plastic indentation responses with self-similar approximations of sharp indentation have been computationally obtained by Giannakopoulos et al.[76] and Larsson et al. [77]. Giannakopoulos and Suresh [74] showed that the yield stress at a plastic strain of 0.29 and the work hardening exponent, *n* can be determined from these values. However, Venkatesh et al.[78] stated that their approach can determine Young's modules, the yield stress and the characteristic stress, $\sigma_{0.29}$, the behaviour of the entire compressive plastic stress-strain beyond yield point could not decide. Therefore, the limitation of determining material properties using this method [78] are existed, if two materials have same material properties E, σ_y and $\sigma_{0.29}$.

From the work of Nayebi et al [79], the plastic properties of material can be determined with only the loading curve. A comparison between the stress-strain behaviour of an aluminium alloy test in uniaxial tension and spherical indentation has been proposed by Herbert et al.

[80]. They used Tabor's relationships [2], which relate normal hardness and stress for a given representative strain which depends on the applied indenter displacement of the sphere in a fully developed plastic contact. From their study, Tabor's equations cannot regenerate the correct shape of the uniaxial stress-strain curve. Therefore, the estimation of a representative strain using Tabor's equation should be reconsidered. Tabor [2] suggested that an additional representative plastic strain of 0.08 is induced by a Vickers indent. This representative plastic strain 0.08 is not an actual plastic deformation of specimen, but rather a statistical best fit to the measured increase of the indentation hardness for the plastically deformed materials. The predicted indentation hardness is shown as

$$\begin{cases} H = C\sigma_r|_{\varepsilon=\varepsilon_r}, & \varepsilon_p^i = 0 \\ H = C\sigma_r|_{\varepsilon=\varepsilon_r+\varepsilon_p^i}, & \varepsilon_p^i > 0 \end{cases} \qquad (2.57)$$

where C is independent of initial plastic strain and the applied indentation displacement due to the self-similarity of Vickers indenters, σ_r is a representative stress and ε_p^i is the initial plastic strain. As can be seen from the above equations, the representative stress σ_r is related to the total sum of the initial plastic strain ε_p^i plus the representative plastic strain. [2]

The increase in indentation hardness of a plastically deformed material can be estimated if its uniaxial stress-strain curve is already known. In a reverse analysis, the stress-strain curve can be predicted from the indentation hardness of the deformed material. Since Tabor [2] proposed the forward and reverse analyses, research efforts have been focused on the definition and calculation of the representative plastic strain.

More recently, the determination of indentation elastic-plastic response using dimensionless analysis and the concept of a representative stress and strain with a single indenter have been studied by Dao et al. [81], in which they developed both forward and reverse algorithms. From their study, a universal representative plastic strain of 0.033 was used to construct dimensional functions. Extending Dao's method [81], Bucaille et al.[64] using conical indenter with different face angle of indenters showed that the representative plastic strain is related to the indenter geometry. Ogasawara et al. [82] mentioned that the proposed representative plastic strain by Dao [81] is limited to apply to a wide range of material properties and it is not associated with elastic or plastic deformations. Therefore, they

proposed a representative plastic strain value of 0.0115, which is able to incorporate the biaxial nature of the plastic deformation [83] obtained from the elastic-plastic indentation response with a single indenter using ε_r=0.0115. Chollacoop and Ramamurty [84] showed that the effect of the indentation loading curve with regard to initial plastic deformation and the stress-strain curves using two different indenters on strain hardening material can be predicted by Dao's method [81]. Cao and Huber [85] stated that the range of representative plastic strain is 0.023-0.095 of ε_r values.

The determination of a representative plastic strain is proposed without using instrumented indentation. Based on the boundary of the large hydrostatic stress 'core' directly under the tip of a sharp indenter, the value of ε_r = 0.07 is reported by Johnson [6]. Chaudhri [86] suggested that the values of ε_r is between 0.25 and 0.36, which is the maximum plastic strain in the plastic zone of a Vickers indenter. A representative plastic strain of 0.07 and 0.225 for Berkovich and cube-corner indenters are proposed by Jayaraman et al. [70], based on the statistical fits with respect to the relationship between the normalised flow stress and hardness. In addition, a value of ε_r = 0.112 is proposed by Tekkaya [87]. Using ε_r = 0.112, the relationship between the yield stress and the Vickers hardness are defined to determine the new local yield stress of specimen. It is clearly noticeable that the values for representative plastic strain vary over a broad range. Most of those values are not based on the physical relationship, rather calculated from curve-fitting. Therefore, it can be said that any suggested representative concept is not universally operative for real materials.

More recently, Chaiwut and Esteban [67] used the combination of inverse analysis and FE simulations with dual indenters to extract accurate unique material properties from indentation loading-unloading data. They used their algorithm to obtain only two material properties (σ_y, n) and Young's modulus (E) from the unloading curve, using the Olive-Pharr method. They could not resolve the issue of uniqueness by using a single indenter. However, by using dual indenters, the optimised results were improved and reached their target values.

2.4 Summary and Knowledge gaps

This chapter has reviewed several relevant aspects of the current knowledge in the field of instrumented indentation tests, especially focused on the determination of material properties from loading-unloading curves. Based on the area of obtaining material properties from loading-unloading indentation curves, the knowledge gaps can be identified as follows:

(i) Only few studies have compared the effects of using different indenter geometries using FE analysis. The effects of using various indenter geometries with different face angles and different tilted angles have not been covered previously.

(ii) Many researchers have used the inverse analysis and dimensional approach in order to obtain elastic-plastic material properties from loading-unloading indentation curves. However, the estimation of material properties cannot be uniquely obtained with a single indenter. In this study, four elastic-plastic parameters (E, σ_y, n and ν) are extracted, for the first time, in a non-linear optimisation approach, fully integrated with FE analysis, using results from a single indentation curve. In order to arrive at the mechanical properties from loading-unloading indentation curves with a single indenter, optimisation algorithm have been developed.

(iii) The values of the representative plastic strain vary over a broad range and any suggested representative strain concept is not universally applicable for all materials. In this work, the combined dimensional analysis and optimisation approaches with a representative strain for determining elastic-plastic properties from indentation tests has been investigated. In general, it is hard to construct mathematical functions of the unloading curves due to the complicated nature of the contact interaction between the indenter and the specimen. Since there is no mathematical formula or function that fits the unloading curve well, a linear and a power-law fitting scheme may be more appropriate. Based on the dimensional analysis with a linear and a power-law fitting scheme, the optimisation approach can be used to obtain elastic-plastic material properties from loading-unloading indentation curves.

(iv)There is a need for more simplified mathematical approaches to obtain the elastic-plastic mechanical properties from loading-unloading indentation curves without the need for FE

analysis. In this work, optimisation techniques combined with simpler mathematical representations of the loading-unloading curves are presented. This is a novel approach to find the material properties from loading-unloading curve.

(v) The determination of time-dependent material properties from loading-unloading curves has not been previously attempted. This work has been extended, for the first time, the determination of visco-elastic-plastic material properties using a two-layer visco-plasticity model with an optimisation approach.

3 Research Methodology

3.1 Research Approach

The aim of this chapter is to clarify and to describe the research methodology used in this thesis in order to address the knowledge gaps mentioned in **Section 2.4**. The instrumented indentation techniques allow measuring a broad range of material mechanical behaviour including elastic-plastic deformation, time dependent behaviour, fracture, residual stresses, and the onset of plastic deformation and dislocation behaviour [88]. This research will only focus on the obtaining material properties of elastic-plastic and visco-plastic behaviour from indentation loading-unloading curves. The literature review has shown that many approaches have been suggested to extract elastic-plastic material properties from instrumented indentation.

Most proposed approaches in the literature to obtain elastic-plastic material properties are based on the characteristic parameters of loading-unloading indentation curves. Furthermore, in order to determine material properties uniquely, most approaches have been used with two or more indenters. This research is mainly focused on alternative methods to obtain the material properties based on optimisation approaches. Firstly, to understand the indentation response beneath the specimen, the FE method (ABAQUS) has been used and then extended to the development of optimisation approaches combining different methods. After a feasibility study and validation of all proposed methods based on the optimisation approach, the proposed methods will be applied to real experimental indentation loading-unloading curves. The schematic diagram of the research methodology is shown and the main contribution of this study is boxed with the dashed line in **Figure 3.1.**

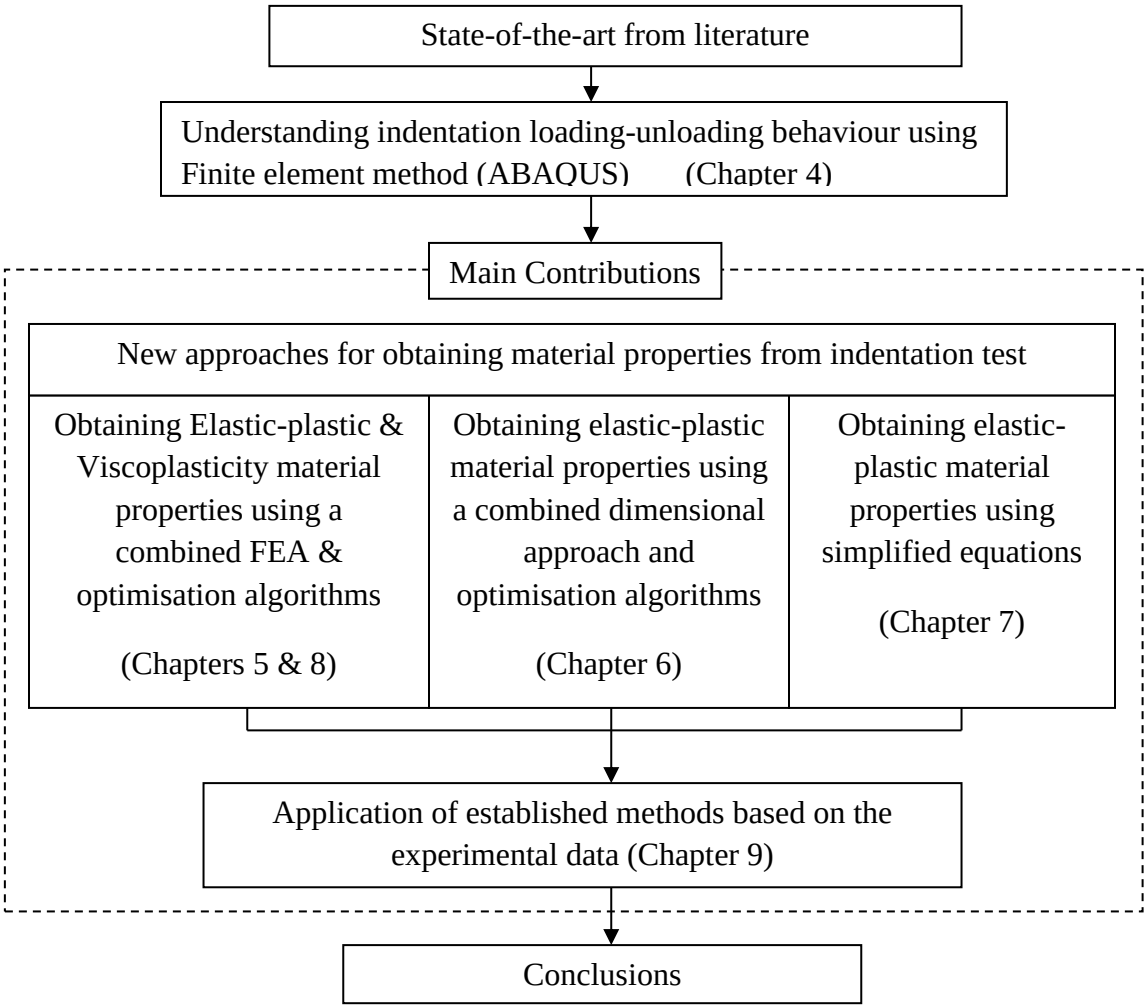

Figure 3.1 Schematic diagram of research methodology

3.2 Development of Methodology

3.2.1 FE model development

At the beginning of this study, attempts have been made to understand the indentation loading-unloading behaviour using FE analysis. All the proposed methods to obtain the material properties have been developed using 'simulated' indentation loading-unloading curves from FEA and the details of FE model used in this study are discussed. The FE analysis of the bulk material indentation system is based on either axisymmetric or 3D continuum elements using ABAQUS Standard 6.8-3 [89]. Contacts between three different types of rigid indenters and an isotropic elastic-plastic specimen are modelled. During each iteration of the optimisation process, FE analysis is performed with the updated elastic-plastic properties determined from the previous optimisation iteration. The friction coefficients at the

contact surfaces between the indenter and the top surface of the bulk material are assumed to be zero, since friction has a negligible effect on the indentation process [64]. The assumption of a perfectly sharp indenter is employed. A "master-slave" contact scheme in the FE procedure is applied on the rigid indenter and the specimen surface. The entire processes have been performed by a PC running Window XP with an Intel Core 2 Duo CPU E8300 processor.

The specimen is modelled as an axisymmetric geometry with three-node axisymmetric triangular continuum elements (CAX3 in ABAQUS) and four-node axisymmetric quadrilateral continuum elements with reduced integration (CAX4R in ABAQUS). For the indenter, an axisymmetric analytical rigid shell/body is used. The region of interest is in the vicinity of the perfect (sharp) indenter tip where a high element density has been used due to the expected high stress gradients immediately beneath the indenter tip, as shown in **Figure 3.2.**

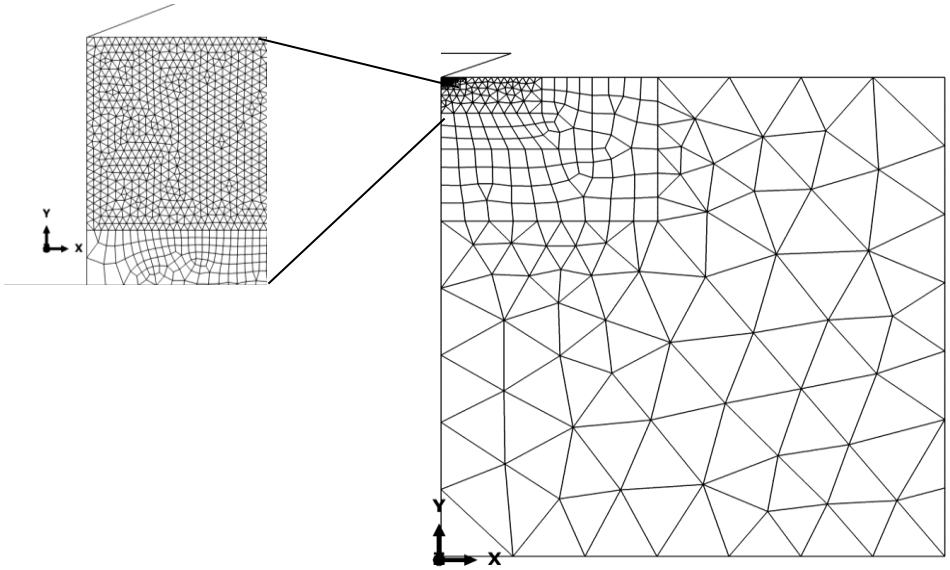

Figure 3.2 FE meshes of the substrate subjected to an axisymmetric conical indenter.

All nodes at the base of the specimen are constrained to prevent them from moving in the x and y directions. A rigid conical indenter with a 70.3° face angle is used, which gives the same projected area to depth-ratio as a Berkovich and Vickers indenters. The simulations are carried out in two distinct steps: a loading step and an unloading step. In the first step, the total indenter displacement is imposed. During the loading step, the rigid cone indenter is

moved downwards along the axial-direction to penetrate the substrate up to the maximum specified depth. During the unloading step, the indenter is unloaded and returns to its initial position. The details of three-dimensional model discussed in **Chapters 4** and **5.** A two-layer elastic-plastic and visco-plastic model is discussed in more detail in **Chapter 8**.

3.2.2 Optimisation model development

The optimisation algorithm has been developed with MATLAB. A non-linear optimisation technique is devised within the MATLAB optimisation toolbox [90] which provides an excellent interface to FE codes such as ABAQUS, through various programming languages such as C and Python. The optimisation technique is used to determine mechanical properties for a given set of target indentation data using an iterative procedure based on a MATLAB nonlinear least-squares routine to produce the best fit between the given 'target' indentation data and the optimised indentation data, produced by the proposed methods. This non-linear least-squares optimisation function (called LSQNONLIN) is based on the trust-region-reflective algorithm [90]. This optimisation procedure is guided by the gradient evaluation and iterates until convergence is reached. The optimisation model is:

$$\mathrm{F}(x) = \frac{1}{2}\sum_{\mathrm{i}=1}^{\mathrm{N}}\left[\mathrm{P}(x)_{\mathrm{i}}^{\mathrm{pre}} - \mathrm{P}_{\mathrm{i}}^{\mathrm{exp}}\right]^2 \rightarrow \min \qquad (3.1)$$

$$x \in R^n \qquad (3.2)$$

$$LB \leq x \leq UB \qquad (3.3)$$

where F(x) is the objective function, x is the optimisation variable set (a vector in the *n*-dimensional space, R^{n}), which for this specific case contains the full set of the material constants in the model.

$$x = \left[material\ proeprites\ (E, \nu, \sigma_y, n \ldots)\right]^T \qquad (3.4)$$

LB and *UB* are the lower and upper boundaries of x allowed during the optimisation. $\mathrm{P}(x)_{\mathrm{i}}^{\mathrm{pre}}$ and $\mathrm{P}_{\mathrm{i}}^{\mathrm{exp}}$ are the predicted total force and the (experimental) force from target data, respectively, at a specific position *i*, within the loops. N is the total number of points used in the measured load-displacement loop. Arbitrary values of material properties have been

chosen as initial values and the proposed optimisation algorithm has been used to find the optimised values of material parameters from which the best fit between the experimental and predicted loading-unloading curve can be achieved. Since the optimisation algorithm is based on curve fitting, generating the 'predicted' loading-unloading curves is one of the essential requirements to fit the experimental ('target') loading-unloading curves. The schematic diagram of the optimisation approach is shown in **Figure 3.3**.

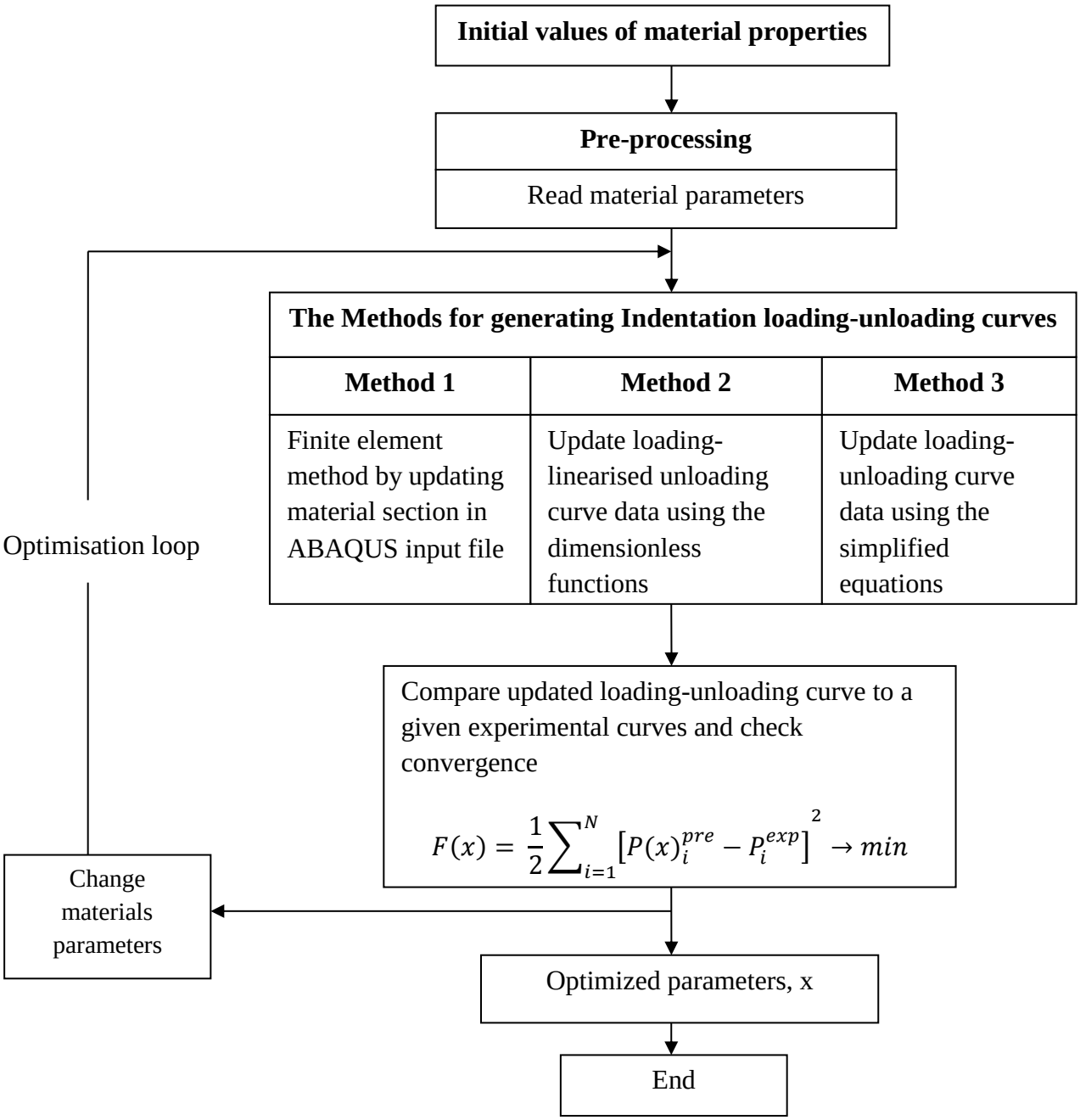

Figure 3.3 Schematic diagram of optimisation approach

Three different methods can be used to generate the indentation loading-unloading curves. 'Method 1' uses a MATLAB optimisation algorithm, with a C language EXE file for pre-processing and a python file for post-processing, with FE analysis (ABAQUS). The 'predicted' loading-unloading curves during optimisation are generated by FE analysis. In order to reduce the FE computational time during the optimisation iterations, FE simulations are only used to construct the dimensional functions in 'Method 2' and the optimisation algorithm is performed with dimensional functions, which are used to generate the 'predicted' loading-unloading curve. Since the loading-unloading relationship between a given material specimen and a given indenter are known from the dimensional functions, simplified equations can be used in 'Method 3' to evaluate the material properties from loading-unloading curves and the 'predicted' loading-unloading curves are generated by simplified equations. The details of optimisation algorithms are presented in the following chapters.

3.3 Conclusions

The research approach and the development of methodology to address the current knowledge gaps have been proposed in this chapter. The fundamental indentation behaviour of an indented material is covered in **Chapter 4**, as well as estimated material properties of hardness and elastic modulus based on the well-known Olive-Pharr method. Subsequently, a combined FE analysis with an optimisation approach is used to determine the elastic-plastic properties in **Chapter 5**. A combined dimensional analysis with an optimisation approach is developed with dimensional functions in **Chapter 6**. Simplified equations are proposed in **Chapter 7** to reduce the computational FE analysis time and to avoid constructing dimensional functions. The methodology is extended to visco-plastic material properties in **Chapter 8**. The verification of the proposed methods and as an illustration of its applicability, real-experimental indentation loading-unloading curves to obtaining material properties are used in **Chapter 9**

4 Effects of indenter geometries on the prediction of material properties

4.1 Introduction

The objective of this chapter is to investigate the influence of indenter geometries on the prediction material properties based on FE simulations. Firstly, numerical indentation tests are carried out to examine the sensitivity of the FE solutions with respect to different types of substrate models. Axisymmetric and 3D indenter geometries with perfectly sharp tips are modelled. Numerical evaluations of three different practical indenter geometries, namely Berkovich, Vickers and conical indenters, are investigated. From the FE simulations, the loading-unloading curves can be obtained. From the slope of the unloading curve, the hardness and elastic modulus can be calculated using the Oliver-Pharr method. The results are compared to investigate the effects of using different indenter geometries. The distribution of the plastic strains and the effects of using different face angles of the indenters are analysed. In addition, material responses with tilted indenter angles are investigated.

4.2 Commonly Used Indenters

The displacement of a rigid indenter of a given geometry is a function of the applied force during the indentation test and the material properties of the substrate. The different face angles of pyramid- sided Vickers and three-sided Berkovich indenters are used to examine the sensitivity of the solutions to the face angles, with different types of substrates. In this study, for comparison purposes, three different types of commonly indenters are used; conical, four sided Vickers and three sided Berkovich indenters, as shown in Figure 4.1. The angle of the Berkovich indenter can be obtained as follows [7]:

$$\begin{pmatrix} 4\mathrm{h_c}\tan^2\emptyset_1 \;=\; \mathrm{A_1}\mathrm{h_c}\tan^2\emptyset_2 \\ 4\mathrm{h_c}\tan^2\emptyset_1 \;=\; \mathrm{A_2}\mathrm{h_c}\tan^2\emptyset_2 \end{pmatrix} \qquad (4.1)$$

where the values of A_1 and A_2 are $3\sqrt{3}$ and π for Berkovich and conical indenters, respectively, $h_c = (h_{max} - h_s)$ is the radius of the contact circle (for a conical indenter), $h_s = \epsilon \frac{P_{max}}{dP_u/dh \;\; at \; h_{max}}$, where h is a constant that depends on the geometry of the indenter, and

$\emptyset_1$ and $\emptyset_2$ is the face angle of indenters shown in **Table 4.1**. It shows the angles of the different types of indenters used in this study. It should be noted that the angles of the conical and Berkovich indenters are chosen to give the same projected area to depth ratio as the projected area of the Vickers indenter and it is assumed that pile-up is negligible, based on Olive-Pharr method [1]. The typical loading-unloading indentation curves are shown in **Section 2.1.**

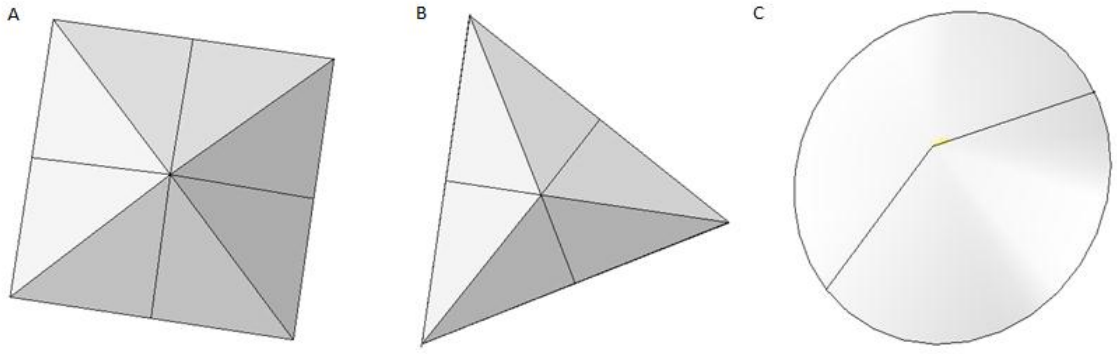

Figure 4.1. Three indenter geometries (a) Vickers; (b) Berkovich; (c) conical

Table 4.1. Indenter angles

	Conical	Vickers	Berkovich
1	68.46˚	66˚	63.09˚
2	70.29˚	68˚	65.27˚
3	72.12˚	70˚	67.46˚

4.3 Finite element modelling

4.3.1 ABAQUS Software Package

ABAQUS is a powerful engineering simulation program, based on the FE method. This commercial simulation software can be applied widely for simple linear analysis to complex nonlinear simulations. In general, two main analysis modules, 'ABAQUS-Standard' and

'ABAQUS-Explicit' are available. ABAQUS-standard can be used to solve a wide range of problems including linear and nonlinear problems, whereas ABAQUS-Explicit is especially focused on dynamic problems such as transient dynamics and quasi-static analyses using explicit time integration. ABAQUS-CAE is the ABAQUS working interface that includes CAD modelling, meshing and visualisation. In this study, ABAQUS-CAE was used for the indentation modelling which includes the creation of the geometry, FE meshing, specifying material properties, boundary conditions and applied load, running the analysis and generating post-processing data.

4.3.2 Types of Load application

There are two different methods that can be used to simulate the indentation of a specimen sample: load control and displacement control. In load control, a concentrated point force is applied on a reference point on the rigid indenter. The indenter, then moves down into the specimen and the total indenter penetration depth can be calculated by measuring the displacement of node just under the indenter. Therefore, the loading-displacement indentation curve can be generated by measuring these two quantities; applied force and the applied indenter displacement. In displacement control, the displacement of the indenter is specified as input, which is equal to the indentation depth. Then, the reaction force from the specimen, which is the summation of forces over the contact area along the penetration direction, can be measured when the indenter moves down. Both simulation methods can be used to simulate the indentation tests. Assuming elastic-plastic behaviour (Young's modulus, E = 218GPa and Yield stress, σ_y=518MPa, work-hardening exponent, n = 0.15 and Poisson's ratio, $v = 0.3$), a typical FE mesh for a rigid conical indenter is shown in **Figure 4.2**. **Figure 4.3** shows the load-displacement curves extracted using both methods for a rigid conical indenter. It can be seen that there are good agreements between the methods of load and displacement control, which indicates that either method can be used. In general, two steps are used in the indentation test; loading and unloading steps. In this study, the 'displacement control' method is employed unless otherwise specified.

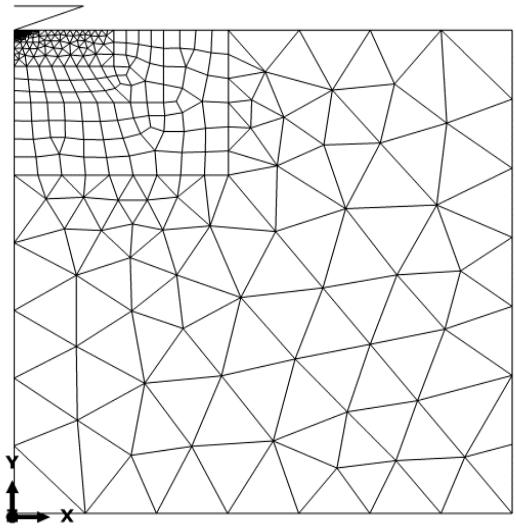

Figure 4.2 Typical FE meshes used in the indentation analysis for axisymmetric conical indenter

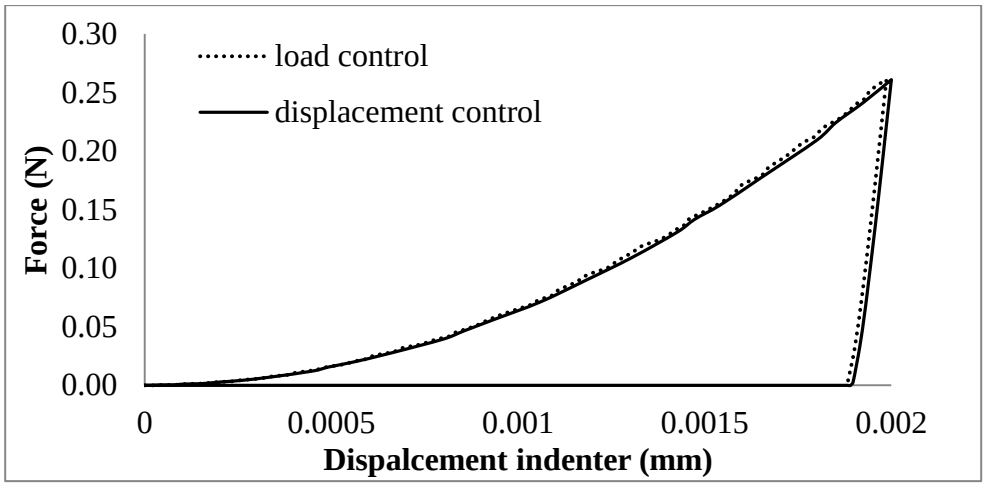

Figure 4.3 Comparison between load and displacement control for a conical indenter

4.3.3 Indenter Geometry Definition

The FE analysis of the bulk material indentation system is based on continuum elements using ABAQUS standard 6.8-3. The material is defined as an isotropic elastic-perfectly plastic material. Generally, the Berkovich pyramid indenter is widely used in indentation tests. In this work, rigid indenters with different face angles are used to examine the sensitivity of the angle of indenter. The friction coefficient at the contact surface between the indenter and the top surface of the substrate is assumed to be zero. Bucaille et al.[64] studied the influence

of the friction coefficient on the normal force in indentation as a function of the included angle, θ based on FEA. They found that the ratio $\mu/\tan\theta$ is small when high values of θ with the friction coefficient $\mu > 0$ are used. Therefore, the friction associated with the Berkovich and Vickers indenters has a negligible effect on the indentation process, whereas friction has a significant effect on the normal force measured on tips with face angles lower or equal to 50°. The indenter tip is assumed to be perfectly sharp. A "master – slave" contact scheme in FE procedure is applied on the rigid indenter and the specimen surface. The stress-strain ($\sigma - \epsilon$) relationship is shown in Eq. (2.46). The material is defined as an isotropic elastic-perfectly plastic material with E = 200 GPa, Yield stress σ_y=20 GPa, work-hardening exponent, n = 0 and Poisson's ratio, v, = 0.25, based on reference [91]. The region of interest is in the vicinity of the indenter tip where a high element density has been used due to the very high stress gradients immediately beneath the indenter tip. The indentation simulations are carried out in two distinct steps, loading and unloading. In the first step, a total indenter displacement of 0.0009mm is imposed. During loading, the rigid indenter moves downwards along the loading axis and penetrates the specimen up to the maximum specified depth. In the second step, the indenter is unloaded and taken back to its initial position.

4.4 FE Models

Details of the axisymmetric conical indenter model are discussed in **Section 3.2.1**. **Figure 4.4**(a) shows the FE mesh for this problem. The simulation is carried out in two distinct steps, a loading step and an unloading step. In the first step, a total indenter displacement was imposed. During the loading step, the rigid conical indenter is moved downwards along the axial-direction and penetrates the substrate up to the maximum specified depth. During the unloading step, the indenter is unloaded and returned to its initial position.

Three-dimensional FE models for a symmetric quarter of a Vickers indenter and a symmetric half of a Berkovich indenter are used. Symmetry surfaces are constrained to slide along the symmetry planes, and the bottom of the substrate is fully constrained. The specimens and indenters are modelled with four-node linear tetrahedron elements (C3D4 in ABAQUS) and 6-node linear triangular prism elements in the vicinity of the indenter tips (C3D6 in ABAQUS). During loading, the indenter is moved downwards to substrate in order to

penetrate the specimen surface. After the loading is released, the indenter is moved upward to the initial position. Typical FE meshes for the Vickers and Berkovich indenters are shown in **Figure 4.4** (b) and (c), respectively.

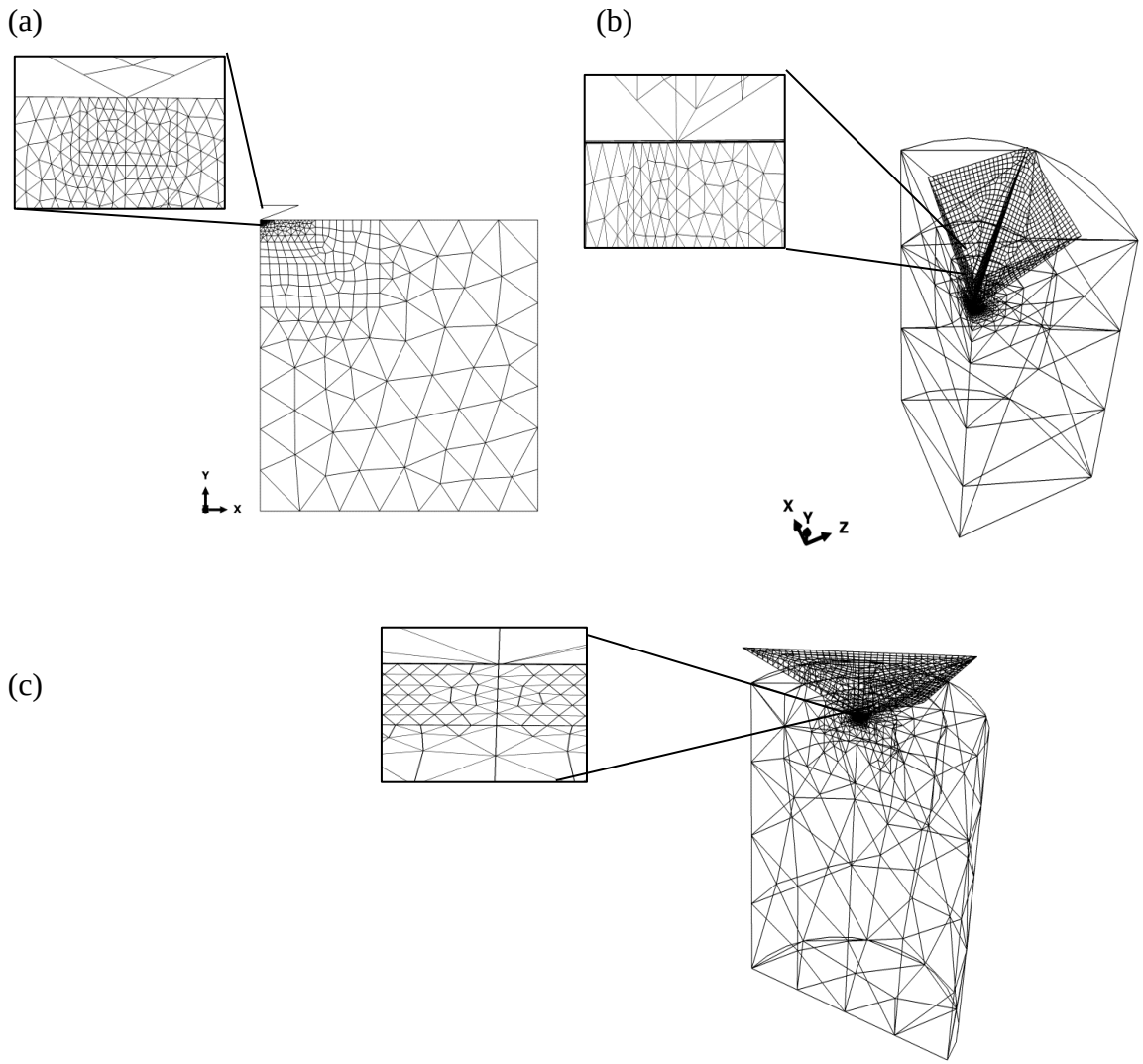

Figure 4.4. Typical FE meshes used in the indentation analysis (a) axisymmetric conical indenter (b) 3D Vickers indenter (c) 3D Berkovich indenter

4.4.1 Typical Indentation Behaviour

In this section, the loading-unloading curves obtained from different FE models of conical indenters are examined in **Figure 4.5** based on the indenter face angles given in **Table 4.1.** It should be mentioned that the FE simulation in this simulation does not consider factors such as bluntness of the indenter tip or time-dependent material behaviour. The 3D conical

indenter models are considerably more time-consuming with regard to the mesh construction as well as the FE running time when compared to the axisymmetric conical analysis. For an applied indenter displacement of 0.0009mm, all FE models of the conical indenter exhibit comparable levels of stresses and strains. For comparison purposes, the axisymmetric conical indenter model is also run as a 3D model. **Figure 4.5** shows that there are good agreements between all conical indenter models.

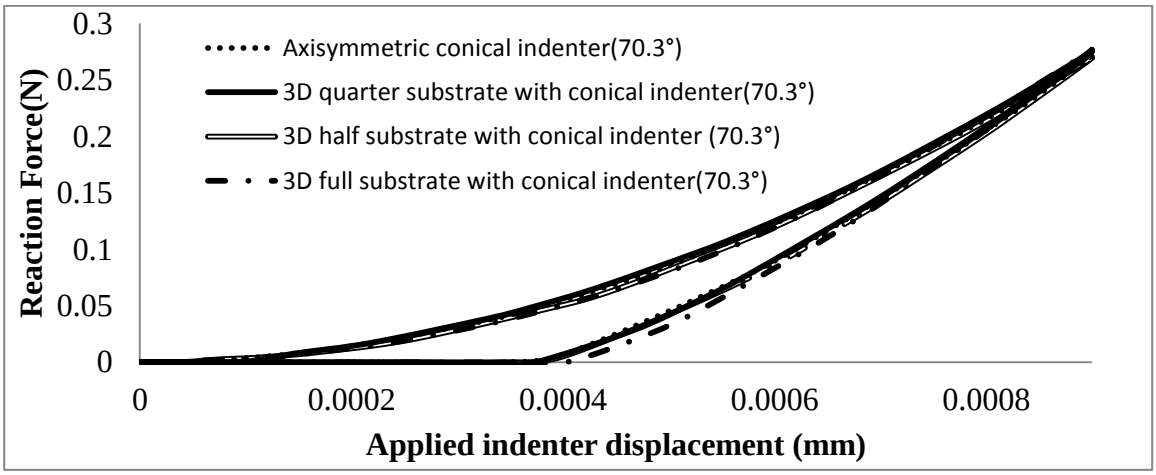

Figure 4.5 Loading-unloading curves for axisymmetric and 3D conical indenters

4.4.2 Mesh Sensitivity

In the initial simulations, an axisymmetric conical indenter and substrate with different element densities in the vicinity of the indenter tips are modelled in order to investigate the sensitivity of the FE solutions to mesh refinement. The comparison of the simulation results obtained for four different mesh densities are shown in **Figure 4.6**. The portion of loading curves with coarse meshes (Mesh size=0.001mm and 0.0005mm) clearly show some differences compared with finer meshes. The differences of the loading-unloading curves generated by using mesh sizes (0.0001mm and 0.0002mm) are negligible. Mesh size 0.00015mm in the vicinity of the indenter tip has been used for subsequent FE analyses.

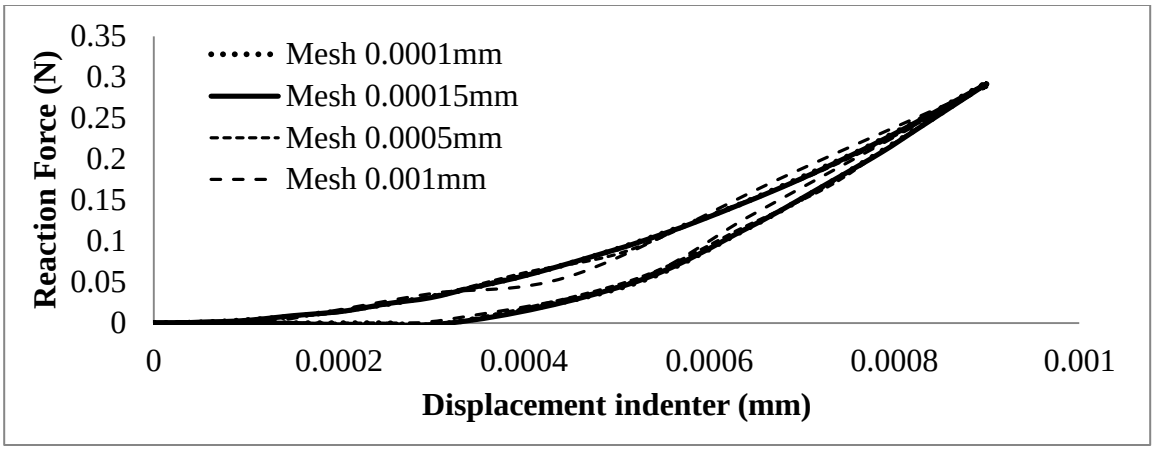

Figure 4.6 Loading-unloading curves for a conical indenter with different meshes sizes

4.5 Comparison between Different Indenter Geometries

The main objective of this section is to investigate the effects of the indenter geometry. For consistency, the same mesh refinement is used in the interest region of the 3D substrate models. From the loading-unloading curve, the slope of unloading curve can be obtained, and hardness and elastic modulus are calculated by using the Oliver-Pharr method [1]. Theoretically, three different types of indenters should generate the same reaction force from the substrate due to the fact that the same projected area to depth ratios are used, as shown in **Table 4.1.** Based on the results of the FE analysis from the substrate, it is noted that the loading- unloading curves of the conical and 3D Vickers and Berkovich indenters slightly deviate from each other when different face angles of the indenters are used, as shown in **Figure 4.7.** The peak reaction force in the axisymmetric FE model is consistently slightly lower than the 3D FE model. This may be attributed to differences in mesh refinement near the tip zone or other factors relating to the differences in stress and strain distributions under the indenter.

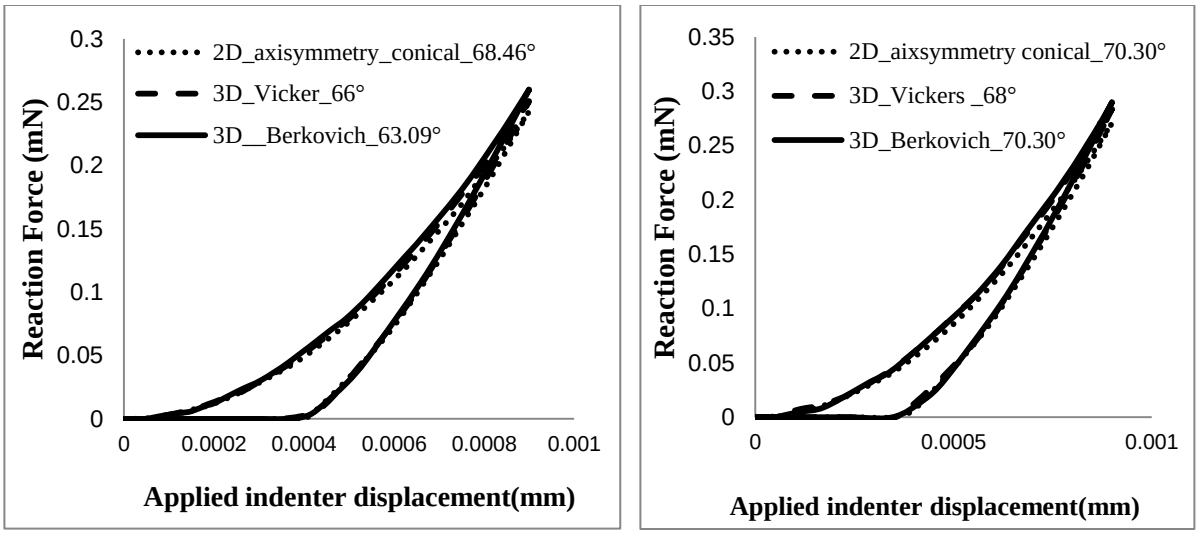

Figure 4.7 Loading-unloading curves with various indenter geometries and face angles

Table 4.2 shows a comparison of the three different indenter geometries, each with three different face angles, where the highest reaction force from the substrate always corresponds to the Berkovich indenter. It is interesting to note that conical indenters always give the lowest reaction force while the Vickers indenter load values are between them. With regard to the values of the computed (evaluated) elastic modulus, it is normalised by the input values used in the FE analysis. The ratios, E_r/E_{input} for conical indenters are always slightly lower than 1 for all indenter angles used. However, the elastic modulus is slightly overestimated with the Vickers and Berkovich indenters. This is related to the stress and strain distributions under the indenter. With regard to hardness, the 3D Vickers and Berkovich indenters always give higher values than the conical indenter due to the fact that the maximum forces are always higher than the conical indenter.

Therefore, although the maximum displacement of the indenter is controlled as 0.009mm, the calculated material parameters are slightly different, depending on the type of indenter used. Furthermore, the contact depths, h_c, are generally in good agreement. It should be noted that the projected areas of the three different types of indenters are similar. These differences are explored in more depth, by comparing the contours of the equivalent plastic stain at the maximum indentation, h_{max}. **Figure 4.8** shows the plastic strain distribution for the maximum force from the FE simulation. The maximum plastic strain regions are located at the surface in the tip of the indentation for conical, Vickers and Berkovich indenters. **Table**

4.2 shows that the plastic strains are larger for the Vickers and Berkovich indenters, for all indenters used. These differences are the main reasons why the loading-unloading curves are not identical. Therefore, the plastic strain differences between the conical axisymmetric indenter and 3D Vickers and Berkovich indenters are sufficient to cause the small differences between the load-displacement behaviour.

Figure 4.8 Equivalent plastic strain distribution obtained at the maximum load with different indenter

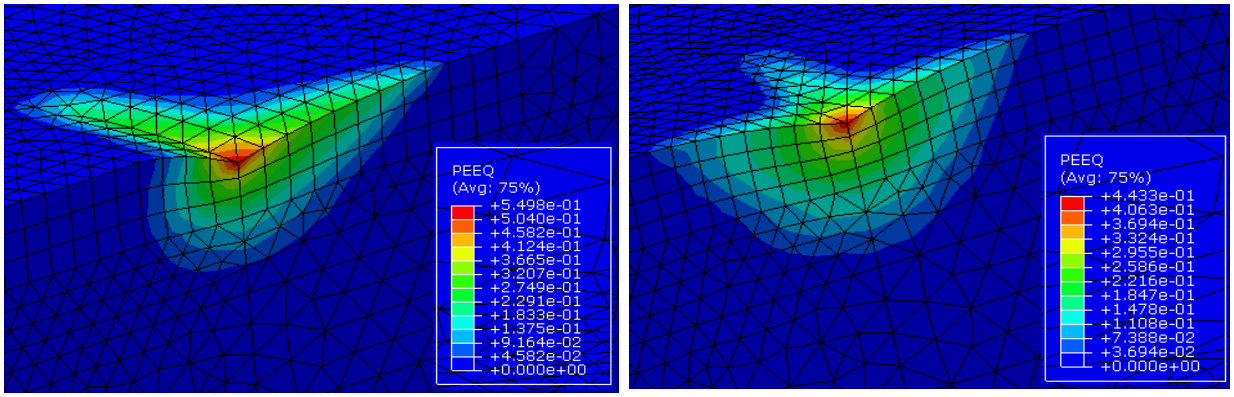

3D half substrate with Berkovich indenter 3D half substrate with Vickers indenter

Table 4.2 FE solutions for the substrate with three different types of indenters

Indenter	Angles	Elastic moduli (GPa)	*Hardness (GPa)	Max Force (mN)	**Er/Einput	hc/hmax	Equivalent Plastic strain
Axisymmetric	68.46	200.21	31.397	0.2428	1.001	0.6878	0.5128
	70.29	198.37	29.979	0.2709	0.992	0.6748	0.4276
Conical	72.12	194.44	28.597	0.3024	0.972	0.6576	0.3524
3D-Vickers	66	207.19	31.926	0.2530	1.036	0.6964	0.5475
	68	206.49	31.596	0.2796	1.032	0.6678	0.5209
	70	205.36	30.69	0.3167	1.027	0.6496	0.4214
3D-Berkovich	63.09	214.52	33.418	0.2599	1.073	0.6897	0.6850
	65.27	212.339	31.999	0.2901	1.062	0.6759	0.5033
	67.47	207.633	30.448	0.32318	1.038	0.6587	0.4749

*Hardness $= M$aximum applied force$/C$ontact area of the indentation

**E_r/E_{input} =Elastic modulus obtained by Oliver-Pharr method$/200$ GPa

4.6 Sensitivity of Indenter Face Angle

In order to examine the differences between the behaviour of the three different face angles, the elastic modulus, hardness and equivalent plastic strains are obtained from FE analysis, see **Table 4.2**. **Figure 4.9** shows the loading-unloading curves for Vickers and Berkovich indenter, where slight differences in the curves are observed and sharper indenters (i.e. indenters with smaller face angles,∅) produce slightly lower forces. This implies that the projected area of the indenter should be increased as the face angle increases. For a low angle indenter (e.g. 66°), the amount of elastic recovery is greater than for a larger angle of indenter (e.g. 70°).

Despite having identical material properties and the same applied maximum displacement (0.0009mm), an indenter with a higher face angle (e.g. 70°) results in higher loads, due to the fact that it displaces more volume and thereby produces greater local stresses. This is because the contact area between the indenter and the bulk material increases as the face angle increases**. Figure 4.10 (**a**)** shows the variation of the ratio of h_c/h_{max} with the indenter face angle, which shows that the lowest face angles lead to higher h_c/h_{max} ratios. The differences between the highest and the lowest ratio h_c/h_{max} with different indenters are about 2%. **Figure 4.10** (b) shows that the ratio E_r/E_{input} remains close to 1 (±3%) for the axisymmetric conical indenters. Both 3D Vickers and Berkovich indenters show that a slight increase in the indenter face angles can slightly decrease the elastic modulus, where the ratio E_r/E_{Input} remains close to 1, ±3.5% and ±6.8%, respectively. **Figure 4.10** (c) shows the equivalent plastic strain plotted against E_r/E_{Input}, where the equivalent plastic strain generally decreases as the tip angle increases. The maximum plastic strain is higher for a low angle indenter due to the fact that the plastic strain region penetrates deeper into the substrate.

With respect to hardness, **Table 4.2** shows that hardness remains close to 30 GPa (±5%), except for the case of the Berkovich indenter with an indenter angle of 63.09° (+11%). **Figure 4.10** (d) shows the variation of the normalised ratio $P_{max}/(A_{projected} \times \sigma_y)$ with the face angle, where it is shown that the ratio is high when the face angle is low. This is also shown in **Table 4.2** where the lower face angles always result in the lowest forces.

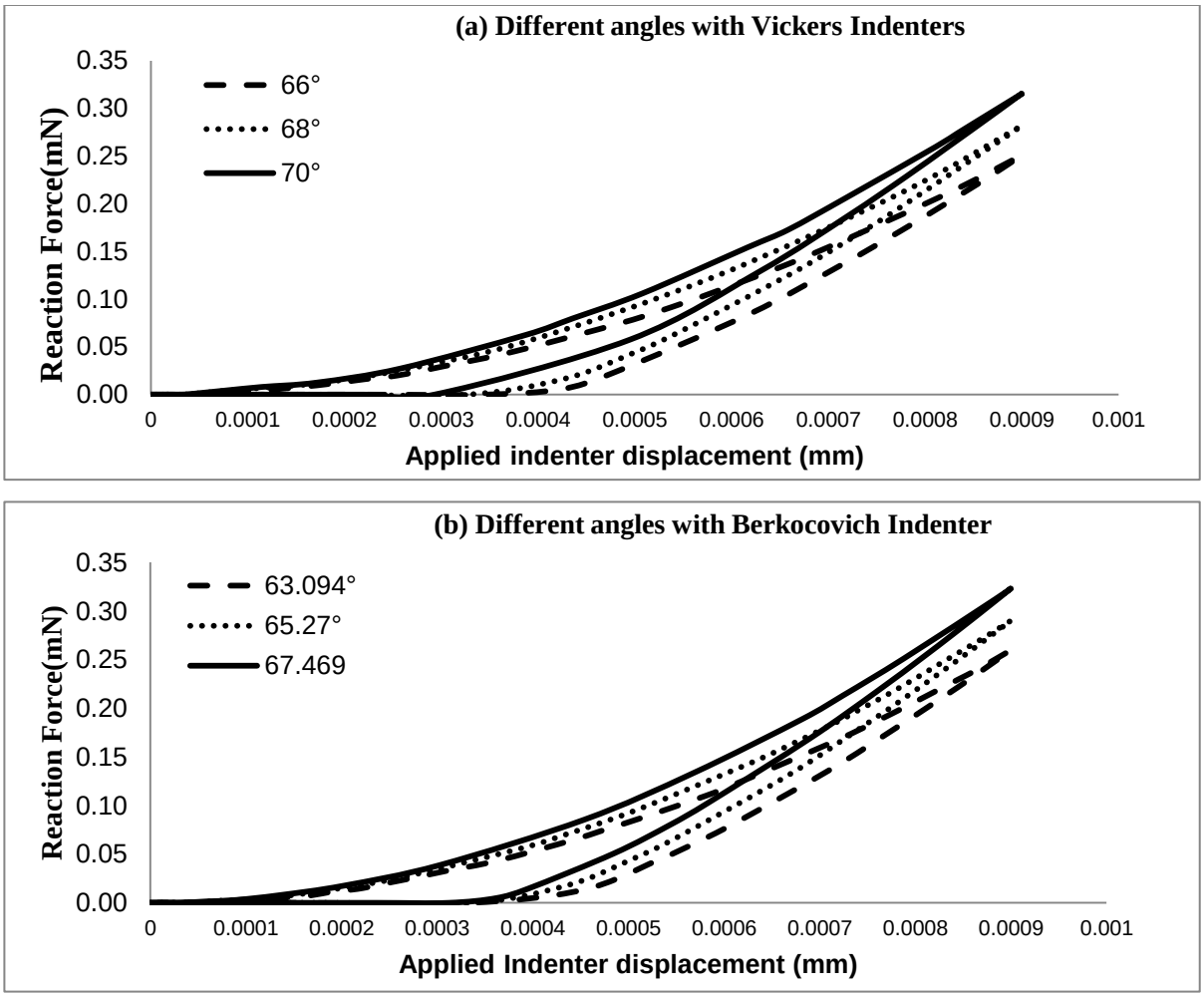

Figure 4.9 Loading-unloading curves with different face angles (a) Vickers (b) Berkovich indenter.

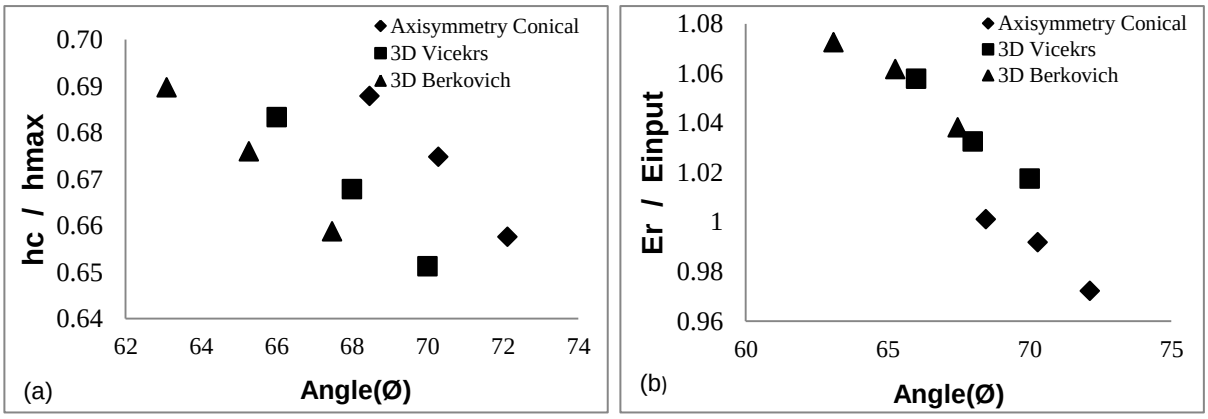

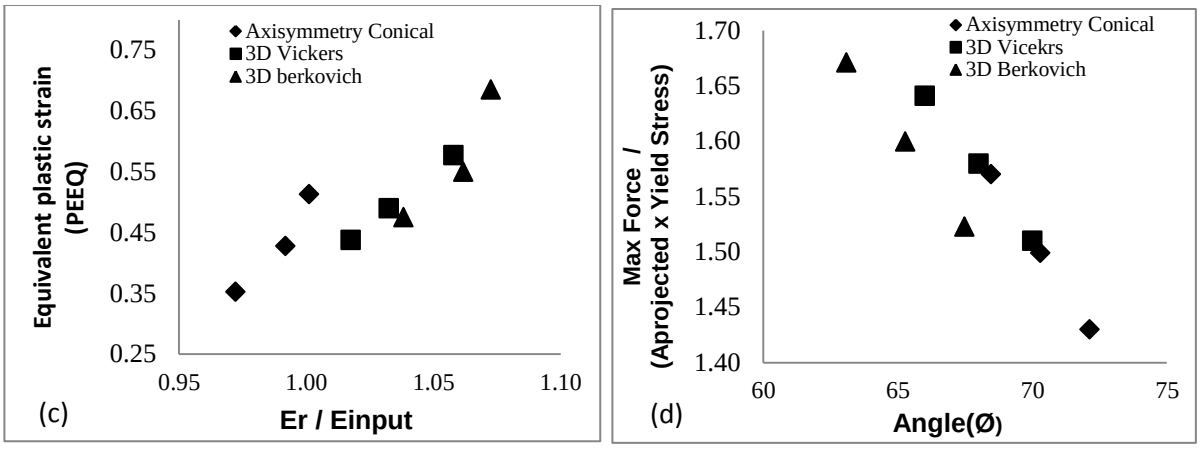

Figure 4.10 Effects of changing indenter face angles (a) Change of normalized depth of residual indenter with indenter face angles ; (b) Change of evaluated elastic modulus/ input elastic modulus with indenter face angles ; (c) Change of equivalent plastic strain obtained at the maximum reaction force with elastic modulus ratio, E_r / E_{input} ; (d) Change of $P_{max}/(A_{projected} \times \sigma_{y)}$with indenter face angles

4.7 Tilted angle of indenters

4.7.1 Problem definition

In real micro or nano-indentation experimental tests, the specimen may not be perfectly aligned with the indenter, which may result in a 'tilt' angle between the indenter and the specimen. Therefore, the influence of the tilt angle of the indenter is investigated based on FE simulations.

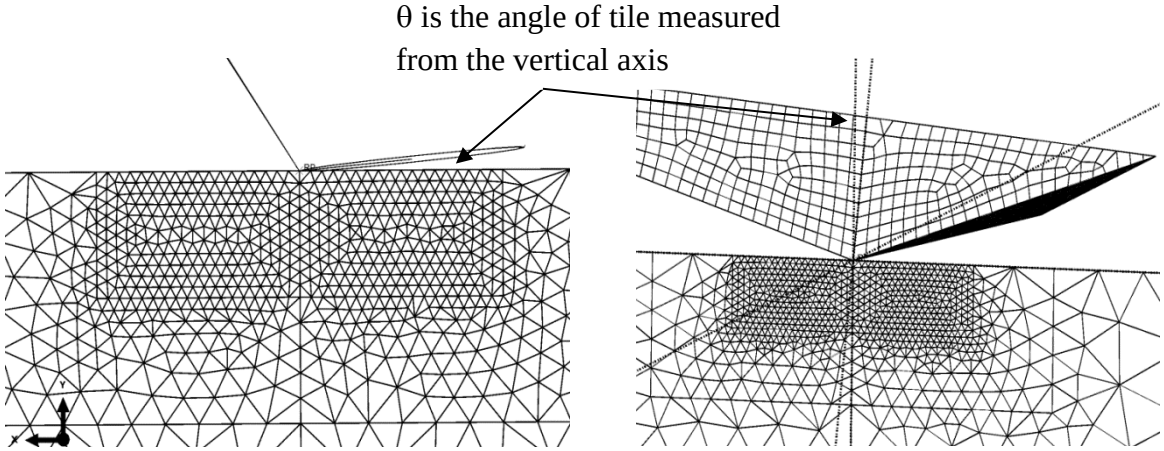

Figure 4.11 Typical FE meshes used in the geometry of the titled flat ended indenter and Berkovich indenter

Figure 4.11 shows the geometry of the titled indenter where θ is the angle of tile measured from the vertical axis. The details of the FE analysis based on a 3D model are covered in **Section 4.4**. A P91 steel homogeneous elastic-plastic specimen with strain hardening is modelled as a half-three-dimensional model. The dimensions of the specimen are 5mm x 5mm x 3mm (height x length x width). A tilted indenter is introduced with displacement control (0.002mm) by rotating the half geometry around the y-direction by an angle of 0° to 5°. The material of the specimen is defined as an isotropic elastic-plastic material, E = 210GPa, Yield stress, σ_y= 550MPa, Poisson's ratio, $\nu = 0.3$ and work-hardening exponent, n = 0.11.

4.7.2 Influence of tilted indenter on load-applied displacement curves

The loading-unloading indentation curve is obtained by recording the reaction force and the corresponding applied displacement. **Figure 4.12** shows the influence of the tilted indenter on the loading-unloading curves for the conical, Berkovich and Vickers indenters. For consistency, the same mesh refinement shown in **Figure 4.11** is used in the interest region of the 3D-half specimen model with displacement control. As can be seen from **Figure 4.12** (a), (b) and (c), the highest reaction force increases with the increase in the tilted indenter angle of indenter due to the fact that a larger force and larger contract area are required to penetrate the specimen to the same maximum depth. It is noted that the maximum reaction force increases by 4%, 11%, and 7% for the conical, Berkovich and Vickers indenters, respectively, compared to the no-tilt reaction force.

(a) Conical indenter

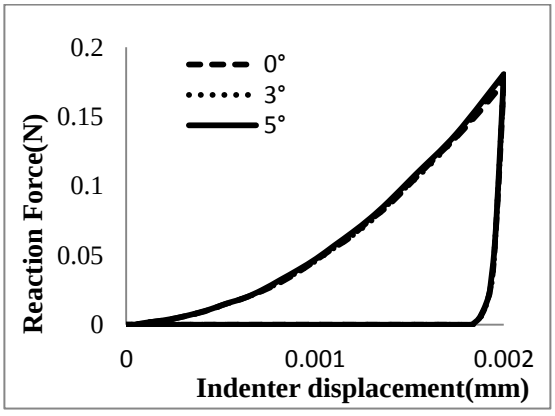

(b) Berkovich indenter

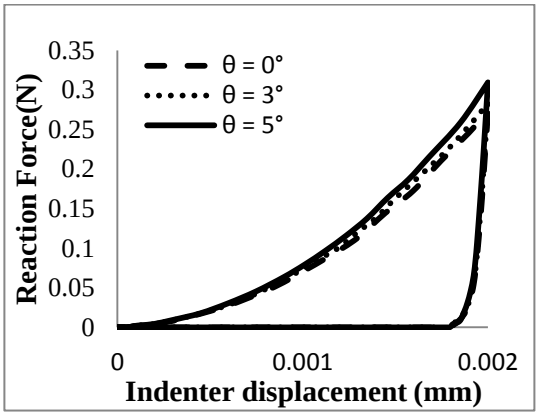

(c) Vickers indenter (d) Flat ended indenter

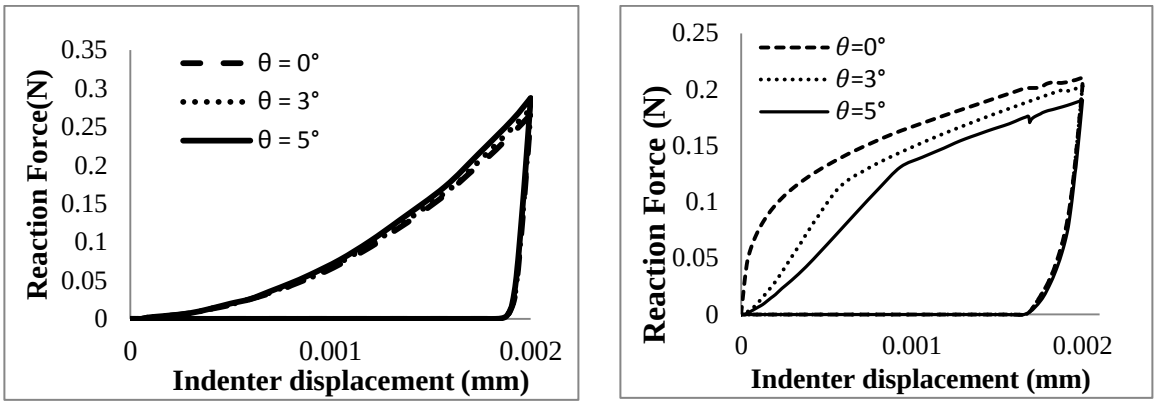

Figure 4.12 Influence of tilted indenter on loading-unloading curves of indentation. (a) Conical indenter (b) Berkovich indenter (c) Vickers indenter (d) Flat-ended 60° cone indenter with force control

It can be clearly seen that the loading part of the curves in **Figure 4.12** (a), (b) and (c) deviate noticeably as the indenter depth increases, whereas in the unloading part of the curves, the deviations are relatively small. This indicates that the elastic recovery during the unloading process is not sensitive to the tilt angle. As can be seen from **Figure 4.12** (d), the behaviour of the loading-unloading curves with tilted flat indenters is very sensitive to the tilt angle due to the fact that the tip of indenter becomes a sharp wedge as the tilt angle increases. It is also interesting to note that the highest reaction force increases with the decrease in the tilt angle. This is due to that a larger contract area of the flat ended tip which leads to a large force needed to penetrate the specimen to the same maximum depth. **Figure 4.13** shows a comparison of the residual von-Mises stress distributions after removing the indenter for tilt angles 0° and 5° for four different types of indenters, where it can be observed that the residual stress field is very different when the tilt angle increases to 5°. **Figure 4.14** shows a comparison of the residual equivalent plastic strains after removing the indenter for tilt angle 0° and 5° for four different types of indenters. It is interesting to observe that the equivalent plastic strains with a tilt angle of 5° for the three indenters are slightly lower than the no-tilt situations, except for the flat ended 60° conical indenter, where more plastic deformations occur due to the sharp edge of flat-ended indenter.

Conical indenter without tilt		Conical indenter for tilt 5°
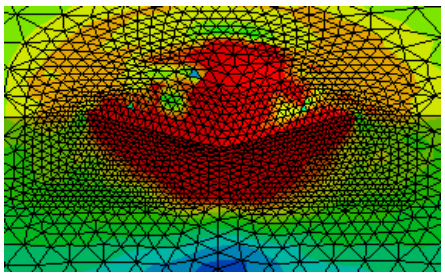	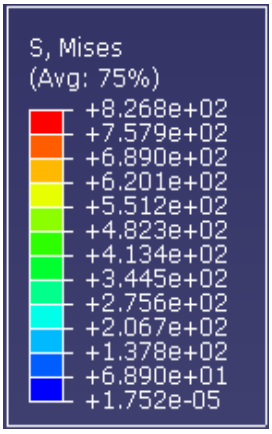	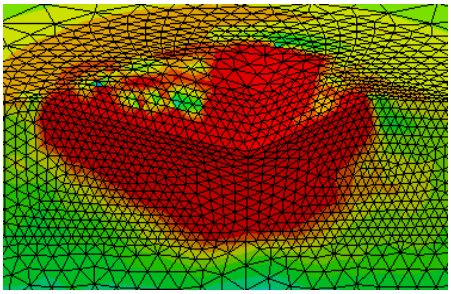
Berkovich indenter without tilt		Berkovich indenter for tilt 5°
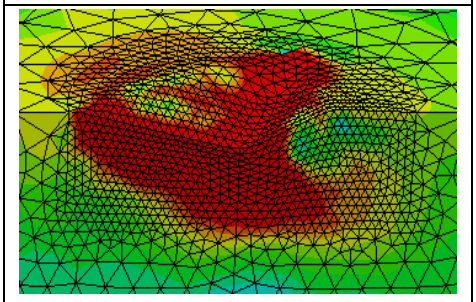		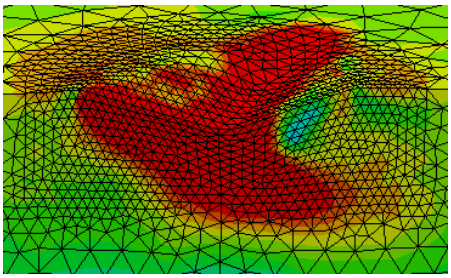
Vickers indenter without tilt		Vickers indenter for tilt 5°
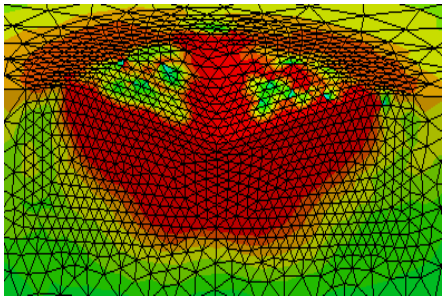		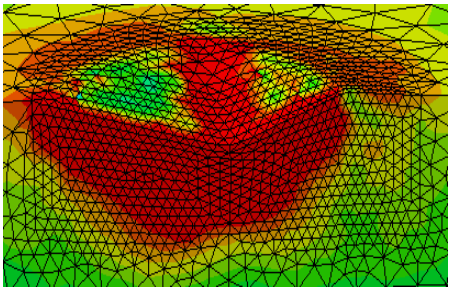
Flat ended 60° cone indenter without tilt	Von Mises stress distribution after indenter removed	Flat ended 60° cone indenter for tilt 5°
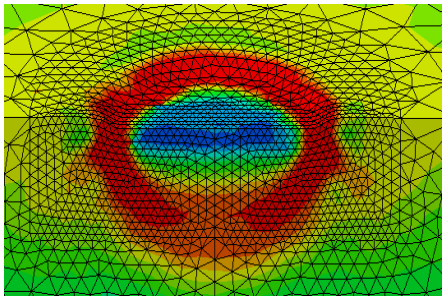		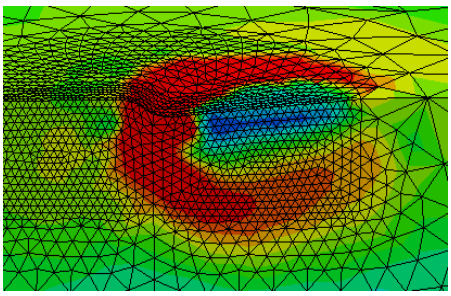

Figure 4.13 Von Mises stress distribution after indenter removed in MPa

Conical indenter without tilt	Conical indenter for tilt 5°
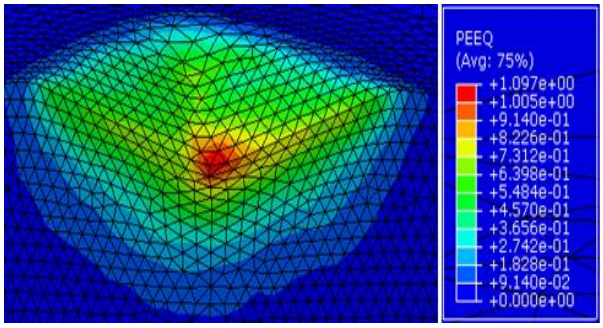	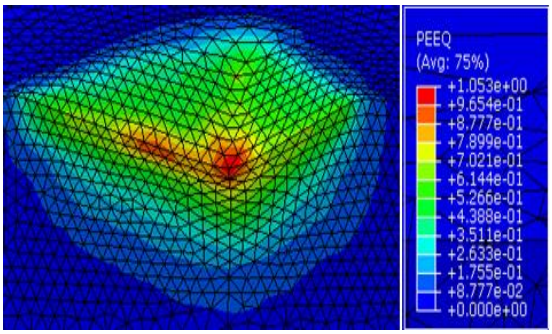
Berkovich indenter without tilt	Berkovich indenter for tilt 5°
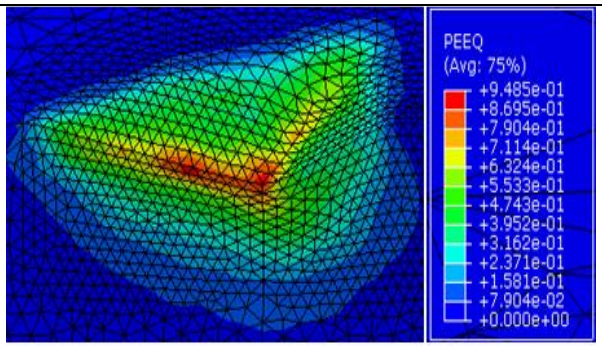	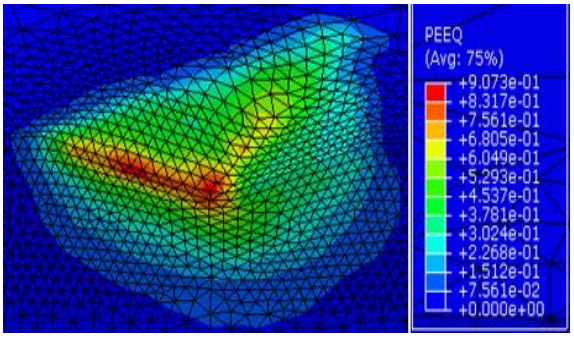
Vickers indenter without tilt	Vickers indenter for tilt 5°
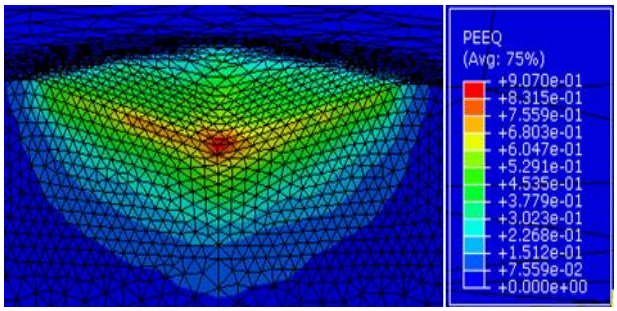	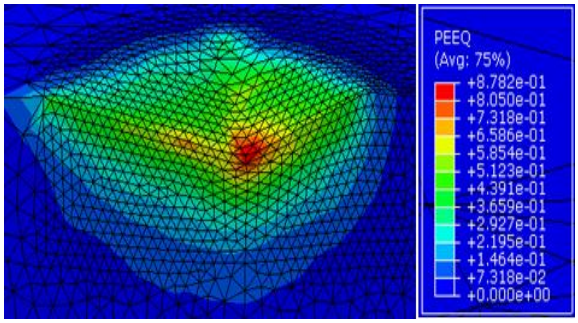
Flat ended 60° cone indenter without tilt	Flat ended 60° cone indenter for tilt 5°
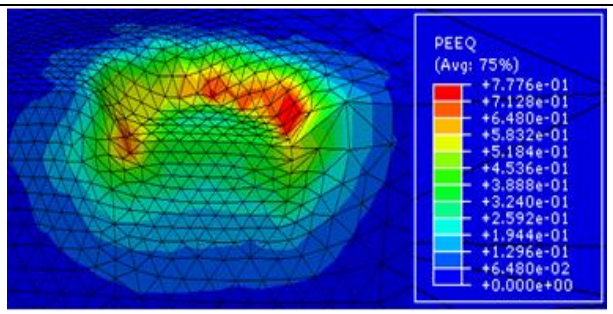	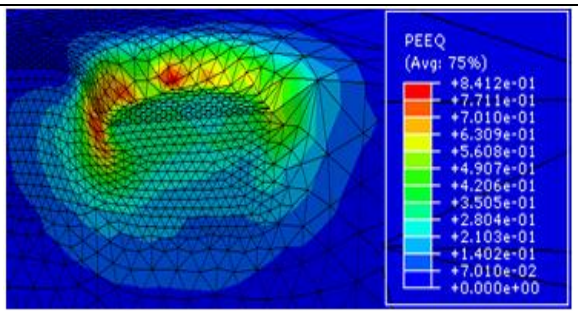

Figure 4.14 Equivalent plastic strain field after indenter removal.

4.8 Conclusions

In this study, the influences of the indenter face angles and indenter geometries are analysed. Generally, the relationships between the applied indenter displacement and the reaction force with axisymmetric and 3D models are in good agreement. A 3D symmetric quarter of the Vickers indenter is used, whereas a 3D symmetric half of the Berkovich indenter is used. The effect of the indenter geometry is investigated with conical, Berkovich and Vickers indenters. Despite having identical material properties and identical maximum applied displacements, there are some differences between the loading-unloading curves obtained from the FE simulations. The predicted elastic modulus for the Berkovich and Vickers indenters is always slightly overestimated, about 3~5% higher than conical indenters. This fact indicates that the indenter geometry affects the predictions of the elastic modulus and hardness. To explore this in more depth, analysis of the residual plastic strain shows that the Berkovich indenter results in about 25% higher values than the other indenters. Therefore, it can be concluded that differences between these indenters exist and caution is needed when the equivalent axisymmetric indenter is used for simplicity. FE analyses for indentations with different indenter face angles show that some differences exist in the loading-unloading curves. Generally, a high face angle can produce up to 20% higher force. In addition, the normalised ratios of E_r/E_{input}, h_c/h_{max} and $P_{max}/(A_{projected} \times \sigma_y)$ always decrease when the face angle of the indenter is increased. For the residual plastic strain, the Berkovich indenter always results in higher values than the Vickers and conical indenters. Therefore, the calculated elastic modulus and hardness are influenced by the face angle of the indenter. Further investigation is needed to compare the FE results with experimental indentation test data and to establish the potential influence of friction and work hardening using different indenter geometries. The influence of misalignment of the indenter has been investigated by changing the indenter tilt angle. In general, the contact surfaces between the indenter and the specimen increase as the tilt angle increases. Further investigation is needed using instrumented indentation loading-unloading curves.

5 Determining Elastic-Plastic Properties from Indentation Data obtained from Finite Element Simulations and Experimental Results

5.1 Introduction

In **Chapter 4**, the influence of indenter geometry on the determination of material properties are investigated using FE analysis based on the Olive-Pharr method, which is mainly focused on obtaining the elastic modulus and hardness indirectly based on the loading-unloading curve. In recent years, research efforts [48, 64, 74, 81, 92-101] have been focused on extracting elastic-plastic material properties directly; Young's modulus (E), yield stress (σ_y) and work hardening exponent (n), by using indentation data in which a power law hardening is generally used to characterise these material parameters. In previous work, the determination of three properties (E, σ_y and n) and two properties (σ_y and n) [94-96 and 101] have been investigated. In this chapter, four elastic-plastic parameter (E, σ_y, n and Poisson's ratio ν) are extracted, for the first time, in a non-linear optimisation approach, fully integrated with FE analysis, using results from a single indentation curve.

Obtaining a unique set of material properties of a power-law material from a single indentation test has proved to be difficult. Consequently, some researchers [64, 94, 96 and 100] used load-displacement curves obtained from more than one indenter geometry (dual indenters) in order to obtain a unique set of material constants. It has been shown that decreasing the indenter angle, i.e. using sharper tip geometry, improves the accuracy of estimation of the mechanical properties [94]. In many approaches, researchers have used a 'simulated' target FE load-displacement curve, as opposed to real-life experimental indentation test data which always contain a certain amount of scatter. Therefore, improved computational approaches based on FE analysis are needed to extract unique and accurate mechanical properties of power law materials from loading-unloading curves. The main objective of this chapter is to introduce a robust and accurate optimisation method for extracting four elastic-plastic mechanical properties (E , σ_y, n and ν) from a given indentation load-displacement curve using only a single indenter. A non-linear MATLAB optimisation algorithm is fully integrated with a commercial FE code, ABAQUS. The new approach is

shown to be accurate and convergent despite using different initial 'guess' values of the material constants, and effective for various common geometries of indenters such as Berkovich, Vickers and conical indenters. Another objective of this study is to examine the effectiveness and accuracy of the optimisation techniques when the target indentation loading-unloading data comes from a real-life experimental indentation curve with random errors, rather than from a simulated FE indentation analysis.

5.2 An Optimisation Procedure for Determining Material Properties

5.2.1 Optimisation Procedure

The optimisation model has been mentioned in the **Section 3.2.2** and the general optimisation algorithm used in this work is illustrated in **Figure 5.1**. Since the initial guess values for (E, ν, σ_y, n) are provided, the optimisation procedure is carried out in several steps with MATLAB, which controls a C language EXE file to automatically generate an ABAQUS input file, run ABAQUS and a Python script to automatically extract the load history from the resulting ABAQUS output file. The MATLAB code is listed in **Appendix 1**. In terms of pre-processing the FE analysis, the material properties in the ABAQUS input file are replaced by new elastic-plastic material properties. Some practical physical constraints have been imposed during the analysis since Poisson's ratio and the work-hardening exponent values for most engineering materials are between 0.0 and 0.5. The boundaries for *E* can be chosen to be between 10 and 600 GPa and σ_y between 10 MPa and 2 GPa [102]. However, in this study, no upper limits have been imposed on the values of Young's modulus and yield stress values in order to cover a wide range of possible engineering materials, i.e.

$$\begin{Bmatrix} E > 0; & 0 < \nu < 0.5 \\ \sigma_y > 0; & 0 < n < 0.5 \end{Bmatrix} \tag{5.1}$$

In ABAQUS, the elastic-plastic material data is specified as Young's modulus, Poisson's ratio, and discrete points on the post yielding true stress-true strain curve. In this study, a power law strain hardening curve has been used to simulate the indentation experiments. The stress-strain ($\sigma - \epsilon$) relationship [102] is assumed to be

$$\sigma = \begin{Bmatrix} E\varepsilon \; for \; \varepsilon \leq \frac{\sigma_y}{E} \\ K\varepsilon^n for \; \varepsilon > \frac{\sigma_y}{E} \end{Bmatrix} \tag{5.2}$$

The decomposition of the strain into elastic and plastic parts is given by

$$\varepsilon_{\text{total}} = \varepsilon_{\text{el}} + \varepsilon_{\text{pl}} \quad (5.3)$$

Since all plastic strains should be input as true strains in ABAQUS, the stress equation can be written as

$$\sigma = K(\frac{\sigma_y}{E} + \varepsilon_{pl})^n \quad (5.4)$$

The coefficient K is given by

$$K = E^n \sigma_y^{1-n} \quad (5.5)$$

In the ABAQUS input file, a discrete set of points is required to represent the uniaxial stress-strain data, rather than specifying the work-hardening exponent n. Therefore, a fixed set of plastic strain values of 0.02, 0.04, 0.08, 0.12, 0.142, 0.172, 0.202, 0.232 and 0.262 are used, in order to specify the plastic stress-strain data in ABAQUS. The coefficient K can be calculated by using Eq. (5.5) and the updated stress data related to these strains can be obtained by Eq. (5.4). It is worth noting that when the last plastic strain value of 26.2% is reached, ABAQUS assumes no further work hardening beyond this point. Since the sharp tip of indenter is discontinuous, a stress singularity occurs at the tip, with extremely high stresses generated at this point. This singularity effect is very localised around the sharp tip, and further tests have shown that the effect of increasing the value of the plastic strain beyond 0.262 on the loading-unloading curve is negligible.

This procedure can be performed by a C language code to calculate the values of K and to replace the current material properties in the ABAQUS input file by the new calculated material properties. This pre-processing procedure is important to determine the material properties of power-law material uniquely. In terms of post-processing, the load history results, extracted by a Python script, are read by a MATLAB program and the objective function calculated. All the procedures are processed automatically until convergence is reached.

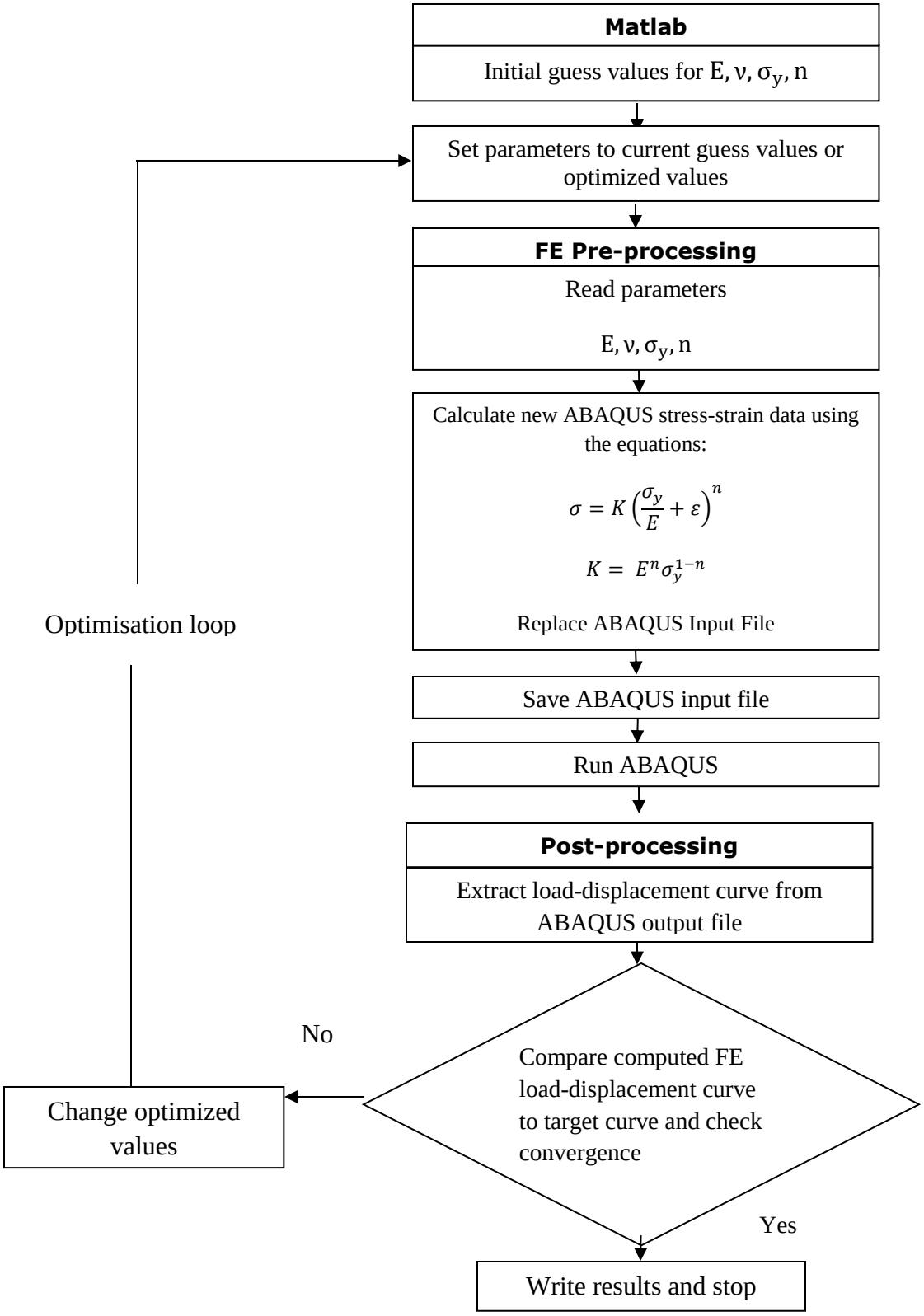

Figure 5.1 Flow chart of the optimisation algorithm to determine the mechanical properties from the load-displacement curves

5.3 Finite Element Indentation Modelling

The details of the FE analysis based on an axisymmetric conical indenter are covered in **Section 3.2.1**. For shallow indentation depths, the size effects in the real-life experimental indentation tests can affect the accuracy of the simulations [103]. It should be noted that the FE simulations do not model the indentation size effects and are therefore limited to simulating macro indentations. The depth of the bulk material is 0.1mm and the maximum displacement of the indenter is 0.0009mm. The simulation is carried out in three distinct steps, a loading step and two different unloading steps. In the first step, a total indenter displacement of 0.0009mm is imposed. During the loading step, the rigid cone indenter moves downwards along the z-direction and penetrates the foundation up to the maximum specified depth. In the second and third steps, the indenter moves upwards in two stages, at 10% of the peak displacement of indenter and then taken back to the initial position, respectively. In the first unloading step, significant nonlinearity occurs which requires very small load increments. In the second unloading step, contact between the indenter and substrate is removed, and larger load increments can be used. [89]

5.3.1 Three-Dimensional Vickers and Berkovich Models

For comparison and validation of the optimisation technique, 3D quarter-symmetry FE models for the conical and Vickers indenters are also used, which are presented in **Figure 5.2**(b) and **Figure 5.2** (c). A half-symmetry FE model for the Berkovich indenter is used in **Figure 5.2** (d). In addition to the symmetry constraints on the symmetry planes, the bottom of the specimen is fully constrained. The specimens are modelled as three-dimensional geometries with a high element density of four-node linear tetrahedron continuum elements (C3D4 in ABAQUS). For the three different types of rigid indenters, a four-node 3-D bilinear rigid quadrilateral continuum element (R3D4 in ABAQUS) is utilized. The loading and unloading procedures are the same as in the axisymmetric model.

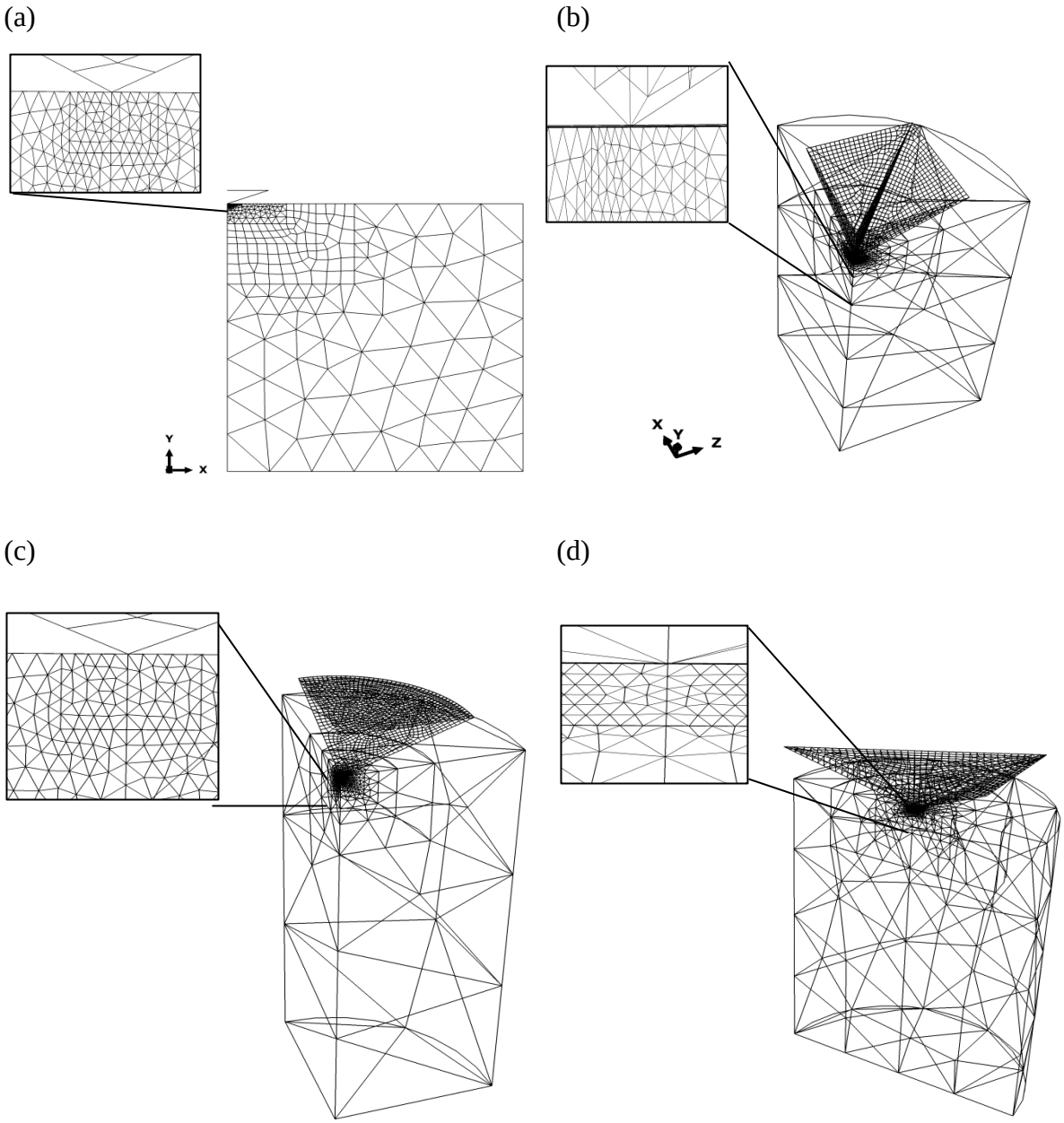

Figure 5.2 The FE meshes: (a) Axisymmetric conical indenter (b) 3D Vickers indenter (c) 3D conical indenter (d) 3D Berkovich indenter

5.3.2 Effect of elastic-plastic properties on the loading-unloading curves

The effect of elastic-plastic properties on the loading-unloading behaviour is examined by changing some material constants and plotting the resulting load-displacement curves for an axisymmetric conical indenter, as shown in **Figure 5.3**. During this process, all others parameter are fixed at their target values. Two cases are investigated; (a) the effect of

Poisson's ratio and (b) the effect of the work-hardening exponent n. As can be seen from **Figure 5.3** (a), a larger Poisson's ratio results in a slightly higher force for the same value of h. However, the load-displacement curves are almost identical. On the other hand, it is obvious from **Figure 5.3** (b) that the force at the maximum indentation load increases with the increasing value of n. It can be said that a larger work-hardening exponent corresponds to a higher stress for a given strain and this can have a significant effect on the load-displacement behaviour.

(a) Effect of Poisson's ratio (b) Effect of Strain hardening

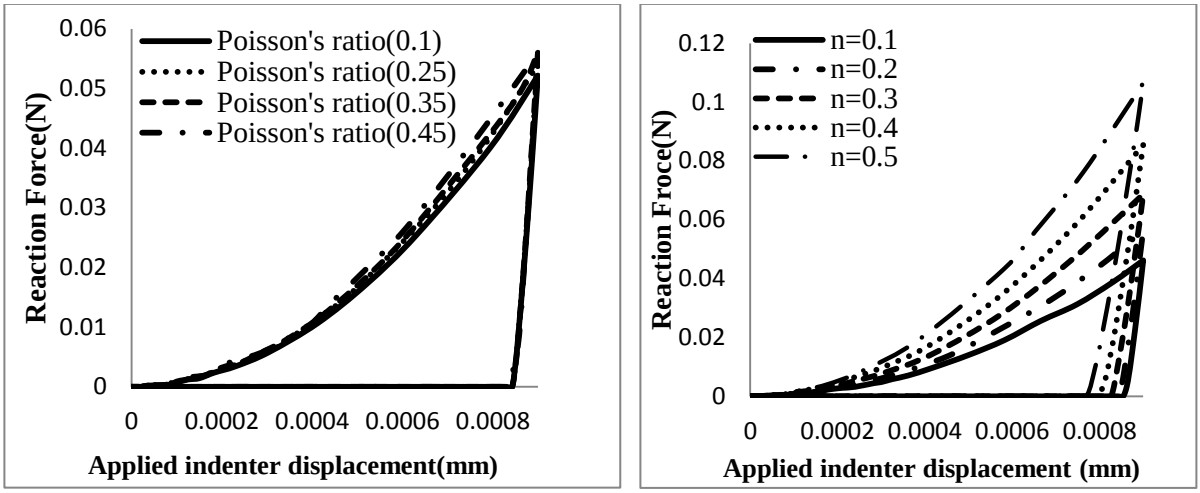

Figure 5.3 Loading-unloading curves for an axisymmetric conical indenter (a) Effect of Poisson's ratio (b) Effect of strain hardening

5.4 Optimisation using a target curve obtained from a FE simulation

5.4.1 Optimisation using an axisymmetric conical indenter analysis

The proposed optimisation algorithm is tested using a single conical indenter. Firstly, a set of material properties are chosen as the target values and FE analyses are performed to obtain a simulated target load-displacement curve (using the target material properties), as shown in **Figure 5.4**. A set of initial 'guess' material parameters are then chosen and implemented in the MATLAB optimisation algorithm which automatically performs a new ABAQUS run for each iteration.

The optimisation results are summarised in **Table 5.1** where the sensitivity of the proposed algorithm is demonstrated by changing two parameters at a time. During this process, all other parameters are fixed at their target values. Various ranges of initial values have been used. Generally, the optimised results are obtained in about 8-12 iterations with a deviation of less than about 1% from the target values. In order to ensure that the stresses are practically independent of element size, mesh sensitivity studies have been carried out, see **Section 5.4.4**.

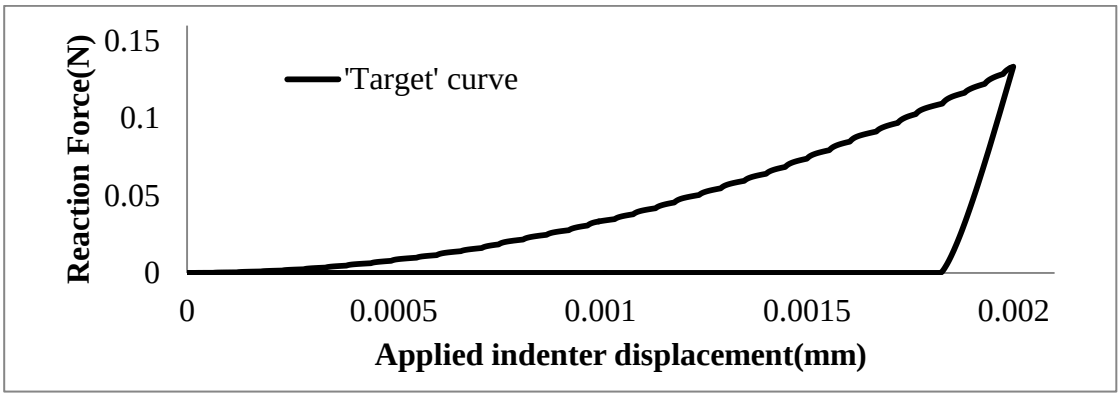

Figure 5.4 Target loading-unloading curve obtained from a FE simulation of an axisymmetric conical indenter

Table 5.1 Two-parameter optimisation for axisymmetric conical indenter

Test	Parameter	Target	Initial values	Boundaries	Final Optimised values	Percentage[a] error(%)	Iterations
1	E(MPa)	1.34E+05	1.00E+03	E >0	1.340E+05	4.78E-04	8
	σ_y(MPa)	3.00E+02	1.00E+03	σ_y> 0	3.000E+02	2.33E-05	
2	E(MPa)	1.34E+05	3.00E+05	E >0	1.340E+05	1.28E-03	11
	v	2.50E-01	1.00E-01	v > 0	2.501E-01	2.98E-02	
3	σ_y(MPa)	3.00E+02	1.00E+03	σ_y> 0	3.000E+02	3.97E-03	10
	n	1.00E-01	4.00E-01	n > 0	1.000E-01	1.28E-02	
4	E(MPa)	1.34E+05	6.00E+05	E >0	1.340E+05	8.49E-03	12
	n	1.00E-01	1.00E-02	n > 0	1.000E-01	3.78E-03	

[a] $\% \left|\left(1-\frac{\text{optimised values}-\text{Target values}}{\text{Target values}}\right)\times 100\right|$

After checking the two-parameter sensitivity, optimisation with four variables is carried out with different initial values, as shown in **Table 5.2**. Three different optimisation tests with different material parameters are performed. The results show that the optimised results are reached in about 36-51 iterations and that all the variables converge from their initial guess parameters to their target values to within 1%, with the exception of the 'n' value in test 1, and the squared norm of the residual error between target and optimised load-displacement curves are in excellent agreement. These results confirm that the material properties of a given material can be accurately obtained by the present optimisation techniques using only a single indenter.

Figure 5.5 presents the convergence history of material properties for each iteration which clearly demonstrates that convergence to the target values can be achieved despite a large variation in the initial values. It is clearly seen in **Figure 5.5**(a) that convergence starts after about 20 iterations in Test 1, which means that all four different parameters approach their target values. In Test 2 and 3, the four parameters converge to the target values after about 81 and 51 iterations in **Figure 5.5**(b) and (c), respectively. The results achieve convergence to within 1% error of the target solutions. Despite the larger initial value of E and σ_y used in Test 3, it is interesting to note that the optimised results in Test 3 are achieved with less iterations than Test 1, since Poisson's ratio, v, converged faster.

Test	Parameter	Target values	Initial values	Boundaries	Final Optimised values	Percentage Error (%)	Iterations
1	E(MPa)	1.34E+05	1.80E+05	E >0	1.339E+05	0.042	36
	σ_y(MPa)	3.00E+02	5.50E+02	σ_y> 0	2.988E+02	0.386	
	v	2.50E-01	3.50E-01	0.1< ν < 0.5	2.512E-01	0.488	
	n	1.00E-01	1.00E-02	0.05<n<0.5	1.102E-01	1.954	
2	E(MPa)	1.34E+05	3.00E+04	E >0	1.340E+05	0.009	81
	σ_y(MPa)	3.00E+02	2.00E+03	σ_y> 0	3.000E+02	0.005	
	v	2.50E-01	3.50E-01	0.1< ν < 0.5	2.498E-01	0.056	
	n	1.00E-01	3.50E-01	0.01<n<0.5	1.001E-01	0.025	

3	E(MPa)	1.34E+05	5.00E+05	E >0	1.34E+05	0.004	51
	σ_y(MPa)	3.00E+02	5.00E+01	σ_y> 0	3.00E+02	0.004	
	v	2.50E-01	1.00E-01	0.1< ν < 0.5	2.498E-01	0.022	
	n	1.00E-01	3.50E-01	0.01<n<0.5	1.00E-01	0.014	

Table 5.2 Four-parameter optimisation for the axisymmetric conical indenter

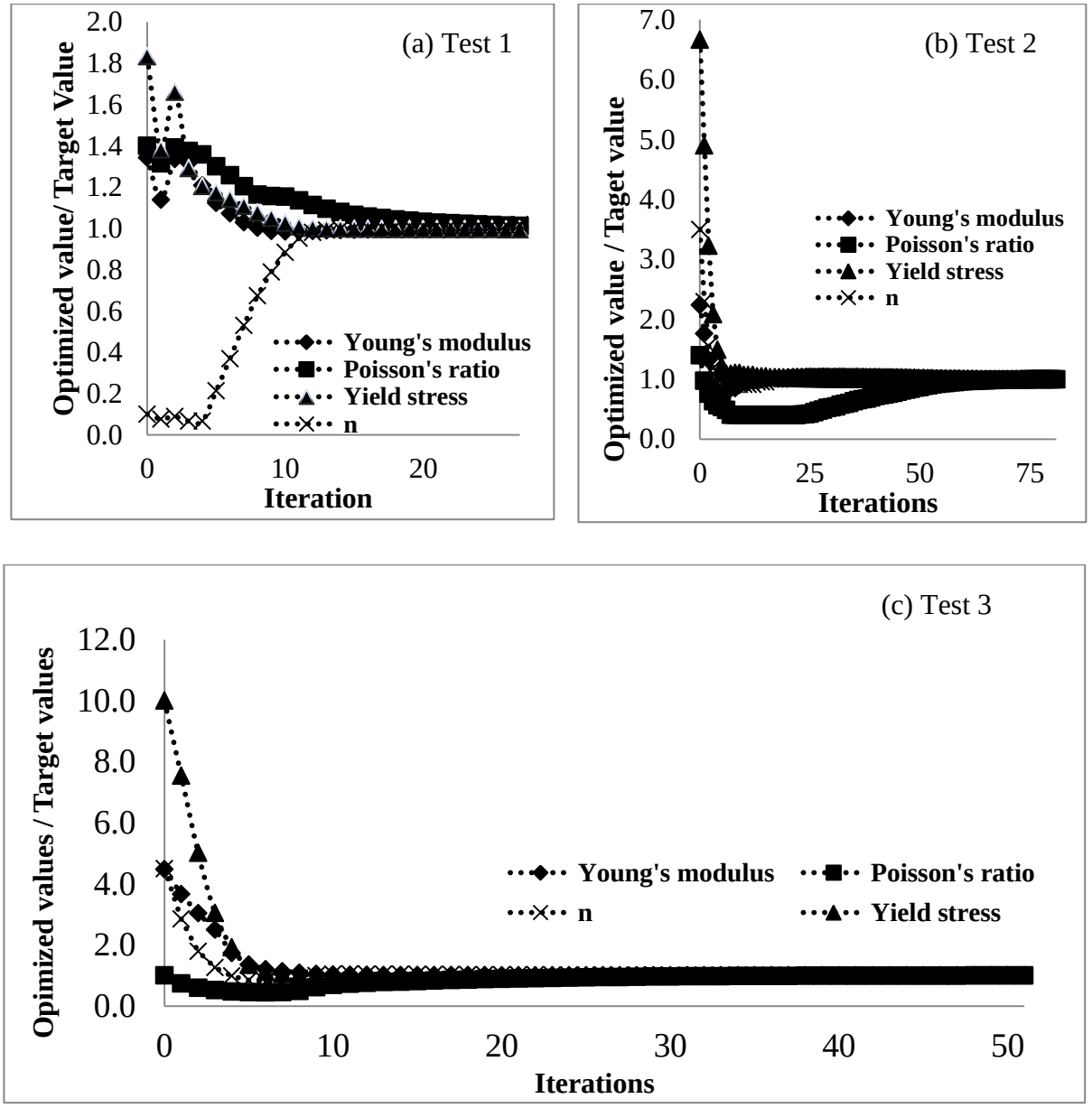

Figure 5.5 Optimised parameter values versus iterations for axisymmetric conical indenters (a) Test 1, (b) Test 2 and (c) Test 3.

5.4.2 Optimisation using 3D Conical, Berkovich and Vickers Indenters

The optimisation algorithm is tested on three different 3D indenter geometries (conical, Berkovich and Vickers Indenters). To reduce optimisation time, the optimisation procedures for the three indenters are carried out using an initial guess of about 50% of the target values. **Table 5.3** shows the initial guess values of the material properties with Test 3 using the same initial values as Test 2 of the axisymmetric conical model. From **Table 5.3**, all results achieve convergence to within 1% error of the target solutions. The squared norm of the residual error between target and optimised load-displacement curves is of the order of 10^{-9}**.** The errors between optimised and target values in Test 4 are slightly larger than the other tests.

Figure 5.6 shows the convergence trends for all four tests. Although the geometries of the models are different, it is interesting to note that the trends shown in **Figure 5.6** (a), **6**(b) and **6**(d) for the four parameters are similar when the same initial guess values are utilized. Furthermore, for the 3D conical indenter test shown in **Figure 5.6** (c), the convergence has the same trend as the axisymmetric conical indenter test (with the same initial values) shown in **Figure 5.5**(b). In terms of the three parameters(ν, σ_y, n) there are sharp increases during the first iteration, but they quickly drop after the second iteration, before gradually reaching the target values. It is interesting to obverse that although Poisson's ratio does not have a strong effect on the results of the indentation, **Figure 5.5**(b) and **Figure 5.6** (c) show that it has some influence the convergence of the iterations.

Figure 5.7 and **Figure 5.8** show the variations in the load-displacement curves during the iterations for the Vickers and Berkovich indenters respectively. Initial values, 2-10 times larger than the target values, have been used in **Figure 5.7**. As the optimisation process is continued, the load-displacement curves gradually approach the target solutions and finally reach the target load-displacement curves.

Despite having identical material properties and the same applied maximum displacement indenter (0.0009mm), it is noted that the Berkovich indenters exhibit more sensitivity than other indenters when the indenter is initially unloaded. It can be said that the Berkovich indenter displaces more volume and thereby produces greater local stresses. This is because the contact area between the Berkovich indenter and the bulk material is larger than the other

indenters. It is also shown that the value of Young's modulus, E, always agrees well with the target value and reaches convergence faster than other material parameters. The entire computation times for the 3D indenters are much longer than the axisymmetric models, but less iteration have been performed. Although the same initial values of the material properties have been used for all three indenters, the computing times and total number of iterations are obviously different.

Table 5.3 Four-parameter optimisation for 3D indenter geometries

Test	Parameter	Target values	Initial values	Boundaries	Finial Optimised values	Percentage Error *(%)*	Iterations
1	E(MPa)	1.34E+05	9.00E+04	E >0	1.340E+05	0.002	
	σ_y(MPa)	3.00E+02	5.00E+02	σ_y> 0	2.498E+02	0.090	
3D Vickers	v	2.50E-01	3.50E-01	0.1< ν < 0.5	3.002E-01	0.060	13
	n	1.00E-01	5.00E-02	0.05<n<0.5	9.982E-02	0.179	
2	E(MPa)	1.34E+05	9.00E+04	E >0	1.339E+05	0.024	
	σ_y(MPa)	3.00E+02	1.00E+03	σ_y> 0	3.002E+02	0.424	
3D	v	2.50E-01	3.50E-01	0.1< ν <0.5	2.510E-01	0.067	13
Conical	n	1.00E-01	1.00E-02	0.05<n<0.5	9.963E-02	0.370	
	E(MPa)	1.34E+05	4.00E+04	E >0	1.341E+05	0.017	
3	σ_y(MPa)	3.00E+02	5.00E+01	σ_y> 0	2.994E+02	0.011	
3D	v	2.50E-01	1.00E-01	0.1< ν < 0.5	2.481E-01	0.188	29
Conical	n	1.00E-01	1.00E-02	0.05<n<0.5	1.010E-01	0.064	
	E(MPa)	1.34E+05	9.00E+04	E >0	1.339E+05	0.032	
4	σ_y(MPa)	3.00E+02	1.00E+03	σ_y> 0	3.011E+02	0.400	
3D	v	2.50E-01	3.50E-01	0.1< ν < 0.5	2.490E-01	0.373	25
Berkovich	n	1.00E-01	1.00E-02	0.05<n<0.5	9.903E-02	0.970	

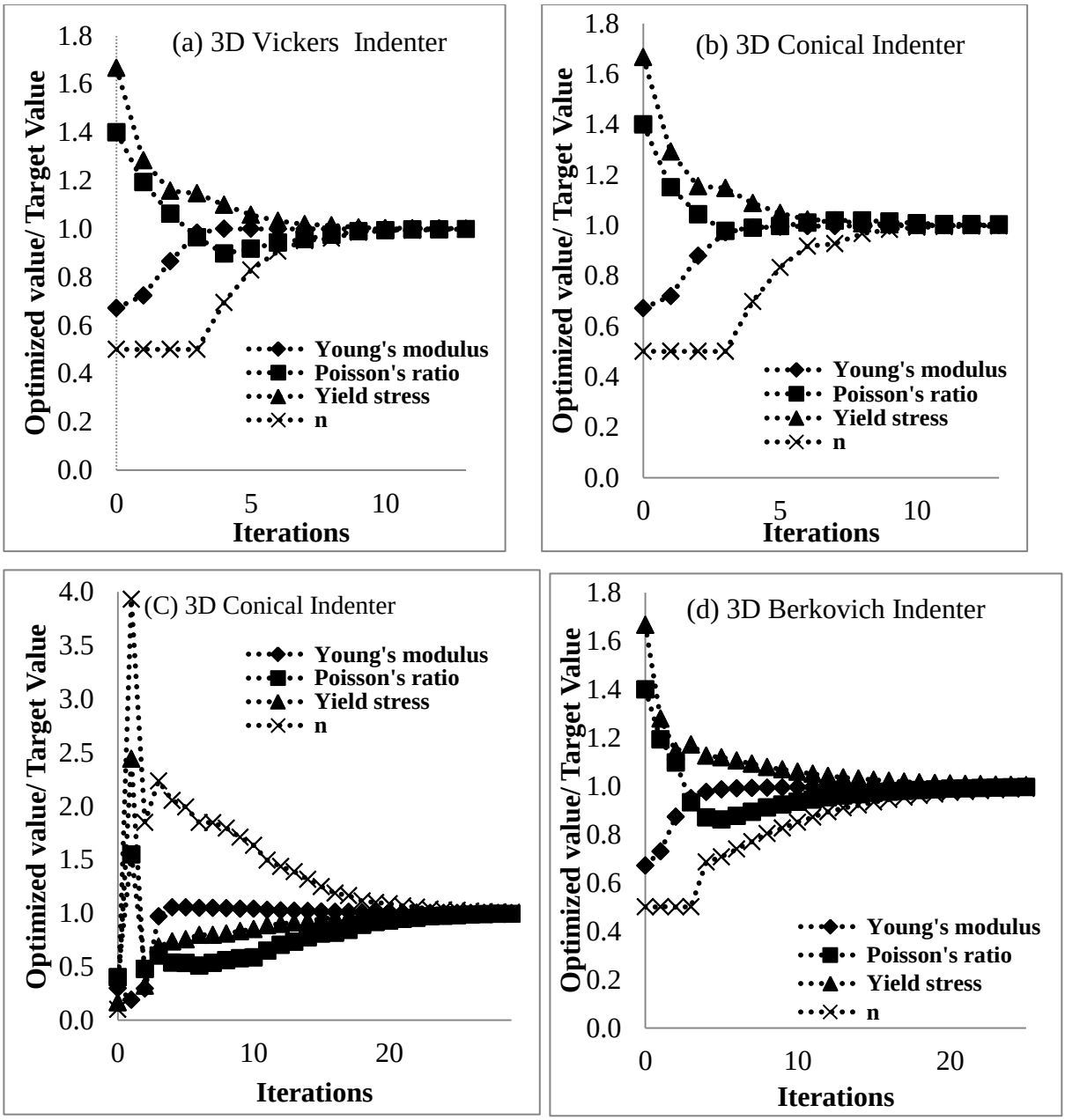

Figure 5.6 Optimised parameter values versus iterations (a) 3D Vickers Indenter, (b) 3D Conical Indenter, (c)3D Conical Indenter with the same initial values as the axisymmetric Test 2, and (d) 3D Berkovich Indenter

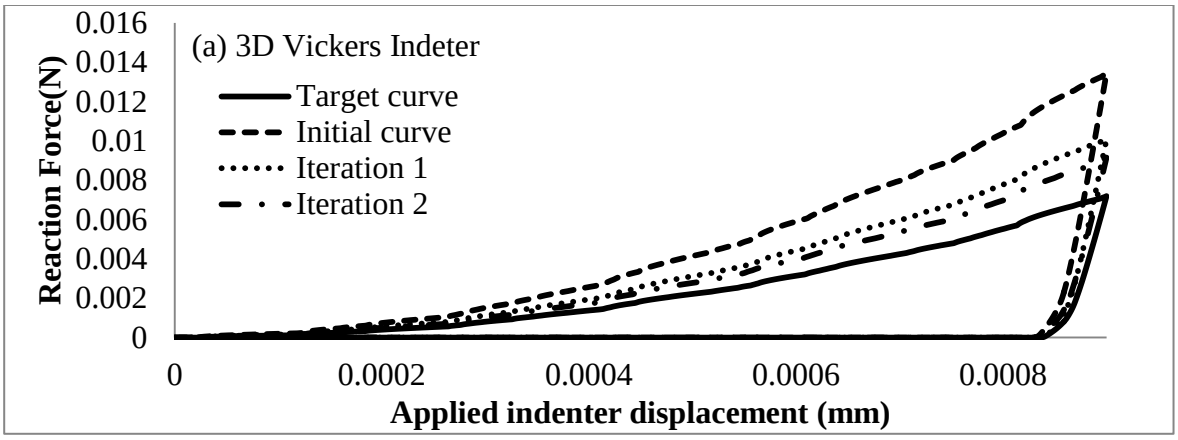

Figure 5.7 Load-displacement curve history of a 3D Vickers indenter (Test 1)

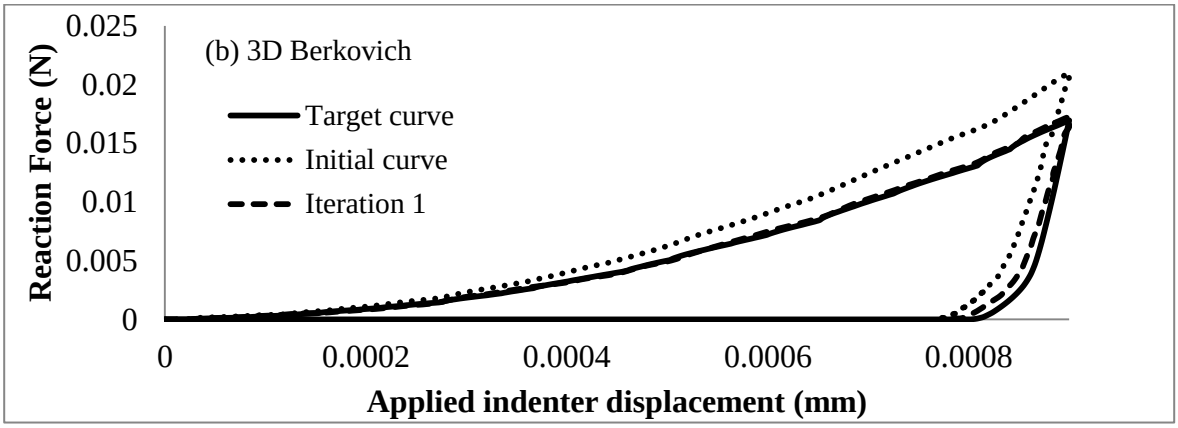

Figure 5.8 Load-displacement loop history of a 3D Berkovich indenter (Test 4)

5.4.3 Effects of initial values and variable ranges

The convergence and computing time obviously depend on the initial guess values, which are presented in **Tables 5.2, 5.3** and **5.4**. Poisson's ratio and the work-hardening exponent values for most engineering materials are between 0.0 and 0.5, but a wider range of material properties for Young's modulus and yield stress exists. Therefore, the ranges of these values have been left as maximum to cover all engineering materials. Generally, initial guess values within 50% of the target values should result in less iterations and less computing time.

5.4.4 Mesh sensitivity

In the initial simulations, a 3D conical indenter and substrate with different element densities in the vicinity of the indenter tips are modelled to investigate the sensitivity of the FE solutions to mesh refinement. Due to severe plastic deformation around the indenter tip, the mesh is much finer in that region. A mesh convergence study is performed by increasing the

mesh density in the vicinity of the indenter until the changes in the loading-unloading indentation curves are negligible, as shown in **Figure 5.9**. The optimisation algorithms with the same initial guess values have been used for different mesh densities. **Table 5.4** shows a comparison of iteration results for two different element sizes near the indenter tip (0.2 μm and 0.5 μm). Using an element size of 0.2μm, the total number of iterations is much less than using an element size of 0.5μm. Moreover, the percentage errors for the 0.2mm element size between the optimised and target values are much lower than the 0.5 μm results. For consistency, therefore, element size 0.5 μm in the vicinity of the indenter tip has been used in the following section with an experimental target indentation curve.

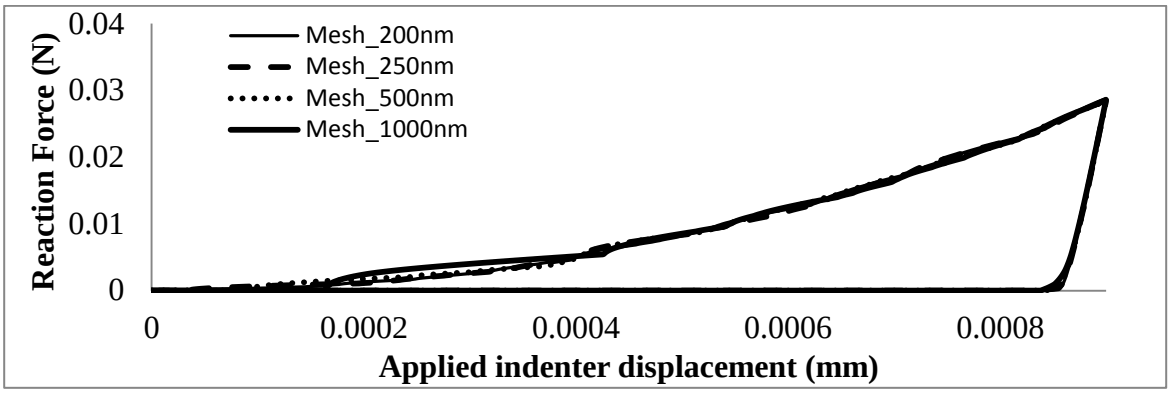

Figure 5.9 loading-unloading curve with different mesh sizes in the vicinity of indenter

Table 5.4 Four parameter optimisation for a 3D conical indenter using two mesh sizes

Test	Parameter	Target values	Initial values	Boundaries	Optimised values	Percentage Error (%)	Iterations
Mesh 1 (Element size 200nm)	E(MPa)	1.34E+05	4.00E+04	0<E< ∞	1.341E+05	5.710E-02	29
	σ_y(MPa)	3.00E+02	5.00E+01	0<σ_y< ∞	2.994E+02	2.138E-01	
	v	2.50E-01	1.00E-01	0.1< ν < 0.5	2.481E-01	7.640E-01	
	n	1.00E-01	1.00E-02	0.01<n<0.5	1.010E-01	9.933E-01	
Mesh 2 (Element size 500nm	E(MPa)	1.34E+05	4.00E+04	0<E< ∞	1.342E+05	1.773E-01	41
	σ_y(MPa)	3.00E+02	5.00E+01	0<σ_y< ∞	2.975E+02	8.168E-01	
	v	2.50E-01	1.00E-01	0.1< ν < 0.5	2.465E-01	1.391E+01	
	n	1.00E-01	1.00E-02	0.01<n<0.5	1.032E-01	2.845E-01	

5.5 Optimisation using a target curve obtained from an experimental test

5.5.1 Experimental indentation test data

In the previous sections, the target loading-unloading indentation curve was obtained using FE analysis with a given set of material properties. To explore the feasibility and robustness of the optimisation algorithm in real-life applications, it is appropriate to consider an experimental load-displacement curve from a laboratory test to extract the material properties. Experimental load-displacement curves for Al 2024-T351 from Khan et al [104] are used in this study based on an MTS Nanoindenter XP with a Berkovich tip.

The elastic-plastic properties of Al 2024-T351 from tensile testing according to ASTM standard E8 [105] are presented in **Table 5.5**. To confirm of the accuracy of the material properties in **Table 5.5**, they are used an input to ABAQUS to arrive at the equivalent FE loading-unloading curve. The FE models consist of two different parts, an indenter and a specimen. The size of the specimen is 2mm x 2mm and the total indenter displacement is 0.002mm [104]. All the FE modelling details are the same as in **Section 3.2.1**.

Figure 5.10(a) shows the load-displacement curves from the experimental indentation test and a FE simulation performed in Ref [104]. The experimental load-displacement curve is used in this study and is regenerated by a digitized graph program.

Figure 5.10 (b) shows the load-displacement curve from Ref [104] and the corresponding ABAQUS FE simulation from this study, based on the material properties in **Table 5.5**, which clearly shows that there are some small differences between the experimental test data and the corresponding FE solution. This is expected since the effects of friction, sharpness of the indenter tip, the indentation size effects in the real-life experimental indentation tests [105] and strain rate effects are not taken into account in the FE analysis. From **Figure 5.10**(b), the maximum reaction force from FEA is slightly lower than the experimental data. In addition, there are differences between the experimental data and FE solutions at the end of unloading portion and it is expected that the accuracy of the optimisation results will be affected by these differences. All the optimisation procedures are based on the experimental load-displacement curve from the digitized experimental curve in **Figure 5.10** (b).

Table 5.5 Material properties of Al 2024-T351 taken from Ref [104]

Elastic Modulus (MPa)	Yield stress (MPa)	Work-hardening exponent	E/Y	UTS (MPa)	Strain-to-Failure (%)
68000	360	0.08	188	478	20

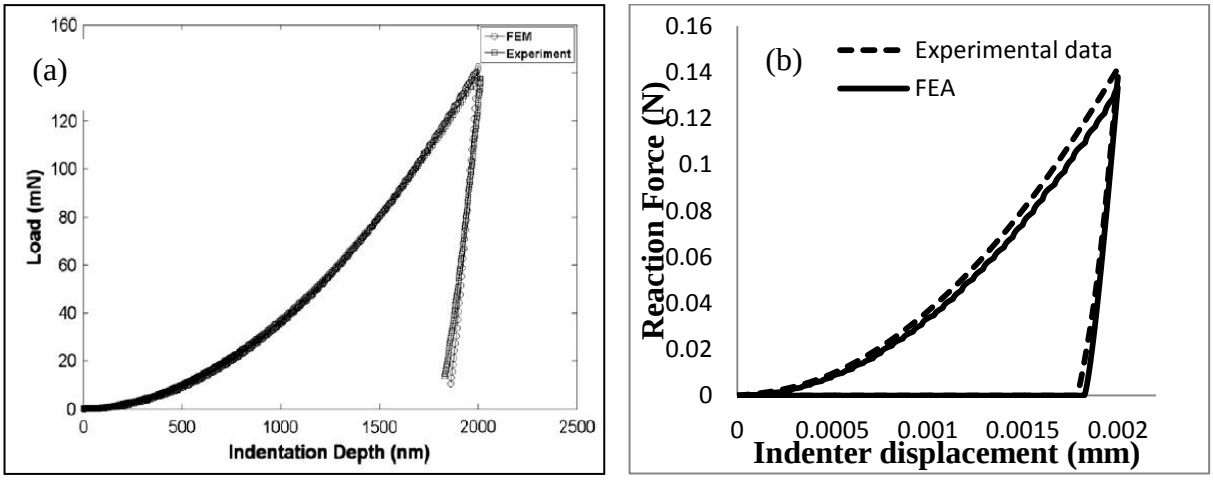

Figure 5.10 Load-displacement curves from experimental indentation data to a depth of 2000nm for Al2024. (a) Load-displacement curves from Ref [104] (b) ABAQUS FE results using the material properties in Table 6 and the experimental load-displacement curve from a digitised graph program.

The optimisation algorithm with a single indenter is used to extract three parameters (E, σ_y, n) from the experimental data, with Poisson's ratio being fixed as 0.33. The relationships between the forward differences ($X_{t+1} - X_t$) versus iterations in Test 1 are illustrated in **Figure 5.11**, which clearly shows how E, σ_y and n reach convergence. The three-parameter optimisation algorithm is carried out with different initial values, as shown in **Table 5.6**. The results show that convergence is achieved in about 11-14 iterations. Despite using three different initial 'guess' values to extract the material properties from the experimental load-displacement curve, similar results are obtained from Tests 1, 2 and 3 in **Table 5.6**. Both the values of Young's modulus, E and yield stress σ_y are close to the target values. The minimum relative errors of estimation for E and σ_y are 6.7% and 0.61%, respectively. The prediction of Young's modulus based on this optimisation technique is more accurate than the Oliver and

Pharr methods [1], which result in a maximum error of 22%. It is noticeable that the errors in the values of work-hardening exponent, n can be as high as approximately 67%. This indicates that, although all material properties coverage, as shown in **Figure 5.11**, using an experimental indentation curve from a single indenter may not be sufficient to arrive at accurate results for the work hardening exponent.

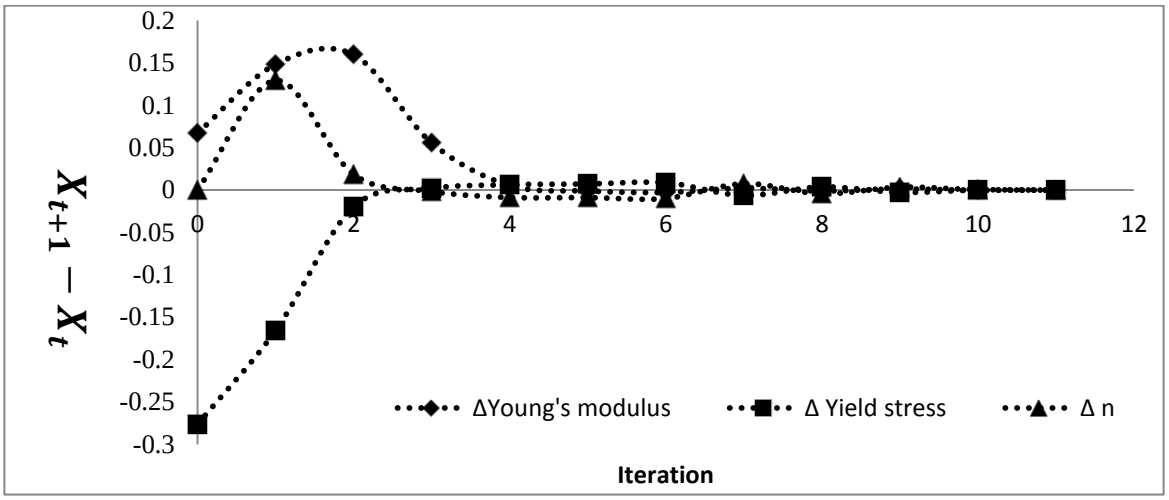

Figure 5.11 $\mathbf{X_{t+1} - X_t}$ versus iterations for axisymmetric conical indenters, Test 1. X= E, σ_y or n

Table 5.6 Material properties of Al 2024-T351 based on an axisymmetric conical indenter

Test	Parameter	Target values	Initial values	Boundaries	Optimised values	Percentage error	Iterations
1	E(MPa)	6.80E+04	2.00E+04	E >0	6.342E+04	6.70%	11
	σ_y(MPa)	3.60E+02	8.00E+02	σ_y> 0	3.562E+02	1.05%	
	n	8.00E-02	1.00E-02	0.01<n<0.499	1.353E-01	69.12%	
2	E(MPa)	6.80E+04	2.00E+04	E >0	6.336E+04	6.8%	14
	σ_y(MPa)	3.60E+02	1.00E+02	σ_y> 0	3.570E+02	2.7%	
	n	8.00E-02	1.20E-01	0.01<n<0.499	1.345E-01	68.12%	
3	E(MPa)	6.80E+04	1.00E+05	E >0	6.324E+04	7%	14
	σ_y(MPa)	3.60E+02	2.00E+02	σ_y> 0	3.578E+02	0.61%	
	n	8.00E-02	1.20E-01	0.01<n<0.499	1.338E-01	67.25%	

5.5.2 Effects of random errors

To test the robustness of the optimisation algorithms when real-life experimental data is used, random errors are introduced in the experimental measurements. Random numbers generated by MATLAB are multiplied by a fixed percentage error and applied to the reaction forces in the 'target' experimental load-displacement curves, as shown in **Figure 5.12** where a random error of 5% is used. It should be noted that the random error of 5% is applied to all points on the curve. The optimisation algorithm is used with same initial guess values with three random error percentages; 1%, 3% and 5%. **Table 5.7** shows the optimised results, where the percentage errors in the optimised values slightly increase when the random error percentage is increased. As before, there are large errors in the optimised work hardening exponent, *n.*

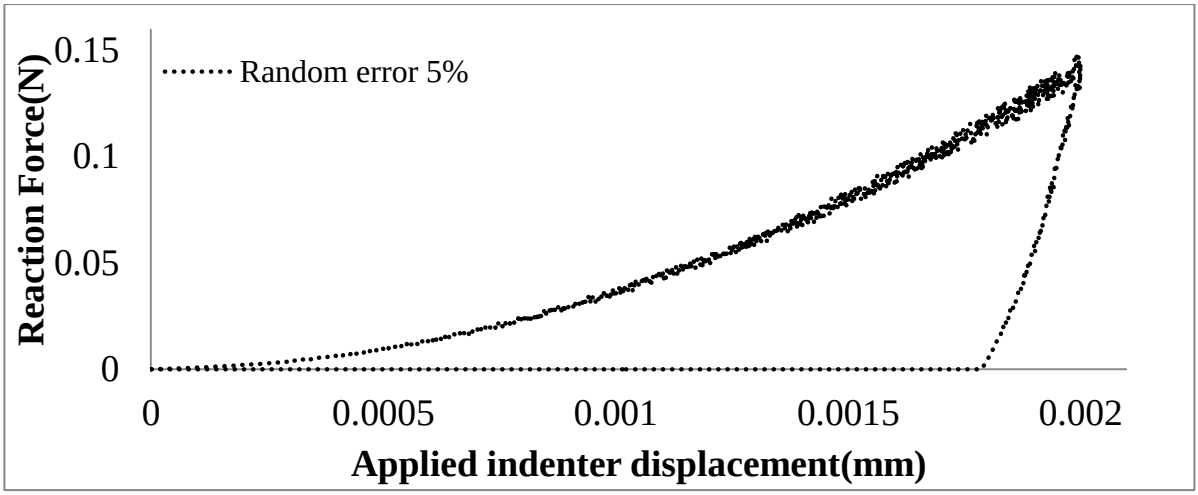

Figure 5.12 Load-displacement curve with random error 5%

Table 5.7 Material properties of Al 2024-T351 Axisymmetric conical indenter with applying random errors.

Test	Parameter	Target values	Initial values	Boundaries	Optimised values	Percentage error	Iterations
1	E(MPa)	6.80E+04	1.00E+05	E >0	6.322E+04	7%	
Random	σ_y(MPa)	3.60E+02	2.00E+02	σ_y> 0	3.575E+02	0.69%	15
Error 1%	n	8.00E-02	1.20E-01	0.01<n<0.499	1.337E-01	67.12%	
2	E(MPa)	6.80E+04	1.00E+05	E >0	6.326E+04	7%	16

Random Error 3%	σ_y(MPa)	3.60E+02	2.00E+02	$\sigma_y > 0$	3.560E+2	1.1%	
	n	8.00E-02	1.20E-01	0.01<n<0.499	1.346E-01	68.25%	
3	E(MPa)	6.80E+04	1.00E+05	E >0	6.323E+04	7.01%	
Random Error 5%	σ_y(MPa)	3.60E+02	2.00E+02	$\sigma_y > 0$	3.583E+02	0.47%	14
	n	8.00E-02	1.20E-01	0.01<n<0.499	1.338E-01	67.25%	

The squared norm of the residual error (SNRE), given Eq. (3.1) in **Section 3.2.2**, can be used as a measure of how close the simulated FE solution is to the real-life experimental load-displacement curve. In **Sections 5.5.1** and **5.5.2**, where the simulation is based on an FE 'simulated' target load-displacement curve, the values of SNRE are of the order of 10^{-9} or 10^{-10}, i.e. the differences between the optimised FE solution and the target load-displacement curve are negligible. In contrast to this, in spite of the fact that the same termination tolerance of 10^{-9} is used for the optimised function values, the SNRE values for the real-life experimental curve are generally of the order of 10^{-3}.

To explore the convergence of the algorithms in more depth, the iteration history of the load-displacement curves obtained from the FE model for Test 1 are compared with those obtained experimentally in **Figure 5.13**. The final optimised FE curves for all three tests are shown in **Figure 5.14** where some 'noise' exists on the loading portion of curves, particularly around the maximum load. This small deviation may have some influence on the accuracy of the optimised values. For this reason, the optimisation process cannot continue until the SNRE value reaches 10^{-9}, and the values of SNRE in this section are approximately 10^{-3}.

The results show that using a real-life target experimental curve results in more convergence difficulties and inaccuracy than a simulated target FE curve. This may be attributed to the fact that the target FE curves do not cater for frictional effects, data scatter and bluntness of the indenter tip. Further investigation may be required to extract more accurate material properties from experimental load-displacement curves, e.g. by using results from dual indenters or narrowing the range of the guess values of the material properties.

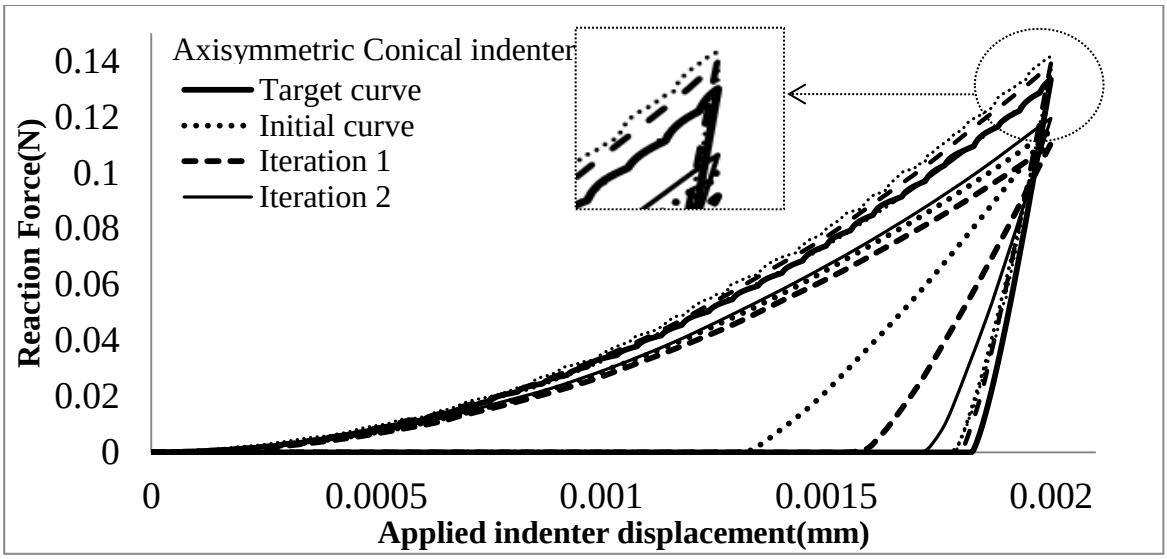

Figure 5.13 FE Load-displacement curve from Test 1 in Table 7

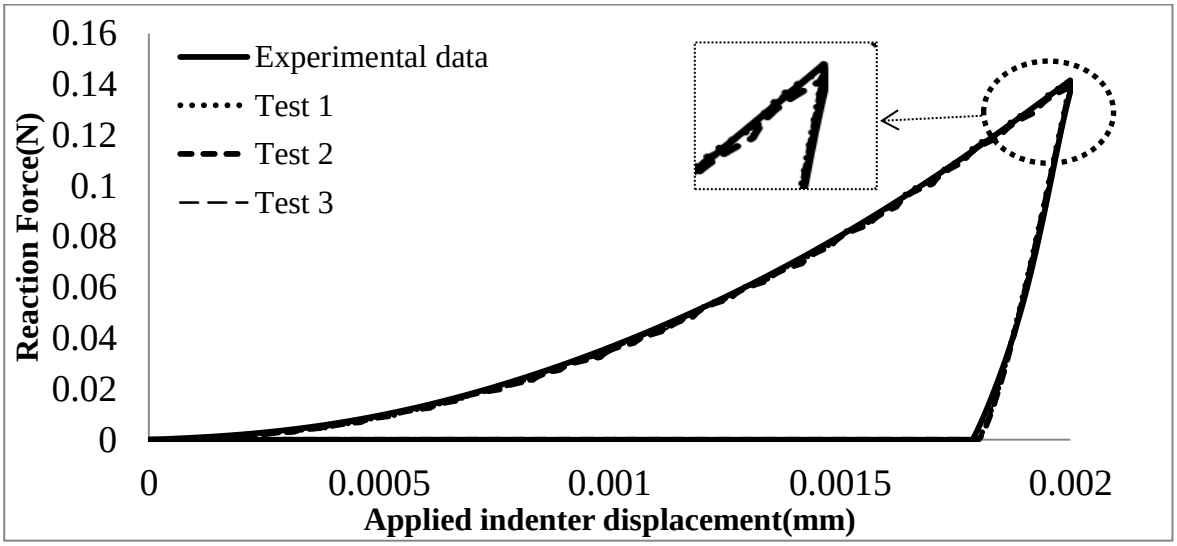

Figure 5.14 Comparison between experimental data from digitized program and FE results from optimised values using an axisymmetric conical indenter

5.6 Conclusions

In this work, a nonlinear least-squares optimisation algorithm is developed and implemented in MATLAB in order to extract four elastic-plastic material properties (E, ν, σ_y, n) of an unknown material by using a single target load-displacement indentation curve. The algorithm automatically feeds input data to ABAQUS and automatically runs FE simulations

to check how close the FE loading-unloading curve is to the 'target' curve. In general, previous work has suggested that indentation data from multiple indenters is required to extract a unique set of material properties. However, the optimisation algorithms devised in this study have been shown to be capable of converging to the target properties, to within 1% error, using results from a single indenter, despite using various initial guess values. Furthermore, it is shown that the optimisation algorithms produce good accuracy for three different indenter geometries; conical, Vickers and Berkovich. It is interesting to note that the elastic modulus and yield stress of both axisymmetric and 3D models converge faster with a greater accuracy than others material parameters. Also, as expected, the convergence and computing time depend on the initial guess values and the model geometry.

The proposed algorithms have also been applied to a real-life target load-displacement curve from an indentation experiment, rather than being based on a 'simulated' FE target curve. Random errors are also applied to reflect experimental measurement errors in the target load-displacement curves, and different initial guess values are used to test the robustness of the optimisation algorithm. The results show that an accurate prediction of yield stress is obtained, but less accurate predictions of Young's modulus and work hardening exponent are obtained. Also, the deviation between the experimental and optimised load-displacement curves, i.e. the squared norm of the residual errors (SNRE) are of the order of 10^{-3} , compared to 10^{-9} when a simulated target FE indentation curve is used. The investigation covers only one real experimental data from literature, in order to demonstrate how the optimisation technique based on FE simulations can be extended to real-life indentation experiments. Further research is required to test the effectiveness of the optimisation technique for a wide range of different materials.

In conclusion, this study has shown that a robust non-linear least-squares optimisation can be used to accurately predict a unique set of four elastic-plastic material properties(E, ν, σ_y, n) without the need for multiple indenters. However, if the target curve is obtained from a real-life experimental test, which inevitably contains some scatter in the data, the accuracy is reduced. Further research is required to improve the accuracy of the predicted material properties from experimental load-displacement curves, e.g. by using results from dual or triple indenters, or narrowing the range of the guess values of the material properties.

6 A Combined Dimensional Analysis and Optimisation Approach for determining Elastic-Plastic Properties from Indentation Tests

6.1 Introduction

In **Chapter 5**, the loading-unloading indentation curves obtained from FE analysis have been used to extract elastic-plastic mechanical properties using the optimisation algorithm. However, extensive computational times are required in such an approach due to the fact that the optimisation procedure is based on iterative FE computations.

Recent research efforts [48,64,75,81,92,94-96 and 97-99] have focused on extracting the elastic-plastic material properties using dimensional analysis of indentation testing [64,74,81,94,97,98]. Specifically, the determination of the yield stress, σ_y, and work-hardening exponent, n, using dimensional analysis and the concept of a representative stress and strain have been studied by Dao et al. [81] and Chollacoop et al. [94] who developed forward and reverse algorithms. The forward algorithm can be used to predict the indentation response for a set of mechanical properties, whereas the reverse algorithm is able to estimate the elastic-plastic properties from the loading-unloading curves. Using these algorithms, three unknown material properties (E, σ_y, n) can be obtained using independent dimensionless functions with very small errors in the elastic modulus and the representative stress $\sigma_{0.033}$ that corresponds to a value of plastic strain of 0.033, whereas the determination of the work-hardening exponent is not very accurate.

An optimisation approach to extract mechanical properties of a power law material has been proposed by Luo et al.[95] and Luo and Lin [96] based on the Zeng and Chiu's fitting scheme [99]. In Zeng and Chiu's method, a straight line is used to represent the unloading curve for elastic-perfectly plastic materials. Luo et al. [95] and Luo and Lin [96] found that the contact area of the indenter gradually decreases after the indenter is removed from the specimens, even for elastic-perfectly plastic materials. Therefore, they proposed a new fitting scheme for the unloading curve. They assumed that the loading portion of the loading-unloading curve of an elastic-plastic material is a function of the corresponding elastic and elastic-perfectly plastic material properties, while at least the upper 50 percent of the unloading curve is a

function of only the elastic properties. Furthermore, in their study, two parameters σ_y and n can be optimised. To reduce the optimisation parameters, Young's modulus was fixed, the values of which can be obtained using the Oliver-Pharr method [1], or it was assumed that it was already known.

Luo et al.[95] and Luo and Lin [96] pointed out that using the entire loading–unloading curve might improve the accuracy of estimation of the mechanical properties of a power law material. In general, the loading portion of the curve is well described by Kick's law, $P = Ch^2$ where P is the load and h is the indentation depth. Nevertheless, it is difficult to construct mathematical functions of the unloading curve since the mechanical properties of a power law material are related to the complicated contact interaction between the test specimen and the indenter. Luo et al. [95] and Luo and Lin [96] fitted the upper 50 percent of the unloading curve which means that at least the lower 50 percent of the curve was not considered in their fitting scheme. Since there is no mathematical formula or function that fits the unloading curve well, it is thought that a linear fitting scheme can still be used, since the information of the initial unloading curves, i.e. the slope of the curve, dP/dh_{max}, and the residual indenter depth, h_r can be obtained from the method proposed in [81, 94]

The objective of **Chapter 6** is to introduce a new approach to the extraction of the three elastic-plastic mechanical properties (E, σ_y, n) from the indentation loading-unloading curves using dimensionless mathematical functions coupled with a numerical optimisation algorithm. A parametric study using FE analysis is first conducted to construct the appropriate dimensional functions. The proposed optimisation algorithm is based on the nonlinear least-square routine in MATLAB. The loading curvature, *C*, the final depth after the indenter, h_r, and the initial slope of the unloading curves, dP/dh, can be calculated by the dimensionless functions, where an executable file is coded using the C language. The elastic-plastic mechanical properties can be obtained from the data provided by the loading-unloading curves. Additionally, the estimation of mechanical properties of power law materials using a single indenter and dual indenters has been carried out. Different sets of materials properties are used and the accuracy and validity of the predicted mechanical properties using the single indenter or dual indenters are assessed.

6.2 Dimensional Analysis

A typical loading-unloading curve of an elastic-plastic material subjected to an instrumented sharp indentation is presented in **Figure 6.1**.

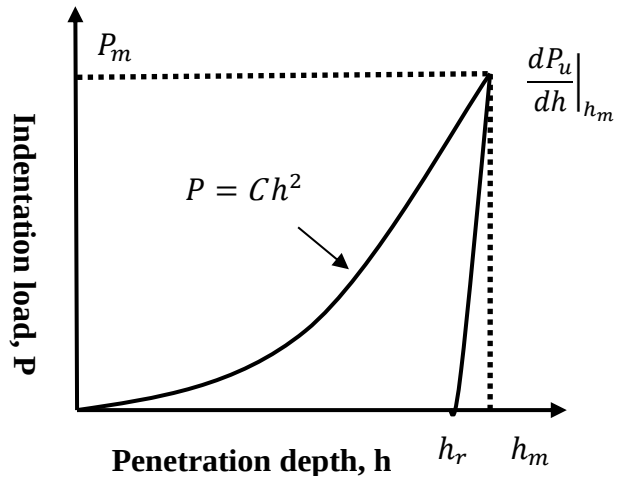

Figure 6.1 Typical load-displacement curve of an elastic-plastic material subjected to a sharp indentation

The loading portion of the curve can be described by Kick's Law, i.e.

$$P = Ch^2 \qquad (6.1)$$

where *C* is the loading curvature which is a related to the geometry of the indenter tip and the material properties of the test material. The maximum applied indenter displacement, h_m, generally occurs at the maximum load, P_m, and the initial unloading slope can be expressed by $S = \frac{dP_u}{dh}\Big|_{h_m}$, where P_u is the unloading load. Giannakopoulos and Suresh [76] mentioned that *C*, *S* and h_r/h_m, where h_r is the final residual depth after the indenter is completely removed, are the three independent governing parameters that can be directly obtained from a single loading-unloading curve. These parameters can be used to obtain unknown material properties from loading-unloading curves.

The elastic-plastic behaviour for many pure and alloyed engineering metals can be expressed by a power law relationship, which is presented schematically in **Figure 6.2.**

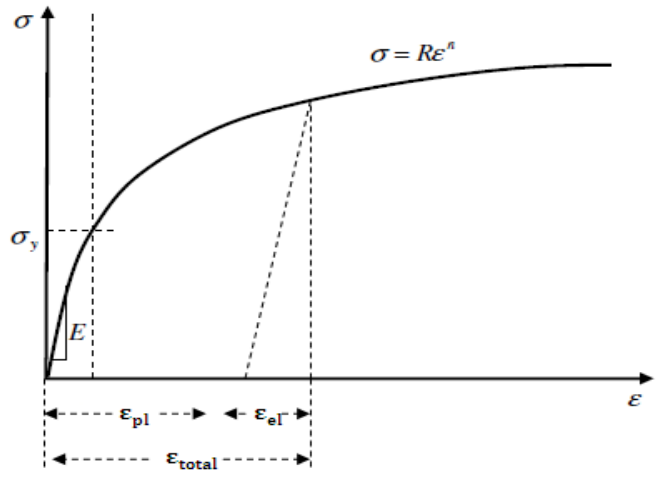

Figure 6.2 Power law elastic-plastic stress-strain behaviour

The stress-strain relationship is assumed to be

$$\sigma = \begin{cases} E\varepsilon \; for \; \varepsilon \leq \frac{\sigma_y}{E} \\ R\varepsilon^n for \;\; \varepsilon > \frac{\sigma_y}{E} \end{cases} \qquad (6.2)$$

where E is Young's modulus, R is a strength coefficient, n is the work-hardening exponent and σ_y is the stress at zero offset strain. The decomposition of the total strain is given by

$$\varepsilon_{\text{total}} = \varepsilon_{\text{el}} + \varepsilon_{\text{pl}} \qquad (6.3)$$

where ε_{el} is the elastic strain component and ε_{pl} is the plastic strain component. The stress equation can be written as

$$\sigma = R(\frac{\sigma_y}{E} + \varepsilon_{pl})^n \qquad (6.4)$$

The coefficient R is given by

$$R = E^n \sigma_y^{1-n} \qquad (6.5)$$

Therefore, four material parameters (E, ν, σ_y, n) are needed to describe the power law elastic-plastic behaviour of the material. For a given geometry of a sharp indenter, the loading portion of the curve for a power law elastic-plastic material can be generally expressed by

$$P = P\left(h, E, \nu, E_i, \nu_i, \sigma_y, n\right), \tag{6.6}$$

where E_i is Young's modulus of the indenter, and ν_i is its Poisson's ratio. In this study, E_i and ν_i are taken to be 1100GPa and 0.07, respectively and ν is assumed to be 0.33. Using a reduced modulus of $E^* = \left[\left(\frac{1-\nu^2}{E}\right) + \left(\frac{1-{\nu_i}^2}{E_i}\right)\right]^{-1}$, this function can be simplified to

$$P = P(h, E^*, \sigma_r, n) \tag{6.7}$$

where σ_r is called the representative stress. According to the Buckingham π-theorem for dimensional analysis [48], the dimensional scaling relationship for the indentation loading curvature can be expressed as

$$P = \sigma_r h^2 f_1\left(\frac{E^*}{\sigma_r}, n\right), \tag{6.8}$$

and thus

$$C = \frac{P}{h^2} = \sigma_r f_1\left(\frac{E^*}{\sigma_r}, n\right), \tag{6.9}$$

where f_1 is a dimensionless function and the normalization is taken with respect to $\frac{E^*}{\sigma_r}$.

At the end of the loading process, the unloading process begins when the indenter reaches the maximum depth and the indentation load, P_u, decreases from P_m to zero. If the elastic effects are characterized by E^*, then the unloading slope can be written as [81]

$$\frac{dP_u}{dh} = E^* h f_2\left(\frac{h_m}{h}, \frac{\sigma_r}{E*}, n\right) \tag{6.10}$$

Hence, the normalized initial unloading slope, $\frac{1}{E^* h_m}\frac{dP_u}{dh}\Big|_{h=h_{max}}$ can be expressed as

$$\frac{1}{E^* h_m}\frac{dP_u}{dh}\Big|_{h=h_m} = f_2\left(\frac{E^*}{\sigma_r}, n\right) \text{ at } h = h_m \tag{6.11}$$

In addition, the unloading force itself can be written as

$$P_u = P_u(h, h_m, E^*, \sigma_r, n) = E^* h^2 \mathrm{f}_u\left(\frac{h_m}{h}, \frac{\sigma_r}{E^*}, n\right) \tag{6.12}$$

When the unloading force is zero, the following expression can be written

$$\frac{h_r}{h_m} = f_3\left(\frac{\sigma_r}{E^*}, n\right) \quad (6.13)$$

The three dimensional functions (f_1, f_2 and f_3) can be used to obtain the mechanical properties.

6.3 Finite Element Analysis to construct dimensional functions

The geometry definition and the axisymmetric conical indentation using FE analysis is mentioned in **Section 3.2.1**. The simulations are carried out in two distinct steps: a loading step and an unloading step. In the first step, a total indenter displacement of 0.002mm is imposed. During the loading step, the rigid cone indenter is moved downwards along the axial-direction and penetrates the substrate up to the maximum specified depth. During the unloading step, the indenter is unloaded and returned to its initial position.

6.4 Result of FE simulations

An elastic–plastic material was used in the FE simulations of indentation in this study. The *E* values range from 10 to 210 GPa, yield stress, σ_y, from 50 to 3000 MPa, and work-hardening exponent, *n*, from zero to 0.5, while Poisson's ratio, *v*, is fixed at 0.33. All the mathematical functions and the material property combinations are presented in **Appendix 2**.

6.4.1 Determination of the representative strain (f_1 function)

Dao et al. [81] and Chollacoop *et al.* [94] reported that a representative strain $\varepsilon_r = 0.033$ could be identified for the conical indenter ($\alpha = 70.3°$) within a specified range of material parameters. Dao *et al*. [81] found that the relationship between $C/\sigma_{0.033}$ and the $E^*/\sigma_{0.033}$ does not depend on the value of n. In this study, a numerical study of this method has been carried out with a parametric analysis of 174 cases using a representative strain of 0.033. The relationship between the normalized $C/\sigma_{0.033}$ and $E^*/\sigma_{0.033}$ is shown in **Figure 6.3**. Subsequently, the f_1 function was determined by fitting all 174 data points to within an error of $\pm$3.14 %. As can be seen from **Figure 6.3**, the relationships between $C/\sigma_{0.033}$ and $E^*/\sigma_{0.033}$ is sensitive to the values of n.

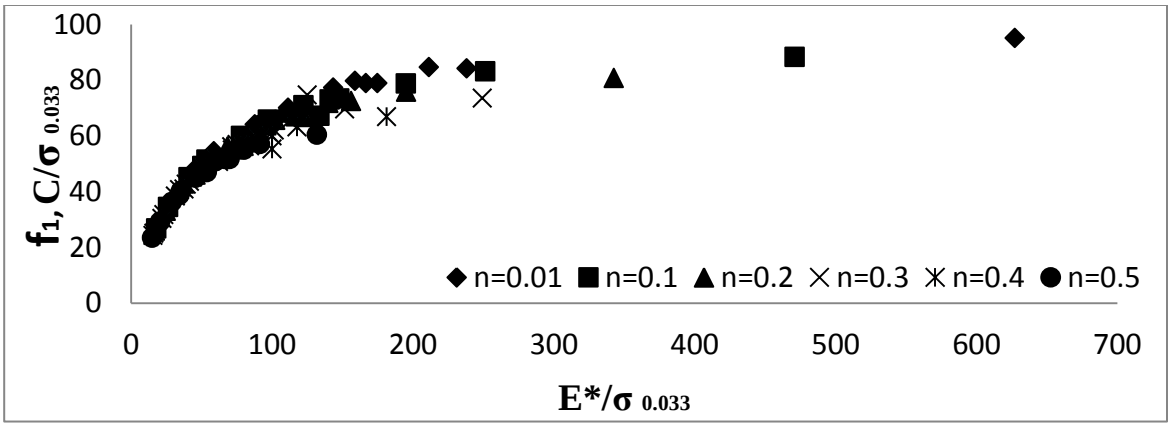

Figure 6.3 Relationship between $C/\sigma_{0.033}$and the $E^*/\sigma_{0.033}$ for different values of the work-hardening exponents (f_1 function) for a conical indenter with 70.3° face angle

The representative strain of ε_r=0.033 (Dao et al. [81]) is based on the uniaxial power-law stress-strain curve. Ogasawara et al. [97] suggested that this representative strain works only for a limited range of material properties and its physical basis is weak. They proposed a new representative strain of ε_r=0.0115, defined as the plastic strain during equi-biaxial loading. To investigate the effectiveness of this new representative strain, FE analysis using ε_r=0.0115 is carried out to construct dimensionless functions based on the axisymmetric indentation model with a conical rigid indenter, as shown in **Figure 6.4**. From the FE results, it is clear that a representative strain ε_r=0.0115 can be applied to practically all power-law engineering materials and the dimensionless relationships between $C/\sigma_y\langle\varepsilon_r\rangle$ and $E^*/\sigma_y\langle\varepsilon_r\rangle$ are practically independent of *n*. Therefore, the representative strain ε_r=0.0115 is used in this study to determine the mathematical functions.

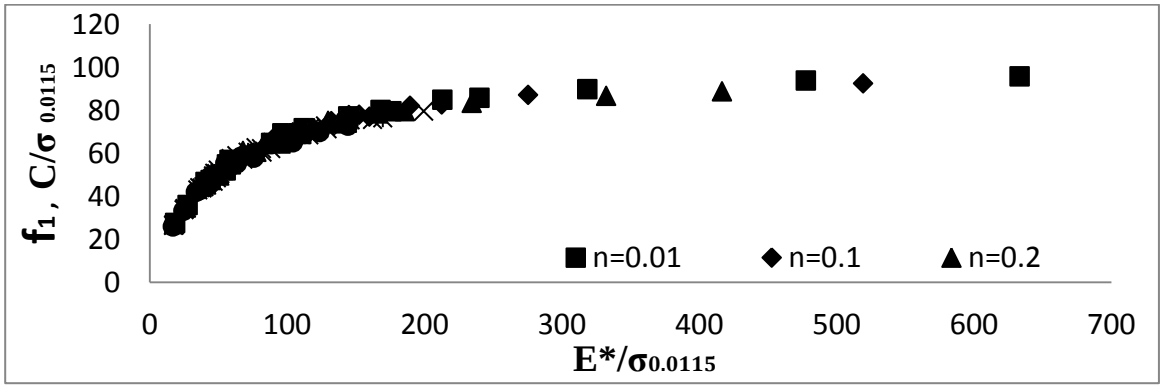

Figure 6.4 Relationship between $C/\sigma_{0.0115}$ and the $E^*/\sigma_{0.0115}$ for different values of the work-hardening exponent (f_1 function) for a conical indenter with 70.3° face angle

The f_1 function is obtained by fitting all 174 data points to within an error of ± 1 percent. There are significant differences between **Figure 6.3** and **Figure 6.4** despite the fact that the same range of materials is used. It is apparent from **Figure 6.4** that the relationship between $C/\sigma_y\langle\varepsilon_r\rangle$ and the $E^*/\sigma_y\langle\varepsilon_r\rangle$ is practically independent of the values of n.

6.4.2 Determination of elastic modulus and h_r/h_m (f_2 and f_3 functions)

The unloading stiffness of an indentation loading-unloading curve is governed by the elastic behaviour of the material. Therefore, the upper portion of an unloading curve can be used to determine the elastic modulus. It is also assumed that the unloading behaviour of indenter is fully elastic with no plastic deformation. Oliver and Pharr [1] found that the unloading curve is usually well represented by a power law fit, $P = C(h - h_r)^m$ and differentiated this equation to obtain the slope of the unloading curve at the maximum depth of penetration, $h = h_{max}$. In this study, approximately two-thirds of the unloading curve is used based on the Oliver and Pharr method.

With respect to the elastic stiffness, Chollacoop et al. [94] derived an elastic modulus function shown in Eq.(6.11). This function includes the effect of pile-up or sink-in on the specimen during the indentation processes. The residual depth of the indenter is also one of the important parameters for determining the mechanical properties. The relationships between the normalised S/E^*h_m and E^*/σ_y for $\sigma_{0.0115}$ is shown in **Figure 6.5** and that between h_r/h_m and σ_y/E^* for $\sigma_{0.0115}$ is shown in **Figure 6.6.**

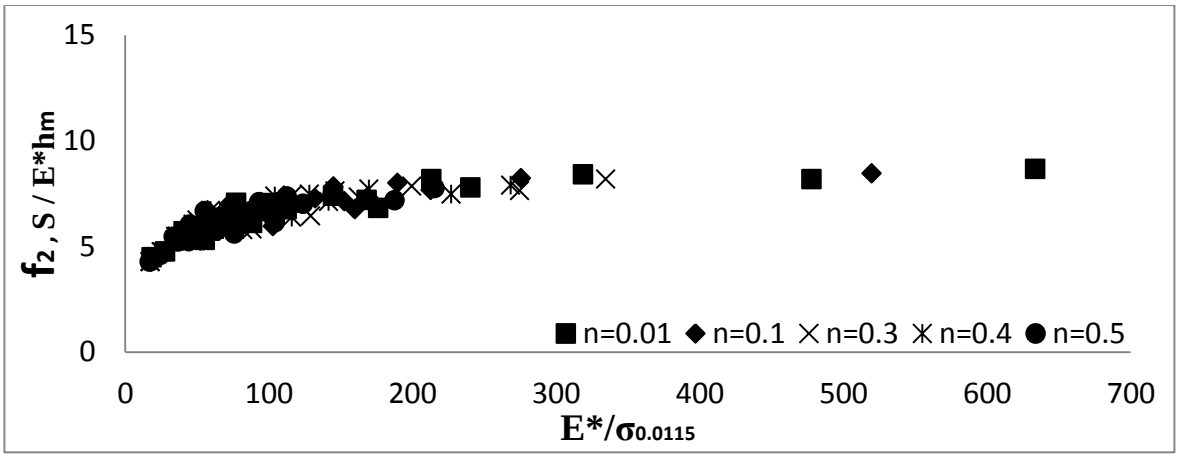

Figure 6.5 Relationship between S/E^*h_m and the $E^*/\sigma_{0.0115}$ for different values of the work-hardening exponent (f_2 function) for a conical indenter with 70.3^0 face angle

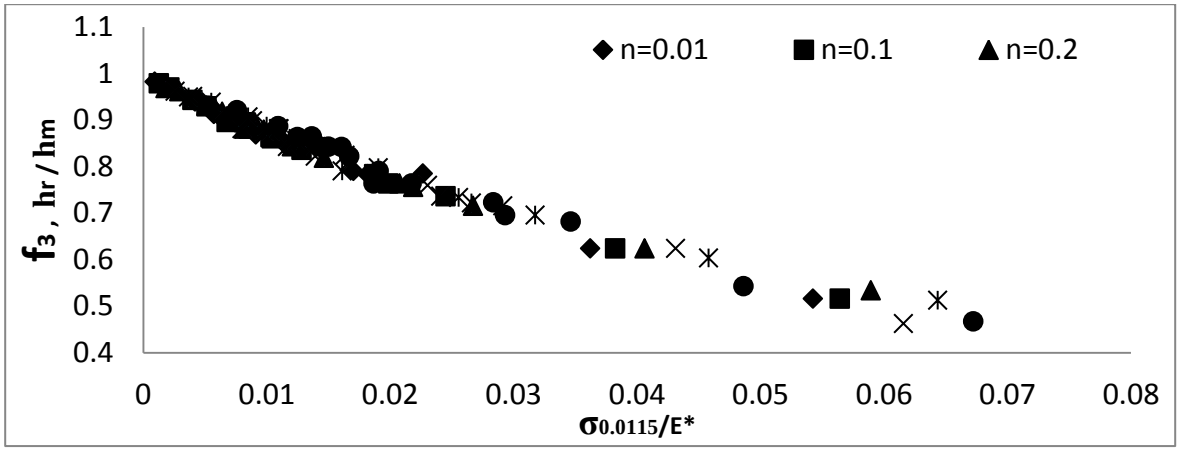

Figure 6.6 Relationship between h_r/h_m and the $\sigma_{0.0115}/E^*$ for different values of the work-hardening exponent (f_3 function) for a conical indenter with $70.3^{\mathbf{o}}$ face angle

6.4.3 Determination of f_1 for a dual indenter situation

Several approaches have been proposed to determine the material properties of a power law material using a single indenter [48, 64, 75, 81, 92, 94-96 and 97-99]. However, in many approaches, the material properties of a power law material cannot be determined uniquely by using a single indenter. Therefore, some researchers, e.g. references [64, 81 and 95], have used loading-unloading curves obtained from more than one indenter geometry (dual indenters) in order to obtain a unique set of material constants. Ogasawara et al. [97] defined the relationship between the representative strain ε_r and the indenter half-apex angle cot θ as:

$$\varepsilon_r = 0.0319\ cot\theta \qquad (6.14)$$

From Eq. (6.14) the representative strain for a conical indenter with a face angle of 60° can be obtained as 0.0184. Numerical FE analyses were performed with parametric studies of 174 cases using a representative strain of 1.84 percent as shown in **Figure 6.7**.

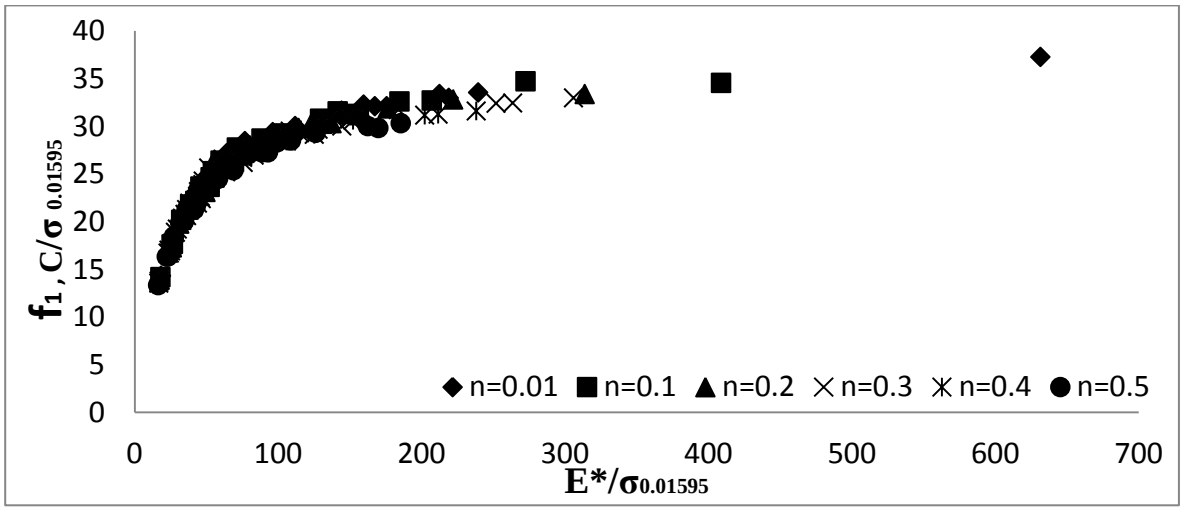

Figure 6.7 Relationship between $C/\sigma_{0.01595}$ and the $E^*/\sigma_{0.01595}$ for different working-hardening exponent (f_1 function) for a conical indenter with 60° face angle

6.5 An optimisation procedure for determining material properties

6.5.1 Optimisation procedure

Based on the proposed dimensionless functions and optimisation techniques, an inverse method is developed to determine the material properties from indentation loading-unloading curves, without using further FE analysis. The optimisation approach is presented in **Section 3.2.2**. In this study, only three different material properties E, σ_y, n are obtained from loading-unloading indentation curves. This specific case contains the full set of the material constants in the model, that is

$$x = \left[E, \sigma_y, n\right]^T \qquad (6.15)$$

Some practical physical constraints were imposed during the analysis. For example, the work-hardening exponent values for most engineering materials are between 0.0 and 0.5. Although a limited range of material properties were chosen in this study, no upper limits were

imposed on the values of Young's modulus and yield stress values in order to cover all possible engineering materials during the optimisation procedures, that is

$$\left\{\begin{array}{c} E > 0 \\ \sigma_y > 0 \\ 0 < n < 0.5 \end{array}\right\} \tag{6.16}$$

The general optimisation algorithm used in this study is illustrated in **Figure 6.8**. After the initial values for E, σ_y and n are guessed, the optimisation procedure is carried out in several steps with MATLAB, which controls the C language executable file to update the indentation forces for loading and unloading. In terms of pre-processing, the displacement of the indenter for the loading and unloading parts is fixed. The indentation force of the loading and unloading parts can be calculated by the functions f_1, f_2 and f_3 during the iterations.

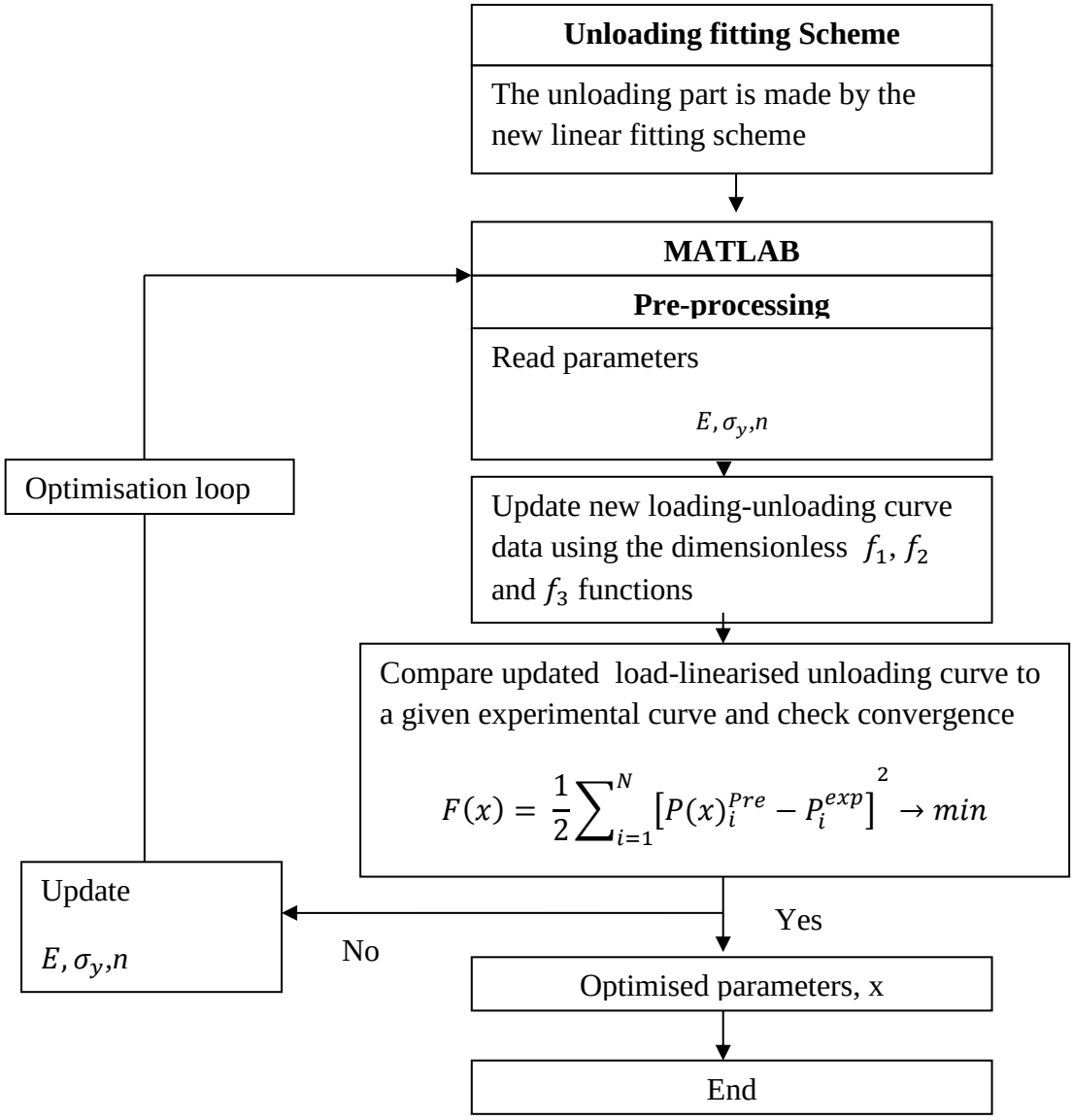

Figure 6.8 Flow chart of the optimisation algorithm to determine the mechanical properties from the loading-linearised unloading curves

With regard to the indentation force for loading, it is proportional to the square of the penetration depth through the coefficient C, as shown in Eq.(6.1). Since the coefficient C can be obtained from the f_1 function, the loading forces can be calculated when the material properties are updated during the iterations. It is noted that the displacement of the indenter for the loading portion is fixed, based on the experimental loading-unloading curve (obtained from FE analysis in this study).

With regard to the unloading force, there are two main methods to obtain the unloading forces; the Oliver-Pharr's method [38] and Doerner and Nix's method [36]. Generally, Doerner and Nix's method can be described by the following equation.

$$P = S(h - h_c) \tag{6.17}$$

where h_c is the depth of residual contact circle after the load has been removed and S is the slope of unloading curve. In contrast, Oliver - Pharr's method can be written as

$$P = A(h - h_r)^m \tag{6.18}$$

where m is the power law index, and A is a constant. The main difference between the two methods is the determination of the contact area at the maximum load. In general, by using the Oliver -Pharr method, the contact area can be obtained from the known geometries of the half angle of the conical indenter as follows:

$$A_m = \pi a_c^2 = \pi(h_c tan\theta)^2 \tag{6.19}$$

The depth of contact circle h_c can be determined from the loading-unloading data using the following equation:

$$h_c = h_{max} - h_s \tag{6.20}$$

where $h_s = \epsilon \frac{P_{max}}{S}$, the geometric constant, ϵ = 0.727 for conical and 0.75 for Berkovich and Vickers indenters, respectively [1]. Unlike the Oliver-Pharr method [38], h_c for Doerner and Nix's method [36] is equivalent to the fitting parameter h_c in Eq. (6.17).

In general, the updated loading-unloading curves are used to fit a given experimental loading-unloading curve data. Even though C, S and h_r are known from the functions f_1, f_2 and f_3 during the iterations, the unloading portions of the curve cannot be directly generated due to the fact that the constant A and the power law index m in Eq.(6.18) remain unknown. This indicates that the loading portion of the force can be calculated using Eq. (6.1), whereas the unloading portion of the force cannot be generated since a practical fitting function is not available. For to this reason, an alternative unloading curve fitting scheme needs to be used. It is assumed that h_c in Eq.(6.17) is the same as in Eq.(6.20), Therefore, Eq.(6.17) can be rewritten as

$$P = S\left(h - \left(h_{max} - \frac{P_{max}}{S}\right)\right) \tag{6.21}$$

The experimental unloading portion of the curve can be regenerated using Eq. (6.21). The unloading curve has effectively been linearised as shown in the line AB in Figure 6.9. It is

worth pointing out that the linearised unloading portion of the curve is interconnected with *S* and h_r, which can be obtained from the proposed dimensionless functions f_2 and f_3 during the iteration process. Consequently, the 'predicted' loading-linearised unloading portion of the curve can be calculated by new functions f_1, f_2 and f_3 to fit the given experimental loading-linearised unloading curve, when new material properties can be updated during iterations. This procedure can be performed by a program written in the C language that updates the loading-linearised unloading curves and can be processed automatically until convergence is reached.

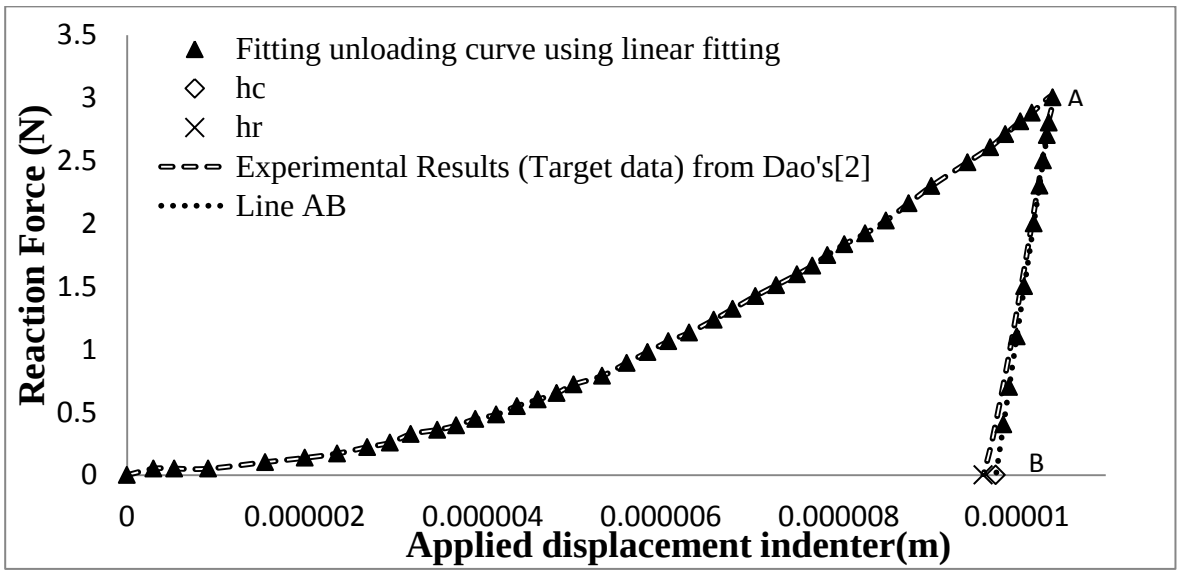

Figure 6.9 Experimental results of 6061-T6511 aluminium specimen obtained using the method of Dao *et al.*[81]

6.5.2 Optimisation results using a single indenter

The proposed optimisation algorithm is used with a single conical indenter. First, a set of material properties are chosen as the target values, as shown in **Table 6.1** and the experimental indentation loading-unloading curve for a conical indenter with an angle of 70.3° is obtained by FE simulation. At the start of the optimisation procedure, the given experimental unloading part of the curve is linearised using Eq.(6.21). The iteration procedure is used to fit the loading-linearised unloading curve and the proposed f_1, f_2 and f_3 functions are used to calculate the mechanical properties of a power-law material. The

number of iterations depends on the initial chosen values of the mechanical properties (E, σ_y, n).

Table 6.1 shows the results of three different optimisation tests with three different target values. The results show that all variables converge from their initial guessed values to their target values. The differences between target and optimised values are about 1% for Young's modulus E with higher differences for the work-hardening exponent, n and initial yield stress, σ_y. In particular, the prediction of n is not very accurate and the error is up to 50% of the target value. The reasons for the large errors in the n values may be related to the unloading slope, dP_u/dh, since it is difficult to obtain dP_u/dh from the unloading curve accurately. Dao et al. [81] also indicated that the error in the initial slope of unloading curve, dP_u/dh can cause -50% and +90% error for extracting σ_y when n>0.1.

Table 6.1 Three parameter optimisation for a single indenter

Case	Parameters	Target values	Optimised values	Percentage error	Iteration
1	E(GPa)	50	50.293	0.5%	28
	σ_y(MPa)	300	265.759	11%	
	n	0.1	0.2107	52%	
2	E(GPa)	100	98.5828	1.42%	14
	σ_y(MPa)	900	1149.892	21.67%	
	n	0.5	0.2328	53.44%	
3	E(GPa)	210	210.234	0.5%	40
	σ_y(MPa)	900	1208.438	25.1%	
	n	0.3	0.0999	67%	

Figure 6.10 shows the variation in the 'predicted' loading-linearised unloading curves during the iteration process for a single indenter. As the optimisation processes are continued, the loading-linearised unloading curves gradually approach the target solutions and finally reach the given experimental loading-linearised unloading curve. The final optimised loading-linearised unloading curve is shown in **Figure 6.11**. There is good agreement between the

given experimental and optimised loading portion of curve, whereas there is some deviation on the linearised unloading portion of the curve. It appears that this small deviation can influence on the accuracy of the optimised values.

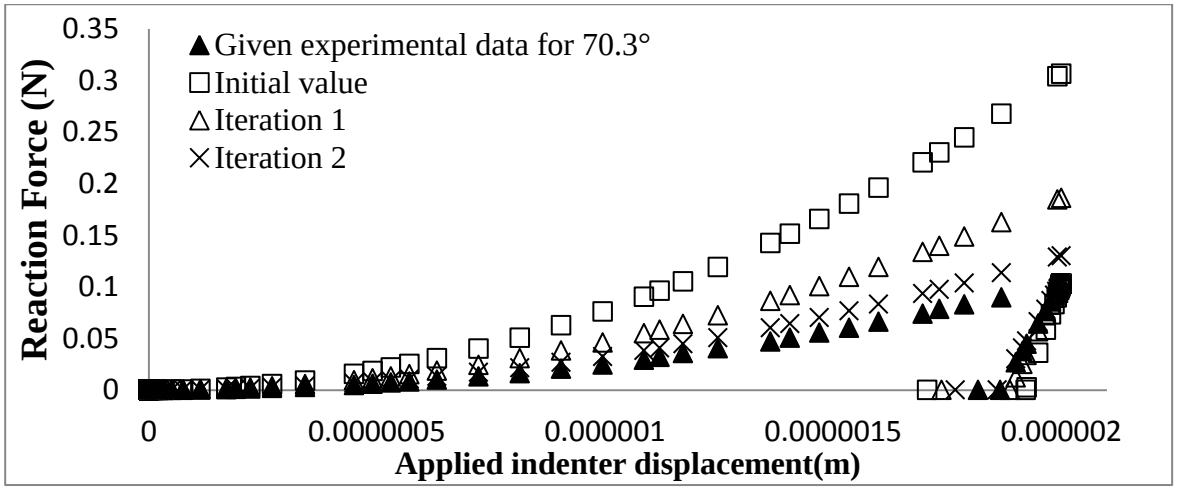

Figure 6.10 Optimisation results and target loading-linearised unloading curve of material properties (E = 50GPa, σ_y = 300MPa and 'n' =0.1)

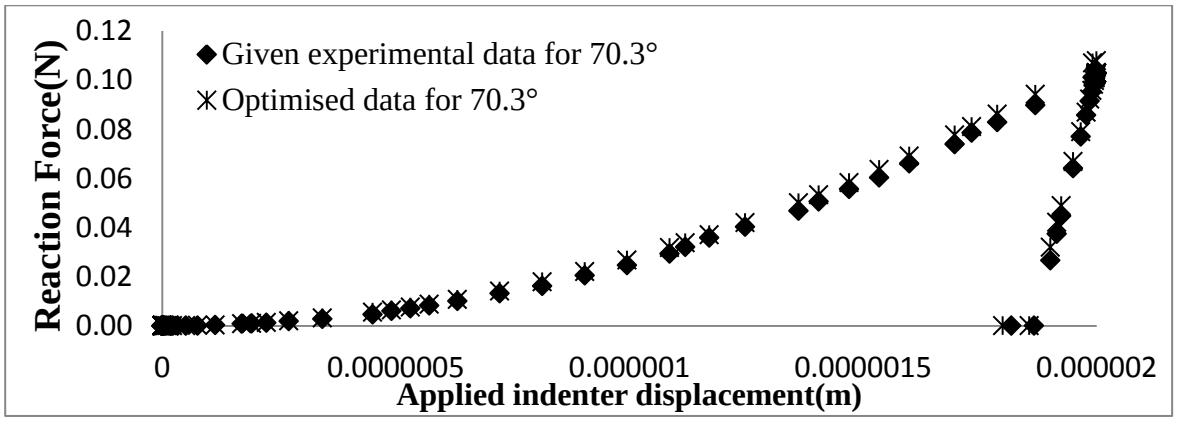

Figure 6.11 Comparison between experimental data and optimised data after iterations (E = 50GPa, σ_y = 300MPa and 'n' =0.1)

6.5.3 Optimisation results using dual indenters

Previous work has shown that, in many inverse approaches, the mechanical properties of a power-law material cannot be uniquely determined from a single indentation test [48].

Therefore, dual indenters have been proposed in order to determine the mechanical properties uniquely. Chollacoop et al. [81] used two different loading-unloading curves to improve the estimation of the elastic-plastic material properties. They found that the accuracy of the material properties is improved when a smaller indenter angle (60°) is used together with the 70.3° angle. Therefore, the present study was extended to extract mechanical properties of a power-law material from two separate loading-linearised unloading curves with half included angles of 60° and 70.3°, obtained by FEA simulation. The same optimisation procedure as performed for the single indenter was applied to the dual indenter problem. The proposed f_1, f_2 , and f_3 functions and $f_{1\ for\ 60^\circ}$ were used to calculate the optimised mechanical properties(E, σ_y, n). The optimisation process with three variables target values for the three variables was carried out with two different loading-linearised unloading curves for the angles of 60° and 70.3°, as shown in **Table 6.2**. For comparison purposes, the same target values as a single indenter test are used. For the three chosen materials, the minimum relative errors of estimation for E, σ_y and n are 0.2, 1.46 and 0 percent, respectively. It is noticeable that the errors in the values of n are up to 4.45 percent higher than the initial values for a given set of material parameters. By contrast the results for σ_y and n are significantly improved, compared with the results from a single indenter.

Table 6.2 Three parameters optimisation for dual indenters

Case	Parameters	Target values	Optimised values	Percentage error	Iteration
1	E(GPa)	50	50.119	0.2%	28
	σ_y(MPa)	300	304.469	1.46%	
	n	0.1	0.10	0%	
2	E(GPa)	100	93.304	6.7%	46
	σ_y(MPa)	900	921.817	2.36%	
	n	0.5	0.5189	3.64%	
3	E(GPa)	210	226.21	7.1%	40
	σ_y(MPa)	900	853.53	5.14%	
	n	0.3	0.314	4.45%	

The determination of plastic mechanical properties of materials using different sharp indenters has been studied by Bucaille et al.[64], based on the method reported in Dao's method [81]. They found that the decreased face angle of the indenter leads to an improved accuracy of the work-hardening exponent, n. This may be attributed to the fact that the material properties$(E, \sigma_y,$ and $n)$ are obtained from the values of the representative stress corresponding to two different indenter face angles. Furthermore, using more than one loading-unloading curve provides more constraints in the optimisation process, which are useful in finding the optimum solution of the objective functions.

Figure 6.12 shows the loading-linearised unloading curves during iterations for the dual indenters. The optimised loading-linearised unloading curve closely fits the given experimental loading-linearised unloading curve during the iterations. From **Figure 6.12** (a), it is clear that the initial values of material parameters result in curves which are larger than the given experimental loading-linearised unloading curve, whereas those in **Figure 6.12** (b) are smaller than the given experimental loading-linearised unloading curve.

Figure 6.13 shows a comparison between the experimental curves and the final optimised curves for a conical indenter with 60° and 70.3° face angles. It clear from this figure that there is a good agreement between the experimental and optimised loading-linearised unloading curves for a conical indenter with 70.3° face angle, whereas there is a small deviation for a conical indenter with a 60° face angle, particularly in the loading curves. These results demonstrate that using two indenters helps to improve the accuracy of the predicted material properties. It also demonstrates that the proposed linear fitting scheme for the unloading part of the curve based on the combination of the dimensional analysis and optimisation algorithm results in an accurate estimation of mechanical properties of a power law material.

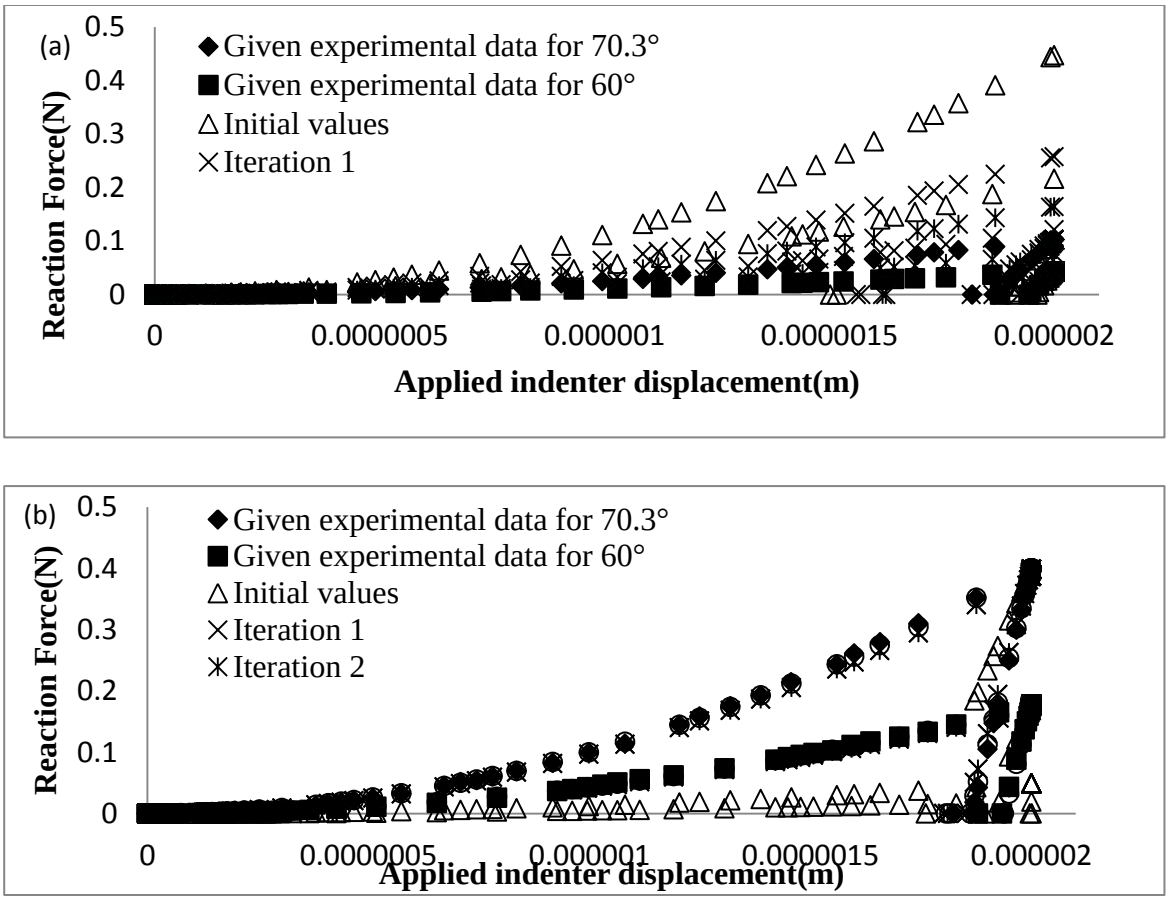

Figure 6.12 Optimisation results and target loading-unloading curve using dual indenters (a) E = 50GPa, $\boldsymbol{\sigma}_y$ = 300MPa and 'n' =0.1 (b) E = 210GPa, $\boldsymbol{\sigma}_y$ = 900MPa and 'n' =0.3

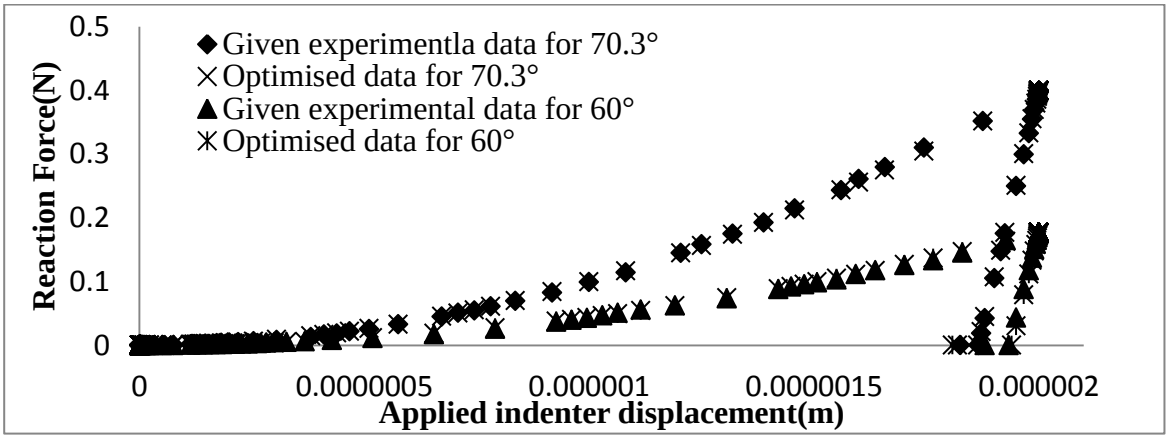

Figure 6.13 Comparison between given experimental curves and optimised curves for a conical indenter with 60° and 70.3° face angles after iterations (E = 210GPa, σ_y = 900MPa and 'n' =0.3)

6.6 Non-linear power-law unloading fitting scheme

Section 6.5.1 mainly focuses on the linearised unloading fitting scheme, which contains the main characteristics of the loading- unloading behaviour. In this section, a new non-linear power-law unloading fitting scheme is used to obtain material properties. This new method can cover a wider range of material properties since the power law fitting, referred to as the Oliver-Pharr method, is more suitable for fitting the unloading curve. In general, the unloading curve can be expressed using the Oliver-Pharr method as follows [1]

$$P = A(h - h_r)^m \tag{6.22}$$

where *m* is the power law index, and *A* is a constant.

The relationship between the normalised $\frac{F_{max}}{(h_m - h_f)^m}$ and A and the relationship between the normalised $\frac{mF_{max}}{(h_m - h_f)}$ and S are shown in **Figure 6.14** and **Figure 6.15**, respectively. From those relationships, the constants A and m in Eq.(6.22) can be expressed as follows

$$A = \frac{F_{max}}{(h_{max} - h_f)^m} \tag{6.23}$$

$$S = \frac{dF}{dh} = \frac{mF_{max}}{(h_{max} - h_f)} \tag{6.24}$$

which can be rewritten as

$$m = \frac{S(h_{max} - h_f)}{F_{max}} \tag{6.25}$$

where h_f and S can be obtained by functions f_2 and f_3. As can be seen in **Figure 6.16,** the new fitting curve is effectively fitted to approximately 68% of the unloading portion of curve. The reason for this is that the value of the constant 'm' becomes zero when $h_{max} = h_f$. Therefore, the full unloading curve cannot be updated during the iterations. Furthermore, it is worth pointing out that this unloading portion of the curve is interconnected with *S* and h_r, which can be obtained from the dimensionless f_2 and f_3 functions during the iteration process. Consequently, the 'predicted' loading-unloading portions of the curve can be

calculated using new f_1, f_2 and f_3 functions to fit the given experimental loading-unloading curve.

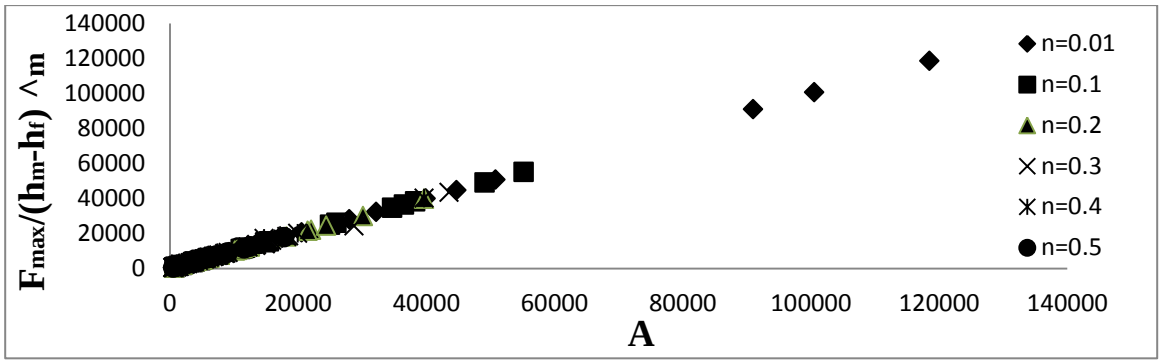

Figure 6.14 Relationship between $\frac{F_{max}}{(h_m-h_f)^m}$ and A for a conical indenter with 70.3° face angle

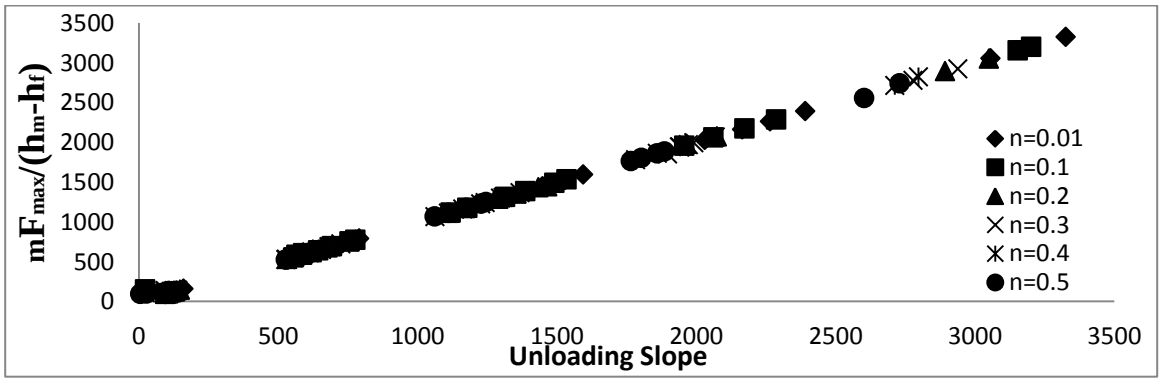

Figure 6.15 Relationship between $\frac{mF_{max}}{(h_m-h_f)}$ and S for a conical indenter with 70.3° face angle

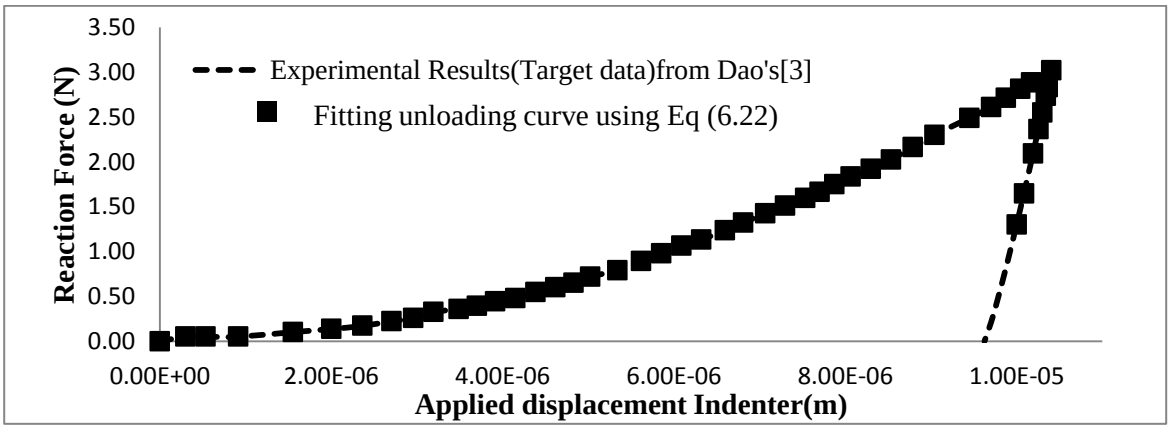

Figure 6.17 Fitting curve and experimental results of 6061-T6511 aluminium specimen from Dao's method [3]

6.6.1 Optimisation results using a single indenter

The proposed optimisation algorithm has been used with a single conical indenter. Firstly, a set of material properties has been chosen as the target values, as shown in **Table 6.3** and the experimental indentation loading-unloading curve for an indenter angle of 70.3° is obtained by FE simulation. A third of the given experimental unloading part of the curve can be deleted to start the optimisation procedures. The iteration procedure is used to fit this loading-unloading curve and the functions f_1, f_2 and f_3 can be used to calculate the mechanical properties of a power-law material. The number of iterations depends on the initial chosen values of the mechanical properties (E, σ_y, n).

Table 6.3 shows the results of three different optimisation tests with three different target values. The results show that the iterations have converged, but the variables are not very close to the target values. The differences between target and optimised values are about 8-10% for Young's modulus E with higher differences for the work-hardening exponent, n and the initial yield stress, σ_y. In particular, the prediction of n is not very accurate and the error is up to 60% from the target value. The reasons for the large errors in the n values may be related to the unloading slope, dP_u/dh, since it is difficult to obtain dP_u/dh from the unloading curve accurately. Dao et al.[81] also indicated that the error in the initial slope of the unloading curve, dP_u/dh can cause approximately ±50% error in extracting σ_y when n>0.1.

Figure 6.17 shows the variation in the 'predicted' loading- unloading curves during the iteration process for a single indenter. As the optimisation processes are continued, the loading-unloading curves gradually approach the target solutions and finally reach the given experimental loading-unloading curves. The final optimised loading-unloading curve is shown in **Figure 6.18**. There is a good agreement between the given experimental and optimised loading portion of curves, whereas there is some deviation on the unloading portion of the curve. It appears that this small deviation can have a large influence on the accuracy of the optimised material constants.

Table 6.3 Three parameter optimisation for a single indenter

Cases	Parameters	Target values	Optimised values	Percentage error	Iteration
1	E(GPa)	50GPa	45.973GPa	8.05%	43
	σ_y(MPa)	300MPa	250.52MPa	16.5%	
	n	0.4	0.519	29.75%	
2	E(GPa)	100GPa	91.45GPa	8.55%	14
	σ_y(MPa)	900MPa	738.25MPa	17.97%	
	n	0.3	0.50	66.7%	
3	E(GPa)	210GPa	186.67GPa	11.10%	41
	σ_y(MPa)	900MPa	1197.90MPa	33.10%	
	n	0.3	0.1	66.7%	

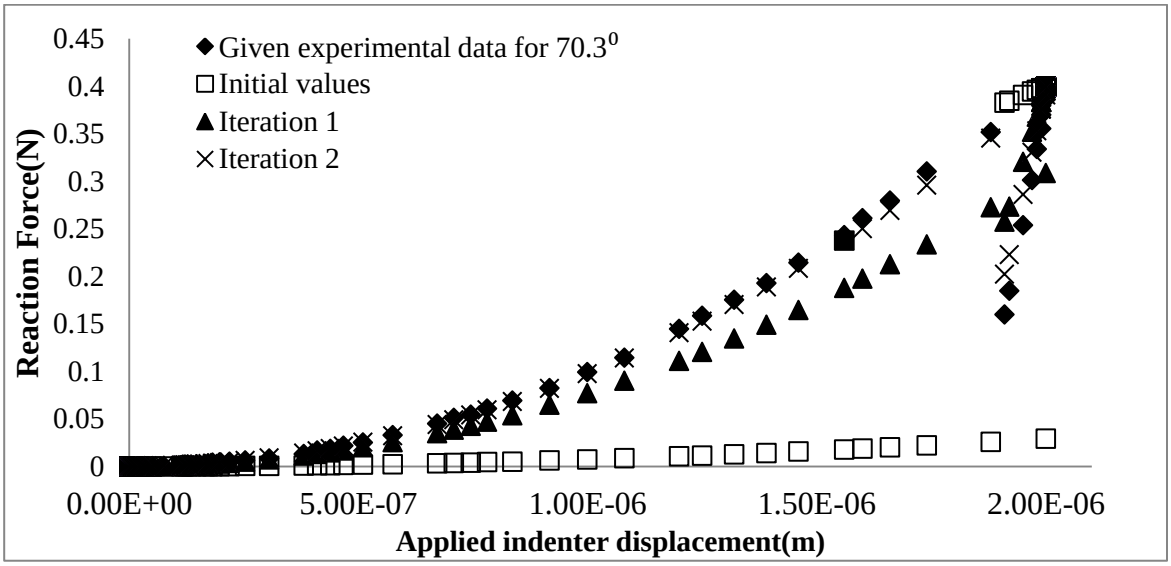

Figure 6.17 Optimisation results and target loading-unloading curve of material properties (E = 210GPa, σ_y = 900MPa and 'n' =0.3)

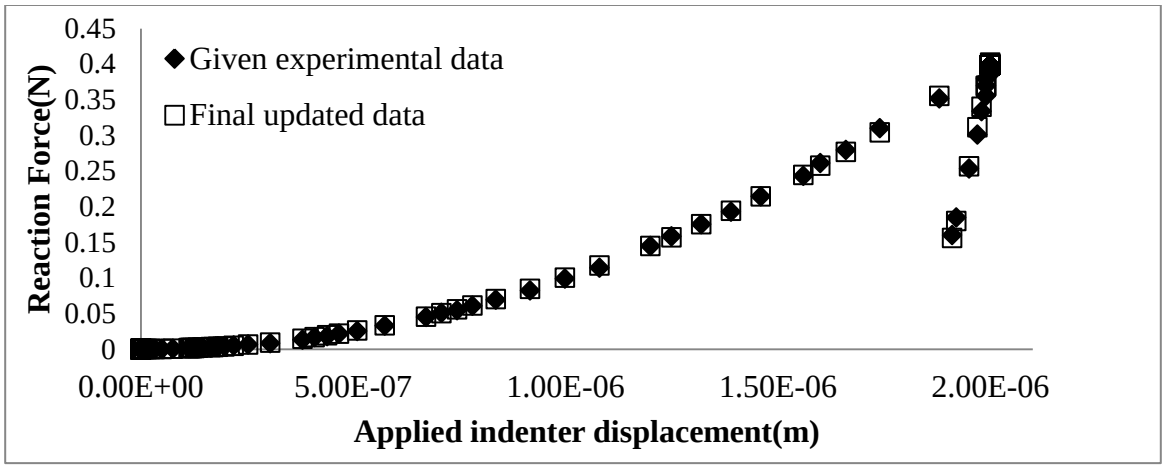

Figure 6.18 Comparison between experimental data and optimised data after iterations (E = 210GPa, σ_y = 900MPa and 'n' =0.3)

6.6.2 Optimisation results using dual indenters

Previous work has shown that, in many inverse approaches, the mechanical properties of a power-law material cannot be uniquely determined from a single indentation test [9]. Therefore, dual indenters have been proposed in order to determine the mechanical properties uniquely. Based on Dao's method [81], two different loading-unloading curves can be used to improve the estimation of the elastic-plastic material properties. They found that the accuracy of the material properties is improved when a smaller indenter angle (60°) is used together with the 70.3° angle. Therefore, the present study is extended to extract mechanical properties of a power-law material from two separate loading- unloading curves with half included angles of 60° and 70.3°, obtained by FE simulation. The same optimisation procedure has been performed as for the single indenter. The proposed functions $f_1, f_2,\ f_3$ and $f_{1\ for\ 60°}$ $f_{2\ for\ 60°}$, $f_{3\ for\ 60°}$ can be used to calculate the optimised mechanical properties (E, σ_y, n).

The optimisation process with three variables has been carried out with two different loading-unloading curves for the angles of 60° and 70.3°, as shown in **Table 6.4**. For comparison purposes, the same target values as a single indenter test are used. For the three chosen materials, the minimum relative errors of estimation for E, σ_y and n are 7.26, 1.5 and 3%, respectively. It is noticeable that the values of Young's modulus are generally underestimated,

compared with the initial values for a given set of material parameters. By contrast the results for σ_y and n are significantly improved, compared with the results from a single indenter.

Table 6.4 Three parameters optimisation for dual indenters

Cases	Parameters	Target values	Optimised values	Percentage error	Iteration
1	E(GPa)	210GPa	194.97GPa	7.26%	41
	σ_y(MPa)	900MPa	913.47MPa	1.5%	
	n	0.3	0.291	3%	
2	E(GPa)	50GPa	46.19GPa	7.62%	36
	σ_y(MPa)	300MPa	306.77MPa	2.25%	
	n	0.4	0.384	4%	
3	E(GPa)	100GPa	91.79GPa	8.21%	13
	σ_y(MPa)	900MPa	896.85MPa	0.35%	
	n	0.3	0.317	5.6%	

The determination of plastic properties using different sharp indenters have been studied by Bucaille et al.[64], based on Dao's method [81]. They found that the decreased face angle of the indenter leads to an improved accuracy of the work-hardening exponent, *n*. The reason for this may be attributed to the fact that the material properties(E, σ_y, n) are obtained from the values of the representative stress corresponding to two different loading situations. Furthermore, using more than one loading-unloading curve provides more constraints in the optimisation process, which are useful in finding the optimum solution of the objective functions.

Figure 6.19 shows the loading-unloading curves during the iterations for dual indenters. The optimised loading-unloading curve fits well with the given experimental loading-unloading curve during the iterations. From **Figure 6.19** (a), it is clearly illustrated that loading-unloading curve, which is generated by the initial values of material parameters, is a few times lower than the given experimental loading-unloading curve, whereas in **Figure 6.19**(b) it is larger than the given experimental loading-unloading curve.

Figure 6.20 shows the comparison between the experimental curves and the optimised curves for a conical indenter with 60° and 70.3° face angles. It clearly shows that there is a good agreement between the given experimental and the optimised loading-unloading curves for a conical indenter with a 70.3° face angle, whereas there is a small deviation for a conical indenter with a 60° face angle, particularly in the loading curves. These results show that using two indenters helps to improve the accuracy of the predicted material properties. This demonstrates that the proposed fitting scheme for the unloading part of the curve based on a combination of the dimensional analysis and optimisation algorithm results in an accurate estimation of mechanical properties of a power law material.

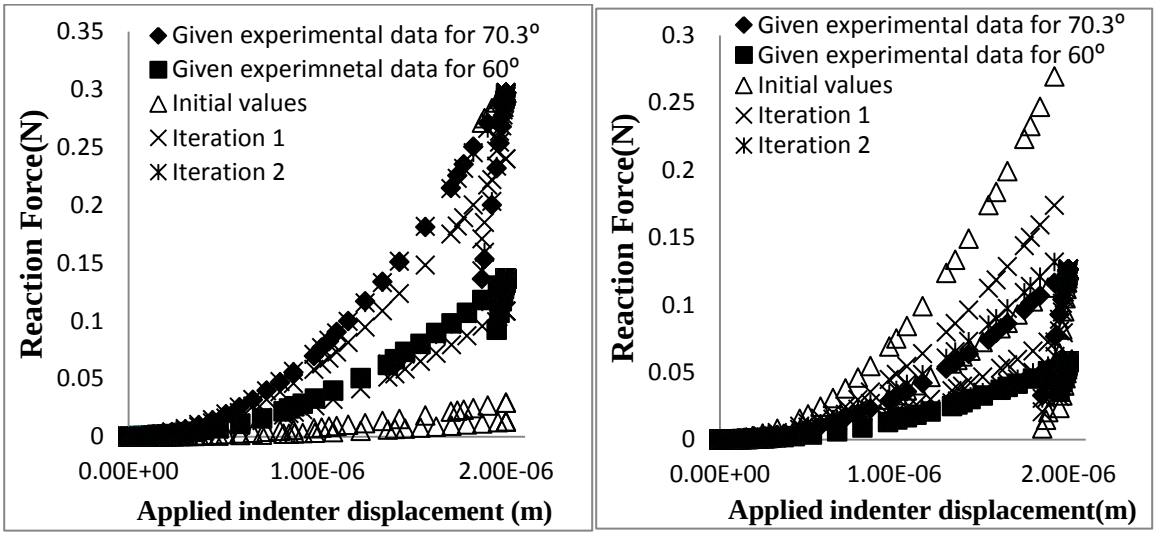

Figure 6.19 Optimisation results and target loading-unloading curve using dual indenters (a) E = 100GPa, σ_y = 900MPa and 'n' =0.3 (b) E = 50GPa, σ_y = 300MPa and 'n' =0.4

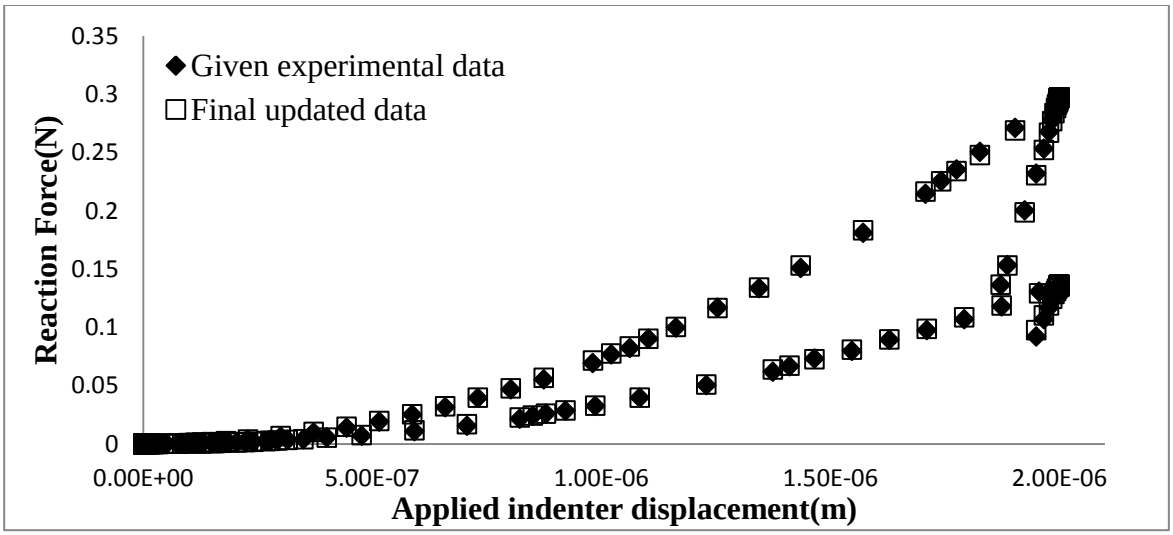

Figure 6.20 Comparison between given experimental curves and optimised curves for a conical indenter with 60° and 70.3° face angles after iterations (E = 210GPa, σ_y = 900MPa and 'n' =0.3)

6.7 Conclusions

In **Chapter 6,** dimensional analysis is combined with a new optimisation algorithm to extract the elastic-plastic mechanical properties from loading–unloading curves without the need to perform FE analysis. In fact, FE analysis is only used to determine the mathematical curve fitting parameters. It has been suggested in the literature [81] that the representative strain 0.033 results in relationships which are independent of the work-hardening exponent, *n*. However, an extensive numerical FE study of 174 cases has shown in this study that the representative strain 0.033 is not independent of the value of *n*. Hence, a different representative strain of 0.0115, as suggested by Ogasawara [97], is used in this study which results in relationships which are practically independent of the value of *n*. A comprehensive parametric FE study of 174 cases is conducted to establish new dimensionless functions to relate the elastic-plastic properties to the indentation response, based on the method reported in Dao et al. [84].

A new algorithm has been used to extract three elastic-plastic mechanical properties (E, σ_y, n) from the loading-unloading curves using the proposed dimensionless functions. This new

technique is based on a non-linear least-square routine MATLAB function (called LSQNONLIN) to produce the best fit between the given experimental loading-unloading data and the optimised data. Both a linearised and a power-law unloading fitting scheme are used. These fitting schemes contain the characteristic initial slope of unloading curve, S, and the residual depth of indenter, which are already known from function f_2 and f_3. However, no specific function is used for the unloading curve due to the fact that the mechanical properties of a power-law material are related to the complicated contact interaction between the test specimen and the indenter. Therefore, further research should be undertaken to obtain better fitting functions for the unloading curve.

With respect to the optimisation results, when a single indenter is used, there are significant differences in the accuracy of the optimised values of n and σ_y used in the target loading-unloading curve. Therefore, two indenter geometries, based on two different face angles of the conical indenter, are used to obtain unique and more accurate estimations of the elastic-plastic material properties.

7 Obtaining material properties from indentation loading-unloading curves using simplified equations

7.1 Introduction

Chapter 5 is focused on the FE simulation with optimisation techniques to extract the material properties directly from loading-unloading curves using a single indentation, without the need for using results from two indentations loading-unloading curves, see Kang et al [106]. Despite using different geometries of indenters (conical, Berkovich and Vickers) and applying various initial guess values, the new algorithms are shown to converge to the correct mechanical properties of a power-law material. The optimisation techniques are also applied to real experimental test data from laboratory tests. However, extensive computational time is required in such an approach due to the fact that the optimisation procedure is based on iterative FE computations.

In **Chapter 6**, a combined dimensional analysis and optimisation approach was developed for determining the elasto-plastic mechanical properties of power law materials, without the need for iterative FE analysis, see Kang et al [107]. A parametric study using FE analysis is first conducted to construct the appropriate dimensional functions. The optimisation algorithm with single and dual indenters is then used to obtain the material properties from the given loading-unloading curves. Different sets of material properties are used and the accuracy and validity of the predicted mechanical properties using a single indenter or dual indenters are assessed.

The objective of this study is to devise more simplified combined mathematical-optimisation approaches to obtain the elastic-plastic mechanical properties (E, σ_y, n) from experimental loading-unloading indentation curves.

7.2 Frame work for analysis

In **Section 6.2**, the relationship between the portions of loading and unloading curves can be investigated based on dimensional analysis. The relationship between the normalised

$\frac{F_{max}}{(h_m - h_f)^m}$ and A and the relationship between the normalised $\frac{mF_{max}}{(h_m - h_f)}$ and S are discussed in **Section 6.6**. Based on these relationships, more simplified equations can be used to obtain material properties from indentation loading-unloading curves.

In order to describe the power law elastic-plastic behaviour of the material, three material parameters (E, σ_y, n) are usually needed. Dao et al. [81, 94] have found that a representative strain $\varepsilon_{pl} = 0.033$ can be identified for the conical indenter ($\alpha = 70.3°$) within a specified range of material parameters. The dimensionless relationship between $C/\sigma_y\langle\varepsilon_r\rangle$ and the $E^*/\sigma_y\langle\varepsilon_r\rangle$ have been shown to be practically independent of n with a representative strain ε_r=0.0115, see **Section 6.4.1**. Therefore, a representative strain ε_r=0.0115 is used in this study. Since the loading-unloading indentation responses are known, the equation covering the loading and unloading portion of the curves can be assumed as follows:

$$C = \sigma_r k_1 \left(\ln\left(\frac{E^*}{\sigma_r}\right)\right) \tag{7.1}$$

and when substituted into Eq.(6.1) in Chapter 6, can be expressed as follows:

$$P_{Loading} = \sigma k_1 \left(\ln\left(\frac{E^*}{\sigma}\right)\right) {h_r}^2 \tag{7.2}$$

where, $\sigma = \sigma_y \left(1 + \frac{E}{\sigma_y} 0.0115\right)^n$, h is the displacement of the indenter, σ_y is the initial yield stress, E is Young's modulus and n is the work-hardening exponent. Moreover, the final residual depth of the indenter h_f can be written as follows:

$$h_r = h_m n k_2 \left(\ln\left(\frac{\sigma}{E^*}\right)\right) \tag{7.3}$$

where h_m is the maximum displacement of the indenter. **Table 7.1** summarises the equations used in this study.

Table 7.1. Equations used to represent loading and unloading curves

Loading portion of curve	Unloading portion of curve
$P_{Loading} = Ch^2$ $C = \sigma k_1 \left(\ln\left(\frac{E^*}{\sigma}\right)\right)$ $\sigma = \sigma_y \left(1 + \frac{E}{\sigma_y} 0.0115\right)^n$	$P_{Unloading} = A(h - h_r)^m$ $m = \frac{S(h_{max} - h_r)}{F_{max}}$ A= $\frac{F_{max}}{(h_{max} - h_r)^m}$ $h_f = h_m n k_2 \left(\ln\left(\frac{\sigma}{E^*}\right)\right)$ where, *S* is the initial slope of unloading curve

7.3 An optimisation procedure for determining material properties

Based on the assumed loading-unloading equations and optimisation techniques, an inverse method is developed to determine the material properties from indentation loading-unloading curves, without using a parametric study and further FE analysis. The optimisation technique is used to determine the elastic-plastic mechanical properties for a given set of indentation data using an iterative procedure based on a MATLAB nonlinear least square routine [90] to produce the best fit between the given data and the predicted optimised data.

In **Chapter 6**, the complicated dimensional functions used to represent the loading-unloading curves are constructed using parametric FE studies. In the simplified approach, these complicated relationships are simply expressed in terms of two key variables, k_1 and k_2 which require proper constraint sets in the optimisation scheme. The non-linear least-square with curve fitting optimisation function (called LSQNONLIN in MATLAB), used in the **Chapter 5**, does not handle equality constraints. Therefore, four different algorithms (Trust Region Reflective, Active Set, SQP and Interior Point) with FMINCON functions are introduced in MATLAB [90]. Firstly, the trust Region Reflective, Active Set and SQP in MATLAB are used to find a suitable optimisation algorithm. However, based on these algorithms, the optimisation solutions are extremely unstable and the first-order optimality, which is a measure of how close a point x is to its optimal value, is never close to zero.

Therefore, the FMINCON function with an interior-point Algorithm, which helps to find the minimum of a constraint nonlinear multivariable function, is used. The optimisation model is:

$$\mathrm{F}(x) = \frac{1}{2}\sum_{\mathrm{i}=1}^{\mathrm{N}}\left[\mathrm{P}(x)_{\mathrm{i}}^{\mathrm{pre}} - \mathrm{P}_{\mathrm{i}}^{\mathrm{exp}}\right]^2 \rightarrow \min \qquad (7.4)$$

$$x \in R^n \qquad (7.5)$$

$$LB \leq x \leq UB \qquad (7.6)$$

where $\mathrm{P}(x)_{\mathrm{i}}^{\mathrm{pre}}$ and $\mathrm{P}_{\mathrm{i}}^{\mathrm{exp}}$ are the predicted indentation force and the experimental force from the target data, respectively, at a specific position *i*, within the loops, N is the total number of points used in the measured loading-unloading loop. F(x) is the objective function, x is the optimisation variable set (a vector in the *n*-dimensional space, R^{n}), which for this specific case contains the full set of the material constants in the model, i.e.

$$x = \left[k_1, k_2, E, \sigma_y, n\right]^T \qquad (7.7)$$

and *LB* and *UB* are the lower and upper boundaries of $\boldsymbol{x}$ allowed during the optimisation. For example, the work-hardening exponent values for most engineering materials are between 0.1 and 0.5. Lower and upper limits have been imposed on the values of Young's modulus between 10 GPa to 210 GPa and yield stress values between 10 MPa and 2500 MPa in order to cover all practical engineering materials during the optimisation procedures. The bounds of $\mathbf{k_1}$ and $\mathbf{k_2}$ are known from the parametric study in **Chapter 6**. The number of sets of material properties means that approximately 180 sets of mechanical properties are used to obtain the minimum and maximum values of $\mathbf{k_1}$ and $\mathbf{k_2}$, based on the proposed range of the material properties**.** In order to obtain the loading curvature, C, the final residual indenter depth, $\mathbf{h_r}$ and the initial slope of unloading curve, S, it is required to fit a power law function to the experimental loading-unloading curve data. In order to obtain the range of the $\mathbf{k_1}$ and $\mathbf{k_2}$ values, the equations of C and $\mathbf{h_r}$ in **Table 7.1** can be re-written as

$$\boldsymbol{k_1} = \frac{\boldsymbol{C}}{\boldsymbol{\sigma}\left(\boldsymbol{ln}\left(\frac{E^*}{\boldsymbol{\sigma}}\right)\right)} \qquad (7.8)$$

$$k_2 = \frac{h_r}{h_m n\left(\ln\left(\frac{\sigma}{E^*}\right)\right)} \qquad (7.9)$$

Therefore, the lower and upper boundaries for all variables can be written as follows:

$$\begin{Bmatrix} 10GPa < E < 300GPa \\ 10MPa < \sigma_y < 2500MPa \\ 0 < n < 0.5 \\ 8 < \mathbf{k_1} < \mathbf{16} \\ -2.5 < \mathbf{k_2} < -\mathbf{0.1} \end{Bmatrix} \quad (7.10)$$

Furthermore, from Eqs (7.1) and (7.3), practical physical equality constraints are imposed during the analysis, as follows:

$$\begin{Bmatrix} \left|\sigma k_1 \left(\ln\left(\frac{E^*}{\sigma}\right)\right) - C\right| = 0 \\ \left|h_m n k_2 \left(\ln\left(\frac{\sigma}{E^*}\right)\right) - h_r\right| = 0 \end{Bmatrix} \quad (7.11)$$

Arbitrary values of $(k_1, k_2, E, \sigma_y, n)$ have been chosen as initial values and the proposed optimisation algorithms are used to find the optimised values of k_1, k_2, E, σ_y and n from which the best fits between the experimental and predicted loading-unloading curve can be achieved. The general optimisation algorithm used in this study is illustrated in **Figure 7.1**. Since the initial guess values for k_1, k_2, E, σ_y and n are provided, the optimisation is carried out to update the indentation force for loading and unloading. In general, the displacements of the indenter for the loading and unloading portions are fixed. The indentation force of the loading and unloading portion of curves can be calculated from the updated parameters (k_1, k_2, E, σ_y and n) to fit the target curve during the iterations.

7.4 Optimisation results using a single indenter

The proposed optimisation algorithm has been used with a single conical indenter. Firstly, a set of material properties have been chosen as the target values, as shown in **Table 7.2** and the experimental indentation loading-unloading target curve for an indenter angle of 70.3° is obtained by FE simulation. Then, the maximum indenter displacement,h_{max}, the maximum reaction force from substrate, F_{max}, the initial slope of unloading curve, S, the loading curvature, C, and indenter residual displacement after unloading, h_r can be obtained by non-linear least square fitting method. Since those constant values are known, the optimisation procedures can be started. The iteration procedure is used to fit the experimental target loading-unloading curve. The proposed equations in **Table 7.1** can be used to calculate the k_1, k_2 parameters and mechanical properties of a power-law material, E, σ_y and n. The

number of iterations depends on the initial chosen values of the mechanical properties ($k_1,\ k_2, E, \sigma_y, n$).

Table 7.2 shows the results of three material properties parameters (E, σ_y and *n*) optimisation for a single indenter with different initial values, where all variables converge from their initial guess parameters to optimised parameters. Despite the fact that different initial values are used, the optimised solutions give almost the same values. However, the differences between the target and optimised values are about 15% for Young's modulus *E* with a higher difference for the working-hardening exponent, n and initial yield stress, σ_y. In particular, the prediction of σ_y is not very accurate and errors go up to 190% from the target values.

Table 7.3 shows the results of three parameters (E, σ_y and *n*) optimisation with different target values. It is interesting to see from all cases that the optimisation solutions for Young's modulus *E* are generally in good agreement compared with the target values, even though a single indenter is used. However, the optimised values of Yield stress and work-hardening exponent, σ_y and n, are not very accurate. It is noticeable that the optimised parameters of case 2 have the smallest relative errors of estimation for E, σ_y and n. **Figure 7.2** shows the variation in the 'optimised' loading- unloading curves during the iteration process for a single indenter. As the optimisation processes are continued, the loading-unloading curves gradually approach the target solutions and finally reach the given experimental loading-unloading curves. The final optimised loading- unloading curve is shown in **Figure 7.3.**

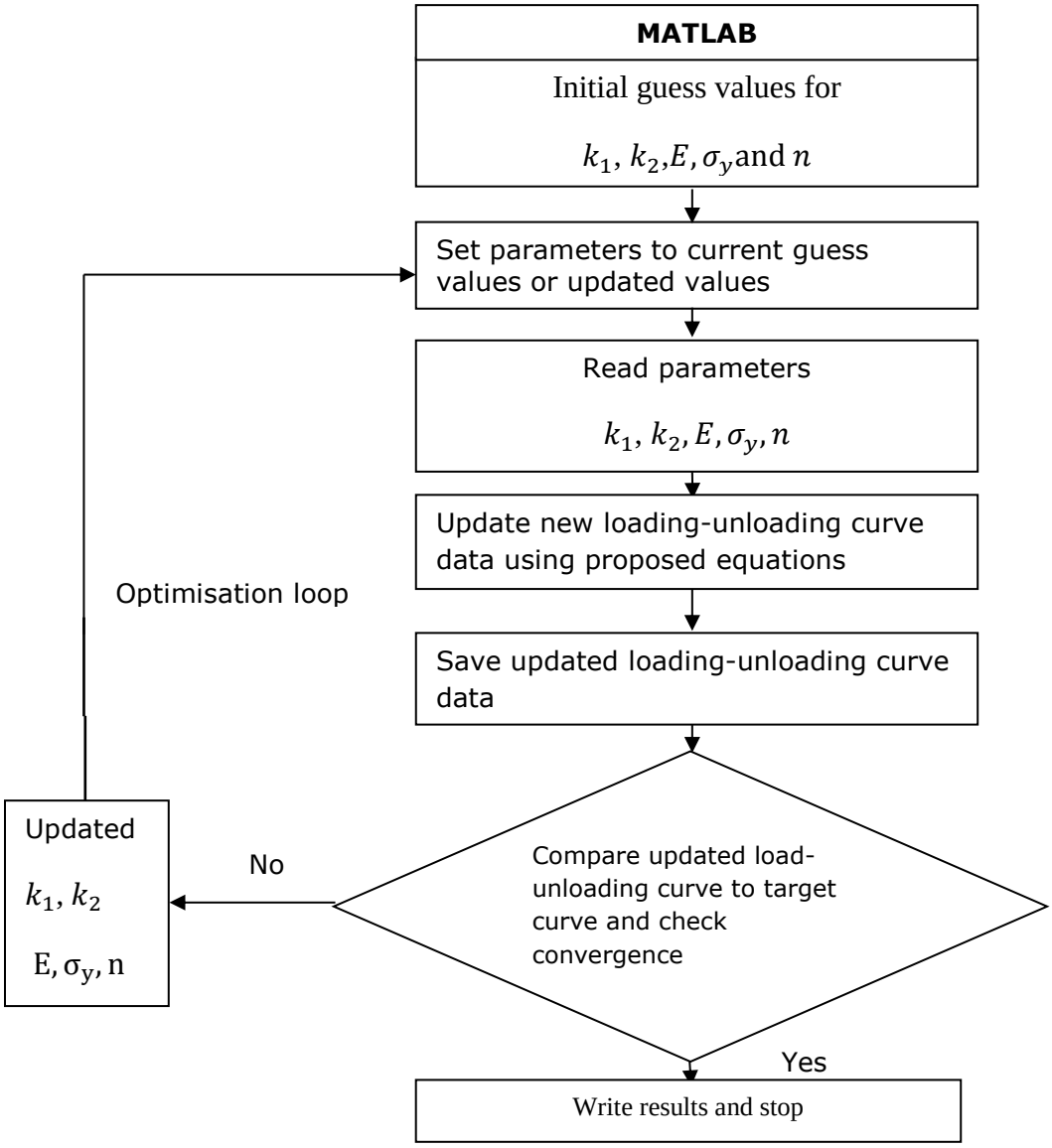

Figure 7.1 Flow chart of the optimisation algorithm to determine the mechanical properties from the loading-unloading

Table 7.2 Three parameters optimisation for a single indenter with different initial values

Case	parameters	Target values	Initial values	Optimised values	Percentage Error for E,σ_y,n	First-order Optimality
1	k_1 k_2 E(GPa) σ_y(MPa) n	12.636 -0.468 210GPa 900MPa 0.4	12.636 -0.468 190GPa 700MPa 0.4	11.428 -0.789 181.71GPa 1731.89MPa 0.254	 -13.4% 192% -36%	3.764e-2
2	k_1 k_2 E(GPa) σ_y(MPa) n	12.636 -0.468 210GPa 900MPa 0.4	12.636 -0.468 120GPa 1500MPa 0.3	11.37 -0.79 183.21GPa 1738.65MPa 0.253	 -13.4% 192% -36%	3.450e-2
3	k_1 k_2 E(GPa) σ_y(MPa) n	12.636 -0.468 210GPa 900MPa 0.4	12.636 -0.468 50GPa 400MPa 0.1	11.401 -0.789 182.38GPa 1735.08MPa 0.2541	 -13.4% 192% -36%	2.288e-2

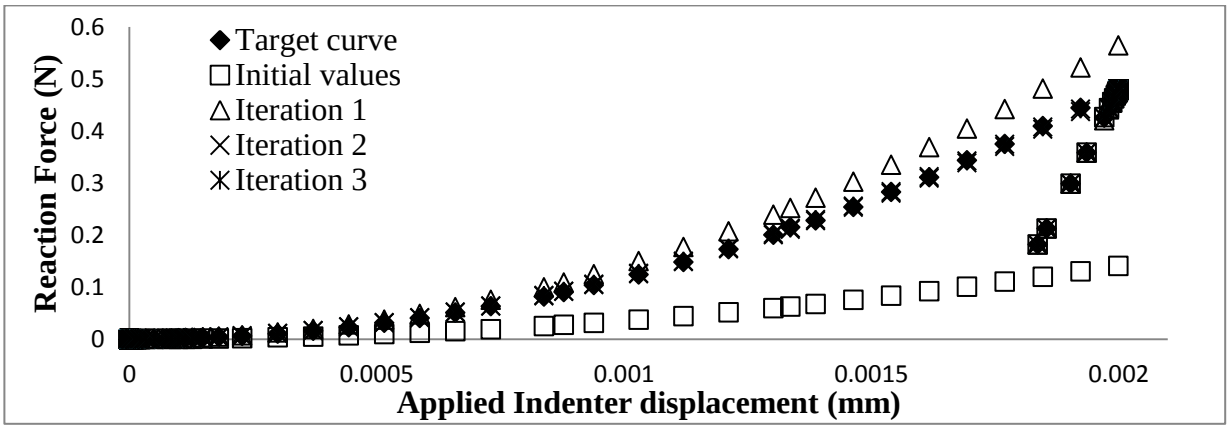

Figure 7.2 Optimisation results and target loading-unloading curve of material properties (Target values, E = 150GPa, σ_y = 1500MPa and 'n' =0.3)

Table 7.3 Three parameters optimisation with different target values

Case	parameters	Target values	Initial values	Optimised values	Percentage Error for E,σ_y,n	First-order Optimality
1	k_1 k_2 E(GPa) σ_y(MPa) n	12.636 -0.468 210GPa 900MPa 0.4	12.636 -0.468 211GPa 910MPa 0.39	11.55 -0.784 178.65GPa 1713.38MPa 0.256	 -15% 190% -36%	4.046e-2
2	k_1 k_2 E(GPa) σ_y(MPa) n	13.444 -0.952 150GPa 1500MPa 0.2	13 -0.5 90GPa 1200MPa 0.24	11.14 -0.779 175.68GPa 1696.77MPa 0.245	 14.6% 13.1% 18.3%	7.506e-2
3	k_1 k_2 E(GPa) σ_y(MPa) n	13.302 -0.592 100GPa 300MPa 0.3	13.302 -0.592 60GPa 200MPa 0.25	 128.23GPa 1127.74MPa 0.23	 22% 375 % -23.3%	3.091e-2

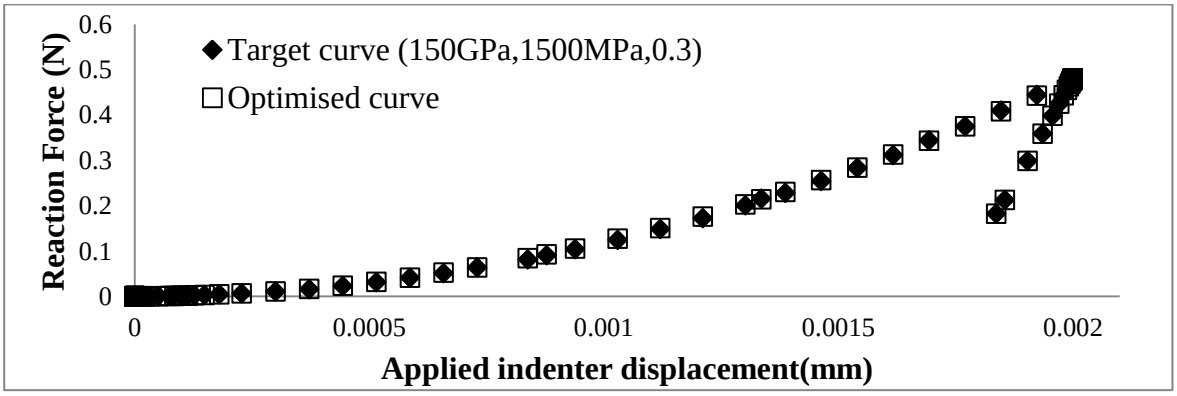

Figure 7.3 Comparison between experimental data and optimised data after iterations (Target values, E = 150GPa, σ_y = 1500MPa and 'n' =0.3)

Since the proposed loading-unloading equations do not consider the complicated physical relationship between indenter and a specimen, it can be thought that the FE simulated 'target' loading-unloading and optimised curves after final optimisation may be virtually matched each other. To prove that, the sets of mechanical properties (E, σ_y and n) obtained in **Table 7.2** (case 1) are inputted in the material section in ABAQUS input file. **Figure 7.4** shows comparison between FE simulated 'target' curve and optimised data after final iteration.

Figure 7.5 shows a comparison between the FE simulated curves based on the final optimised values and the final optimised loading-unloading curve generated by MATLAB for case 1 in **Table 7.2**. As can be seen from two different curves, loading-unloading curves in **Figure 7.4** are perfectly matched after obtained by optimisation solution in MATLAB, whereas the sets of optimised parameters after final iterations is resubmitted in the material section of ABAUS input file and it could not be exact match with a FE simulated 'target' curve in **Figure 7.5**.

The deviation between the optimised and target parameters, shown in **Table 7.2,** and significant changes of the optimised (E, σ_y and n) parameters, despite small changes of k_1 and k_2, indicates the proposed equations are very sensitive to the values of k_1 and k_2. The physical mechanical relationships between k_1 and k_2 and the mechanical properties (E, σ_y and n) are not embedded in the simplified equations. This means that the mechanical properties based on a single indentation loading-unloading curve cannot be uniquely obtained without further mechanical relationships governing the complicated responses between a specimen and an indenter.

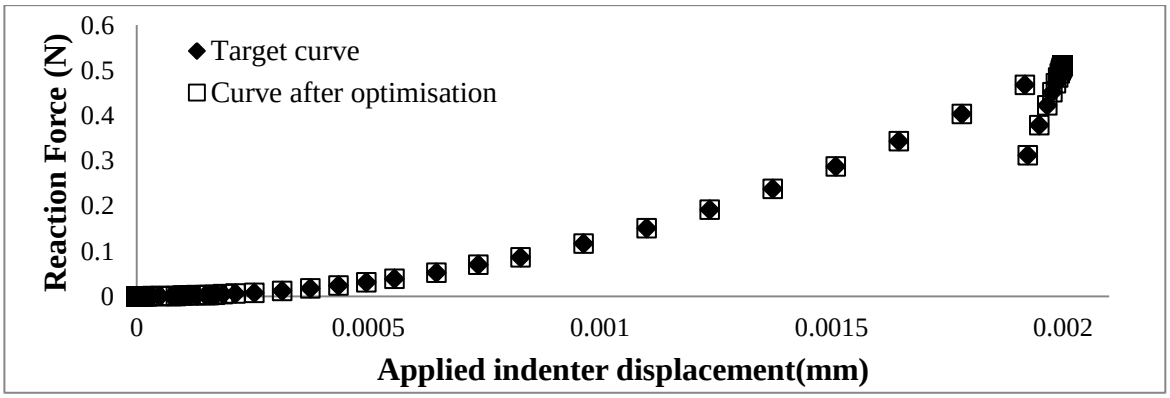

Figure 7.4 Comparison between FE simulated 'target data' base on target value, E = 210GPa,

σ_y = 900MPa, n = 0.4 and optimised data after final iterations for case 1 in **Table 7.2**, which generated by MATLAB algorithm.

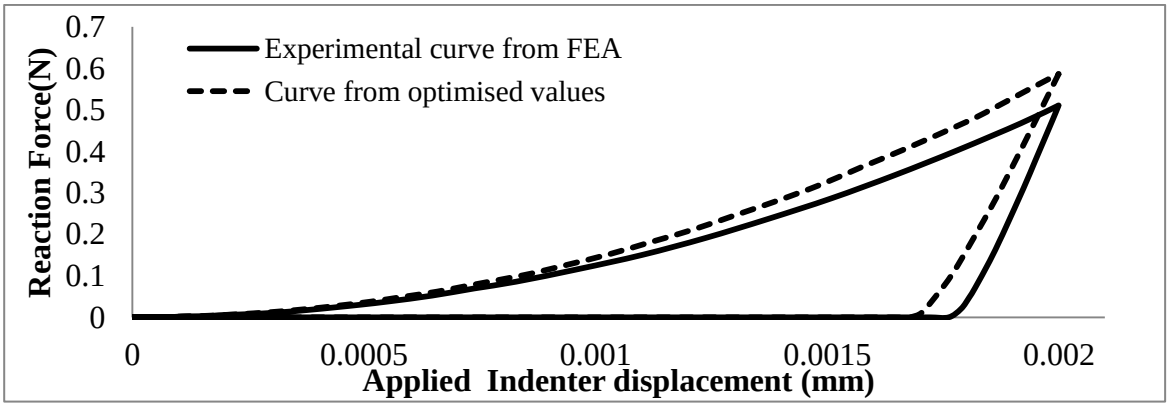

Figure 7.5 Comparison between the FE simulated curves after resubmit the final optimised values in the material section of ABAQUS input file and the curve generated from MATLAB with final optimised values for case 1 in **Table 7.2**. It is noted that the final optimised values is E = 181.71GPa, σ_y = 1731.89MPa, n = 0.254

7.5 Optimisation results using dual indenters

In **Section 7.3**, it has shown that, in many inverse approaches, the elastic-plastic mechanical properties of a power-law material could not be determined uniquely from a single indentation loading-unloading curve. Therefore, dual indenters have been proposed in order to determine the mechanical properties uniquely. Based on Dao's method [81], two different loading-unloading curves can be used to improve the estimation of the elasto-plastic material properties. They found that the accuracy of the material properties is improved when a smaller (sharper) indenter angle (60°) is used together with the 70.3° angle. The present study is extended to extract mechanical properties of a power-law material from two separate loading- unloading curves with half included angles of 60° and 70.3°, obtained by FEA simulation. The above optimisation procedure is used for dual indenters with seven parameters. From the parametric study in **Chapter 6**, the range of bounds $k_{1\ for\ 70.3°}$, $k_{2\ for\ 70.3°}$, $k_{1\ for\ 60°}$, $k_{2\ for\ 60°}$, can be decided.

$$\begin{Bmatrix} 10GPa < E < 300GPa \\ 10MPa < \sigma_y < 2500Mpa \\ 0 < n < 0.5 \\ 9 < \ k_{1\ for\ 70.3°} < \mathbf{17} \\ -20 < k_{2\ for\ 70.3°} < \mathbf{-0.1} \\ \mathbf{4.73} < k_{1\ for\ 60°} < 6.29 \\ -23 < k_{2\ for\ 60°} < \mathbf{-0.35} \end{Bmatrix} \quad (7.12)$$

Despite using dual indenters, choosing the initial values of parameters still significantly effects of the convergence of the proposed optimisation algorithms. Therefore, the range of initial values of k_1 and $k_{2\ \text{for}\ 60°\ \text{and}\ 70.3^0}$ is based on the parametric study in **Chapter 6**. In general, the FMINCON function in MATLAB returns a local minimum, but it may be a global minimum. Using a global optimisation method can lead to a better optimisation solution, although it is computationally expensive. However, it is possible to check the global minima using the optimisation tool box, is available in the MATLAB optimisation toolbox manual. In order to avoid a local minimum rather than a global minimum, the first estimated sets of mechanical parameters are first used. After the first optimised parameters are obtained, they are used as initial parameters for the FMINCON function in the MATLAB optimisation toolbox to investigate better minimum values. This process is repeated until the same minimum and best first-order optimality can be obtained. For comparison purposes, the same target parameters for a single indenter test are used for the dual indenters. The simplified optimisation processes with three different target parameters (E, σ_y and n) have been carried out with two different loading-unloading curves for the angles of 60° and 70.3°, as shown in **Table 7.4**. For three chosen materials, the minimum relative estimation errors for E, σ_y and n are -1.93% 10.7% and 0%, respectively. The prediction of Young' modulus, E shows a significant improvement in all cases. In terms of σ_y and n, although there are still large differences between the sets of target parameters and the sets of final optimised parameters, the sets of optimised parameters show slight improvements, compared with those from a single indenter.

Figure 7.6 shows the loading-unloading curves during iterations for dual indenters, where the optimised loading-unloading curves converge to the given experimental loading-unloading curve. **Figure 7.7** shows the comparison between the experimental curves and the final optimised curves for a conical indenter with 60° and 70.3° face angles. Clearly, there is a

good agreement between the given experimental curve and the optimised loading-unloading curves for a conical indenter with 60° face angle, whereas there is a small deviation for a conical indenter with 70.3° face angle, particularly in the loading curves.

Table 7.4 Three parameters optimisation (E, σ_y and n) with different target values using dual indenters

Case	parameters	Target values	Initial values	Optimised values	Percentage Error for E,σ_y,n	First-order optimality
1	k_1 for 70.3°	12.636	12.636	12.328	3.91% 81% -56.7%	1.386e-01
	k_2 for 70.3°	-0.468	-0.468	-1.079		
	E(GPa)	210GPa	200GPa	218.219GPa		
	σ_y(MPa)	900MPa	700MPa	1630.06MPa		
	n	0.4	0.35	0.173		
	k_1 for 60°	5.985	5.985	5.187		
	k_2 for 60°	-0.466	-0.466	-1.109		
2	k_1 for 70.3°	13.444	12.444	12.149	-1.93% 10.7% 0%	6.394e-03
	k_2 for 70.3°	-0.952	-0.952	-0.955		
	E(GPa)	150GPa	165GPa	161.811GPa		
	σ_y(MPa)	1500MPa	1650MPa	1681.03MPa		
	n	0.2	0.15	0.20038		
	k_2 for 60°	6.174	6.1747810	5.575		
	k_2 for 60°	-0.977	-0.977	-0.983		
3	k_1 for 70.3°	13.302	13.302	13.016	-6.24% 33% 37.67%	4.585e-03
	k_2 for 70.3°	-0.592	-0.592	-0.969		
	E(GPa)	100GPa	90GPa	93.76GPa		
	σ_y(MPa)	300MPa	350MPa	448.03MPa		
	n	0.3	0.32	0.187		
	k_1 for 60°	5.866	5.866	5.376		
	k_2 for 60°	-0.587	-0.587	-0.981		

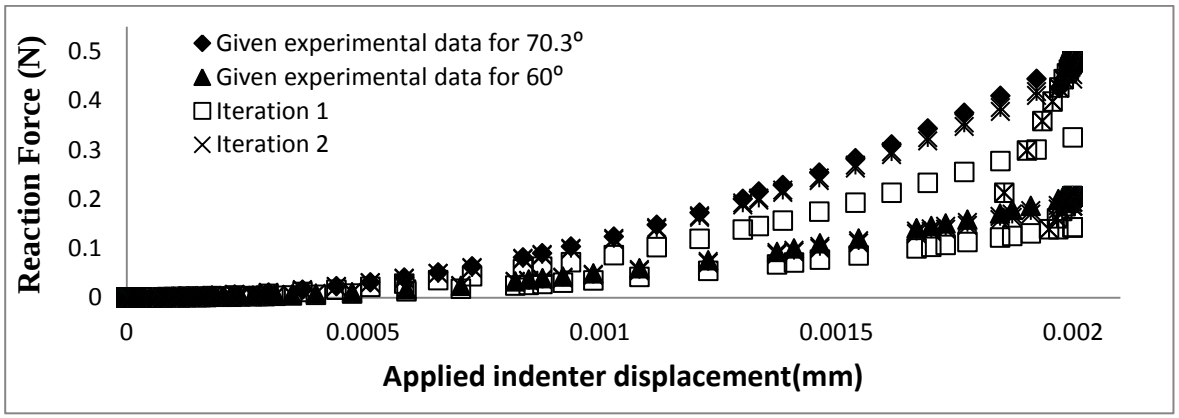

Figure 7.6 Optimisation results and target loading-unloading curve using dual indenters (a) E = 150GPa, σ_y = 1500MPa and 'n' =0.2

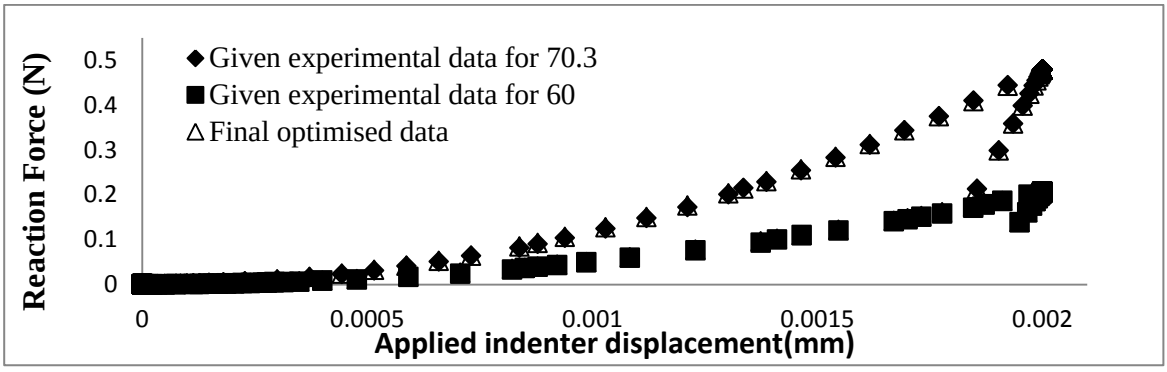

Figure 7.7 Comparison between given experimental curves and optimised curves for a conical indenter with 60° and 70.3° face angles after iterations (Target values, E = 150GPa, σ_y = 1500MPa and 'n' =0.2)

(a) 210GPa, 900MPa, 0.4

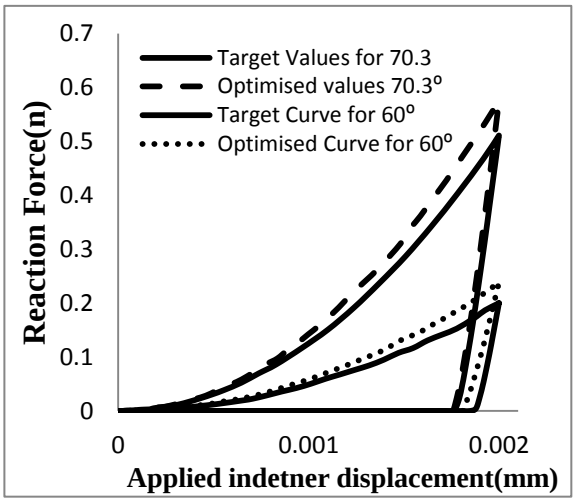

(b)1500GPa, 1500MPa, 0.2

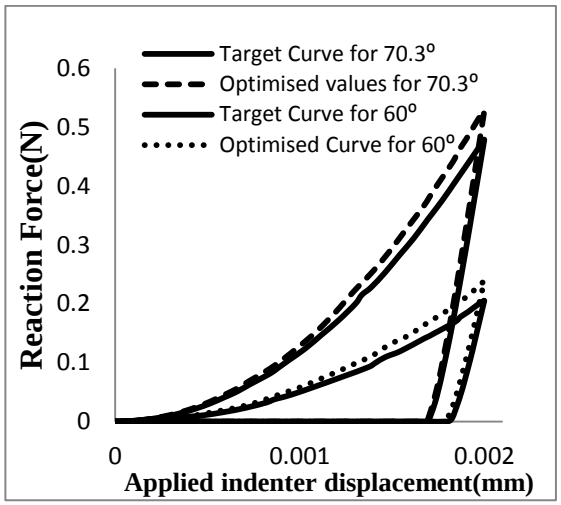

(c) 100GPa, 300MPa, 0.3

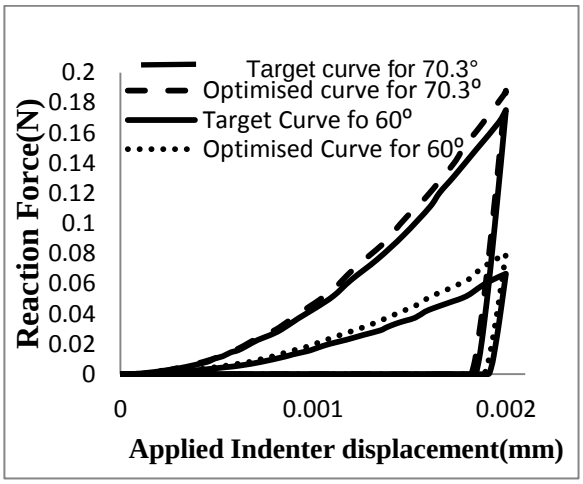

Figure 7.8 Comparison between the experimental target curve and the curve obtained by inputting the converged material parameters into ABAQUS for cases 2, 3 in Table 2 (a) E = 210GPa, σ_y = 900MPa, n = 0.4 , (b) E = 1500GPa, σ_y = 1500MPa, n = 0.2, (c) E = 100GPa, σ_y = 300MPa, n = 0.3

Figure 7.8 shows the comparison between the experimental target loading-unloading curves and the corresponding curve obtained by inputting the converged material properties in **Table 7.4** into ABAQUS (post-optimisation curve) for a conical indenter with 60 and 70.3° face angles. It undoubtedly shows that there is still a small deviation between these loading-unloading curves, where a slightly higher reaction force is predicted by the post-optimisation

ABAQUS run. The residual indenter depth after unloading, h_r is in good agreement, except for the loading-unloading curve for a conical indenter with 60° in **Figure 7.8** (a). Furthermore, the initial slope of the unloading curve, *S*, which is related to Young's modulus *E*, is in good agreement.

Since there is no investigation of the physical mechanical relationship between an indenter and a specimen, the feasibility of the simplified mathematical equations is still uncertain. From the results of the single and dual indenters, the optimised results can be very different from the target parameters. However, it is found that at least the estimation of Young's modulus *E* is more accurately than the standard Olive-Pharr's method [1], based on the results of the dual indenters. It is noted that the maximum error of Young's modulus based on the Olive-Pharr's method is 22%.

7.6 Alternative approach with LSQNONLIN function in MATLAB

There are still considerable differences of the yield stress, σ_y and the work-hardening exponent, *n* between the FE-simulated 'target' and the 'optimised' values using the FMINCON function in MATLAB. Therefore, a different algorithm (LSQNONLIN function) is investigated, even though this algorithm cannot handle constraints. The same assumed equations for the portions of the loading-unloading curves in **Table 7.1** are used; except that the value of m is fixed for convenience. Since practical physical equality constraints cannot be used with the LSQNONLIN function, the values of the loading curvature, *C* and the residual indenter displacement, h_r in Eq. (7.2) are used as a constraint point, as shown in **Figure 7.9**.

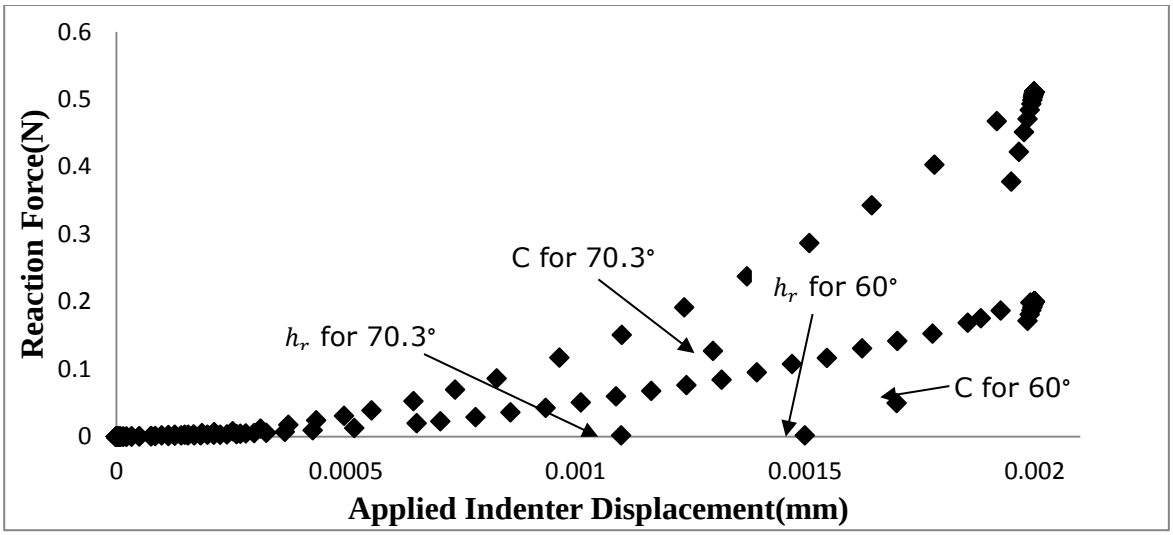

Figure 7.9 The constraint points of *C* and h_r based on the LSQNONLIN function in MATLAB.

7.6.1 Optimisation procedure

The general optimisation algorithm used in this study is described in **Figure 7.10.** Unlike **Figure 7.1**, the C language executable file is used for convenience. Since the initial values for (k_1, k_2, E, σ_y and n) are provided, the optimisation procedure is carried out to update the loading and unloading portions of the indentation curves. Firstly, MATLAB calls the initial guess values and controls the C language EXE file to generate the loading and unloading portions of force data, which is then read by MATLAB to fit the target curve during the iterations.

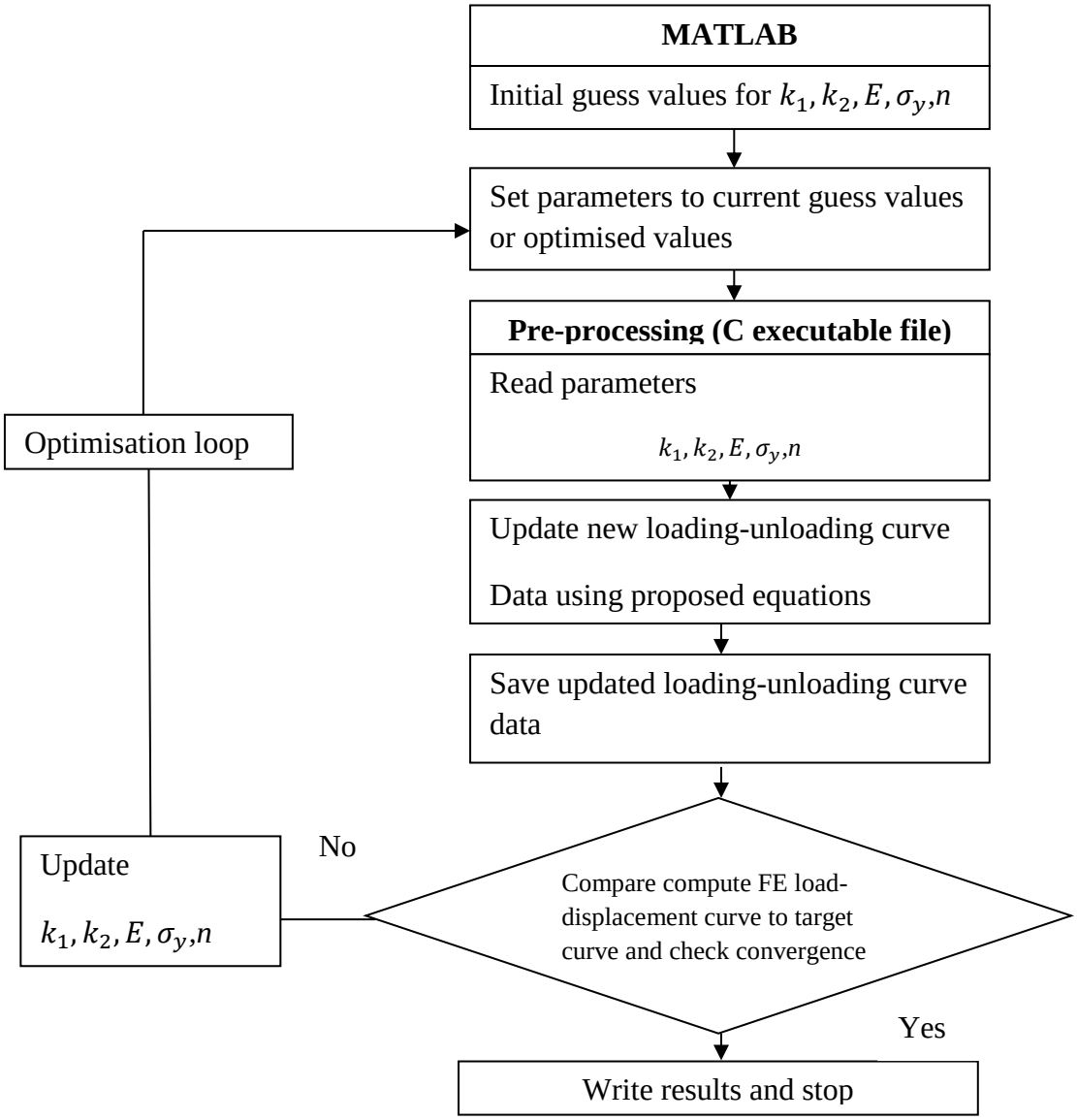

Figure 7.10 Flow chart of the optimisation algorithm to determine the mechanical properties from the loading- unloading curve based on the LSQNONLIN function.

7.6.2 Optimisation results using dual indenters

For convenience, the proposed optimisation algorithm is used with only dual indenters. For comparison, the same sets of material properties have been chosen as the target values, as shown in **Table 7.5**. As can be seen, the results of three parameters (*E*, σ_y and *n*) seem to be

in good agreement with the target values. However, it is noticeable that the sets of initial values are closer to the target values, within approximately 10%.

Table 7.5 Seven parameters optimisation for dual indenter with different target values

Case	parameters	Target values	Initial values	Optimised values	Percentage Error for E,σ_y,n	First-order optimality
1	k_1 for 70.3° k_2 for 70.3° E(GPa) σ_y(MPa) n k_1 for 60° k_2 for 60°	12.636 -0.468 210GPa 900MPa 0.4 5.985 -0.466	12.636 -0.468 180GPa 600MPa 0.35 5.985 -0.466	13.012 -0.503 205.53GPa 948.67MPa 0.371 6.074 -0.504	2.38% 5.4% 8.1%	2.56e-07
2	k_1 for 70.3° k_2 for 70.3° E(GPa) σ_y(MPa) n k_1 for 60° k_2 for 60°	13.302 -0.592 100GPa 300MPa 0.3 5.866 -0.587	12.302 -0.592 120GPa 250MPa 0.3 5.866 -0.587	12.51 -0.585 117.92GPa 299.17 0.2962 5.542 -0.5838	14% 0% 1.2%	4.5e-09
3	k_1 for 70.3° k_2 for 70.3° E(GPa) σ_y(MPa) n k_1 for 60° k_2 for 60°	12.44 -0.952 150GPa 1500MPa 0.2 6.174 -0.9777	12.44 -0.952 165GPa 1650MPa 0.15 6.174 -0.9777	13.03 -1.038 155.7GPa 1585.53 0.1825 5.946 -1.071	3.7% 5.39% 8.75%	2.7e-09

Table 7.6 Seven parameters optimisation for dual indenters with different initial values

Case	parameters	Target values	Initial values	Optimised values	Percentage Error for E,σ_y,n	First-order optimality
1	k_1 for 70.3°	12.636	12.636	13.012		2.56e-07
	k_2 for 70.3°	-0.468	-0.468	-0.503	2.38%	
	E(GPa)	210GPa	180GPa	205.53GPa		
	σ_y(MPa)	900MPa	600MPa	948.67MPa	5.4%	
	n	0.4	0.35	0.371		
	k_1 for 60°	5.985	5.985	6.074	8.1%	
	k_2 for 60°	-0.466	-0.466	-0.504		
2	k_1 for 70.3°	12.636	12.636	12.63		5.23-07
	k_2 for 70.3°	-0.468	-0.468	-0.469	0%	
	E(GPa)	210GPa	210GPa	209.7GPa		
	σ_y(MPa)	900MPa	900MPa	900MPa	0%	
	n	0.4	0.4	0.399		
	k_1 for 60°	5.985	5.985	5.99	0%	
	k_2 for 60°	-0.466	-0.466	-0.467		
3	k_1 for 70.3°	12.636	12.302	13.39		2.93e-7
	k_2 for 70.3°	-0.468	-0.592	-0.5813	2.04%	
	E(GPa)	210GPa	170GPa	205.7GPa		
	σ_y(MPa)	900MPa	400MPa	1048.5MPa	14%	
	n	0.4	0.25	0.318		
	k_1 for 60°	5.985	5.866	6.083	20.5%	
	k_2 for 60°	-0.466	-0.587	--0.586		

Figure 7.11 shows the comparison between the FE-simulated 'target' curve and the optimised curve for a conical indenter with 60° and 70.3° face angles, which shows excellent agreements between the two curves. Using the optimised values (E, σ_y and n) of cases 1, 2 and 3 in **Table 7.6,** the optimised material properties are input into ABAQUS (post-optimisation run) in order to check the validity of the optimised values. **Figure 7.12** and **Figure 7.13** show a comparison between the post-optimisation FE curve and the target curves for 60° and 70.3° face angles obtained for two sets of target material properties. In general, using two indentation loading-unloading curves helps to improve the accuracy and uniqueness of the predicted material properties. However, the results based on the simplified equations cannot be guaranteed to be unique, even though dual indentation curves are used with the proposed functions. As can be seen from **Table 7.6**, the optimised material

properties are different in each case. However, the differences between the post-optimisation FE generated loading-unloading curves and the target curves, for both 60° and 70.3° face angles, are very small.

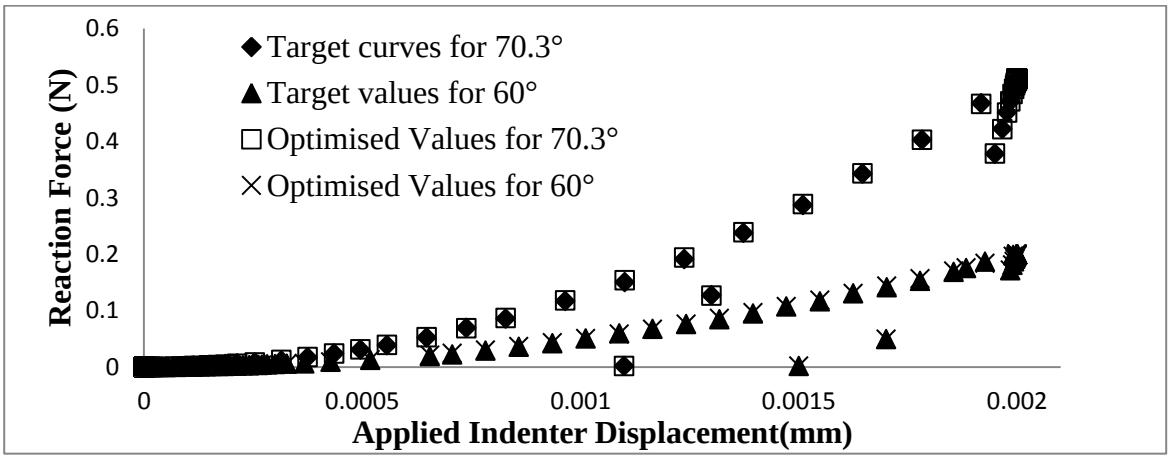

Figure 7.11 Comparison between the experimental target curve and the optimised curves for a conical indenter with 60° and 70.3° face angles after iteration E = 210GPa, σ_y = 900MPa, n = 0.4

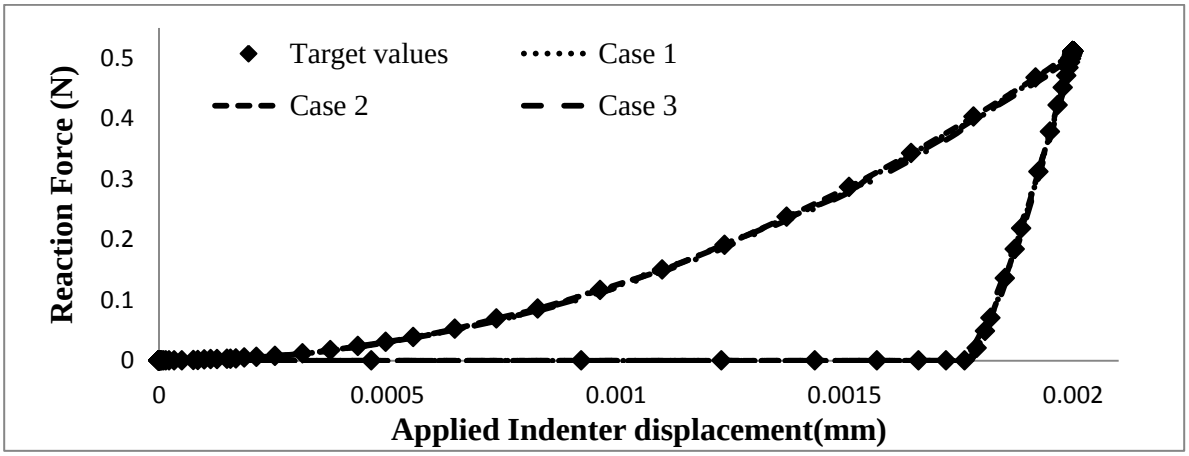

Figure 7.12 Post-optimisation FE generated loading-unloading curves with 70.3° face angles for Cases 1, 2, and 3 in **Table 7.6** corresponding to the target material properties of E = 210GPa, σ_y= 900MPa and n = 0.3

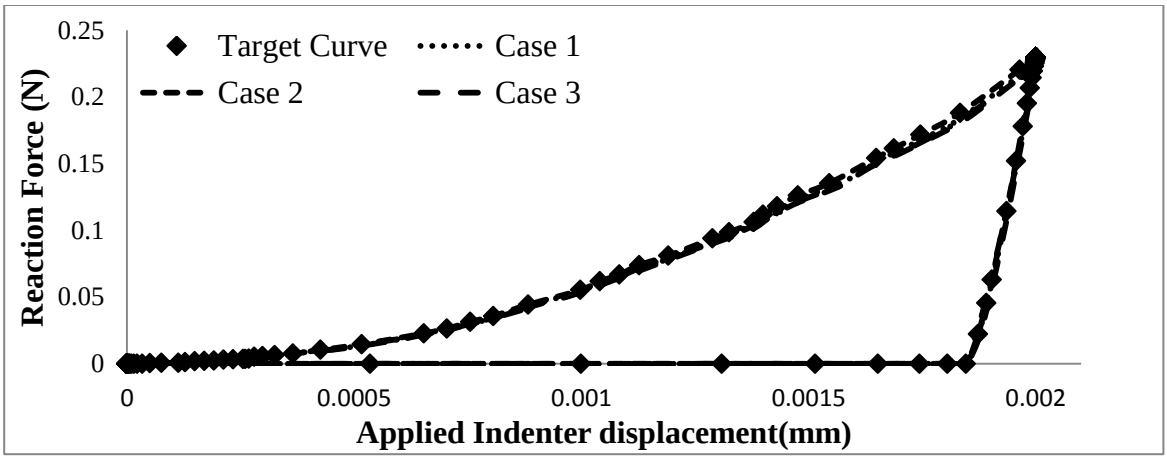

Figure 7.13 Post-optimisation FE generated loading-unloading curves with 60° face angles for Cases 1, 2, 3 and 4 in **Table 7.6** corresponding to the target material properties of E = 210GPa, σ_y= 900MPa and n = 0.3

In general, the results of first-order optimality are much lower using the LSQNONLIN function in MATLAB than using the FMINCON function in **Table 7.4**. Moreover, it is shown that the optimised sets of mechanical properties are strongly dependent on the initial sets of parameters.

7.7 Conclusion

A novel optimisation algorithm is proposed to extract the elastic-plastic mechanical properties from loading-unloading curves without using a parametric study and further FE analyses, although the bounds of the constants k_1 and k_2 and the mathematical relationships of the unloading curves have been obtained from a previous study in **Chapter 6**.

It is assumed that the portions of loading and unloading curves are significantly dependent on the mechanical properties (E, σ_y and n). The bounds of the parameters k_1 and k_2 obtained from the parametric study in **Chapter 6**, are also introduced to check convergence during the iterations. A new algorithm is used to extract three material parameters (E, σ_y, n) from the loading-unloading curves using the simplified equations. This new technique is based on a MATLAB minimisation routine function with equality constraints (called FMINCON) to

produce the best fit between the target loading-unloading curve (FE simulated) and the optimised curve.

With respect to the optimisation results based on the FMINCON function in MATLB, the predictions of Young's modulus, E are generally much more accurate than the prediction of yield stress, σ_y and work-hardening exponent, n using both a single and dual loading-unloading curves for a conical indenter. However, there are significant errors in the accuracy of the optimised values of n and σ_y.

Therefore, an alternative approach based on the LSQNONLIN function in MATLAB is used. This approach still cannot arrive at a unique set of material properties using a single indenter. However, using dual indenters, the optimised parameters are much closer to the target parameters, compared with the FIMICON function in MATLAB. The optimised parameters are strongly dependent on the initial guess parameters. Some limitations of this algorithm still exist due to the use of the k factors. Therefore, a parametric study of the k factors and further investigations of the mechanical relationships between the indenter and the specimen are required. This further study can help to reduce the number of unknowns and the bounds of the parameters leading to improved accuracy of the optimisation results.

8 Determination of elastic and viscoplastic material properties from indentation tests using a combined finite element analysis and optimisation approach

8.1 Introduction

Indentation creep tests [109-114] have been used to obtain the creep properties of materials, despite the fact that uniaxial tensile creep tests are the standard techniques to obtain creep parameters. There are several advantages of indentation creep tests. For example, only a small amount of the material is needed and the test can be used for the characterization of the local deformation behaviour. In general, creep is usually used to describe a time-dependent material behaviour of metals at high temperature that is a result of visco-elastic deformation when stress or strain is applied. Elastic-plastic behaviour usually refers to elastic and time-independent plastic deformation, whereas visco-elastic and viscoplastic behaviours refer to time-dependent elastic and time-dependent plastic deformations respectively.

Recent studies [115-119] have found that the determination of material properties from time-dependent material behaviour based on conventional indentation tests, based on the Oliver-Pharr method, does not provide an accurate estimation of material properties. The contacts between an indenter and a material specimen is visco-elastic and not purely elastic, in which creep occurs during the instrumented (nano-scale) indentation unloading which leads to an overestimation of Young's modulus.

Research efforts [115-119] have focused on extracting the time-dependent mechanical properties, which are limited to viscoelastic materials and do not consider the plastic deformations of the materials, but some researchers [21-22] have assumed that plastic-viscoelastic procedures occur separately in an indentation test. Tweedie and Van Vliet [119] stated that the plastic deformation can be negligible as the indentation is relatively shallow, hence a purely viscoelastic behaviour can be analysed for the time-dependent response. However, plastic deformation may not be negligible, since time-dependent indentation tests may involve very high localised contact stresses resulting in plastic strains.

The main objective of this study is to determine the elastic-plastic and creep material properties from indentation loading-unloading curves using a Finite Element (FE) approach combined with optimization algorithms for a combined two-layer viscoplasticity material model available in the ABAQUS FE code [89] combined with optimisation algorithms. The optimisation approaches discussed in the previous chapters are extended in this study to elastic-plastic and creep material properties using a spherical indenter. The current investigation builds on previous studies evaluating elastic-plastic material properties from indentation loading-unloading curves, using a novel two-layer viscoplasticity model and combined FE and optimisation methods to arrive at the mechanical properties of elastic-plastic and creep material to within an error of less than 10%.

8.2 Two-layer viscoplasticity model

The FE analysis of the bulk material indentation is based on an axisymmetric indenter that is modelled using the ABAQUS Standard FE code. The two-layer viscoplasticity model within ABAQUS [89] is chosen as an example to demonstrate both creep and elastic-plastic material behaviour occurring in the indentation test. A two-layer viscoplasticity model is developed for modelling materials in which both significant time-dependent and time-independent behaviour are observed, which for metals typically occurs at elevated temperatures. A one-dimensional idealization of the two-layer viscoplasticity model is presented in **Figure 8.1**, which describes the combined effect of a rate-independent (elastic-viscous network) and a rate-dependent (elastic-plastic network) material behaviours. It is noted that the rate-independent behaviour exhibits permanent deformations after the load application, whereas the rate-dependent behaviour exhibits permanent deformation of the material under load over time. The model consists of an elastic-plastic network that is in parallel with an elastic-visco (Maxwell model) network, where K_p is the elastic modulus of elastic-plastic network, K_v is the elastic modulus of elastic-viscous network, σ_y is the initial yield stress, H' is the power law hardening with work hardening exponent, n_1, and A and n_2 are the Norton creep parameters (based on the Norton Law: creep strain rate = $A\,\sigma^{n_2}$).

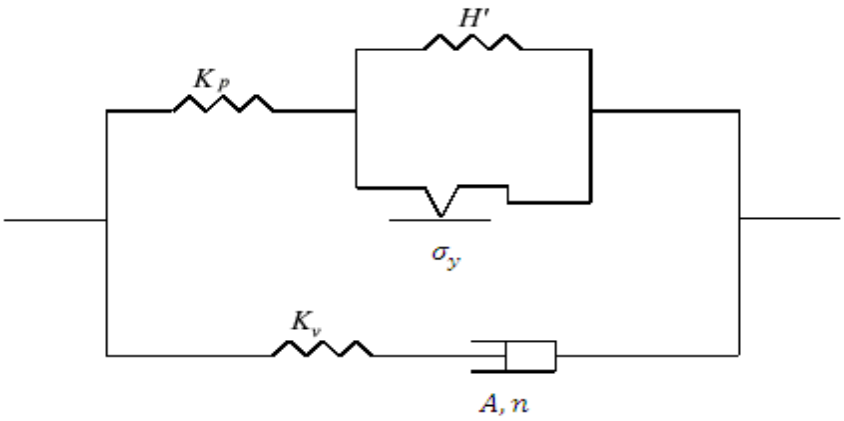

Figure 8.1 One-dimensional idealization of the two-layer viscoplasticity model [89]

The elastic-plastic network predicts the time-independent behaviour of the material, whereas the elastic-viscous network predicts the time-dependent behaviour of the material. The two-layer viscoplasticity model is based on the von-Mises yield condition in the elastic-plastic network and the Norton power law (secondary creep) for the viscoplastic behaviour in the elastic-viscous network. The two mechanisms are assumed to be independent, and the total stress σ is the sum of the stress σ_v in the elastic-viscous network and the stress σ_p in the elastic-plastic network. In this study, the two-layer viscoplasticity model is combined with a power-law strain hardening for the time-independent behaviour and the viscoplastic behaviour of the material is assumed to be governed by the Norton Law, also known as the Norton-Hoff law (secondary creep).

The material behaviour in the two-layer viscoplasticity model in ABAQUS covers elastic, plastic, and viscous deformations. The elastic part of both networks in **Figure 8.1** is defined by a linear isotropic elasticity model. A parameter f is introduced define the ratio of the elastic modulus of the elastic viscous network (K_v) to the total (instantaneous) modulus $(K_p + K_v)$ as follows:

$$f = \frac{K_v}{(K_p + K_v)} \qquad (8.1)$$

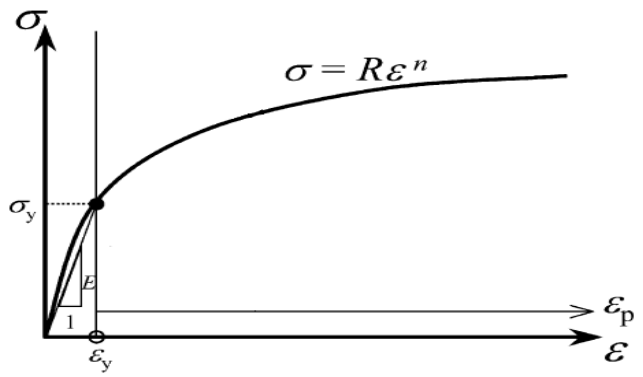

Figure 8.2 Power law elasto-plastic stress-strain behaviour

A simple elastic-plastic, true stress–true strain behaviour is assumed to be

$$\sigma_p = \left\{ \begin{matrix} K_p\varepsilon \ \ if\ \sigma_p \leq \ \sigma_y \\ R\varepsilon^{n_1}\ if \ \ \sigma_p \geq \ \sigma_y \end{matrix} \right\} \tag{8.2}$$

where σ_y is the initial yield stress, n_1 is the work hardening exponent and the coefficient R can be expressed as

$$R\varepsilon^{n_1} = \frac{\sigma_y}{\varepsilon_y^{n_1}}\left(\varepsilon_y + \varepsilon_p\right)^{n_1} = \sigma_y\left(1 + \frac{\varepsilon_p}{\varepsilon_y}\right)^{n_1} = \sigma_y\left(1 + \frac{K_p}{\sigma_y}\varepsilon_p\right)^{n_1} \tag{8.3}$$

where ε_y is the strain at the initial yield stress σ_y and ε_p is the plastic strain. The viscous behaviour of the material is assumed to be governed by the Norton Law, also known as the Norton-Hoff law (secondary creep). A time-hardening power law can be chosen for the viscous behaviour and setting *m* =0:

$$\sigma_v = A^{-\frac{1}{n_2}}\dot{\varepsilon}^{\frac{1}{n_2}} \tag{8.4}$$

$$\dot{\varepsilon} = A\sigma_v^{n_2}t^m \tag{8.5}$$

where σ_v is the viscous stress in the viscoelastic network and A and n_2 are Norton constants. It is assumed that the mechanisms are independent and can be written as:

$$\sigma = \sigma_p + \sigma_v \tag{8.6}$$

Therefore, the elastic strain is defined as:

$$\varepsilon^{el} = f\ \varepsilon_v^{el} + \ (1-f)\varepsilon_p^{el} \qquad (8.7)$$

The total strain comprising elastic, plastic and viscous strains can be expressed as follows:

$$\varepsilon_{total} = \varepsilon^{el} + f\varepsilon^{v} \ + (1-f)\varepsilon^{pl} \qquad (8.8)$$

where $\varepsilon^{pl} = \varepsilon_p^{pl}$ is the elastic strain in the elastic-plastic network and $\varepsilon^{v} = \varepsilon_V^{v}$ is the elastic strain in the elastic-viscous network. In the ABAQUS input file, a discrete set of points is required to represent the inelastic stress-strain behaviour, which is calculated based on Eq. (8.3). The data lines used to define the two-layer viscoplastic material model within the ABAQUS input file are shown below.

*Elastic

(Values of Young's modulus, Poisson's ratio)

*Plastic

(Values of stress, plastic strain)

*Viscous, law=Time (time-hardening rule)

A, n_2, m, f

The flow chart of the two-layer viscoplasticity model is shown in **Figure 8.3**

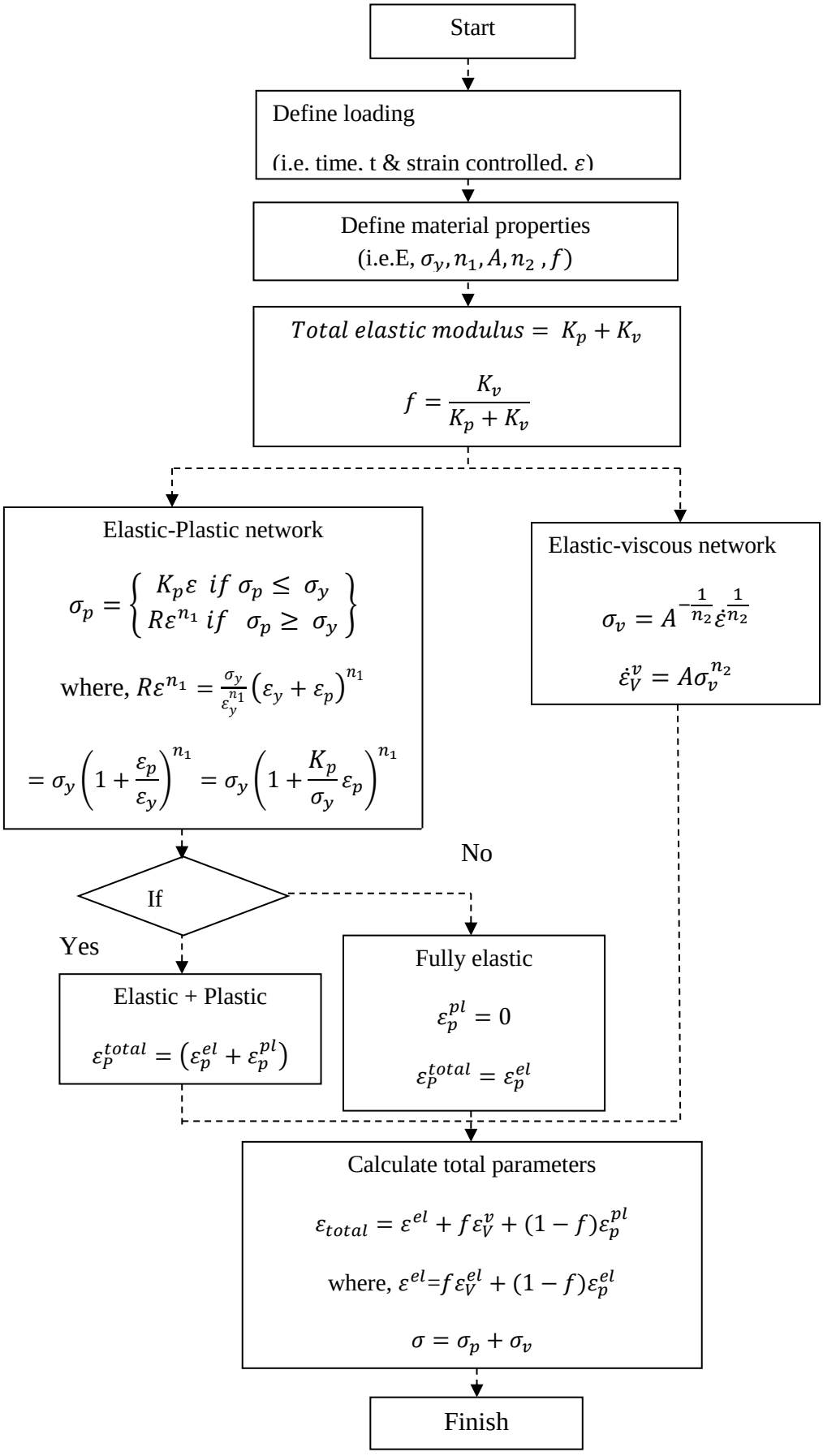

Figure 8.3 Flow chart of the two-layer viscoplasticity model used in this study

8.3 An Optimisation Procedure for Determining Viscoplastic Material Properties

8.3.1 Optimisation Model

The optimisation model is mentioned in the **Section 3.2.2** and the optimisation variable sets, *x* (a vector in the *n*-dimensional space, R^n), which for this specific case contains the full set of the material constants in the model, as follows:

$$x = \left[E, \sigma_y, n_1, A, n_2, f\right]^T \tag{8.9}$$

LB and *UB* are the lower and upper boundaries of x allowed during the optimisation. For the basic case in the viscoplasticity model, e.g. by choosing the time-hardening power law for the viscous behaviour, there can be six material parameters.

Scaling is very important in this optimisation approach due to the fact that the objective function gradients are calculated using very small variations of the parameter values. Since the parameter values span a very large range (e.g. E of the order of 10^9 Pa and the creep parameter A of the order of 10^{-14}), scaling factors have been used as shown in Eq.(8.10). The physical boundary constrains in the optimisation algorithm can be set to be of the same order as in Eq. (8.10 (a) (e.g. E is 210) and then scaled to the values required in the FE simulation as in Eq. (8.10).(b) (e.g. E is 210×10^9). Some practical physical constraints have been imposed during the optimisation analysis since Poisson's ratio and the work-hardening exponent values for most engineering materials are between 0.0 and 0.5. The boundaries for *E* have been chosen to be between 10 and 300 GPa and σ_y between 10 MPa and 2 GPa [102]. The lower and upper limits imposed on the material parameters are given below.

$$\left\{\begin{array}{c} 0 < E < 300; \\ 0 < \sigma_y < 2; \\ 0 < n_1 < 5; \\ 0 < A < 10; \\ 0 < n_2 < 10; \\ 0 < f < 10; \end{array}\right\}_{in\ optimisation\ (a)} \times \left\{\begin{array}{c} E \times 10^6; \\ \sigma_y \times 10^3; \\ n_1 \times 10^{-1}; \\ A \times 10^{-13}; \\ n_2; \\ f \times 10^{-1}; \end{array}\right\}_{in\ ABAQUS\ (b)} \tag{8.10}$$

Since the indenter is load-controlled, $D(x)_i^{pre}$ and D_i^{exp} are the predicted total displacement and the (experimental) displacement from target data, respectively, at a specific position i, within the loops. N is the total number of points used to represent the experimental (measured) load-displacement curves. Arbitrary values of $(E, \sigma_y, n_1, A, n_2, f)$ have been chosen as initial values and the proposed optimization algorithm has been used to find the optimised values of these parameters from which the best fit between the experimental and predicted load-displacement loops can be achieved.

8.3.2 Optimisation Procedure

The general optimization algorithm used in this work is illustrated in **Figure 8.4**. Since the initial guess values for $(E, \sigma_y, n_1, A, n_2, f)$ are provided, the optimization procedure is carried out in several steps using MATLAB, which controls the C language EXE file to automatically generate an ABAQUS input file, running ABAQUS and a Python script to extract the load history from the resulting ABAQUS output file. In terms of pre-processing the FE analysis, the material properties in the ABAQUS input file are replaced by new two-layer viscoplasticity material properties. In ABAQUS, these are Young's modulus, Poisson's ratio, and discrete points on the post yielding true stress-true strain curve.

In the ABAQUS input file, a discrete set of points is required to represent the uniaxial stress-strain data, rather than specifying the work-hardening exponent n_1 [106]. Therefore, a fixed set of plastic strain values of 0.005, 0.01, and 0.0115 are used in order to specify the plastic stress-strain data in ABAQUS. The coefficient R can be calculated by using Eq. (8.3) and the updated stress data related to these strains can be obtained by Eq. (8.2). The viscous behaviour of the material is governed by the Norton power-law with creep parameters, A and n_2 and the fraction, *f*, is defined in the viscous section of ABAQUS input file. This procedure can be performed by a C language code or a similar computing language to replace the current material properties in the ABAQUS input file by the new calculated material properties. In terms of post-processing, the load history results, extracted by a Python script, are read by a MATLAB program and the objective function calculated. All the procedures are processed automatically until convergence is reached.

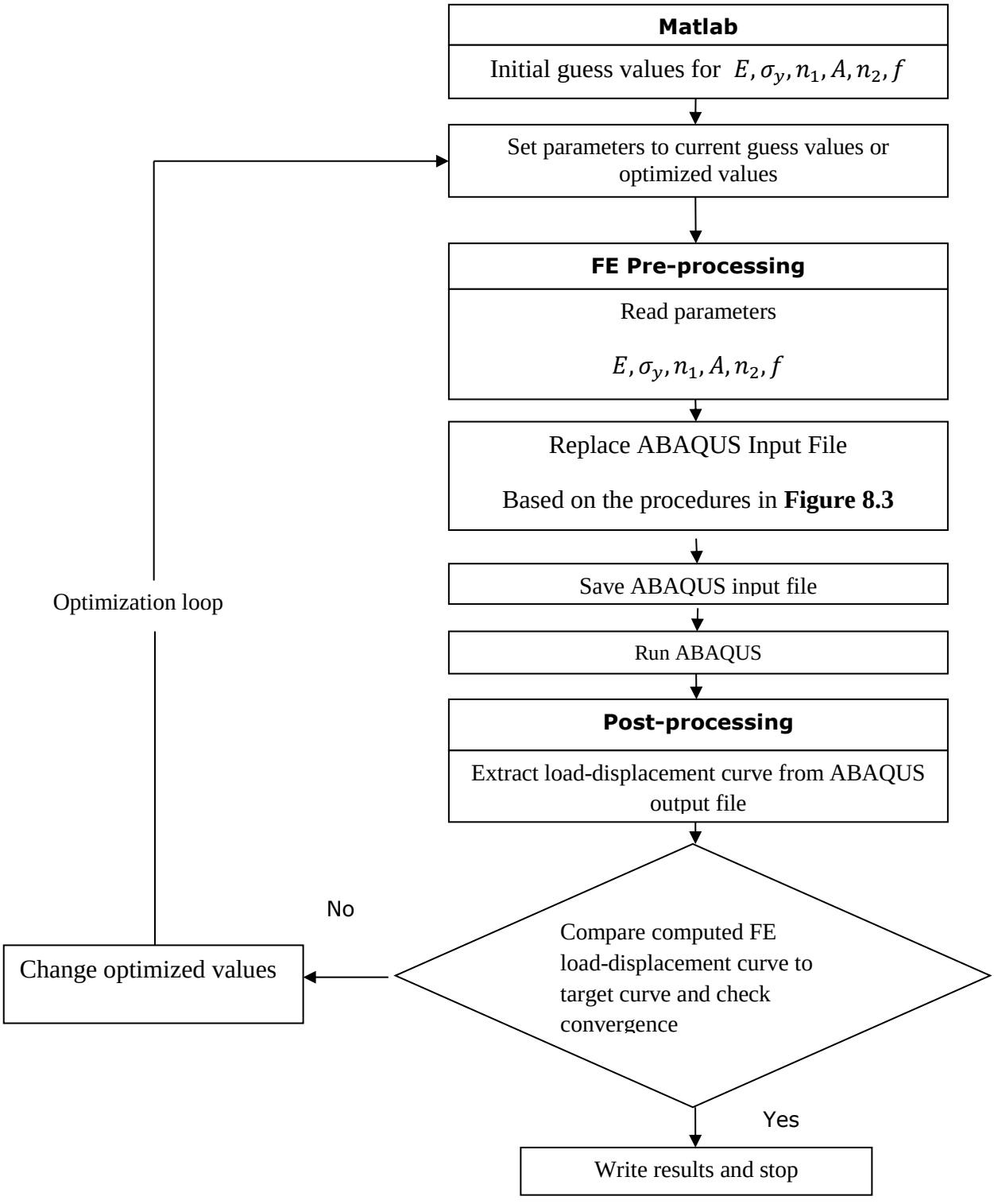

Figure 8.4 Flow chart of the optimisation algorithm to determine the mechanical properties from the load-displacement curves

8.4 Finite Element Indentation modelling

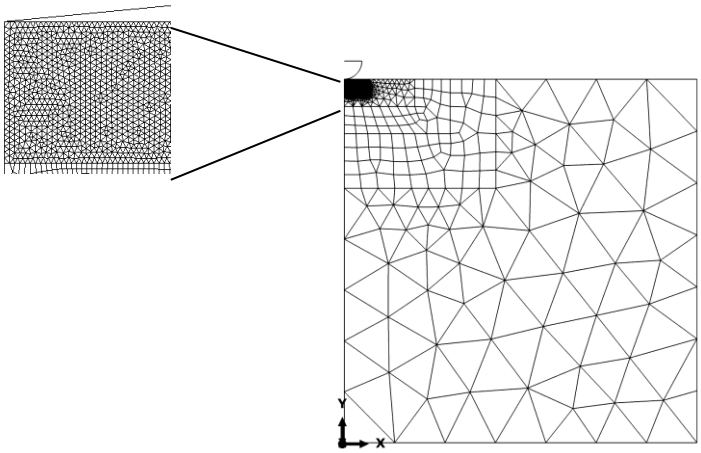

Figure 8.5 The FE meshes: Axisymmetric spherical indenter

The details of FE model is mentioned in the **Section 3.2.1**. The FE mesh for the axisymmetric spherical indenter is shown in **Figure 8.5**. The depth of the bulk material is 2mm and the maximum load on the indenter is 4.62N under load-control conditions. The simulation is carried out in three distinct steps: loading, holding and unloading. In the first step, a total indentation load 4.62N is applied. During the loading step, the rigid indenter moves downwards along the y-direction and penetrates the foundation up to the maximum specified force. In the second step, the indenter is held at the maximum specified force with a dwell time (3s) to induce viscoelastic deformation. In the third step, the load is reduced to zero. In the first unloading step, significant nonlinearity occurs which requires very small load/time increments. In the second and third steps, contact between the indenter and substrate is maintained and removed, respectively and larger load increments can be used.

8.5 Optimisation using a target curve obtained from a FE simulation

The optimisation scheme has been applied to determine the material properties of two-layer viscoplasticity model using a spherical indenter. Firstly, a set of material properties are chosen as the target values and FE analysis is performed to obtain a simulated target loading-unloading curve. A set of initial 'guess' material parameters are then selected and implemented in the MATLAB optimisation algorithm which automatically performs a new

ABAQUS run for each iteration. The target material properties are shown in **Table 8.1** for two materials, XN40F (a high nickel-chromium material) at 900℃ and P91 steel at 600℃. The given material properties have been obtained by uniaxial tensile creep testing. Previous work, see. e.g. [121,122], has shown that creep parameters obtained from impression creep agree well with those obtained from conventional uniaxial creep testing.

In order to check the sensitivity of the optimisation algorithms, each parameter is changed in turn, while all other parameters are fixed at their target values. Generally, the optimised results are obtained in about 8-10 iterations with a deviation of less than about 1% from the target values. Moreover, optimisations based on a combination of parameters involving two or four parameters are performed, as shown in **Table 8.2**. The parameter 'Errnorm' is the sum of the squares of the differences between the target and optimised curves. The results show that all the variables converge from their initial guess parameters to their target values to within 1% and 'Errnorm' is nearly zero, while it takes more iteration to reach the target values when more parameters are added, except in Test 4 in **Table 8.2**. It is noted that convergence is faster, and with improved accuracy, when the initial guess values are chosen closer to the target values. These results demonstrate that the proposed optimisation algorithms are capable of obtaining the material properties accurately.

Figure 8.6 presents the convergence history of the material properties during the iteration process. It clearly demonstrates that convergence to the target values can be achieved despite a large variation in the initial guess values. As can be seen from **Figure 8.6** (a), convergence starts after about 6 iterations for Young's modulus and creep parameter n_2, whereas the creep parameter A goes up and then steadily decreases until the target value is reached. The four parameters converge to their target values after 9 iterations in **Figure 8.6** (b), which is much faster than in **Figure 8.6** (a).

Table 8.1 Material properties obtained from experimental tests used in this study, obtained from the uniaxial tensile creep testing.

Material	E(MPa)	σ_y(MPa)	n_1	A	n_2	f
XN40F at 900℃	60.00E+03	209	0.3	9.14E-14	4.66	0.92
P91 steel at 600℃	136.00E+03	230	0.22	6.31E-06	2.7	0.54

Table 8.2 Parameter optimisation for the XN40F material using a spherical indenter

Test	Parameter	Target values	Initial values	Final Optimized values	Percentage[a] error(%)	Iterations	[b]ErrNorm
1	A	9.14E-14	6.14E-14	9.139E-14	4.45E-03	7	2.011E-11
2	n_1	0.30	0.12	0.30	5.15E-01	25	7.20E-10
	σ_y(MPa)	2.09E+02	6.00E+02	2.08E+02	9.44E-03		
3	E(MPa)	6.0E+04	4.00E+04	5.99E+4	3.0E-03	45	1.60E-10
	A	9.14E-14	7.18E-14	9.145E-14	5.75E-02		
	n_2	4.66	3.66	4.659	2.71E-03		
4	E(MPa)	6.00E+04	7.00E+04	6.00E+04	3.01E-02	17	3.4E-10
	n_1	0.3	4.5E-01	3.01E-01	2.42E-01		
	σ_y(MPa)	2.09E+02	4.00E+02	2.08E+02	4.65E-01		
	n_2	4.66	3.5	4.66	5.1E-04		

[a] $\left|\left(1-\frac{optimised\ values-target\ values}{target\ values}\right)\times 100\right|$

[b] $ErrNorm = sum((target\ curve - optimised\ curve)^2)$

(a) Test 3 in Table 2

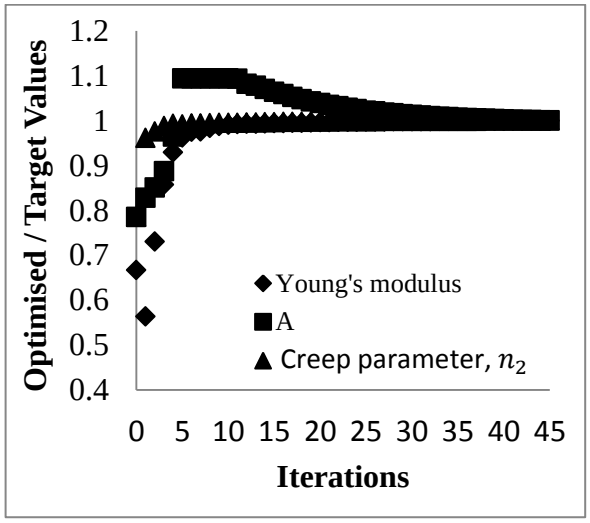

(b) Test 4 in Table 2

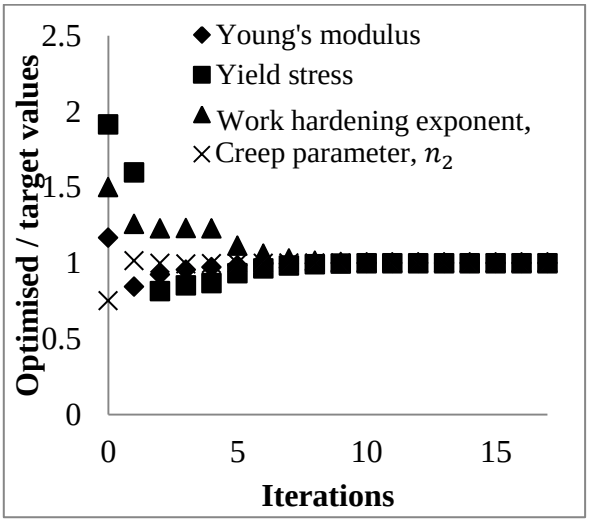

Figure 8.6 Optimised parameter values versus iterations for a spherical indenter (a) Test 3 and (b) Test 4

After checking the sensitivity of the optimisation algorithms, the optimisations of the full combination of six parameters of the XN40F material are investigated. **Table 8.3** shows the initial values and final optimised values for the XN40F material, where it is shown that, in

general, good convergence is obtained with the different variations of guess values. Although the percentage errors between the target and optimised values are much larger than when a combination of set of parameters involving only two or four parameters is used, all results have achieved convergence to within 10% error of the target solutions. In particular, the optimised values for Test 1 are much closer to the target values than the other test results, whereas the yield stresses in Test 2 and creep parameter A are generally higher than the other parameters. **Figure 8.7** shows the convergence trends for all three tests for XN40F. Although the initial guess values are different, it is interesting to see that the trends shown in **Figure 8.7**(a), (b) and (c) for the six parameters are similar, and gradually reach their target values.

Table 8.3 Six parameter optimisation for the XN40F material using a spherical indenter

Test	Parameter	Target values	Initial values	Final Optimized values	Percentage[a] error(%)	Iterations	[b]ErrNorm
1	E(MPa)	60000	80000	60305	0.50	22	3.53E-09
	σ_y(MPa)	209	350	208.325	0.32		
	n_1	0.30	0.35	0.305	1.71		
	A	9.14E-14	8.5E-14	9.03E-14	1.20		
	n_2	4.66	3.9	4.66	0.130		
	f	0.92	0.85	0.92	0.05		
2	E(MPa)	60000	100000	57760	3.7	19	5.09E-08
	σ_y(MPa)	209	550	190.77	8.72		
	n_1	0.30	0.4	0.286	4.50		
	A	9.14E-14	8.2E-14	9.12E-14	0.13		
	n_2	4.66	3.5	4.65	0.19		
	f	0.92	0.75	0.91	0.93		
3	E(MPa)	60000	120000	60800	0.03	17	4.06E-09
	σ_y(MPa)	209	600	226.40	7.68		
	n_1	0.30	0.45	0.270	10		
	A	9.14E-14	9.6E-14	9.59E-14	0.1		
	n_2	4.66	3.8	4.66	0.01		
	f	0.92	0.76	0.921	0.01		

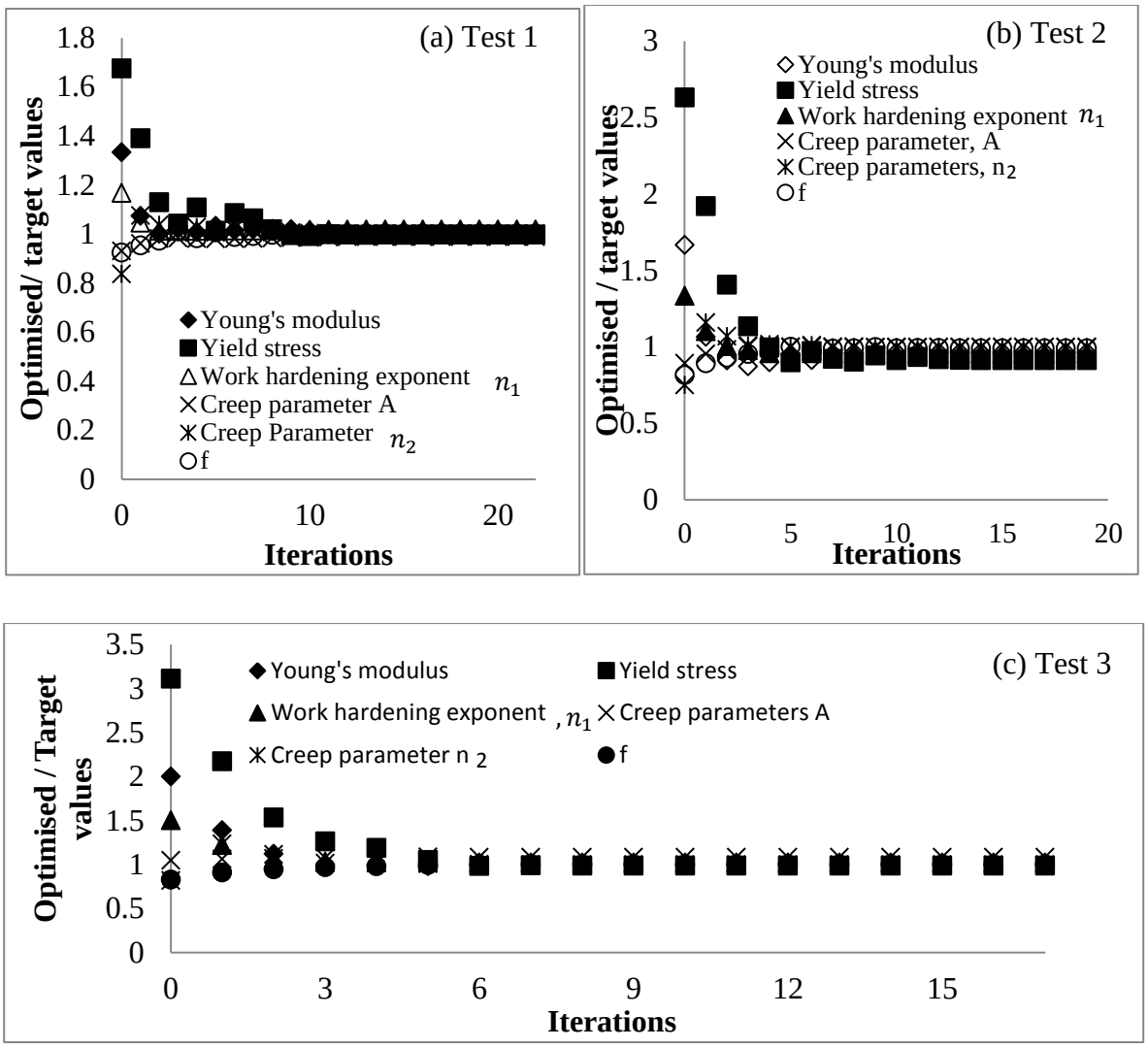

Figure 8.7 Optimised parameter values versus iterations for a spherical indenter (a) Test 1, (b) Test 2 and (C) Test 3 in Table 3 for XN40F material

The combination sets of six parameters optimisation for another material, P91 steel, are also investigated. **Table 8.4** shows the details of the initial values and final optimised values for P91 steel material. Most of the final optimised parameters in each case converge to within 10%, but higher errors occur in the creep parameter A. **Figure 8.8** shows the convergence history of the material properties for each iteration which clearly illustrates that convergence to the target values can be achieved despite a large variation in the initial values. In test 1, where the differences between the target and initial values are small, the convergence trend is similar for all material parameters, whereas the convergence trends are different in Tests 2

and 3. It is interesting to note that the convergence trend of the work hardening exponent in **Figure 8.8**(c) goes down and then steadily increases until the target value is reached. As before, the convergence rate and accuracy depend on the initial guess values. Since this is a non-linear material behaviour, there is no guarantee that the optimization algorithm will always converge to the 'target' parameters (whether obtained by FE analysis or an experiment). The optimization approach produces impressive accuracy in **Table 8.2**, whereas less accurate optimised results with six parameters are shown in both **Tables 8.3** and **8.4**. Further studies should be undertaken to analyse the parameter correlation in terms of six parameters.

It is clearly illustrated that the convergence accuracy of creep parameter A in Tests 2 and 3 in Table 4 is not as good as the other parameters. Therefore, the sensitivity of the loading-unloading curves to changes in the creep parameter A is investigated in **Figure 8.9**. **Figure 8.9** (a) shows the loading-unloading curves based on the optimised and target values of the creep parameter A, based on the results of test 3 in **Tables 8.4**. **Figure 8.9** (b) shows the loading-unloading curves obtained based on two different values of the creep parameter A, 5.77×10^{-6} and 6.5×10^{-6} , while all other parameters are fixed at their optimised values in test 3 in **Tables 8.4**. It is interesting to note that changes of the creep parameter A of up to 11% have a very small influence on the loading-unloading curves.

Tables 8.4 Six parameters optimisation for the P91 material using a spherical indenter

Test	Parameter	Target values	Initial values	Final Optimized values	Percentage[a] error(%)	Iterations	[b]ErrNorm
1	E(MPa)	136000	140000	144462	6.22	24	9.45E-08
	σ_y(MPa)	230	250	224	2.47		
	n_1	0.22	0.26	0.224	1.90		
	A	6.31E-6	6E-6	6.39E-6	1.28		
	n_2	2.7	2.9	2.71	0.44		
	f	0.54	0.5	0.564	4.59		

2	E(MPa) σ_y(MPa) n_1 A n_2 f	136000 230 0.22 6.31E-6 2.7 0.54	80000 500 0.15 5.0E-6 4 0.70	137743 232.27 0.214 5.7E-6 2.73 0.549	1.28 0.98 2.34 9.67 1.08 1.8	80	1.234e-09
3	E(MPa) σ_y(MPa) n_1 A n_2 f	136000 230 0.22 6.31E-6 2.7 0.54	250000 150 0.30 5.7E-6 3.5 0.65	142803 236.4 0.2048 6.85E-6 2.70 0.567	5% 3% 8% 7% 0.1% 6%	86	3.886E-09

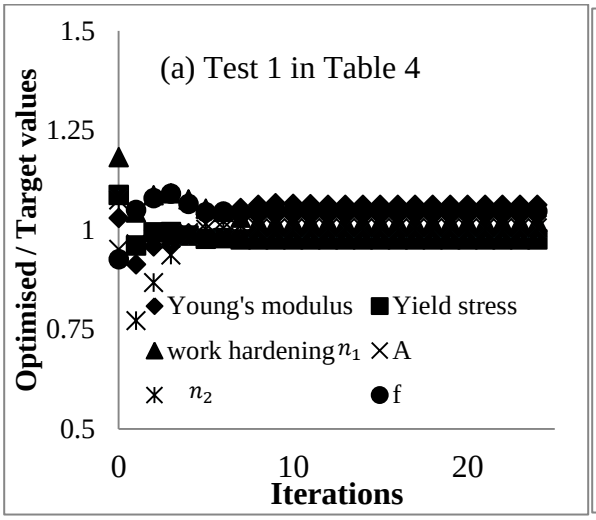

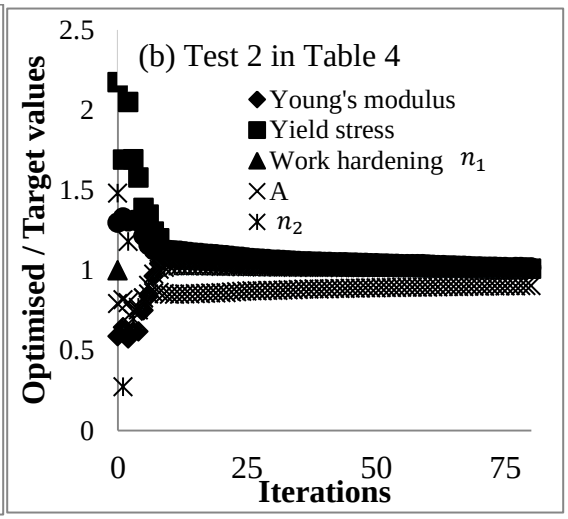

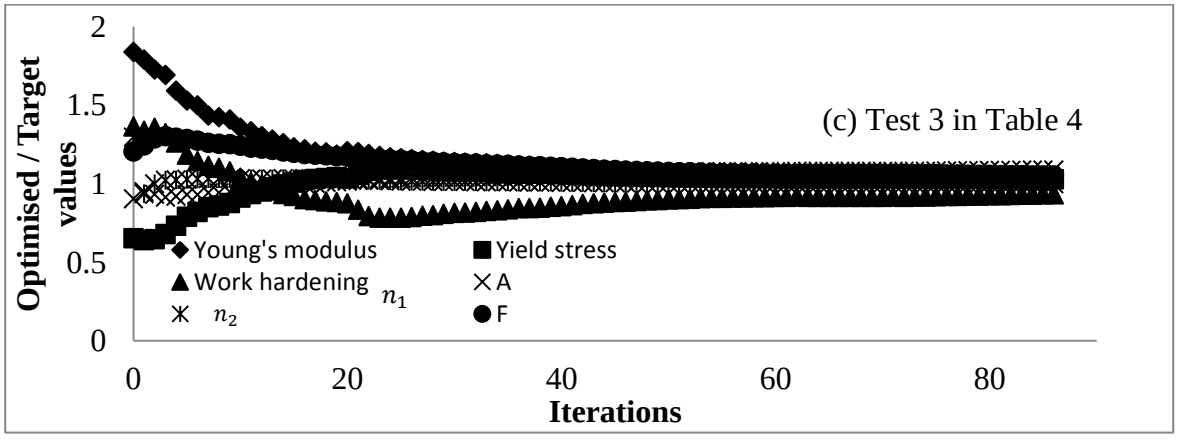

Figure 8.8 Optimised parameter values versus iterations for the P91 material using a spherical indenter (a) Test 1, (b) Test 2 and (c) Test 3 in **Table 4**

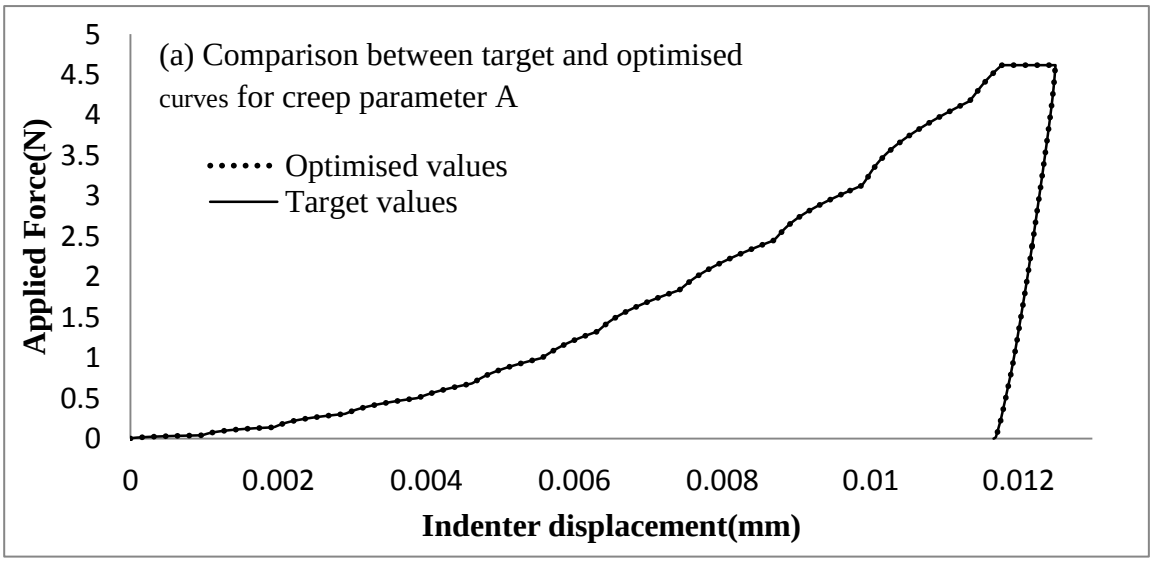

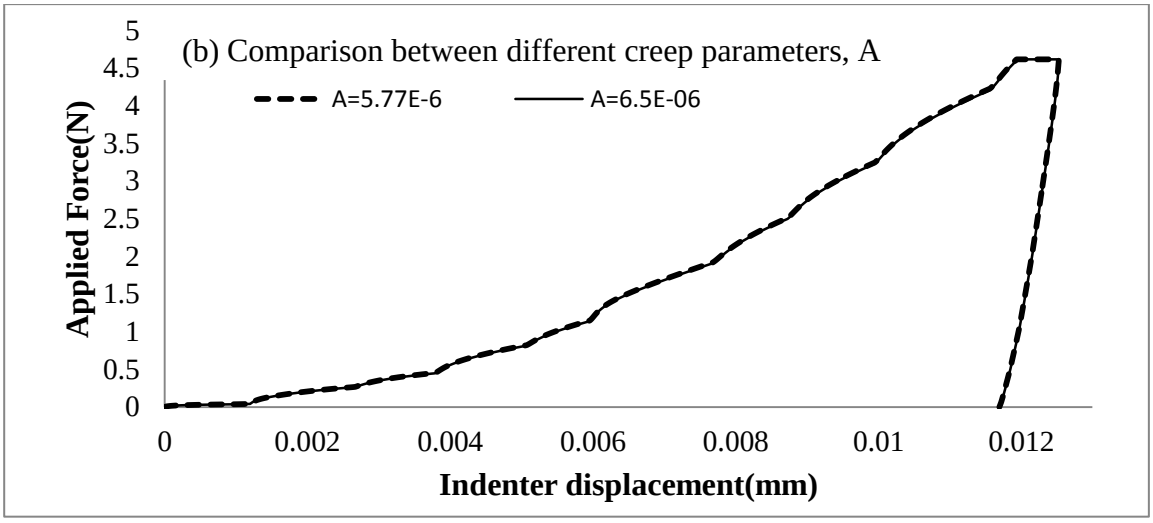

Figure 8.9 (a) Comparison between target and optimised curves for creep parameter, A, for a spherical indenter (b) Indentation curves obtained from two different creep parameters, A, for a spherical indenter.

8.6 Optimisation approach using a conical indenter

A previous study [106] has shown that Berkovich and Vickers indenters displace more volume and thereby produce greater local stresses due to fact that the contact areas between

the indenters and the bulk materials are larger than in the case of conical indenters. Despite these differences, conical indenters have the advantage of possessing axial symmetry and equivalent projected areas of contact can be used between conical and pyramid-shaped indenters such as Berkovich and Vickers indenters. In order to check the feasibility and the sensitivity of the optimisation approach, it is appropriate to consider a numerical experimental load-unloading curve from a conical indenter to determine the time-dependent material properties.

Table 8.5 shows the optimised results for axisymmetric conical indenters for the P91 steel material. The differences between the target and optimised parameters with a conical indenter are within 10%. For comparison purposes, the same initial values are used for both spherical and conical indenters in test 1 in both **Table 8.4** and **Table 8.5** and the percentage errors are shown in **Figure 8.10**. Despite using the same initial input data, it is interesting to obverse that the optimised results from both indenter geometries are different. Differences exist in the number of iterations and the final optimised parameters, especially Young's modulus, creep parameter A and parameter *f*. The differences between spherical and conical indenters may be attributed to the different shapes of the simulated target loading-unloading curves. As can be seen form **Figure 8.11**, different types of indentation loading-unloading curves are obtained despite using the same material properties. It is also observed that, for the same maximum indentation load, the displacement of a conical indenter is about two times larger than that of a spherical indenter due to the fact that there are more plastic deformations in the vicinity of a conical indenter.

Table 8.5 Six parameters optimisation for the P91 material using an axisymmetric conical indenter for P91 steel material

Test	Parameter	Target values	Initial values	Final Optimized values	Percentage[a] error(%)	Iterations	[b]ErrNorm
1	E(MPa)	136000	140000	135967	0.02	56	2.27E-09
	σ_y(MPa)	230	250	226.06	1.17		
	n_1	0.22	0.26	0.226	2.97		
	A	6.31E-6	6.0E-6	5.78E-6	3.70		
	n_2	2.7	2.9	2.71	0.67		
	f	0.54	0.5	0.538	0.27		
2	E(MPa)	136000	200000	145385	6.90	11	2.36e-09
	σ_y(MPa)	230	300	236.84	2.97		
	n_1	0.22	0.27	0.207	7.91		
	A	6.31E-6	6.0E-6	6.28E-6	0.38		
	n_2	2.7	3.5	2.72	0.63		
	f	0.54	0.45	0.577	6.85		

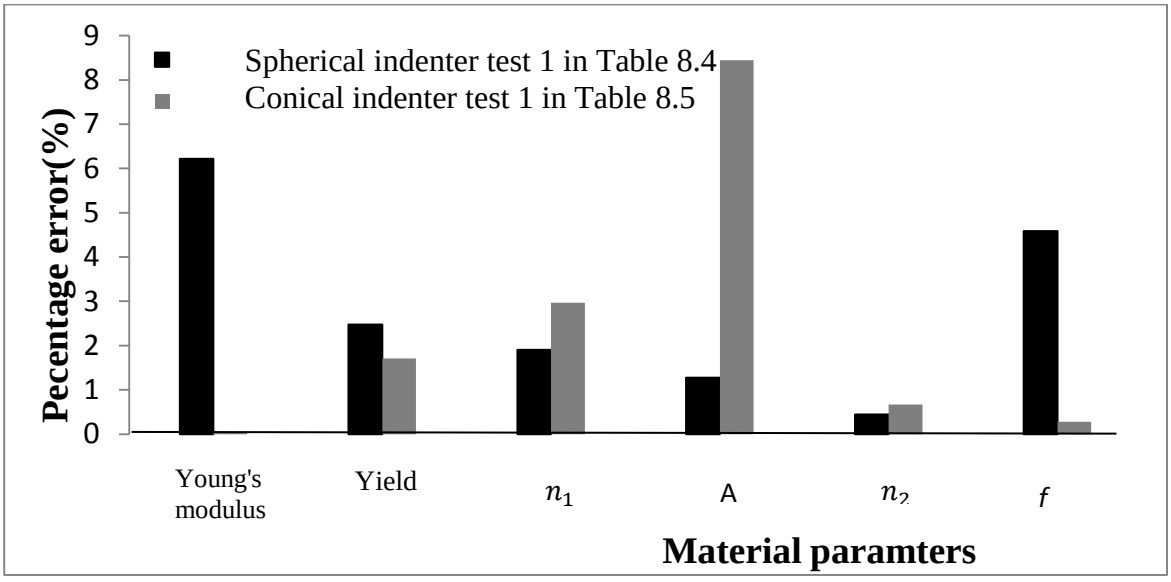

Figure 8.10 Comparison between errors in the optimised results from spherical and conical indenter

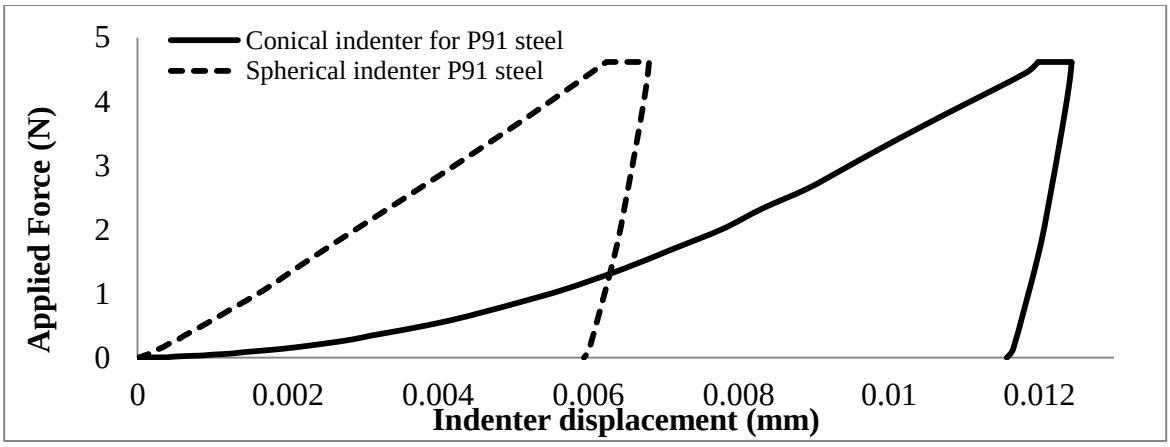

Figure 8.11 Simulated target loading-unloading curve for a spherical and a conical indenter.

8.7 Conclusions

In this study, a combined FE analysis based on a two-layer viscoplasticity model, and optimisation approach is presented to determine six time-dependent material properties (E, σ_y, n_1, A, n_2, f) of unknown materials from a given loading-unloading indentation curve. Two different materials are investigated, XN40F at 900℃ and P91 steel at 600^{o}C. The optimisation algorithm automatically provides input data for the material section in the ABAQUS FE input file and automatically runs FE simulations until the optimised loading-unloading curve reaches the given simulated target loading-unloading curve.

Previous studies have shown that the determination of material properties from time-dependent material behaviour based on conventional indentation test methods does not provide an accurate estimation of the material properties of the indented specimen. The proposed approach can be used to investigate the visco-elastic-plastic material behaviour based on the two-layer viscoplasticity model and determine the time-dependent material properties from the target simulated loading-unloading curve, to within 1-10% error, using results from a spherical indenter, despite using various initial guess values and using different materials. Moreover, there are good agreements between the target and optimised values based on using a conical indenter, although the convergence rate and accuracy depend on the initial input values. Further research may be targeted at using experimental target loading-unloading indentation curves for a wider range of materials.

9 Implementation of Optimization Techniques in Determining Elastic-Plastic Properties from 'real' Instrumented Indentation Curves

9.1 Introduction

In previous chapters, three different approaches to determine the elastic-plastic material properties from the loading-unloading curves have been established. (i) Combined FE Simulation and optimisation (ii) Combined dimensional analysis and optimisation (iii) Optimisation using simplified equations. However, the optimisation techniques have been mainly applied on 'simulated' target FE loading-unloading curves. This chapter highlights the estimation of elastic-plastic properties from 'real' experimental instrumented indentation loading-unloading curves, using the developed optimization techniques. The 'real' experimental optimisation results based on FE analysis, dimensional analysis and a simplified empirical method are compared. The general performance and the applicability of those techniques are evaluated and some of limitations and areas that need to be exploited in the future are briefly addressed.

9.2 The results of nanoindentation and tensile experimental data

Micro Material Nano-Test instrument can be used for the depth-sensing indentation tests, which is load controlled and can be applied a wide range of loads between 0.1-500mN for low loads and 0.1-20N for high loads. Room temperature nanoindentation tests with Berkovich and spherical indenters have been performed [123] on P91 steel [124] specimen with maximum loads of 150mN, 200mN as shown in **Figure 9.1**. Ten indentation tests have been completed at each load level to provide accurate indentation curves. The details of the nanoindentation tests are presented in **Table 9.1**.

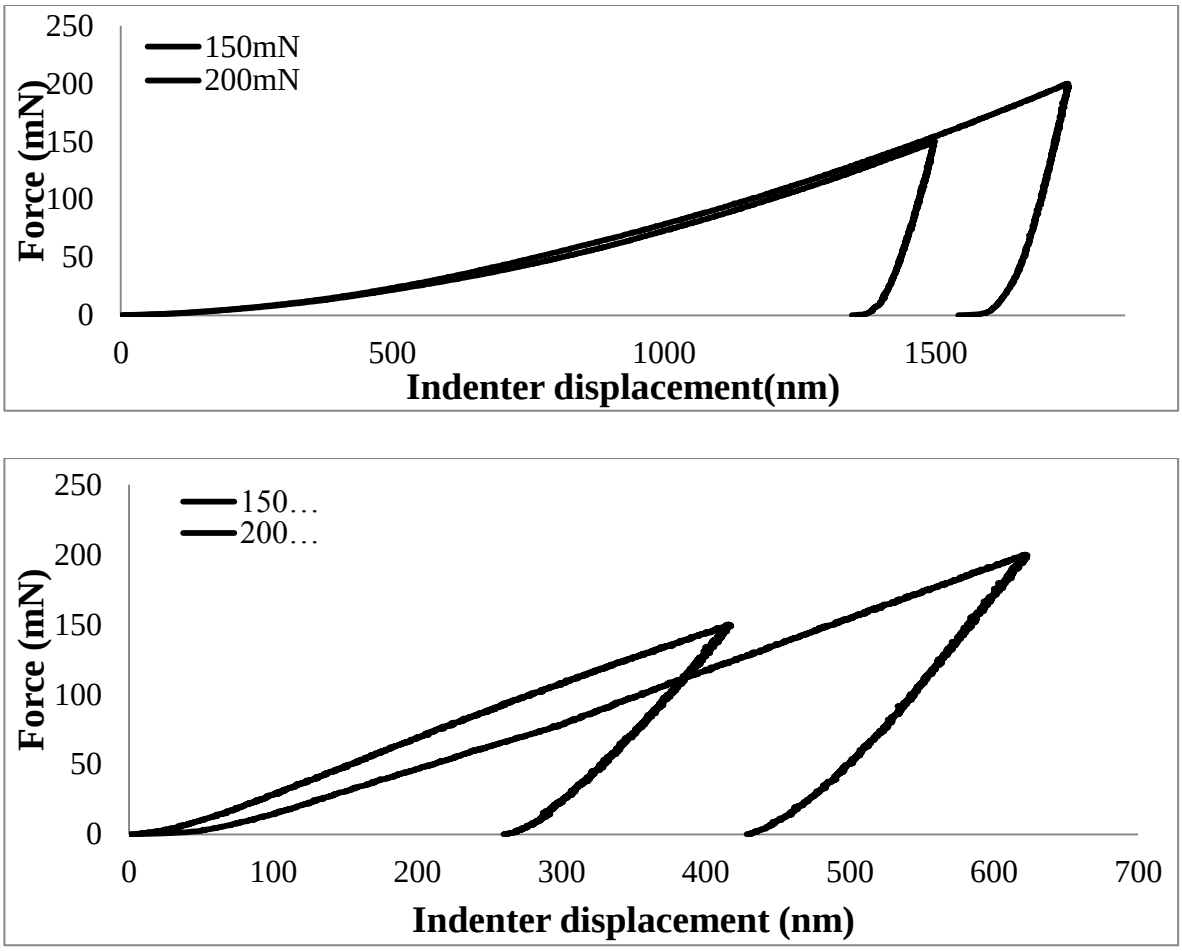

Figure 9.1 Experimental loading-unloading curves at different load levels using (a) Berkovich and (b) Spherical indenters

Table 9.1 The detail of nanoindentation test [124]

	Geometry of indenter	**Temperature**	**Applied Force**	**Dwell times**
P91 steel	Berkovich indenter	Room (23°C)	(100mN, 150mN and 200mN)	Loading time set at 20s Unloading time set at 10s

Uniaxial tensile tests at room temperature 23°C on P91 steel specimens have also been performed [124]. The P91 true stress-true strain curve is shown in **Figure 9.2** where Young's modulus is 215 GPa, the yield stress is 515 MPa at a strain of 0.0033 and work hardening exponent is 0.136. These tensile stress-strain data can be used to validate the optimised results

based on the three different optimisation techniques. Young's modulus value of the P91 steel at the room temperature can be obtained based on the Oliver-Pharr method. The average values of Young's modulus at each load are presented in **Table 9.2**. It is interesting to note that P91 Young's modulus values obtained from nanoindentation tests are approximately 14% higher than those from the tensile tests.

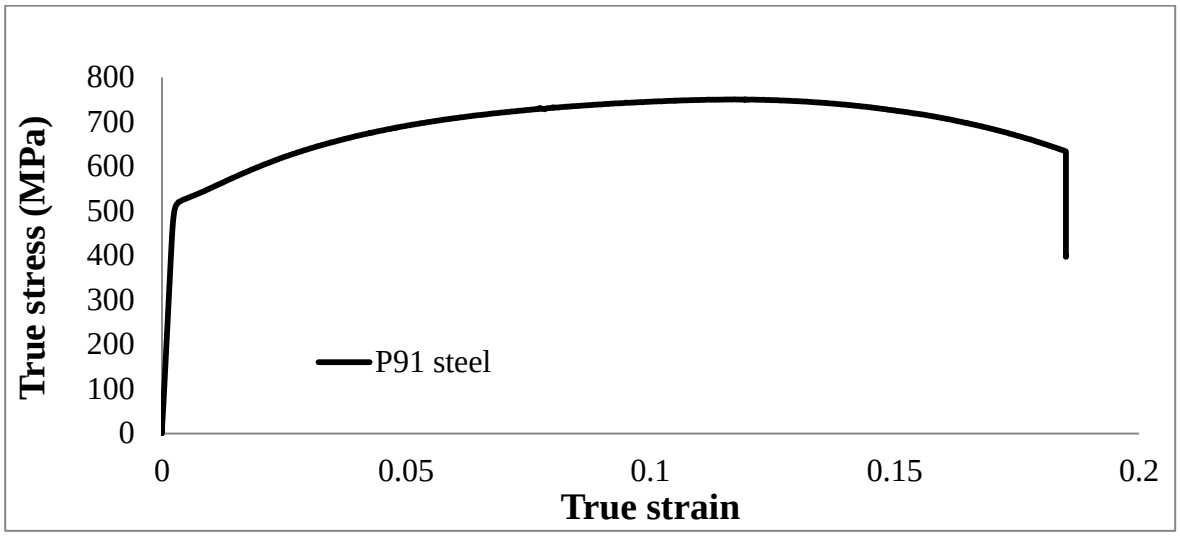

Figure 9.2 True stress-strain curves for the P91 parent steel specimen

Table 9.2 The results of Young's modulus from nanoindentation tests based on the Oliver-Pharr method

Load (mN)	100	150	200
Young's modulus (GPa)	251	253	244

9.3 Applying the three different methods to real experimental indentation loading-unloading curves

9.3.1 Optimisation Method 1: A Combined FE simulation and optimisation algorithm approach

A combined FE simulation and the optimisation approach has been developed in **Chapter 5**, using three types of indenters (namely, Berkovich, Vickers and conical) to determine the elastic-plastic material properties. In **Chapter 5**, 'simulated' FE loading-unloading curves are

assumed as 'real-life' experimental loading-unloading curves. Excellent convergence and optimised results can be obtained from those loading-unloading curves, but less accurate results have been obtained with real-life experimental loading-unloading curve, as discussed in **Section 5.5**. It is noted that the real-life experimental loading-unloading curve in **Chapter 5** is obtained from Ref [104]. The experimental nanoindentation tests are performed at the University of Nottingham with Berkovich and spherical indenter with different applied loads. The details of 3D FE indentation models with Berkovich and spherical indenters are mentioned in **Section 3.2.1**. The depth and diameter of bulk material are 1.5 mm and 10 mm respectively and the radius of spherical indenter is 25μm, as shown in **Figure 9.3.**

(a) (b)

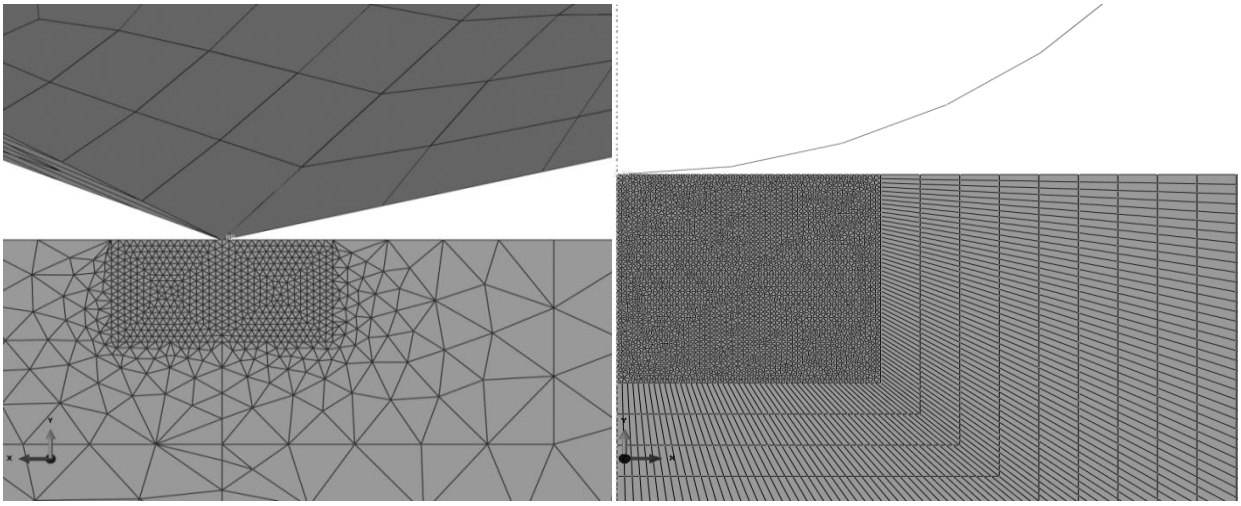

Figure 9.3 FE meshes of substrate subjected to (a) 3D Berkovich indenter and (b) axisymmetric spherical indenter

3D and axisymmetric indentation model can be used and the maximum applied forces of the Berkovich and spherical indenters are 150mN and 200Nm. The simulation is carried out in two distinct steps, a loading step and an unloading step. In the first step, a maximum load indenter 150mN or 200mN is imposed. During the loading step, the rigid Berkovich indenter moves downwards along the vertical direction and penetrates the foundation up to the maximum specified load. In the second step, the indenter moves upwards to the initial position. **Figures 9.4** (a) and (b) show a comparison of the FE solutions (run with the uniaxial stress-strain data as input) with the corresponding instrumented load-displacement

nanoindentation curves for the P91 steel specimen under the Berkovich and spherical indenters, respectively. Ten nanoindentation loading-unloading curves from a Berkovich indenter and a FE simulated curve based on the P91 tensile stress-strain data under the maximum load of 150 mN generally agree well. The FE results with a spherical indenter provide an excellent approximation in the portion of loading curve, but there is a clear deviation in the unloading portion, as shown in **Figure 9.4**(b). The discrepancies may be due to uncertain material properties, failure mechanisms and their interactions that are not accounted for, and the difficulties of realizing a truly rigid support in the experiments [124]. Therefore, the experimental results from the spherical indenter are not used used in Optimisation Method 1.

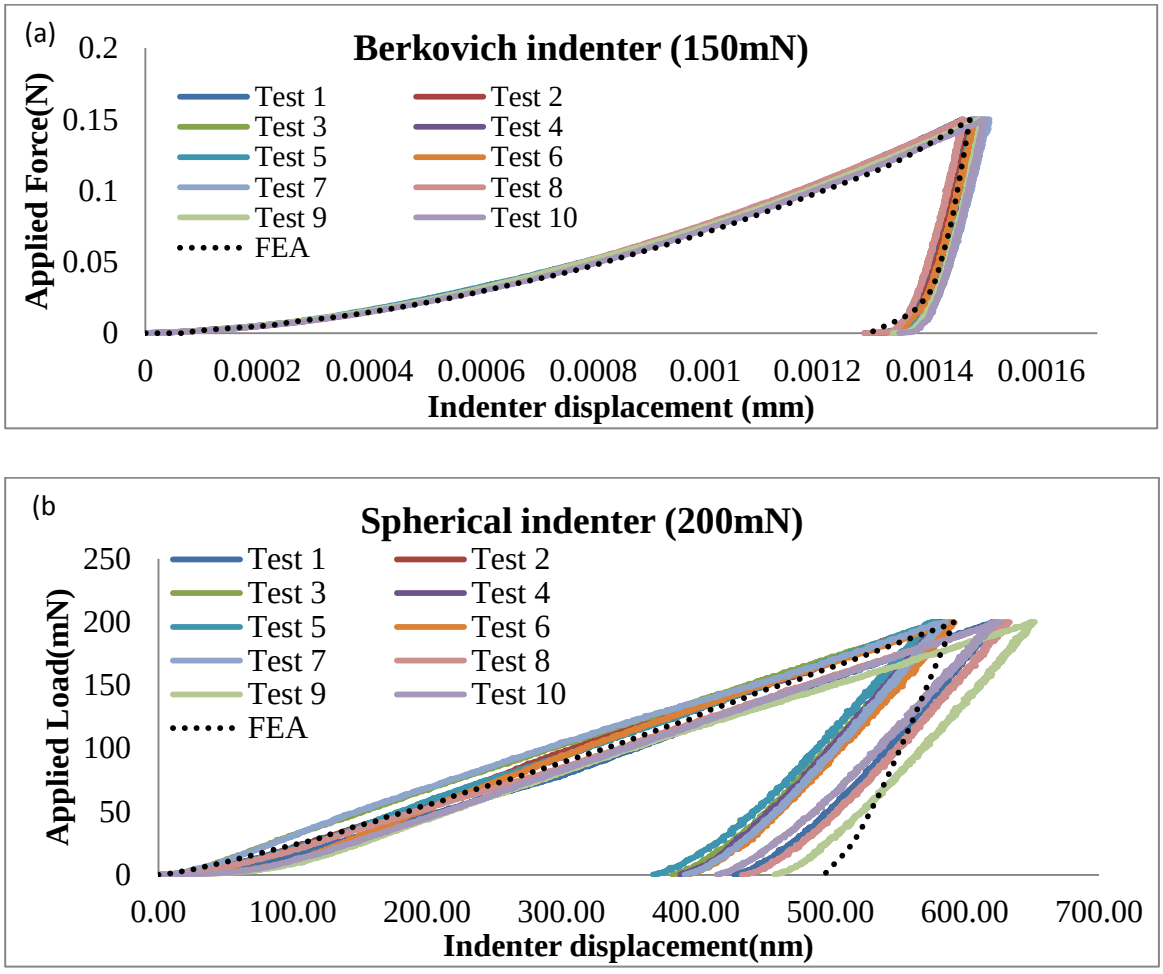

Figure 9.4 Ten nanoindentation experimental (a) Berkovich tests with 150mN and (b) spherical tests with 200mN versus FEA indentation results of P91 steel specimens

Previous optimisation results in **Chapter 6** and **7** showed that a single loading-unloading curve with a single indenter could not arrive at a unique set of elastic-plastic material properties. To compare with other optimisation methods, therefore, two different loading-unloading curves based on the same Berkovich geometry but with two different applied loads (150 mN and 200 mN) are used as the dual loading-unloading curves, since indentation data for different indenter geometries were not available. To determine the elastic-plastic material properties, loading-unloading curves for tests 3 and 7 have been selected due to the best agreement with the FE generated curve shown in **Figure 9.4**. The optimised results with a combined FE simulation and optimisation algorithm approach are shown in **Table 9.3** for test 3 and **Table 9.4** for test 7. The results show that optimised results are reached in about 18-38 iterations and the total number of iterations increases as the initial values are deviate from the target values. Young's modulus and yield stress are generally in good agreement compared with the uniaxial tensile test data. However, both optimised results of the working hardening exponent are approximately 5-12% less than those obtained from the tensile test data, which is n=0.136. **Figures 9.5 and 9.6** show the convergence history of the material properties for tests 3 and 7, respectively. In general, convergence starts after 15 iterations, with the exception of case 1(b) in **Figure 9.5**.

Table 9.3 Three optimisation results with two different initial values for Test 3

Case	Parameters	Target values	Initial values	Optimised values	Percentage Error	Iteration
1	E(GPa)	215000	180000	214357.0	0.3%	18
	σ_y(MPa)	515	400	504.45	2.04%	
	n	0.136	0.1	0.126	7.3%	
2	E(GPa)	215000	110000	214045.4	0.4%	25
	σ_y(MPa)	515	592	497.77	3.3%	
	n	0.136	0.193	0.129	4.8%	
3	E(GPa)	215000	80000	214857.80	0.7%	38
	σ_y(MPa)	515	2500	512.90	0.40%	
	n	0.136	0.45	0.127	6.6%	

Table 9.4 Three optimisation results with two different initial values for Test 7

Case	Parameters	Target values	Initial values	Optimised values	Percentage Error*	Iteration
1	E(GPa)	215000	180000	21712	1.3%	21
	σ_y(MPa)	515	400	495.40	4.5%	
	n	0.136	0.1	0.127	6.62%	
2	E(GPa)	215000	110000	217895	0.92%	27
	σ_y(MPa)	515	592	490.20	3.9%	
	n	0.136	0.193	0.121	11.0%	
3	E(GPa)	215000	80000	208471	3%	39
	σ_y(MPa)	515	2500	489.81	4.89%	
	n	0.136	0.45	0.128	5.88%	

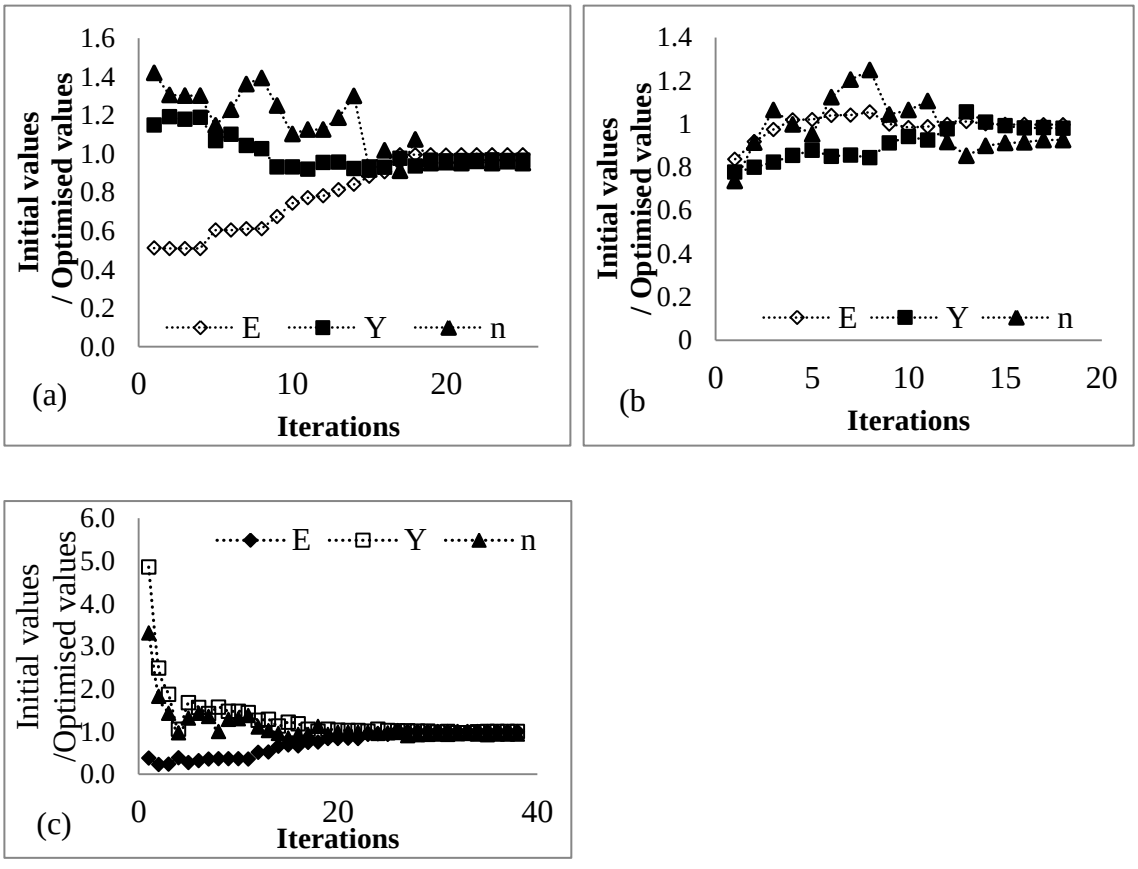

Figure 9.5 Optimised parameter values versus iterations for test 3(a) case 1, (b) case 2 and (c) case 3 using Optimisation Method 1

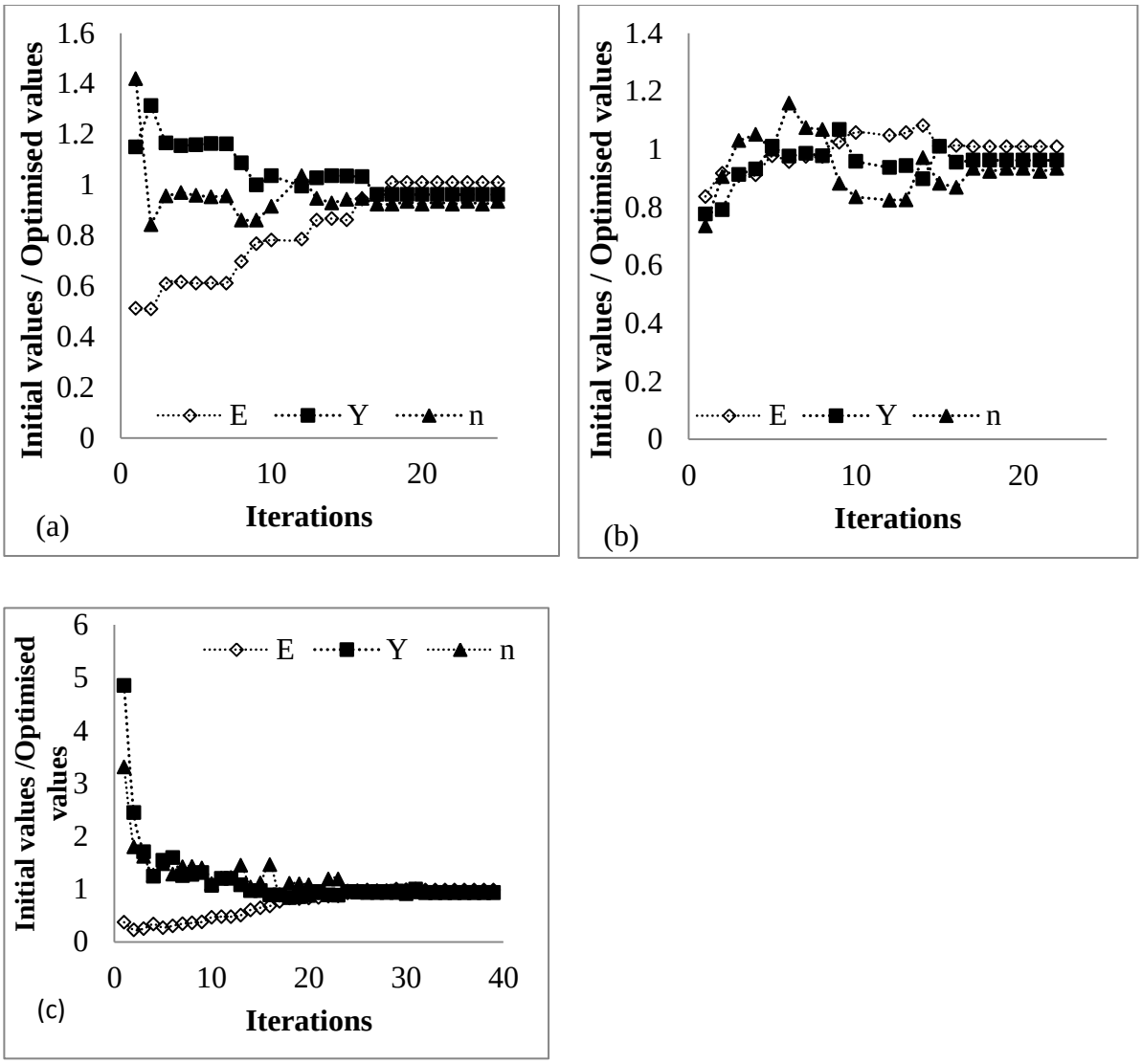

Figure 9.6 Optimised parameter values versus iterations for test 7 (a) case 1, (b) case 2 and (c) case 3 using Optimisation Method 1

Figure 9.7 shows the comparison between 'real' experimental loading-unloading curves and the FE simulated loading-unloading curves for a conical indenter with 150mN and 200mN based on the set of the final optimised parameters in **Table 9.3** and **9.4**, respectively. **Figure 9.8** shows the comparison of the equivalent plastic strain (PEEQ in ABAQUS) of the final optimised results of cases 1 in **Table 9.3** and **9.4** after removing the indenter. The maximum plastic strain occurs directly beneath the tip of conical indenter and the specimen experiences strains exceeding approximately 7~9% for both 150mN and 200mN loads. Therefore, the FE simulated curves shown in **Figure 9.7** agree well with 'real' experimental loading-unloading

curves. Optimisation Method 1 generally estimates the elastic-plastic material properties well, despite the under-estimation of the value of the work hardening exponent.

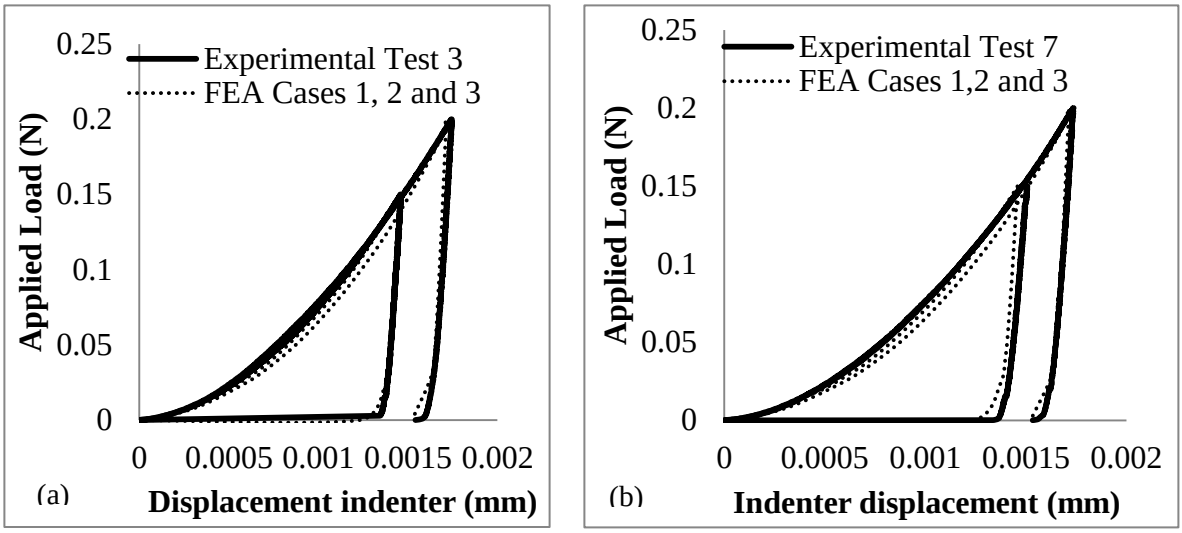

Figure 9.7 Comparison between Experimental curves and FE curves from final optimised results (a) Experimental test 3 (b) Experimental test 7 using Optimisation Method 1

150mN Test 3 case 1	200mN Test 3 case 1
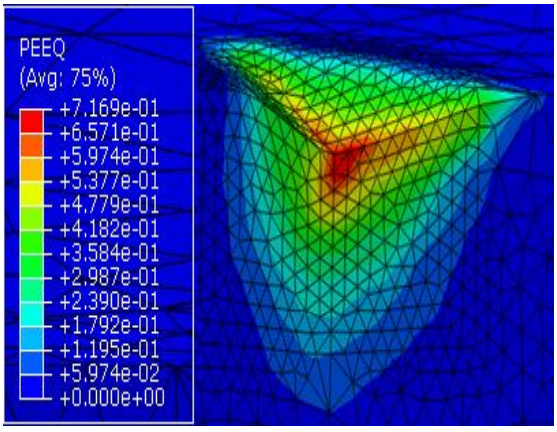	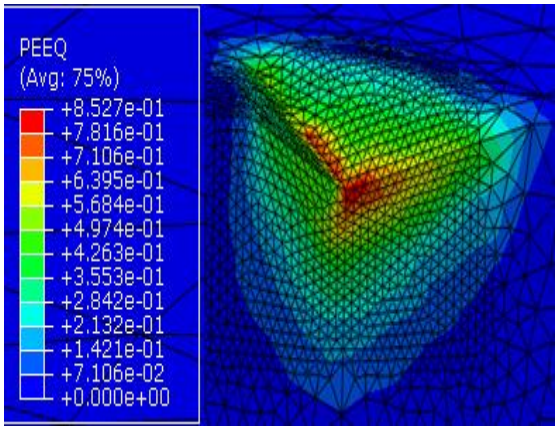

150mN Test 7 case 1	200mN Test 7 case 1

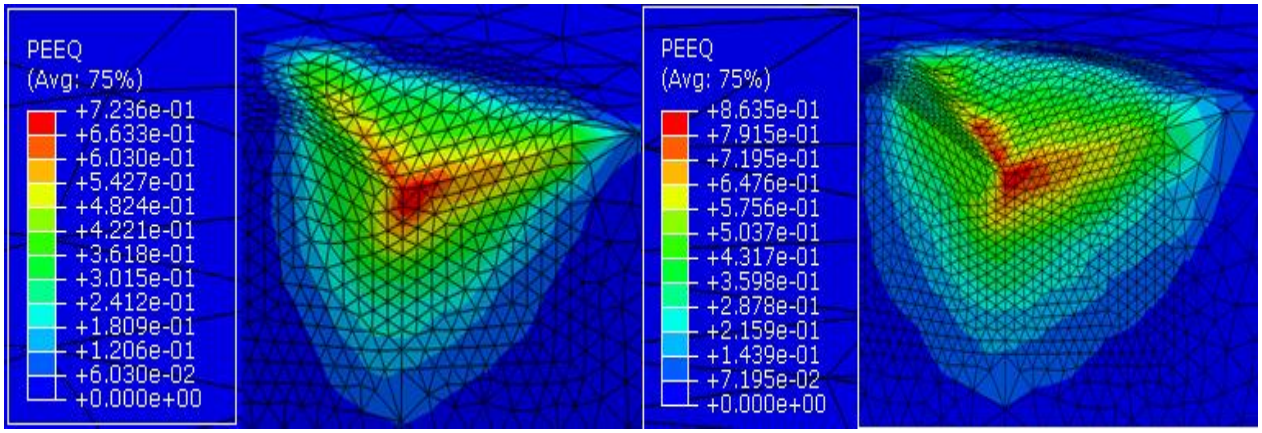

Figure 9.8 Contours of the equivalent plastic strain (PEEQ in ABAQUS) of the final optimised results of each case 1 in **Table 9.3** and **9.4** using Optimisation Method 1

9.3.2 Optimisation Method 2: Combined dimensional approach and optimisation

In **Chapter 6**, a combined dimensional analysis and optimisation approach has been developed and used to determine the elastic-plastic material properties from loading-unloading curves. To construct the dimensional functions, a parametric study using FE analyses with a wide range of material properties and a sharp indenter has been performed. In general, the elastic-plastic material properties could not uniquely be determined using a single indentation loading-unloading curve, but more accurate estimated results can be obtained from dual indenters with different angles.

In this section, 'real experimental' loading-unloading curves can be used as the 'target' loading-unloading curves to determine the elastic-plastic material properties based on the dimensional functions used in **Chapter 6**. It is noted that the 'real experimental' loading-unloading curves are based on a single Berkovich indenter with different loads, despite the fact that using dual indenters with different angles gives more accurate optimised results. The dimensional functions used in **Chapter 6** were constructed with a representative plastic strain

value of 0.0115. From the P91 true stress-strain curve in **Figure 9.2**, a representative stress at a strain value of 0.0115 is approximately 560 MPa, which is the target value for a representative stress for Optimisation Method 2.

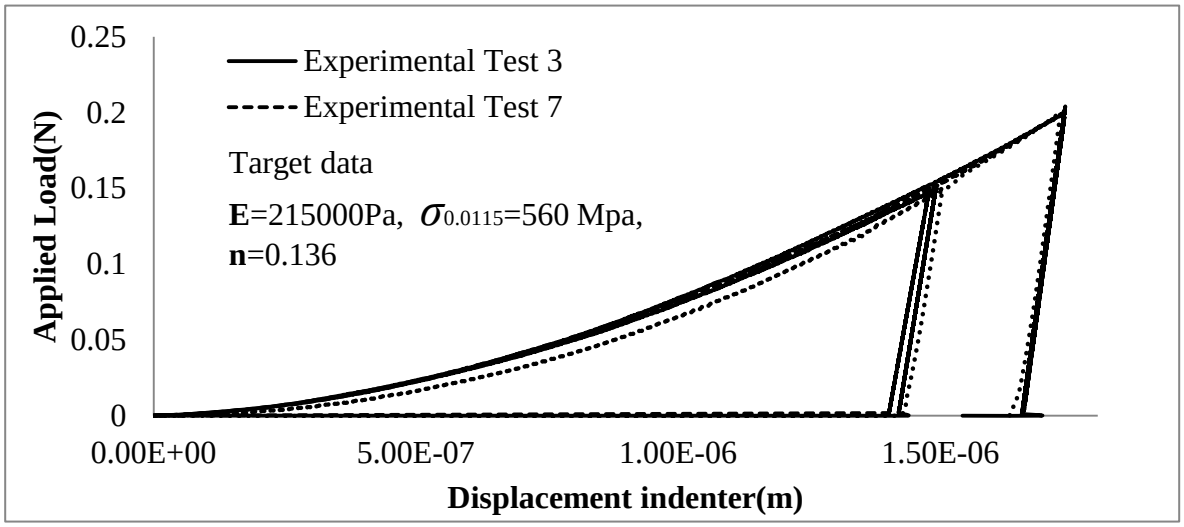

Figure 9.9 Comparison between Experimental loading-unloading curves of the experimental test 3 and test 7 and FE simulated curves.

The portions of the experimental unloading curves are regenerated by using Eq. (6.21). **Figure 9.9** shows the comparison between the experimental loading-linearized unloading curves of the experimental tests and the FE simulated curve, based on the properties E=215GPa, $\sigma_{0.0115}$=560MPa, n=0.136. FE simulated curves based on the set of target material properties generally agree well with both experimental loading-linearized unloading curves.

Two experimental loading-linearized unloading curves for tests 3 and 7 are used to extract the elastic-plastic material properties. **Table 9.5** clearly shows that the proposed approach estimates Young's modulus more accurately than the values of $\sigma_{0.0115}$ and n. Compared with the Oliver and Pharr's method shown in **Table 9.2,** the prediction of Young's modulus using this approach gives more accurate results. However, the prediction of a representative stress $\sigma_{0.0115}$ and n for both experimental tests are relatively large, with errors of approximately 10% for $\sigma_{0.0115}$ and 5-10% for n. From **Figure 9.9**, it is clear that the FE simulated loading curve deviates from the experimental loading curve. The deviation may cause prediction errors for

$\sigma_{0.0115}$ and n, since plastic deformation in the indented specimen occurs as the indenter moves down.

Figure 9.10 shows the experimental loading-unloading curves, FE simulated curves based on the final optimised results in **Tables 9.6** and **9.7** and the final optimised curves from MATLAB. It is clearly indicated that the final optimised curve from MATLAB agrees well with the experimental loading-unloading curves. FE simulated curves based on the final optimised results also agree well with the experimental loading-unloading curves, despite the large prediction errors of $\sigma_{0.0115}$ and n. This means that the dimensional functions can capture the physical relationships between the indenter and the specimen due to the fact that the functions have been generated by FE simulation with a wide range of material properties.

Five different sets of optimised elastic-plastic properties obtained during the optimisation procedure have been re-simulated using FEA, as shown in **Figure 9.10** which shows that, visually, it is hard to distinguish the differences between the different loading-unloading curves. This means that using dual loading-unloading curves with different loads would not be as beneficial as dual curves with the different angles of indenter, and a combined dimensional approach and optimisation algorithm could not arrive at the elastic-plastic material properties uniquely without further background information. Therefore, to improve the accuracy and uniqueness of the Optimisation Method 2, dual loading-unloading curves with different indenter face angles should be used.

Table 9.5 Three optimisation results with two different initial values for Test 3

Case	Parameters	Target values	Initial values	Optimised values	Percentage Error*	Iteration
1	E(GPa)	215000	180000	203100	5.5%	36
	$\sigma_{0.0115}$(MPa)	560	400	628.90	10.8%	
	n	0.136	0.1	0.128	5.9%	
2	E(GPa)	215000	110000	203056	5.5%	25
	$\sigma_{0.0115}$(MPa)	560	592	638.46	12.3%	
	n	0.136	0.193	0.122	10.3%	

Table 9.6 Three optimisation results with two different initial values for Test 7

Case	Parameters	Target values	Initial values	Optimised values	Percentage Error*	Iteration
1	E(GPa)	215000	180000	197486	8.0%	24
	$\sigma_{0.0115}$(MPa)	560	400	633.65	11.6%	
	n	0.136	0.1	0.128	5.9%	
2	E(GPa)	215000	110000	197505	8.0%	26
	$\sigma_{0.0115}$(MPa)	560	592	629.37	11.0%	
	n	0.136	0.193	0.130	4.4%	

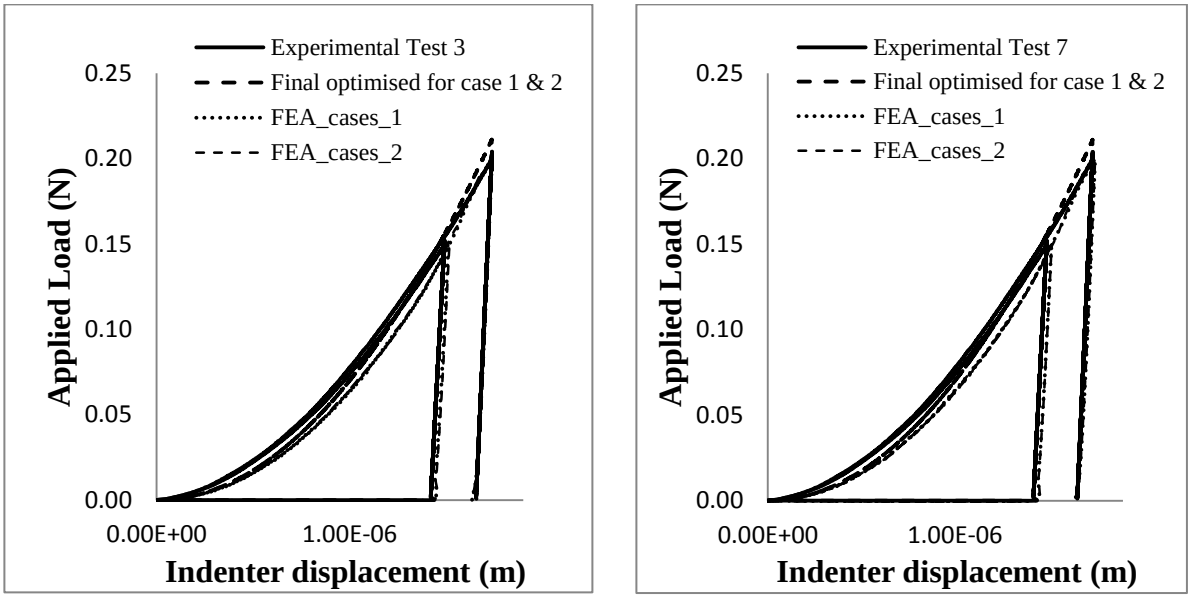

Figure 9.9 Loading-unloading curves for experimental tests, curves generated by FE simulation based on the final optimised values in **Tables 9.6** and **9.7** and the final curves from the optimisation algorithm using Optimisation Method 2

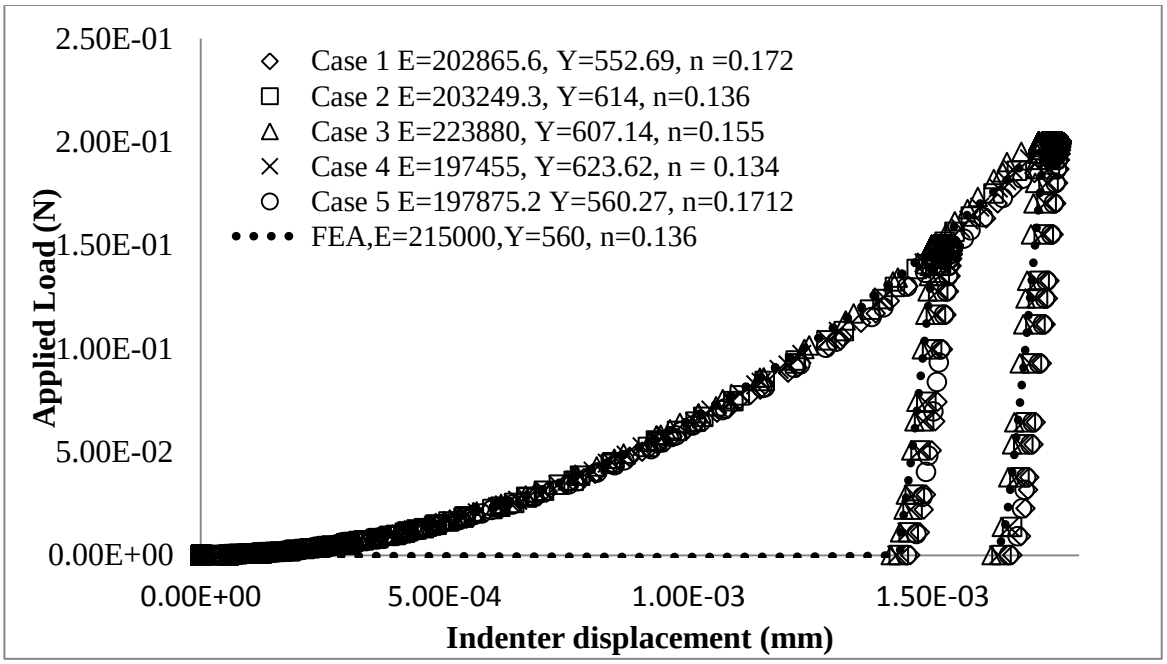

Figure 9.10 Loading-unloading curves for FE simulated curves based on the different elastic-plastic material properties from the optimised values and the target value of FEA curves using Optimisation Method.

9.3.3 Optimisation Method 3: Obtaining material properties from indentation loading-unloading curves using simplified equations

Since the characteristic loading-unloading indentation response can be determined using the dimensional analysis discussed in **Chapter 6**, an attempt has been made to obtain material properties from indentation loading-unloading curves using simplified equations. For predicting the sets of material properties from the experimental loading-unloading curves, a MATLAB nonlinear least square routine with LAQNONLIN function is used to produce the best fit between the experimental loading-unloading curve and the predicted optimised curves. The simplified equations are shown in **Table 7.1**. Previous studies in **Chapter 6** have indicated that the solutions are very sensitive to the values of k_1 and k_2 compared to other parameters. Therefore, the optimisation has been performed by reducing the bounds of the k_1 and k_2 factors.

Table 9.7 Three optimisation results with two different initial values for Test 3

Case	parameters	Target values	Initial values	Optimised values	Percentage Error for E,σ_y,n
1	k_1 for 150mN k_2 for 150mN E(GPa) σ_y(MPa) n k_1 for 200mN k_2 for 200mN	215GPa 560MPa 0.136	16.0 -1.10 180GPa 400MPa 0.10 16.0 -1.10	216960.09 635.94 0.141	1% 12% 3.5%
2	k_1 for 150mN k_2 for 150mN E(GPa) σ_y(MPa) n k_1 for 200mN k_2 for 200mN	215GPa 560MPa 0.136	16.0 -1.10 110000 592 0.193 16.0 -1.10	214670 635.49 0.140	1% 12% 3.5%

Table 9.8 Three optimisation results with two different initial values for Test 7

Case	parameters	Target values	Initial values	Optimised values	Percentage Error for E,σ_y,n
1	k_1 for 150mN k_2 for 150mN E(GPa) σ_y(MPa) n k_1 for 200mN k_2 for 200mN	215GPa 560MPa 0.136	16.0 -1.10 180GPa 400MPa 0.10 16.0 -1.10	217685.61 638.31 0.138	1% 12% 1.4%
2	k_1 for 150mN k_2 for 150mN E(GPa) σ_y(MPa) n k_1 for 200mN k_2 for 200mN	215GPa 560MPa 0.136	16.0 -1.10 110000 592 0.193 16.0 -1.10	218371 635.634 0.1396	1% 12% 2.6%

In this study, a seven-parameter optimisation algorithm with different initial values is performed. **Tables 9.7** and **9.8** show the target and final optimised values. In general, there are excellent agreements for Young's modulus and the work-hardening exponent, which agree within 5% with both experimental loading-unloading curves. However, the yield stress values $\sigma_{0.0115}$ are approximately 12% over-estimated. The relationships between the forward differences ($X_{t+1} - X_t$) versus iterations in case 2 in **Table 9.8** are illustrated in **Figure 9.11**, which clearly shows how elastic-plastic material parameters reach convergence.

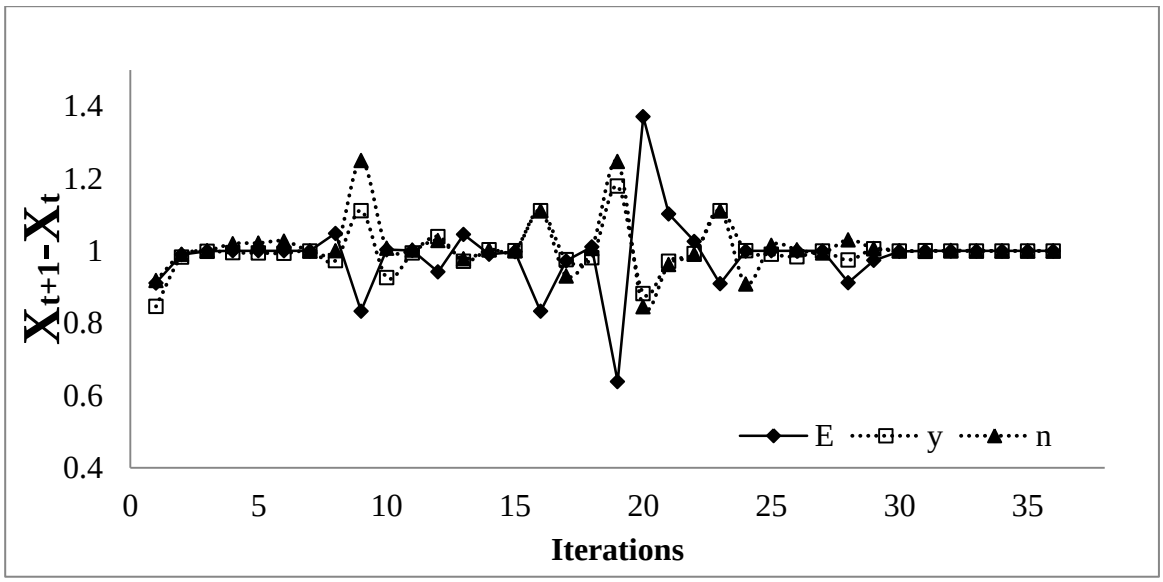

Figure 9.11 $X_{t+1} - X_t$ versus iterations for the case 2 in **Table 9.8** using Optimisation Method 3

Figure 9.12 shows the comparisons between the optimised and the experimental loading unloading curves. In addition, the final optimised results are re-submitted in the FE simulation to generate FE simulated loading-unloading curves. The final optimised curves from MATLAB agree well with the experimental test curves. On the other hand, there is some deviation of the curves between the FE simulated loading-unloading curves from the final optimised values and the final optimised curves from MATLAB. This may be caused by the sensitivity of the values k_1 andk_2. Therefore, accurate and unique material properties using simplified mathematical equations cannot be guaranteed based on dual-loading-unloading curves with different loads. It can be also said that the mathematical equations may not accurately capture the physical relationships between the indenter and the specimen.

Therefore, further investigations with more experimental tests using different indenter geometries may be required to improve this optimisation method.

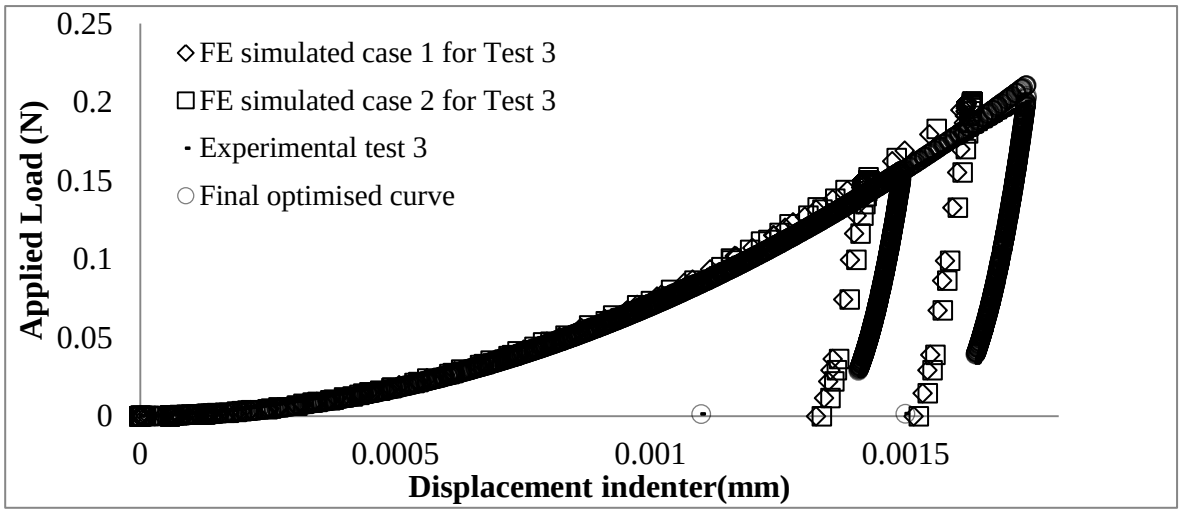

Figure 9.12 Loading-unloading curves for FE simulated curves based on the different elastic-plastic material properties from the optimised values and the target value of FEA curves using Optimisation Method 3

9.4 Discussions and conclusions

In this chapter, three different optimisation methods (namely, FE analysis, dimensional analysis and a simplified empirical method) are applied on 'real' experimental loading-unloading curves to extract elastic-plastic material properties (E, σ_y, n). The Micro Material Nano-Test instrument has been used for depth-sensing indentation tests to obtain the experimental loading-unloading curves using only a Berkovich indenter. The room temperature nanoindentation tests have been performed on a P91 specimen with 100 mN, 150 mN and 200 mN maximum loads. Therefore, dual loading-unloading curves with different loads are used instead of different indenter angles, since indentation data from different indenter geometries was not available.

With regards to Optimisation Method 1 (FE method), there are small differences between the experimental test curves and the corresponding FE generated curves, especially the loading portion of the curve. This is expected since the effects of friction, sharpness of the indenter tip, the indentation size effects in the real-life experimental indentation tests [105] and strain rate

effects are not taken into account in the FE analysis. The optimised results are very similar to the results obtained in **Table 5.6**. Both the values of Young's modulus, *E* and yield stress σ_y are close to the results obtained from the uniaxial tensile test. However, the values of the work-hardening exponent, *n* are over-estimated compared to the values of *n* from a power law fit of the uniaxial stress-strain data in **Figure 9.2**. This indicates that using an experimental indentation curve from a single indenter may not be sufficient to arrive at accurate predictions of the work hardening exponent.

With respect to Optimisation Method 2 (dimensional functions approach), the dimensional functions used in **Chapter 6** were constructed using a representative plastic strain 0.0115. Therefore, the target value of yield stress of this method is approximately 560 MPa, obtained from the P91 true stress-strain curve. The final optimised results from this method show the values of Young's modulus and work hardening exponents are relatively more accurate than the values of yield stress at $\sigma_{0.0115}$. However, the issues of uniqueness have clearly been illustrated in **Figure 9.10**, since similar loading-unloading curves from different sets of material properties are obtained corresponding to the experimental loading-unloading curve from the original set of material properties. This means that the proposed dimensional functions capture the physical relationships of the response between the indenter and the specimen, but some background information of the indented material is needed to arrive at accurate elastic-plastic material properties. It can be also said that using the same indenter geometry with different loads to produce the dual loading-unloading curves, does not guarantee a unique set of elastic-plastic material properties.

With reference to Optimisation Method 3 (simplified approach), simplified equations to generate the portion of loading-unloading curves have been developed since the characteristic loading-unloading response of indenter is known by the dimensional analysis used in **Chapter 6**. The results show that the values of Young's modulus and work hardening exponents agree well with those obtained from uniaxial tensile tests, but the final optimised values of the yield stress are generally over-estimated. Compared with the dimensional analysis approach, the physical relationships between the indenter and the specimen are not captured, since the values of k_1 and k_2 are introduced in the simplified approach. **Figure 9.12** shows that the FE simulated loading-unloading curves do not match well with the

experimental curves, even though the final simulated curves from MATLAB agree well with the experimental curves.

In general, the elastic-plastic material properties from these three proposed methods estimate the values of Young's modules to within 6%, compared to the values obtained from the uniaxial tensile tests. Furthermore, the estimations of Young's modulus are much better than those obtained from the Olive-Pharr method, which are approximately 20% over-estimated. To obtain the elastic-plastic material properties uniquely, especially the yield stress and work hardening exponent, using dual loading-unloading curves from different indenter geometries, rather than the same indenter geometry with different loads, is necessary.

10 Conclusions and future work

This work has been focused on the determination of elastic-plastic and visco-plastic material properties from indentation loading-unloading curves. Three different methods (namely, FE analysis, dimensional mathematical functions and simplified mathematical equations approaches) have been developed by using optimisation approaches. The three approaches have been validated against two types of indentation curves; FE-simulated curves and real experimental loading-unloading curves.

10.1 Conclusions

To determine the material properties from instrumented indentation loading-unloading curves, the research methodology has been established. To understand the material response of an indented specimen, the effects of indenter geometries on the prediction of material properties have been investigated by using the commercial FE software ABAQUS with the new optimisation approaches combining different methods.

All of the proposed methods have been applied to real instrumented indentation loading-unloading curves with only a Berkovich indenter, with experiments being performed at the University of Nottingham. The FE simulation has been implemented in the ABAQUS software based on the material properties obtained from the uniaxial tensile tests of P91 steel. The simulated FE loading-unloading curves agree well with experimental loading-unloading curves.

A combined FE analysis and optimisation approach for determining the sets of elastic-plastic and visco-plastic material have been developed. To validate the optimisation method, 'FE simulated' loading-unloading curves have been used as 'target' indentation curves. The optimised results from the FE simulated loading-unloading curves show excellent comparison with the sets of 'target' material properties, despite the fact that only a single indenter with a single load has been used. After the validation and feasibility of the optimisation algorithm, this approach is extended to examine the effectiveness and accuracy of the optimisation techniques using a real-life experimental indentation loading-unloading curve. The

estimations of the values of Young's modules and yield stress are much more accurate than that of the work-hardening exponent.

A parametric study with a wide range of material properties has been conducted by using FE analysis to construct appropriate dimensional functions. These dimensional mathematical functions are coupled with a numerical optimisation algorithm to determine the elastic-plastic material properties from the indentation loading-unloading curves. Unlike the FE approach, using a single indenter is not sufficient to arrive at a unique set of elastic-plastic material properties. Therefore, dual loading-unloading curves with different face angles of sharp indenters have been used. The optimised results show that dual loading-unloading curves can help to improve the accuracy of the predicted material properties. Since only experimental data from single indenter geometry (Berkovich indenter) is available for this investigation, dual loading-unloading curves have not been used. The optimised results are generally in good agreement with the material properties obtained from uniaxial tensile tests, despite using a single loading-unloading curve. However, if single indenter geometry is used, it is possible to arrive at very similar indentation curves even when using different optimised sets of material properties. This means that using a single indenter is not sufficient to guarantee arriving at a unique set of material properties.

Since the characteristic loading-unloading curves can be obtained from the dimensional analysis, more simplified mathematical equations have been devised to obtain the elastic-plastic material properties. Various optimisation approaches have been used. The optimisation algorithm has been performed by reducing the bounds of the parameters, and accurate optimised results are obtained by using the LSQNONLIN functions in MATLAB with dual loading-unloading curves. This approach shows that the prediction of the value of Young's modulus from real experimental loading-unloading curves is much better than the Oliver-Pharr method, which is approximately 20% over-estimated, but the error of the yield stress is generally higher than that obtained from the uniaxial tensile tests. Furthermore, the FE-simulated loading-unloading curves based on the final optimised values do not match well with the corresponding experimental loading-unloading curves, despite the fact that the final optimised curves in MATLAB match well with the experimental loading-unloading curves. This is due to the fact that the values of the k_1 and k_2 parameters used in the simplified

equations may not capture the complicated physical relationships between the indenter and the specimen.

The optimisation approaches based on the FE analysis, dimensional analysis and simplified empirical method have been used to determine nonlinear elastic-plastic as well as visco-plastic material properties. In general, the proposed methods can accurately estimate the values of Young's modulus from both real experimental and FE-simulated loading-unloading curves, compared with the Oliver-Pharr method. They can also determine reasonably accurate values of the yield stress and work hardening exponent from both experimental and FE-simulated curves when dual loading-unloading curves with different indenter face angles are used, On the other hand, using real experimental loading-unloading curves from a single indenter geometry does not accurately and uniquely arrive at the values of yield stress and work hardening exponent. To improve the prediction of accurate elastic-plastic material properties, at least two loading-unloading indentation curves from different indenter face angles are recommended.

10.2 Future work

Based on the research work presented in this study, potential future work to improve the current work is listed below.

(i) Instrumented indentation tests with different indenter face angles should be implemented to obtain accurate estimations of elastic-plastic material properties. The investigation of the effect of indenter parameters, such as titled indenter angles, blunt indenter, thin-film coated specimen and the behaviour of the material under high temperature should be undertaken.

(ii) Some limitations of the simplified mathematical functions approach exist due to the values of the k factors. Therefore a parametric study of the k factors and further work for investigating the relationships between the material properties and the geometry of the indenter should be undertaken. This can help to reduce the number of unknowns and the bounds of the parameters leading to improved accuracy of the optimisation results.

(iii)To establish more accurate dimensional mathematical functions and the simplified equations, instrumented indentation tests should be performed on a wide range of materials.

Close examination of the contact area during unloading should be undertaken using AFM observations, since the most complex plastic response between the indenter and the specimen occurs during the elastic recovery of the specimen when the indenter is removed.

(iv)Global optimisation functions in MATLAB may help to improve the estimation of the material properties with more efficiency and accuracy and it may improve the robustness of the current optimisation algorithms.

References

[1] W.C. Oliver. and G.M. Pharr., An improved technique for determining hardness and elastic modulus using load and displacement sensing indentation experiments, Journal of Materials Research, 1992, 7(6), 1564-1583.

[2] D. Tabor., The hardness of metals, Oxford University press, Cambridge, Great Britain, 1951

[3] J.A. Brinell, II Congress International de Methodes d'Essai: Iron and steel institute journal, 1900, 59., 243

[4] E. Meyer , Investigations of hardness testing and hardness. Phys.Z. 1908 9, 66 -74.

[5] H. Hertz, Uber Die Beruhrung Fester Elastischer Korper (on the contact of elastic solids). J.Reine Angew.math., 1881, 92, 156-171.

[6] K. L. Johnson, Contact Mechanics, Cambridge University Press, Cambridge, 1985.

[7] A.C. Fischer-Cripps, Nanoindentation, 2nd ed., Springer, New York, 2004.

[8] J**.** Boussinesq**,** Application des Potentials a l'etude de l'equilibre et du mouvement des solides elastiques**.** Gauthier-Villars, Paris, 1885**.**

[9] I.N. Sneddon, Boussinesq's Problem for a rigid cone. Proc.cambridge Philos. Soc. 44, 1948. 492-507

[10] I.N. Sneddon, The relation between load and penetration in the axisymmetric boussinesq problem for a punch of arbitrary profile, Int. J. Engng. Sci., Int.J.Engng.Sci. 1965.3(1), 47-57.

[11] D. Tabor, A simple theory of static and dynamic hardness. Proc. R. Soc., Lond.. A , 1948, 192(1029), 247-274.

[12] N.A. Stilwell, and D. Tabor, Elastic recovery of conical in-dentations. Proc. Phys. Soc. London, 1961, 78(2), 169-179.

[13] G.Dumas, Elastoplastic indentation of a half-space by an infinitely long rigid circular cylinder. Int.J.Mech.Sci.1971, 13(6), 519-528

[14] H. Ford, J.M. Alexander, Advanced mechanics of materials. Longmans, London, 1963.

[15] C. Hardy, Indentation of an elastic-perfectly-plastic half-space by a hard sphere. J.Basic Eng. 1972, 94(1), 251.

[16] R., Hill, The mathematical theory of plasticity. Oxford University Press, London, 1950.

[17] L.E. Goodman, Contact stress analysis of normally loaded rough sphere. Trans. ASME, Series E, J.Appl.Mech. 1962, 29(3), 515-522

[18] J.Grunzweig, Calculations and measurements on wedge-indentation.J.Mech. Phys.Solids 1954, 2(2), 81-86.

[19] A.I. Kuznetsoy, Penetration of rigid dies into a half-space with power-law strain hardening and nonlinear creep, 1962. J. Appl. Math. Mech. 26(3), 717-732.

[20] E.H. Lee, J.R.M. Radok,. The contact problem for viscoelastic bodies. Trans. ASME, Series E, J. Appl. Mech. 1960. 27(3), 438-444.

[21] J.R. Matthews, Indentation hardness and hot pressing. Acta Metall. 1980, 28 (3), 311–318.

[22] J.R.M., Radok, Viscoelastic Stress Analysis. Q. Appl. Math, 1957, 15, 198-202.

[23] W.H. Yang, The contact problem for viscoelastic bodies. Trans. ASME, Ser. E, J. Appl. Mech. 1966, 33, 395-401

[24] R.S. Bradley, The cohesive force between solid surfaces and the surface energy of solids. Philos. Mag.,1932, 13(86), 853–862.

[25] B.V. Derjaguin, Analysis of friction and adhesion IV: The Theory of the Adhesion of Small Particles. Koll.-Zeit. 1934, 69 (2), 155–164.

[26] B.V. Derjaguin, V.M. Muller, Y.P. Toporov, Effect of contact deformations on adhesion of particles. J. Coll. Interface Sci. 1975, 53(2), 314–326.

[27] K.L. Johnson, K. Kendall, A.D. Roberts,. Surface energy and the contact of elastic solids. Proc. R. Soc. Lond. A, Math. Phys. Sci. 1971, 324(1558), 301–313.

[28] D. Maugis, Adhesion of Spheres: The JKR-DMT transition using a Dugale model. J. Colloid Interface Sci. 1992, 150 (1), 243–269.

[29] V.M. Muller, V.S. Yushchenko, B.V. Derjaguin, On the influence of molecular forces on the deformation of an elastic sphere and its sticking to a rigid plane. J. Coll. Interface Sci. 1980, 77(1), 91–101.

[30] D. Tabor, Surface forces and surface interactions. J. Coll. Interface Sci. 1977, 58 (1), 2–13.

[31] S.I. Bulychev, V.P. Alekhin, M.K. Shorshorov, A.P. Ternovskii, G.D. Shnyrev, Determining young's Modulus from the indenter penetration diagram. Zavodskaya Laboratoriya 1975, 41 (9), 1137–1140.

[32] J.L. Loubet, J.M. Georges, O. Marchesini and G. Meille,. Vickers indentation curves of magnesium oxide (MgO). J. Tribol.Trans. ASME 1984, 106, 43–48.

[33] D. Newey, M.A Wilkins and H.M. Pollock, , An ultra-low-load penetration hardness tester., 1982, J. Phys. E: Sci. Instrum. 15(1), 119–122.

[34] J.B. Pethica, R.. Hutchings and W.C. Oliver, Hardness measurement at penetration depths as small as 20 Nm. Philos. Mag. A, 1983, 48(4), 593–606.

[35] A.P. Ternovskii, V.P. Alekhin, M.K. Shorshorov, M.M. Khrushchov and V.N. Skvortsov, Micromechanical testing of materials by depression. Zavodskaya Laboratoriya 1974, 39(10), 1242–1247.

[36] M.F. Doerner and W.D. Nix, A method for interpreting the data from depth-sensing indentation instruments. J. Mater.Res., 1986, 1(4), 601-609.

[37] G.M. Pharr, and W.C. Oliver and F.R.. Brotzen, On the generality of the relationship among contact stiffness, contact area, and elastic modulus during indentation. J. Mater. Res., 1992, 7(3), 613-617.

[38] W.C. Oliver and G.M. Pharr, Measurement of hardness and elastic modulus by instrumented indentation: Advances in understanding and refinements to methodology. J. Mater. Res.,2004. 19(1), 3-20.

[39] C.M. Cheng, and Y.T. Cheng, On the initial unloading slope in indentation of elastic-plastic solids by an indenter with an axisymmetric smooth profiles. Appl.Phys. Lett., 1997, 71(18), 2623-2625.

[40] C.M. Cheng, and Y.T. Cheng, Relationships between hardness, elastic modulus, and the work of indentation. Appl.Phys. Lett., 1997, 73(5), 614-616.

[41] C.M. Cheng, and Y.T. Cheng, Further analysis of indentation loading curves: Effects of tip rounding on mechanical property measurements. J. Mater.Res., 1998. 13(4), 1059-1064.

[42] C.M. Cheng and Y.T. Cheng, Effects of 'sinking in' and 'piling up' on the estimating the contact area under load in indentation. Phil. Mag. Lett., 1998. 78(2), 115-120.

[43] C.M. Cheng and Y.T. Cheng, Scaling approach to conical indentation in elastic-plastic solids with work-hardening. J.App.Phys., 1998, 84(4), 1284-1291.

[44] C.M. Cheng and Y.T. Cheng, Analysis of indentation loading curves obtained using conical indenters. Phil. Mag. Lett., 1998, 77(1), 39-47.

[45] C.M. Cheng and Y.T. Cheng, Scaling relationships in conical indentation of elastic-perfectly plastic solids. Int. J. Solids Structures, 1999, 36(8), 1231-1243.

[46] C.M. Cheng and Y.T. Cheng, Y.T. Can stress-strain relationships be obtained from indentation curves using conical and pyramidal indenters?. J. Mater.Res., 1999, 14(9), 3493-3496.

[47] C.M. Cheng and Y.T. Cheng, What is indentation hardness?. Surf. Coat. Tech. 2000, 133-134, 417-424.

[48] C.M. Cheng and Y.T. Cheng,. Scaling, dimensional analysis, and indentation measurements. Mater Sci Eng., 2004, 44(4-5), 91-149.

[49] C. Hary, C.N. Baronet and G.V. Tordion, The indentation of an elastic-perfectly-plastic half-space by a hard sphere, J.Basic Eng. 1972, 94(1), 251-254.

[50] G. Dumas, C.N. Baronet, Elastoplastic indentation of a half-space by an infinitely long rigid circular cylinder. Int.J. Mech.Sci. 1971, 13(6), 519-530

[51] A.K. Bhattacharya and W.D. Nix. Analysis of elastic and plastic deformation associated with indentation testing of thin films on substrate 1988, 24(12) 1287-1298

[52] T.A. Laursen and J.C. Simo A study of the mechanical of micro-indentation using finite elements. J Mater Res., 1992, 7(3), 618-626

[53] M, Lechinichi, C, Lenardi, J, Haupt and R, Vitali., Simulation of Berkovich nanoindentation experiments on thin films using finite element method. Thin Solid Films, 1998, 312(1-2), 240-248

[54] A, Bolshakov, W.C. Oliver, G.M. Pharr., Influences of stress on the measurement of mechanical properties using nanoindentation: Part II. Finite element simulations. J Mater Res, 1996, 11(3), 760-768.

[55] J.M. Antunes, L.F. Menezes and J.V. Fernandes., Numerical study of the influence of imperfection of the tip of a Vickers indenter on ultramicrohardness, Key Engineering Materials, 2002, 230(2), 525–528.

[56] H.F.Wang ,and H. Bangert., Three-dimensional finite-element simulation of Vickers indentation on coated systems. Materials Science and Engineering: A, 1993, 163(1), 43–50.

[57] Li, Min, C. Wei-min., L. Nai-gang, W. Ling-dong., A numerical study of indentation using indenters of different geometry, Journal of Material Research, 2004, 19(1), 73-78.

[58] N.A. Sakharova, J.V. Fernandes, J.M. Antunes and M.C. Oliveira, Comparison between Berkovich, Vickers and conical indentation tests: A three-dimensional numerical simulation study. International Journal of Solid and Structure, 2009, 46(5), 1095-1104.

[59] S.I. Bulychev, V.P. Alekhin, M.K. Shorshorov, and A.P. Ternovskii, Mechanical properties of materials studied from kinetic diagrams of load versus depth of impression during microcompression. Strength of Materials, 1976, 8(9), 1084-1089

[60] X. Chen, J. Yan and A.M., Karlsson, On the determination of residual stress and mechanical properties by indentation. Materials Science and Engineering: A, 2006, 416(1-2), 139–149.

[61] J. Yan, X. Chen, A.M. Karlsson, Determining equi-biaxial residual stress and mechanical properties from the force–displacement curves of conical micro indentation. J.Eng.Mater.Techol., 2007a, 129(2), 200–206.

[62] J. Yan, A.M. Karlsson and X. Chen. Determining plastic properties of a material with residual stress by using conical indentation. International Journal of Solids and Structures, 2007b. 44(11-12), 3720–3737.

[63] T.W. Capehart, Y.T. Cheng, Determining constitutive models from conical indentation: sensitivity analysis. J. Mater, Res., 2003, 18(4), 827–832.

[64] J.L. Bucaille, S. Stauss, E. Felder and J. Michler. Determination of plastic properties of metals by instrumented indentation using different sharp indenters. Acta Mater., 2003, 51(6), 1663–1678.

[65] Y. Cao, N. Huber, Further investigation on the definition of the representative strain in conical indentation. J. Mater. Res., 2006, 21(7), 1810–1821.

[66] S. Swaddiwudhipong, K.K, Tho, Z.S. Liu, K. Zeng. Material characterization based on dual indenters. Int. J. Solids Struct., 2005, 42(1), 69–83.

[67] G. Chaiwut. and P.B. Esteban. Characterization of elastoplastic properties based on inverse analysis and finite element modelling of two separate indenters. Int.J. Engineering materials & Techonology, 2007, 129(4), 603-608.

[68] A.G. Atkins and D. Tabor. Plastic indentation in metals with cones, J.Mech.Phys. Solid 1965,13(3), 149-164.

[69] J.S. Field, M.V. Swain. Determining the mechanical properties of small volumes of material from submicrometer spherical indentations. J. Mater. Res. 1995, 10 (1), 101– 112.

[70] S. Jayaraman, G.T. Hahn, W.C. Oliver, C.A. Rubin and P.C. Bastias. Determination of monotonic stress–strain curve of hard materials from ultra-low-load indentation tests. Int. J. Solid Struct. 1998, 35 (5-6), 365–381.

[71] B., Taljat, T. Zacharia and F. Kosel, New analytical procedure to determine stress–strain curve from spherical indentation data. Int. J. Solid Struct. 1998, 35 (33), 4411–4426.

[72] N. Huber and C. Tsakmakis, Determination of constitutive properties from spherical indentation data using neural networks. Part I: the case of pure kinematic hardening in plasticity laws, J. Mech. Phys. Solids, 1999, 47 (1), 1569–1588.

[73] K.D. Bouzakis and N. Vidakis, Superficial plastic response determination of hard isotropic materials using ball indentations and a FEM optimisation technique. Mater. Charact. 1999, 42 (1), 1–12.

[74] A.E. Giannakopoulos and S. Suresh, Determination of elasto-plastic properties by instrumented sharp indentation, Scripta Mater. 1999, 40(10), 1191–1198.

[75] R. Hill, B. Storakers and A.B. Zdunek. A Theoretical Study of the Brinell hardness Test. Proc. Roy. Soc. Lond. A, 1989, 423(1965), 301-330.

[76] A.E. Giannakopoulos, P.-L. Larsson and R. Vestergaard. Analysis of Vickers indentation, Int. J. Solids Struct. 1994, 31(19). 2679-2708.

[77] P.L. Larsson, A.E. Giannakopoulos, E. Soderlund, D.J. Rowcliffe and R. Vestergaard. Analysis of Berkovich indenter. Int. J. Solids Struct. 1996, 33(2), 221-248

[78] T.A. Venkatesh, K.J. Van Vliet, A.E. Giannakopoulos and S. Suresh, Determination of elasto-plastic properties by instrumented sharp indentation: guidelines for property extraction, Scripta Mater., 2000, 42(9), 833–839

[79] A. Nayebi, R.E., Abdi, O. Bartier, and G. Mauvoisin, New procedure to determine steel mechanical parameters from the spherical indentation technique, Mech. Mater. 2004, 34(4), 243-254

[80] E.G.Herbert, G.M, Pharr, W.C. Oliver, B.N, Lucas, J.L, Hay, On the measurement of stress-strain curves by spherical indentation. Thin Solid Films, 2001, 398-399, 331-335

[81] M. Dao, N, Chollacoop, K.J. VanVliet, T.A. Venkatesh, and S. Suresh. Computational modelling of the forward and reverse problems in instrumented sharp indentation. Acta Mater 2001, 49(19), 3899-3918

[82] N. Ogasawara, N. Chiba and X.J. Chen, Representative strain of indentation analysis. J. Mater Res, 2005, 20(8), 2225-2234

[83] N. Ogasawara, N. Chiba and X.J. Chen, Measuring the plastic properties of bulk material by single indentation test. Scr Mater, 2006, 54(1), 65-70

[84] N. Chollacoop and U. Ramamurty, Experimental assessment of the representative strains in instrumented sharp indentation. Scr mater, 2005, 53(2), 247-251

[85] Y.P. Cao, J.Lu, A new scheme for computational modeling of conical indentation in plastically graded materials. J. Mater. Res.2004, 19 (6), 1703–1716

[86] M.M. Chaudhri. Subsurface strain distribution around Vickers hardness indentations in annealed polycrystalline copper. Acta Mater, 1998, 46 (9), 3047-3056

[87] A.E. Tekkaya, An improved relationship between Vickers hardness and yield stress for cold formed materials and its experimental verification, CIRP Ann Manuf Technology. 2000, 49(1), 205-208

[88] I Szlufarska, Atomistic simulations of nanoindentation, Mater. Today. 2009, 9(5), 42-50

[89] ABAQUS, 2000. Tutorial manual version 6.8, Pawtucket: Hibbitt, Karlsson and Sorensen, Inc

[90] Matlab, Optimisation toolbox TM 4 users guide, 2008 (T.M.Inc.).

[91] A.A. Pelegri, X. Huang. Nanoindentation on soft film/hard substrate and hard film/soft substrate material systems with finite element analysis. Composites Science and Technology. 2008, 68(1), 147-155

[92] J.M. Antunes, J.V. Fernandes, L.F. Menezes and B.M. Chaparro, A new approach for reverse analysis in depth-sensing indentation using numerical simulation, Acta Mater. 2007, 55(1) 69-81

[93] Y.P. Cao and J. Lu, A new method to extract the plastic properties of metal materials from an instrumented spherical indentation loading curve, Acta Mater. 2004, 52(13) 4023-4032

[94] N. Chollacoop, M. Dao and S. Suresh, Depth-sensing instrumented indentation with dual sharp indenters, Acta Mater. 2003, 51(13), 3713-3729

[95] J. Luo, J. Lin and T.A. Dean, A study on the determination of mechanical properties of a power law material by its indentation force-depth curve, Philosophical magazine, 2006, 86(19), 2881-2905

[96] J. Luo, J. Lin, A study on the determination of plastic properties of metals by instrumented indentation using two sharp indenters, Int. J. Solids Struct., 2007, 44(18-19) 5803-5817

[97] N. Ogasawara, N. Chiba and X. Chen, Representative strain of indentation analysis, J. Mater Res. 2005, 20(9), 2225-2234

[98] N. Ogasawara, N. Chiba and X. Chen, Measuring the plastic properties of bulk materials by singles indentation test, Scripta Mater. 2006, 54 (1), 65-70

[99] K. Zeng. C.H. Chiu, An analysis of load-penetration curves from instrumented indentation, Acta Mater. 2001, 49(17), 3539-3551

[100] S. Swaddiwudhipong, K.K. Tho, Z.S. Liu and K. Zeng, Material characterization based on dual indenters, Int. J. Solids Struct. 2005, 42 (1), 69–83.

[101] G. Chaiwut and P.B. Esteban, Characterization of elastoplastic properties based on inverse analysis and finite element modelling of two separate indenters, J. Engineering Materials and Technology. 2007, 129(4), 603-608

[102] G.E. Dieter, Mechanical Metallurgy, McGraw-Hill, New York, 1976.

[103] Y. Wei, X. Wang and M. Zhao. Size effect measurement and characterization in nanoindentation test, Journal of Materials Research, 2004, 19(1), 208-217

[104] M.K. Khan, S.V. Hainsworth, L.E. Fitzpatrick, A combined experimental and Finite element approach for determining mechanical properties of aluminium alloys by nanoindentation, Comput.Mater.Sci. 2010, 49(4), 751-760.

[105] ASTM E8M Test Methods for Tension Testing of Metallic Materials (Metric), Annual Book of ASTM Standards vol. 03.01,2003

[106] J.J. Kang, A.A. Becker, and W. Sun, Determining Elastic-plastic properties from Indentation data obtained from Finite Element Simulations and Experimental Results, Int.J.Mech.Sci. (Accepted)

[107] J.J. Kang, A.A. Becker, and W. Sun, A combined dimensional analysis and optimisation approach for determining elastic-plastic properties from indentation tests. J. Strain. Analysis. 2011, 46 (8), 749-759.

[108] M. Boris, Determining elastic-plastic properties from indentation tests using finite element simulations, Msc thesis in computational engineering.

[109] M. J. Mayo and W. D. Nix, A micro-indentation study of superplasticity in Pb, Sn, and Sn–38 wt% Pb, Acta Metall., 1998, 36 (8), 2183–2192

[110] A. R., Geranmayeh and R. Mahmudi, Room-temperature indentation creep of lead-free Sn–5% Sb solder alloy, J. Electron. Mater, 2005, 34 (7) 1002–1009

[111] S. N. G. Chu. and J. C. M. Li, Impression creep; A new creep test, J. Mater. Sci.,1977, 12(11), 2200–2208.

[112] A. Juhasz, P. Tasnadi, P. Szaszvari and I. Kovacs, Investigation of the superplasticity of Tin-lead eutectic by impression creep Tests, J. Mater. Sci. 1986, 21(9), 3287–3291.

[113] P. M. Sargent and M. F. Ashby, Indentation creep, Mater. Sci. Technol. 1992, 8(7), 887–897.

[114] K. Zhang, J. R. Weertman and J. A. Eastman, The influence of time, temperature, and grain size on indentation creep in high-purity nanocrystalline and ultrafine grain copper, Appl. Phys. Lett. 2004, 85 (22) 5197–5199

[115] A.H.W. Ngan and B. Tan, Viscoelastic effects during unloading in depth-sensing indentation. J. Mater.Res. 2002, 17(10), 2604-2610

[116] A.H.W. Ngan, H.T. Wang, B.Tang. and K.Y. Sze, Correcting power-law viscoelastic effects in elastic modulus measurement using depth-sensing indentation, Int.J.Solids struct., 2005, 42 (5-6) 1831-1846

[117] A.C. Fischer-Cripps, Multiple-frequency dynamic nanoindentation testing, J.Mater Res., 2004, 19, 2981-2988

[118] G. Huang, B. Wang, and H. Lu, Measurements of viscoelastic functions of polymers in the frequency-domain using nanoindentation, Mech Time-depend Mater. 2004, 8(4) 345-364

[119] C.A. Tweedie, and K. Van Vliet, Contact creep compliance of viscoelastic materials via nanoindentation, J. Mater Res., 2006, 21 (6), 1576-1589

[120] M.F. Ashby, Material Selection in Mechanical Design, 2nd ed. Elsevier, Amsterdam, 1999.

[121] T.H. Hyde, K. Yehia, and A.A. Becker, Interpretation of impression creep data using a reference stress approach. Int.J.Mech.Sci., 1993, 35(6), 451-462

[122] A.A, Becker, T.H. Hyde and L. Xia, Numerical analysis of creep in components. J. Strain. Analysis. 1994, 29 (3), 185-192

[123] M.I. Davies and Nicola Everitt, Nano-indentation data for P91 specimens, University of Nottingham, 2012

[124] A. H. Yaghi, T. H. Hyde, A. A. Becker, W. Sun, G. Hilson, S. Simandjuntak, P. E. J. Flewitt, M. J. Pavier, D. J. Smith, A comparsion between measured and modelled residual stresses in a circumferentially butt-welded p91 steel pipe. J. Pressure vessel Technol. 2010, 132(1)

[125] A.M. Majed, S.Y, Ahmet, P.C. Andreas, Elastoplastic contact/impact of rigidly supported composites", Composites: Part B, 2012(43),1244–1251

Appendix 1

This is MATLBA optimization algorithms, including Optimization.m and Objective_function.m. There are four different initial guess values, Young's modulus, Poisson's ration, Yield stress and work hardening exponent. For replacing the material section in ABAQUS input file, pre_processing.exe is based on C language. After ABAQUS job is finished, post_processing.py can be used to extract loading-unloading curve from ABAQUS.odb file.

This is code for 'Optimization.m'

```
clear;close all;
format longE
%Declaration of global variables
global History Evals Iter s1 s2 s3 s4
global nop E v y n

%starting initial guess values
IGV =[600000 0.25 3000 0.45];
%Young's modulus, Poisson's ratio, Yield stress, work hardening exponent
E=IGV(1,1); v=IGV(1,2); y=IGV(1,3); n=IGV(1,4);
%The number of parameters
nop=4;

%The scale coefficients for each parameters
s1=1.0e-9; s2=1.0e-4; s3=1.0e-7; s4=1.0e-4;
InitialParameter=[E*s1,v*s2, y*s3, n*s4];

%Initialize counters
Iter=0; Evals=0; History=[];
%setting optimisation options
Set_options=optimset('TolFun',1e-15,'TolX',1e-15,'MaxIter',10000)

%invoke optimizer
[x, resnorm]=LSQNONLIN(@objfunction,InitialParameter, [0 1.0000E-05 0 5.000E-06],[inf
4.99999E-05 inf 4.99999E-05],Set_options)

%Scale the optimized parameters to normal values
x1=x(1)/s1; x2=x(2)/s2; x3=x(3)/s3; x4=x(4)/s4;
OptParam=[x1 x2 x3 x4];

%Save the optimized parameters in "parameter.txt"
parameter = fopen('parameters.txt', 'w');
fprintf(parameter,'%12.8f %12.8f %12.8f %12.8f', OptParam);
fclose(parameter);
```

```
%save('parameter.txt','OptParam','-ascii')
%Save the parameter evolution history in "Parameter_history.txt".
History=[History; [Iter Evals x1 x2 x3 x4 resnorm]];
Parameter_history = fopen('Parameter_history.txt', 'w');
fprintf(parameter,'%6.1f %6.2f %12.8f %12.8f %12.8f %12.8f %12.8f', History);
fclose(Parameter_history);
%save ('Parameter_history.txt', 'History','-ascii')

%Call external program
%Pre_processing: replacing material parameters in ABAQUS input file%
%ABAQUS job
%Post_processing: extracting loading-unloading curve from ABAQUS odb.file%
!del tempatefile.*  %Deleting previous tempatefile.odb
!pre_processing  %Replacing material parameters in ABAQUS input file
!copy ABAQUS_INPUT_FILE_NAME.inp tempate_file.inp
!abaqus job=tempate_file interactive %input ABAQUS job
!abaqus cae noGUI=post_processing.py % Extracting loading-unloading curve from
ABAQUS odb.file
```

This is code for ‘Objective_function.m’

```
%This function computes the difference between
%target and simulated loading-unloading curve
function err=f(params)
global Iter Evals History s1 s2 s3 s4 nop nob
global nob nop E v y n
%Scale the paramteres to normal values
x1=params(1)/s1; x2=params(2)/s2; x3=params(3)/s3; x4=params(4)/s4;
OptParam=[x1 x2 x3 x4];

%Save the parameters in parameter.txt
parameter = fopen('parameters.txt', 'w');
fprintf(parameter,'%12.8f %12.8f %12.8f %12.8f', OptParam);
fclose(parameter);

!del tempatefile.*
!pre_processing
!copy ABAQUS_INPUT_FILE_NAME.inp tempatefile.inp
!abaqus job=tempatefile interactive
!abaqus cae noGUI=post_processing.py

% Invoke the target loading & unloading curve
load loading.txt
Dis=loading(:,1); Force=loading(:,2);
load unloading.txt
```

```
Dis1 = unloading(:,1); Force1 = unloading(:,2);
A1=[Force; Force1];
A=[Dis; Dis1];

nob=length(A);
plot(A,A1,'g-'), hold on
% Invoke the loading & unloading curve from FEA
load loading_FEA.txt
loading_Dis_FEA=loading_FEA(:,1); loading_Force_FEA =loading_FEA(:,2);
load unloading_FEA.txt
unloading_Dis_FEA=unloading_FEA(:,1); unloading_Force_FEA=unloading_FEA(:,2);
B1=[loading_Force_FEA; unloading_Force_FEA];
B=[loading_Dis_FEA; unloading_Dis_FEA];

%Plot both target and simulated loading-unloading curve.
plot(B,B1,'r-'), hold on
ylabel('Load');
xlabel('Indentation displacement');

%The difference between the displacement portions of target and
%simulated loading & unloading curves.
err=A1-B1;
%calculate the norm of error vector
resnorm=0.5*sum(err.^2);

History=[History;[Iter Evals x1 x2 x3 x4 resnorm]];
save ('history.txt', 'History', '-ascii')

Evals=Evals+1;
if rem(Evals,nop)==0
Iter=Iter+1;
end
```

Appendix 2

$$f_1\left(\frac{E^*}{\sigma_r}\right) = \frac{C}{\sigma_{0.0115}}$$

$$= -0.374\left[ln\left(\frac{E^*}{\sigma_{0.0115}}\right)\right]^3 + 2.666\left[ln\left(\frac{E^*}{\sigma_{0.0115}}\right)\right]^2 + 19.759\left[ln\left(\frac{E^*}{\sigma_{0.0115}}\right)\right] - 44.101$$

$$f_2\left(\frac{E^*}{\sigma_r}, n\right) = \frac{1}{E^* h_m}\frac{dP_u}{dh}\Big|_{h_m}$$

$$= (-0.0270n^3 + 0.295n^2 - 0.0903n + 0.0127)\left[ln\left(\frac{E^*}{\sigma_{0.0115}}\right)\right]^3 + (-2.972n^3 - 1.575n^2 + 0.708n - 0.341)\left[ln\left(\frac{E^*}{\sigma_{0.0115}}\right)\right]^2 + (28.235n^3 - 5.054n^2 - 0.635n + 3.415)\left[ln\left(\frac{E^*}{\sigma_{0.0115}}\right)\right] + (-62.696n^3 + 26.380n^2 - 3.141n - 2.989)$$

$$f_3\left(\frac{\sigma_r}{E^*}, n\right) = \frac{h_r}{h_m}$$

$$= (0.0737n^3 - 0.0282n^2 + 0.001n - 0.0114)\left[ln\left(\frac{\sigma_{0.0115}}{E^*}\right)\right]^3 + (0.995n^3 - 0.348n^2 + 0.0151n - 0.201)\left[ln\left(\frac{\sigma_{0.0115}}{E^*}\right)\right]^2 + (4.088n^3 - 1.141n^2 + 0.021n - 1.221)\left[ln\left(\frac{\sigma_{0.0115}}{E^*}\right)\right] + (4.979n^3 - 0.658n^2 - 0.114n - 1.609)$$

$$f_{1\ for\ 60^\circ} = \frac{C}{\sigma_{0.0184}}$$

$$= -0.205\left[ln\left(\frac{E^*}{\sigma_{0.0184}}\right)\right]^3 + 4.170\left[ln\left(\frac{E^*}{\sigma_{0.0184}}\right)\right]^2 + 31.224\left[ln\left(\frac{E^*}{\sigma_{0.0184}}\right)\right]$$

$$- 46.645$$

The combinations of E and σ_y used in this study are listed in Table 1. The work-hardening exponent, n, has values of 0.01, 0.1, 0.2, 0.3, 0.4 and 0.5, resulting in a total of 174 cases.

Table 1 Combinations of E and σ_y used in this study

E(GPa)	σ_y(MPa)	E(GPa)	σ_y(MPa)
10	50	100	1800
	100		2500
	200		3000
	400		
	600		
50	100	150	300
	300		600
	600		1000
	900		1500
	1200		2500
	2000		3000
100	200	210	300
	600		600
	900		900
			1200
			2500
			3000

List of Publications

[1] J. Kang, A.A., Becker, W. Sun, Effect of indenter geometries on material properties:, Applied mechanics and Material, Vol. 70 (2011), 219-224

[2] J. Kang, A.A., Becker, W. Sun, A Combined dimensional analysis and optimisation approach for determining elastic-plastic properties from indentation tests, Journal of Strain analysis, Vol. 46 (2011), 749-759

[3] J. Kang, A.A., Becker, W. Sun, Determining elastic-plastic properties from indentation data obtained from Finite element simulations and experimental results, Int.J. Mech.Sci. Vol. 62 (2012) 34-46

[4] J. Kang, B.Martin, A.A, Becker and W. Sun, Obtaining material properties from indentation loading unloading curves using simplified equations, Proc. Eleventh Int. Conf. on Computational Structures Technology, B.H.V. Topping, (Editor), Civil-Comp Press, Stirlingshire, Paper 263, 4-7 September 2012, Dubrovnik Croatia

[5] J. Kang, A.A., Becker and W. Sun, Implementation of optimization techniques in determining elastic-plastic and visco-plastic properties from Instrumented Indentation curves", 38th solid mechanics conference, IPPT, Zaklad Graficzny Uniwersytet Warszawski,zam, Page 308, 27-31 August 2012, Warsaw

[6] J. Kang, A.A., Becker and W. Sun, A comparison between dimensional analysis and finite element simulation approach based on the optimisation with real experimental results, Journal of Materials:Design and Application. (Under considering)